1. Report No.	2. Government Accession No.	3. Recipient's Catalog No.
FHWA/TX-07/0-4519-1		

4. Title and Subtitle	5. Report Date
VERIFICATION OF THE LOAD-THICKNESS DESIGN CURVES IN THE MODIFIED TRIAXIAL DESIGN METHOD	February 2007 Published: June 2008
	6. Performing Organization Code

7. Author(s)	8. Performing Organization Report No.
Emmanuel G. Fernando, Jeongho Oh, Cindy Estakhri, and Soheil Nazarian	Report 0-4519-1

9. Performing Organization Name and Address	10. Work Unit No. (TRAIS)
Texas Transportation Institute The Texas A&M University System College Station, Texas 77843-3135	11. Contract or Grant No. Project 0-4519

12. Sponsoring Agency Name and Address	13. Type of Report and Period Covered
Texas Department of Transportation Research and Technology Implementation Office P. O. Box 5080 Austin, Texas 78763-5080	Technical Report Sept. 2003 to Dec. 2006
	14. Sponsoring Agency Code

15. Supplementary Notes

Project performed in cooperation with the Texas Department of Transportation and the Federal Highway Administration.
Project Title: Verification of the Modified Triaxial Design Procedure
URL: http://tti.tamu.edu/documents/0-4519-1.pdf

16. Abstract

The Texas Department of Transportation (TxDOT) uses the modified triaxial design procedure to check pavement designs from the flexible pavement system program. Since its original development more than 50 years ago, little modification has been made to the original triaxial design method. There is a need to verify the existing load-thickness design chart to assess its applicability for the range in pavement materials used by the districts, and the range in service conditions encountered in practice. Additionally, there is a conservatism in the current method, which assumes the worst condition in characterizing the strength properties of the subgrade. While this approach may be applicable for certain areas of the state such as east Texas, it can lead to unduly conservative assessments of pavement load capacity in districts where the climate is drier, or where the soils are not as moisture susceptible. Clearly, there is a need to consider regional differences to come up with a more realistic assessment of pavement thickness requirements for the given local conditions. To verify the existing triaxial design method, researchers executed a comprehensive work plan that included a literature review of the current method, load bearing tests on full-scale field sections, laboratory tests on small-scale pavement specimens at various moisture conditions, and comparisons of load bearing capacity estimates from the existing method with corresponding estimates determined from analyses of test data. This report documents the verification of the modified triaxial design method implemented by TxDOT.

17. Key Words	18. Distribution Statement
Pavement Design, Modified Triaxial Design Method, Pavement Thickness Design, Pavement Structural Evaluation, Mohr-Coulomb Failure Criterion, Plate Bearing Test, Allowable Wheel Loads, Small-Scale Pavement Models	No restrictions. This document is available to the public through NTIS: National Technical Information Service Springfield, VA 22161 http://www.ntis.gov

19. Security Classif.(of this report)	20. Security Classif.(of this page)	21. No. of Pages	22. Price
Unclassified	Unclassified	272	

VERIFICATION OF THE LOAD-THICKNESS DESIGN CURVES IN THE MODIFIED TRIAXIAL DESIGN METHOD

by

Emmanuel G. Fernando
Research Engineer
Texas Transportation Institute

Jeongho Oh
Associate Transportation Researcher
Texas Transportation Institute

Cindy Estakhri
Program Manager
Texas Transportation Institute

Soheil Nazarian
Professor of Civil Engineering
The University of Texas at El Paso

Report 0-4519-1
Project 0-4519
Project Title: Verification of the Modified Triaxial Design Procedure

Performed in cooperation with the
Texas Department of Transportation
and the
Federal Highway Administration

February 2007
Published: June 2008

TEXAS TRANSPORTATION INSTITUTE
The Texas A&M University System
College Station, Texas 77843-3135

DISCLAIMER

The contents of this report reflect the views of the authors, who are responsible for the facts and the accuracy of the data presented. The contents do not necessarily reflect the official views or policies of the Texas Department of Transportation or the Federal Highway Administration. This report does not constitute a standard, specification, or regulation, nor is it intended for construction, bidding, or permit purposes. The United States Government and the State of Texas do not endorse products or manufacturers. Trade or manufacturers' names appear herein solely because they are considered essential to the object of this report. The engineer in charge of the project was Dr. Emmanuel G. Fernando, P.E. # 69614.

ACKNOWLEDGMENTS

The work reported herein was conducted as part of a research project sponsored by the Texas Department of Transportation and the Federal Highway Administration. The authors gratefully acknowledge the support and guidance of the project director, Mr. Mark McDaniel, of the Materials and Pavements Section of TxDOT. Mr. McDaniel provided a compilation of Texas triaxial classifications for soils found across the state that researchers incorporated into the soils database of the improved computerized procedure for triaxial design developed from this project. In addition, the authors give thanks to members of the Project Monitoring Committee for their support of this project. A special note of thanks is extended to Ms. Darlene Goehl and Mr. Billy Pigg of the Bryan and Waco Districts, respectively, for their assistance in identifying and testing materials used in field sections to verify TxDOT's modified triaxial design method. Mr. Miguel Arellano of the Austin District also compiled information on the statewide use of various base materials that was helpful in developing the field test plan for this project. The assistance provided by TxDOT engineers in this regard is sincerely appreciated.

The authors are also thankful to the following colleagues who assisted in the field and laboratory tests done on this project to verify the modified triaxial design method:

- Mr. Gerry Harrison and Mr. Lee Gustavus provided technical expertise in setting up and conducting the plate bearing tests on full-scale field sections. In addition, Mr. Gustavus assisted in monitoring the construction of test sections, and in characterizing material properties for construction quality control and quality assurance, and for analyses of test data.
- Ms. Stacy Hilbrich characterized the soil-water characteristic curves of the base and subgrade materials used in constructing the test sections in this project.
- Dr. Wenting Liu wrote the data acquisition program for the plate bearing test and assisted in collecting the data from these tests.

Finally, a special note of thanks is extended to Dr. Robert Lytton who provided expert advice in the characterization of regional moisture conditions across Texas, particularly in the application of the integrated climatic effects model he developed in a project sponsored by the Federal Highway Administration.

TABLE OF CONTENTS

CHAPTER Page

APPENDIX Page

APPENDIX Page

LIST OF FIGURES

Figure Page

Figure Page

Figure Page

Figure Page

Figure Page

Figure Page

Figure Page

Figure Page

Figure Page

Figure Page

LIST OF TABLES

Table Page

Table Page

CHAPTER I. INTRODUCTION

The Texas Department of Transportation (TxDOT) uses the Texas modified triaxial design procedure as a design check to the Flexible Pavement System (FPS) program. The current version of this design program, FPS-19, uses the backcalculated layer moduli from falling weight deflectometer (FWD) measurements and the expected number of 18-kip equivalent single axle loads (ESALs) to determine design thicknesses for the specified pavement materials. On many Farm-to-Market (FM) roads where the expected number of cumulative 18-kip ESALs is low, it is not uncommon to find trucks with wheel loads that exceed those corresponding to the standard 18-kip single axle configuration used in pavement design. These occasional overloads could give rise to subgrade shear failure, particularly under conditions where the base or subgrade is wet. Thus, pavement engineers check the results from FPS against the Texas modified triaxial design procedure to ensure that the design thickness provides adequate cover to protect the subgrade against occasional overstressing. In cases where the thickness requirement from the triaxial method is greater than the pavement thickness determined from FPS, current practice recommends using the pavement thickness based on the modified triaxial design method unless the engineer can justify using the FPS results.

Since its original development more than 50 years ago, little modification has been made to the original triaxial design method. There is a need to verify the existing load-thickness curves to assess their applicability for the range in pavement materials used by the districts, and the range in service conditions that pavements are subjected to. Additionally, there is conservatism in the existing design method that is manifested in the way the subgrade is characterized. Specifically, the subgrade material is tested under capillary wetting to define the Texas triaxial class. While this approach may be representative of climatic and soil conditions in certain areas of the state such as east Texas, it can be notably conservative in districts where the climate is drier, or where the soils are not as moisture susceptible. Clearly, there is a need to consider regional differences in climatic and soil conditions in the existing triaxial design method to come up with a more realistic assessment of pavement thickness requirements for the given climatic and soil moisture conditions, pavement materials, and the wheel load assumed for pavement design (referred to as the design wheel load in this report).

There is also an issue about the rationality of using a load adjustment factor of 1.3 to account for differences in pavement damage potential between single and tandem axle configurations. In current practice, this factor is used to determine the design wheel load for the modified triaxial design check in Test Method Tex-117E. Specifically, if the percent of tandem axles is 50 percent or more, the average of the ten heaviest wheel loads daily (ATHWLD) is multiplied by 1.3 to come up with the design wheel load for determining the depth of cover above the subgrade using the existing flexible base design chart in Tex-117E. For design projects where the percent of tandem axles is less than 50 percent, the design wheel load equals the ATHWLD.

In a load-zoning project conducted for the Pennsylvania Department of Transportation, Fernando, Luhr, and Saxena (1987) found that the predicted compressive strain at the top of the subgrade did not vary significantly between single, tandem, and triple axle configurations provided that the load per tire and tire pressure remained constant between axle configurations. However, the researchers also noted that while the magnitudes of the maximum vertical compressive strain may be similar, different strain cycles are produced between axle configurations, with triple axles producing three strain cycles versus two and one for the tandem and single axles, respectively. This observation indicates that different axle configurations would produce varying damage effects, even if the load per tire and tire pressure are the same between axle assemblies. To investigate this issue further, Fernando, Luhr, and Saxena (1987) examined performance data from the road test conducted by the American Association of State Highway Officials (AASHO, 1962). Specifically, they examined the data from Loop 3 of the AASHO road test, which were trafficked with 12-kip single axles and 24-kip tandem axles on adjacent lanes. These are the only data from the road test in which single and tandem axles carried the same load per tire on identical pavement sections constructed on the test lanes.

Figures 1.1 and 1.2 compare the number of weighted load applications to reach terminal present serviceability indices (PSIs) of 1.5 and 2.5, respectively, between the tandem and single axles used during the test. It is observed that the data points are scattered along the line of equality, which indicates that the two axle configurations caused similar pavement performance. This observation appears to be consistent with the previous finding on the similarity of predicted subgrade compressive strain between axle configurations that have the same load per tire and tire pressure.

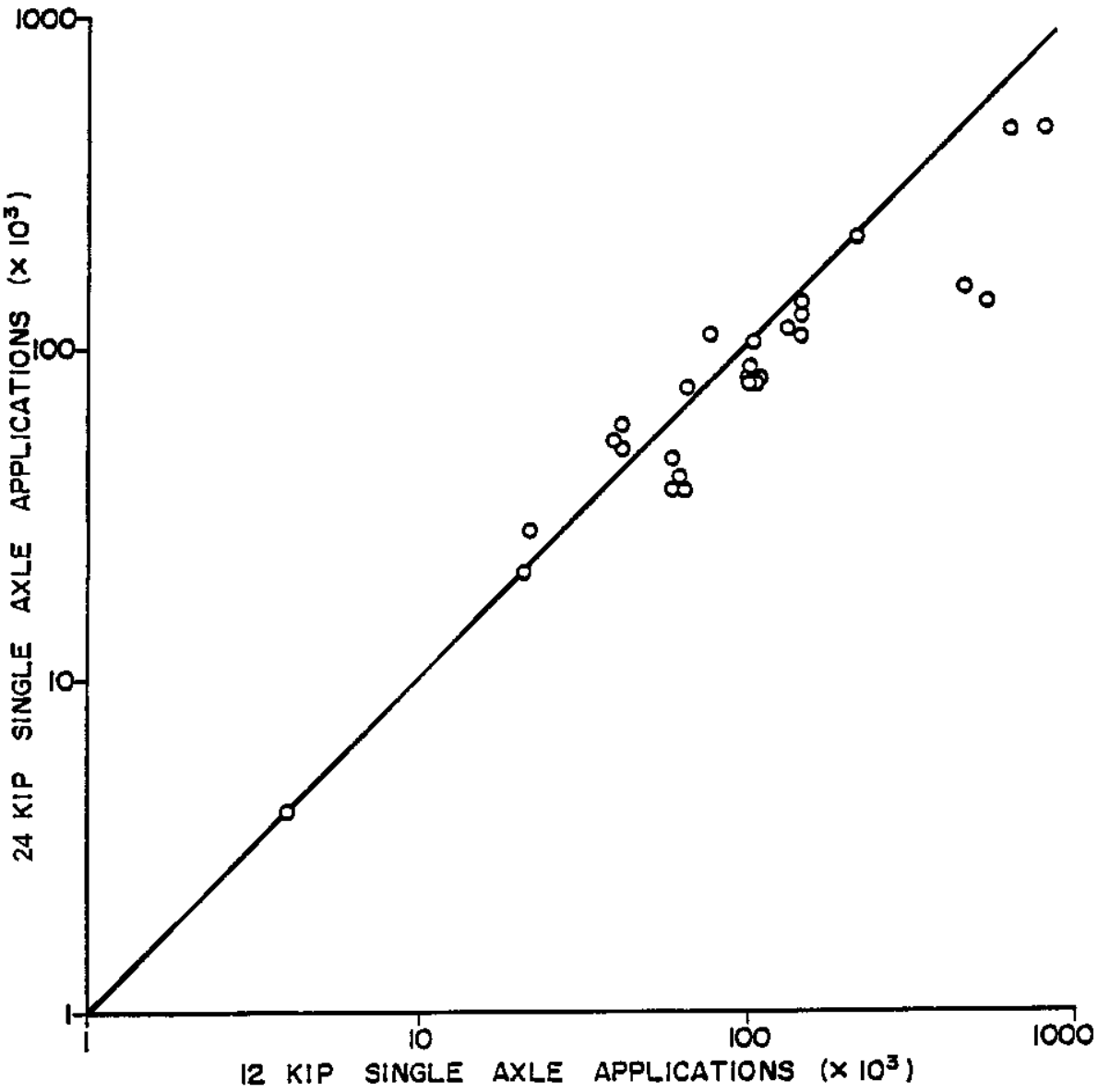

Figure 1.1. Number of Load Applications of 24-kip Tandem and 12-kip Single Axles for AASHO Loop 3 Sections to Reach a Terminal PSI of 1.5 (Fernando, Luhr, and Saxena, 1987).

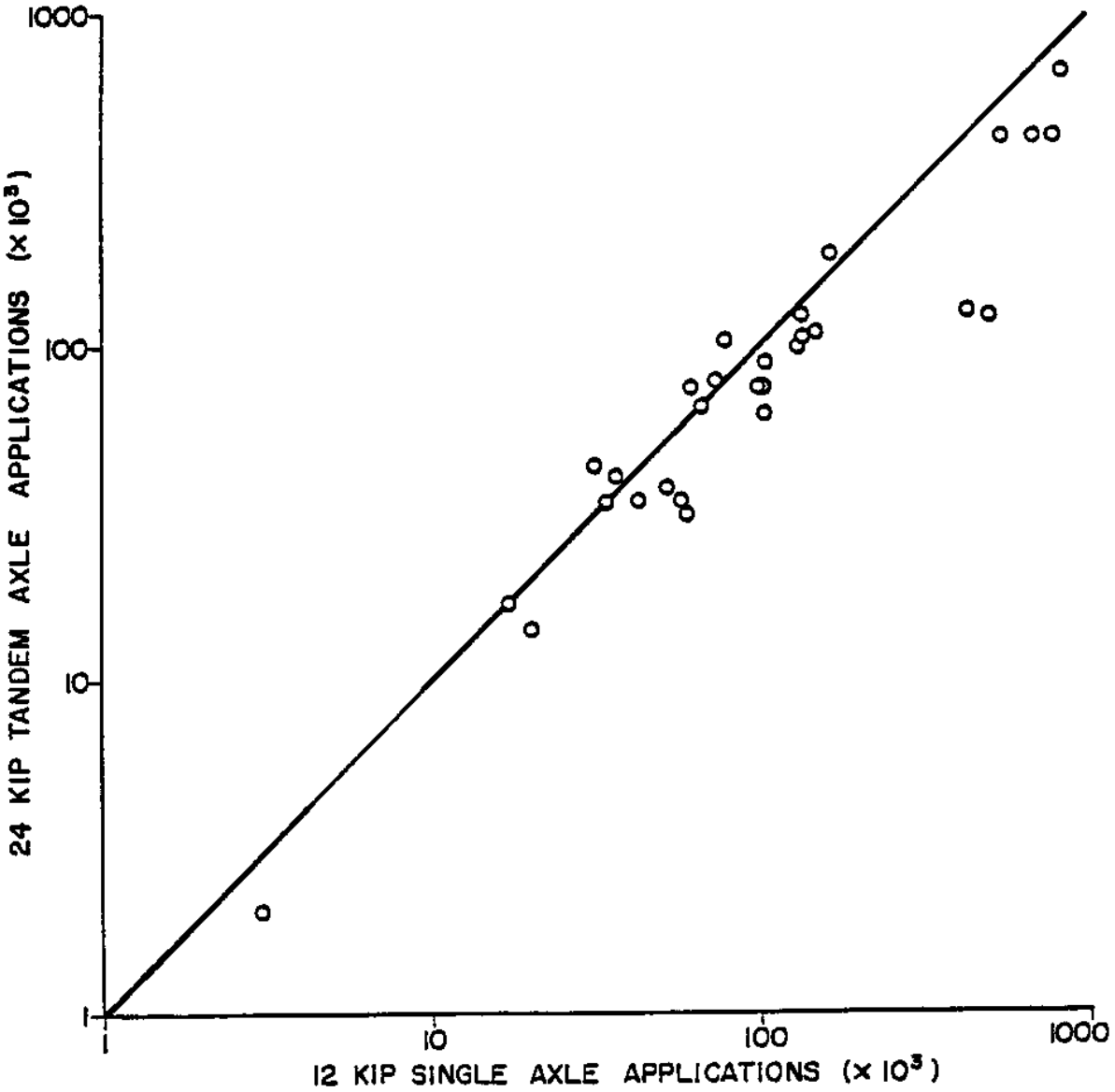

Figure 1.2. Number of Load Applications of 24-kip Tandem and 12-kip Single Axles for AASHO Loop 3 Sections to Reach a Terminal PSI of 2.5 (Fernando, Luhr, and Saxena, 1987).

RESEARCH OBJECTIVES

The primary objectives of this project are to:

- verify the load-thickness design curves in TxDOT's Test Method Tex-117E that are used in the current modified triaxial design method; and
- account for regional variations in climatic and soil conditions across Texas in the pavement design check of FPS-generated flexible pavement designs.

Researchers accomplished these objectives by carrying out a comprehensive work plan that covered the following tasks:

- a literature review of the development of the load-thickness design curves that enabled researchers to re-create the curves based on the review findings;
- development of a plan to verify the load-thickness design curves based on testing full-scale field sections and small-scale pavement models;
- construction of test sections and fabrication of small-scale pavement models;
- field and laboratory testing to characterize pavement materials and evaluate load carrying capacity of test sections built to verify the thickness design curves;
- investigation of the correspondence between small-scale and full-scale pavement test results;
- analysis of test data to verify the current load-thickness design curves;
- compilation of climatic and soils data on the different Texas counties;
- evaluation of expected moisture contents using a comprehensive model of climatic effects originally developed by Lytton et al. (1990) in a project conducted for the Federal Highway Administration;
- investigation of relationships between soil moisture and soil strength properties; and
- development of a stress-based analysis program for checking FPS-generated pavement designs based on the Mohr-Coulomb strength criterion.

This report documents the research work conducted to verify the existing load-thickness design curves. A companion report by Fernando, Oh, Ryu, and Nazarian (2008) documents the development of a methodology to account for variations in climatic and soil conditions in checking the adequacy of pavement designs from the FPS program. Researchers implemented this methodology as an option in the *LoadGage* program developed from this project. Among the enhancements to the current modified triaxial design method implemented in *LoadGage* are:

- a stress-based analysis procedure that provides users with greater versatility in modeling flexible pavement systems compared to the limited range of approximate layered elastic solutions represented in the existing modified triaxial thickness design curves;
- more realistic modeling of pavement wheel loads, in lieu of the current practice of using a load adjustment factor of 1.3, which was found to be overly conservative from the verification efforts conducted in this project;
- an extensive database of soil properties covering each of the 254 Texas counties for evaluating the effects of moisture changes on soil strength properties; and
- a moisture correction procedure (to account for differences between wet and dry regions of the state) that provides users the option of adjusting strength properties determined from laboratory triaxial tests (such as TxDOT Test Method Tex-117E) to the expected in-service moisture conditions.

Instructions on the operation of the computer program are given in the *LoadGage User's Manual* by Fernando, Oh, and Liu (2007).

SCOPE OF RESEARCH REPORT

This report documents the research conducted to verify the existing load-thickness design curves in the modified triaxial design method. It is organized into the following chapters:

- Chapter I provides the impetus for this project and states its objectives.
- Chapter II documents the work done to understand the development of the existing load-thickness design curves by reviewing published literature. This chapter also presents the efforts made by researchers to re-create the existing design curves based on information obtained from the literature review.
- Chapter III presents the field and laboratory test programs executed in this project to verify the existing design curves. This chapter identifies the flexible base and stabilized materials selected for constructing full-scale pavement sections and for fabricating small-scale pavement models to verify the design curves. The field and laboratory tests to characterize materials and evaluate load carrying capacity are also presented.
- Chapter IV documents the construction of the flexible base and stabilized test sections.

- Chapter V investigates the correspondence between small-scale and full-scale pavement tests. Researchers used the findings from this investigation to establish the applicability of using small-scale pavement models for verifying the existing load-thickness design curves.
- Chapter VI presents the verification of the design curves using field and laboratory test data. For this analysis, researchers compared allowable wheel loads determined from test data with corresponding predictions from the existing design charts and from a number of pavement models.
- Finally, Chapter VII summarizes the findings from the verification of the existing load-thickness design curves and recommends modifications to the current design method.

The appendices provide supporting material referred to in the different chapters, beginning with the plans and specifications given in Appendix A for constructing full-scale pavement sections used in verifying the triaxial design curves. Data from laboratory tests to characterize properties of the base and subgrade materials found on these test sections are provided in Appendix B, while Appendix C presents test data collected for the purpose of verifying the quality of the sections built. Finally, Appendix D presents load-displacement curves from the plate bearing tests.

CHAPTER II. LITERATURE REVIEW

Chester McDowell, former Soils Engineer of what was then the Texas Highway Department (THD) spearheaded the development of the Texas triaxial design method in the mid-1940s to the early 1960s. To verify the load-thickness design curves in this project, researchers initially reviewed published information to establish how the existing design method was developed and identify underlying principles and assumptions made to generate the design charts. From this literature review, researchers put together the historical timeline given in Figure 2.1 that identifies certain key events in the development of the Texas triaxial design method. The findings from this literature review are presented in this chapter.

BASIC PREMISE OF TRIAXIAL DESIGN METHOD

The triaxial design method is based on the theory that elastic bodies recover from an enormous number of deflections caused by loads as long as the induced stresses are within the strength of the materials subjected to such loads. Thus, the design method boils down, in simple terms, to determining the design thickness of better material to prevent overstressing the soil foundation or subgrade under the design wheel load. It is important to note that, even if the induced stresses are within the elastic range of the materials comprising the pavement, McDowell did recognize that pavement deterioration can eventually take place due to fatigue from repetitive load applications. Indeed, he writes in the closure to the paper he wrote for the 33rd Annual Meeting of the Highway Research Board that:

> *It does not seem illogical to expect a pavement to eventually suffer from fatigue even though it is supported by an elastic medium (McDowell, 1954).*

However, as originally developed, the mechanism of fatigue from repetitive loading was not included as a criterion in the determination of design thickness. It was after the flexible base design chart was developed that McDowell came up with an approximate procedure to consider the effect of repetitive loading on the thickness design through the introduction of a load-frequency design factor (LFDF). Researchers note that this factor is not used in the current procedure implemented by TxDOT. Instead, a design based on repetitive loading is determined using FPS, which is then checked against the modified Texas triaxial design method to verify that the FPS design provides adequate cover to prevent overstressing the subgrade due to one application of the ATHWLD. With this in mind, the following

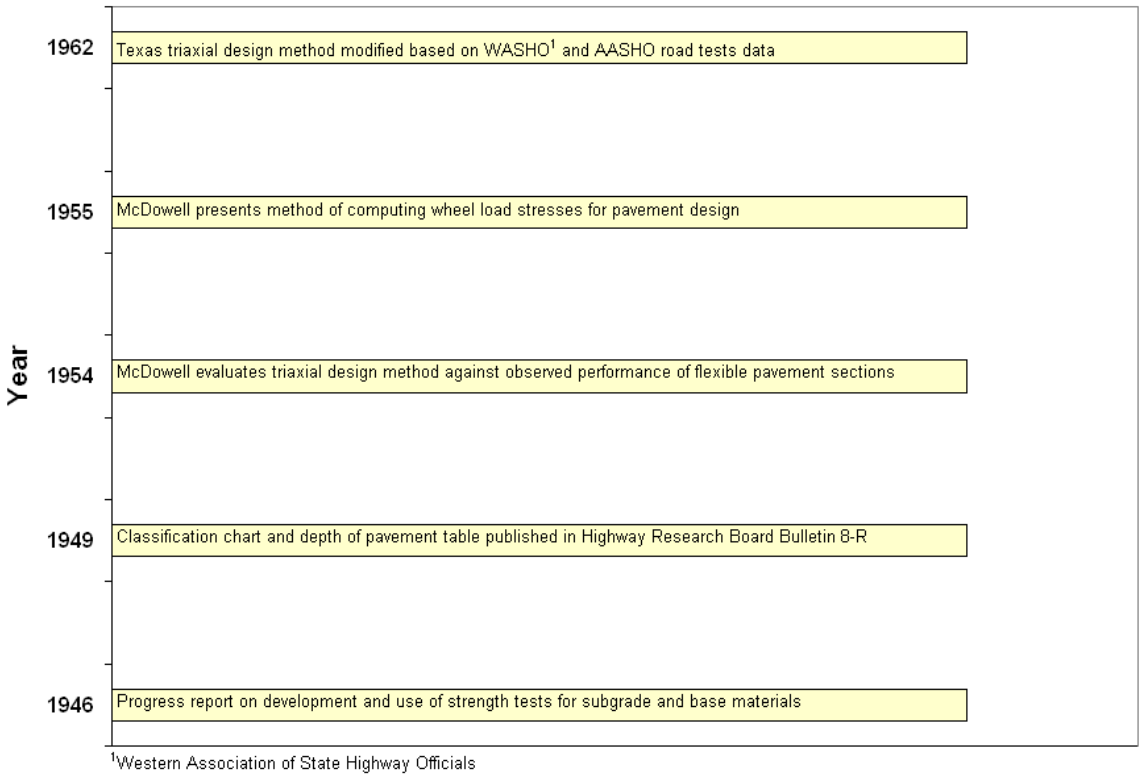

Figure 2.1. Stages of Development of the Texas Triaxial Design Method.

discussion on the load-frequency design factor is simply intended to provide historical information about its development for the purpose of this literature review.

DEVELOPMENT OF THE LOAD-FREQUENCY DESIGN FACTOR

The concept of the load-frequency design factor came out of road life studies conducted by McDowell to verify the triaxial design method. The earliest such study was reported by McDowell in 1954 when he evaluated the correlation between observed performance data on in-service pavement sections in Texas with the ratios of actual to design pavement thickness from the triaxial design method. Figure 2.2 shows the correlation McDowell reported from this investigation. McDowell expressed the relationship shown in Figure 2.2 in terms of the number of load applications to failure. Assuming ten applications of the heaviest wheel loads per day, he came up with the following equation to estimate service life in terms of the allowable number of load applications (in lieu of service life in years as shown in Figure 2.2):

$$Allowable\ load\ applications = 3504 \times 10^{0.01465\ (percent\ design)} \qquad (2.1)$$

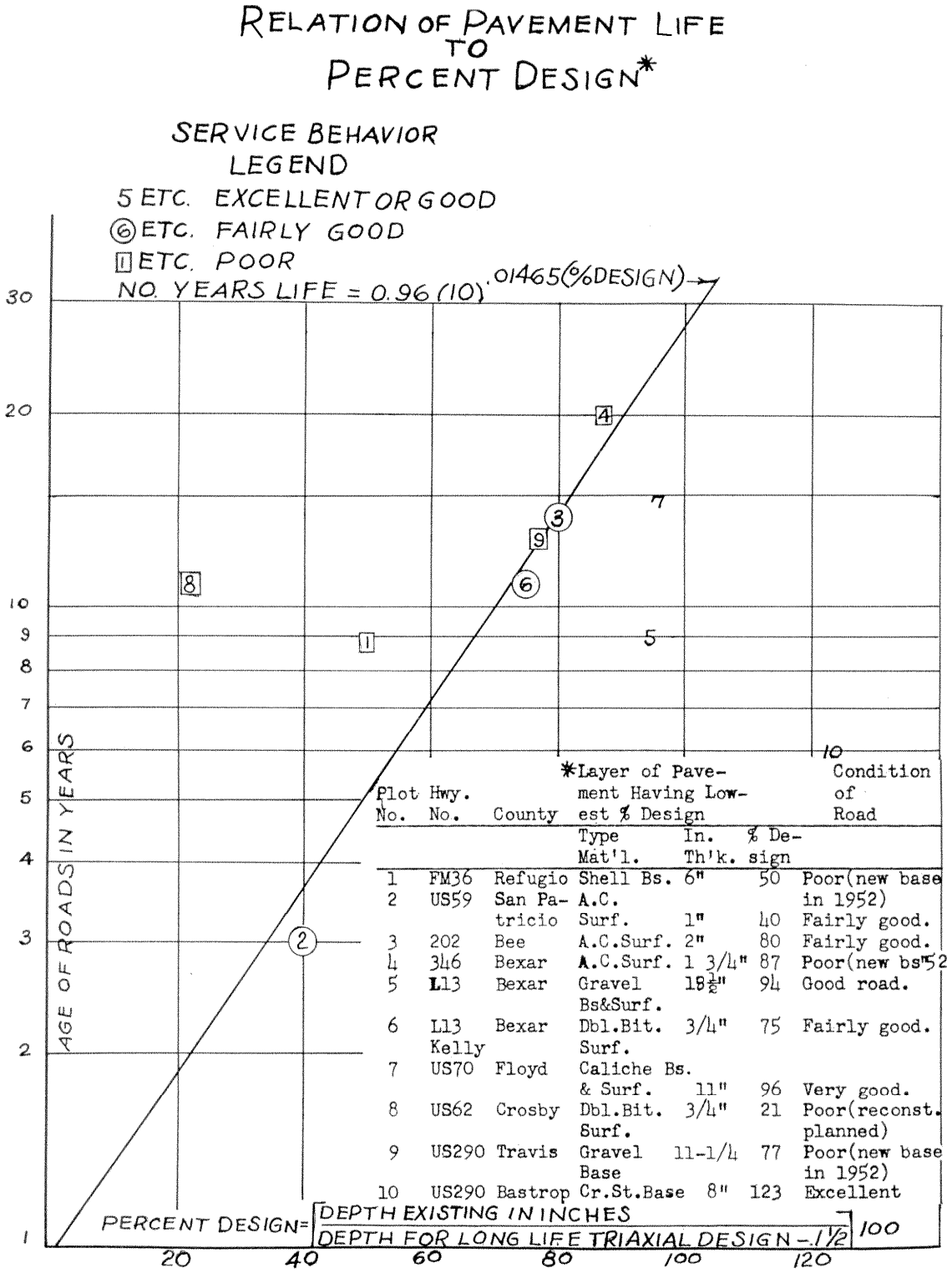

Plot No.	Hwy. No.	County	*Layer of Pavement Having Lowest % Design: Type Mat'l.	In. Th'k.	% Design	Condition of Road
1	FM36	Refugio	Shell Bs.	6"	50	Poor(new base
2	US59	San Patricio	A.C. Surf.	1"	40	in 1952) Fairly good.
3	202	Bee	A.C.Surf.	2"	80	Fairly good.
4	346	Bexar	A.C.Surf.	1 3/4"	87	Poor(new bs'52
5	L13	Bexar	Gravel Bs&Surf.	18½"	94	Good road.
6	L13	Bexar Kelly	Dbl.Bit. Surf.	3/4"	75	Fairly good.
7	US70	Floyd	Caliche Bs. & Surf.	11"	96	Very good.
8	US62	Crosby	Dbl.Bit. Surf.	3/4"	21	Poor(reconst. planned)
9	US290	Travis	Gravel Base	11-1/4	77	Poor(new base in 1952)
10	US290	Bastrop	Cr.St.Base	8"	123	Excellent

Figure 2.2. Correlation between Service Life and Pavement Thickness as a Percentage of Triaxial Design Thickness (McDowell, 1954).

where percent design is as defined in Figure 2.2 and pavement failure is taken as the condition where 5 percent or more of the surface area shows distress (Flexible Pavement Design Correlation Study, 1956). McDowell noted that the correlation line given in the figure divides the data into two groups. Left of the line are pavements exhibiting poor condition while right of the line are pavements in good to excellent condition. However, McDowell noted that the data associated with the correlation are rather limited. Thus, he later expanded the evaluation to include test data from road tests conducted by the Western Association of State Highway Officials (WASHO) and AASHO.

Figures 2.3 and 2.4 show the correlation line based on analysis of WASHO road test sections having 2-inch and 4-inch surfacings, respectively. The ordinate axes on both figures show the number of load repetitions required to produce 200 ft^2 of cracking for each WASHO road test section. The correlation line was drawn so as to separate sections of poor performance, on the left side of the line, from sections that showed good performance on the right side of the line (McDowell, 1962). McDowell noted that the WASHO correlation line provided an approximate relationship to perform a pavement design on the basis of load repetitions. Specifically, he noted that:

> *In using this relationship, triaxial design depths were varied as much as 35 percent depending on the number of heavy load applications anticipated during the life of the facility (McDowell, 1962).*

Table 2.1 shows the initial procedure implemented by TxDOT for adjusting triaxial design thickness on the basis of the expected number of load repetitions. In this initial procedure, the number of load repetitions corresponds to the expected number of wheel loads (on dual tires) equal to or greater than 8000 lb. The load-frequency design factors in Table 2.1 track the WASHO correlation line shown in Figures 2.3 and 2.4 for the given numbers of load repetitions. Note that McDowell coined the term "load-frequency design factor" in Table 2.1 to replace the term "percent design" in Figures 2.3 and 2.4.

After results from the AASHO road test became available, McDowell conducted a similar analysis to evaluate the load-frequency design factors against AASHO road test data. Figure 2.5 shows a chart similar to Figures 2.3 and 2.4 with the WASHO correlation line superimposed on AASHO road test data. In this figure, the number of axle load applications at the time a section was taken out of test is plotted against the corresponding depth design ratio or load-frequency design factor. There is a wide range in the scatter of the data as noted

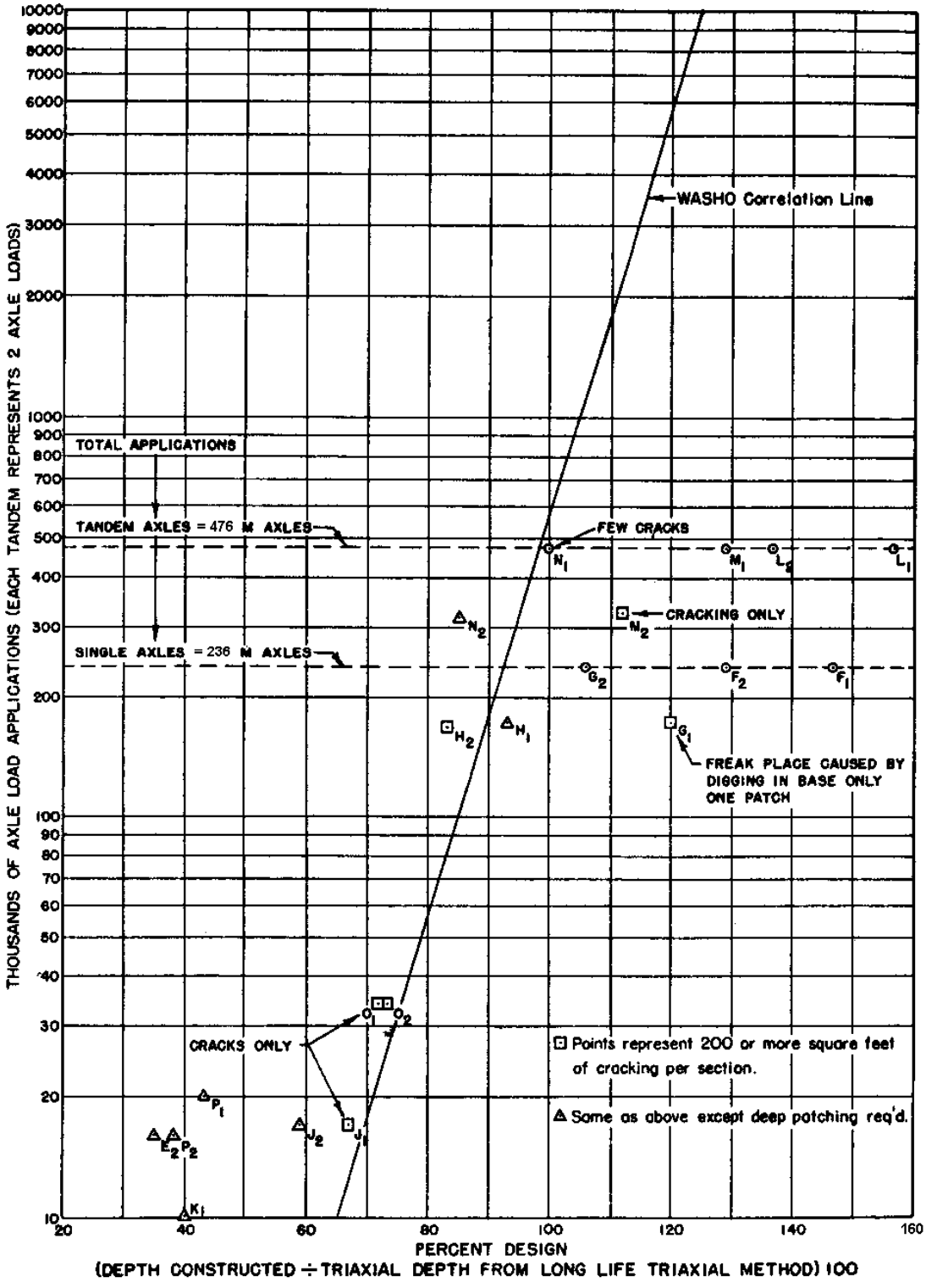

Figure 2.3. Analysis of WASHO Road Test Sections with 2-inch Surfacings (McDowell, 1962).

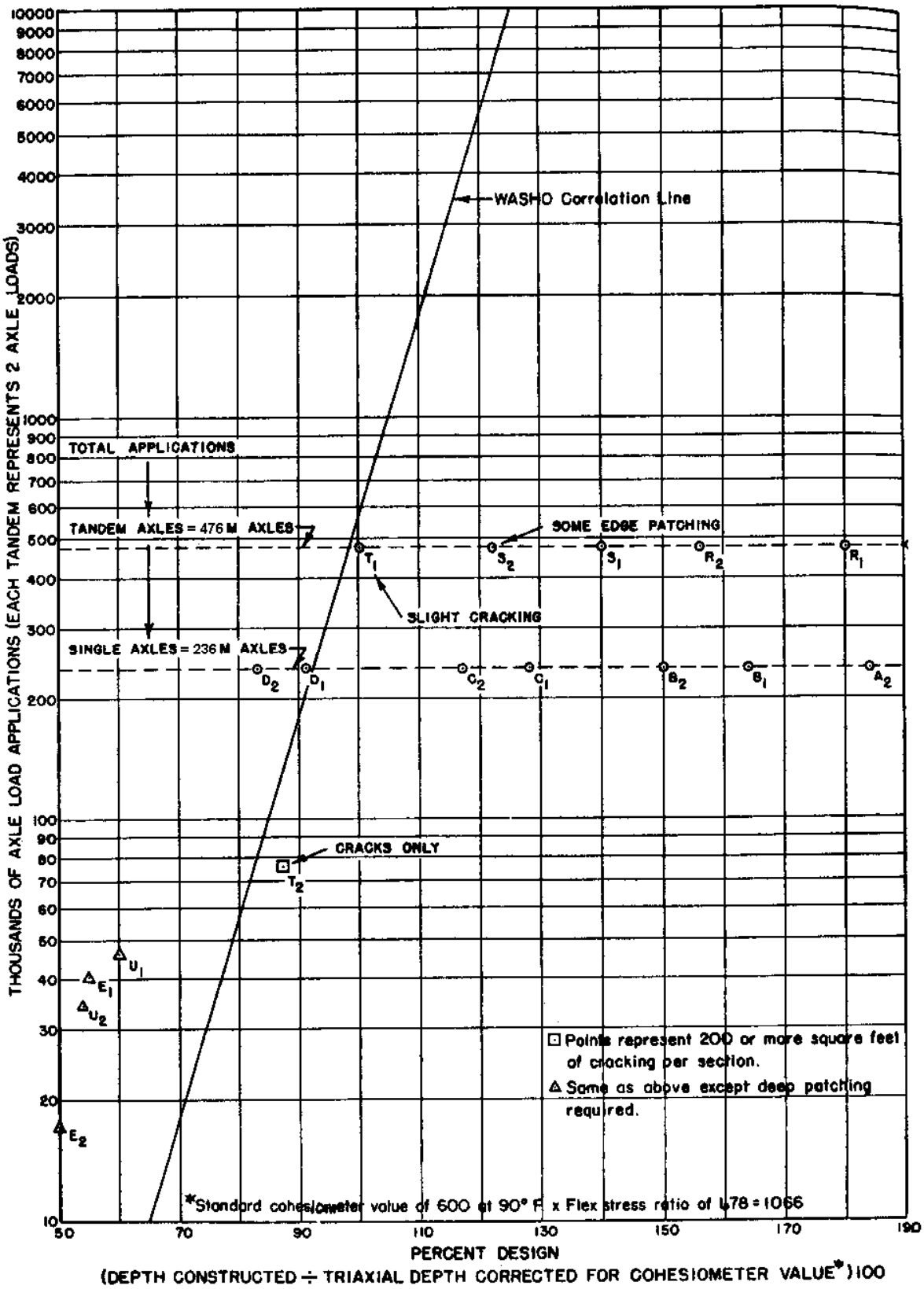

Figure 2.4. Analysis of WASHO Road Test Sections with 4-inch Surfacings (McDowell, 1962).

Table 2.1. Initial Load-Frequency Design Factors Used with Triaxial Design Method (McDowell, 1962).

Test Method Tex-117E

CRITERIA FOR OBTAINING THE LOAD-FREQUENCY DESIGN FACTOR

Number of Applications of Wheel Loads in Excess of 8000 Pounds		Load Frequency
Total Estimated During Design Life	Approximate Daily Applications for a 25 Year Design Life	Design Factor*
10,000	1	0.65
18,000	2	0.70
30,000	3	0.75
56,000	6	0.80
100,000	11	0.85
175,000	19	0.90
300,000	33	0.95
550,000	60	1.00
1,000,000	110	1.05
1,700,000	186	1.10
3,000,000	330	1.15
5,200,000	570	1.20
10,000,000	1100	1.25
30,000,000	3300	1.35

*A load-frequency design factor less than 1.0 shall not be used for the design of the main lanes of a controlled access highway.

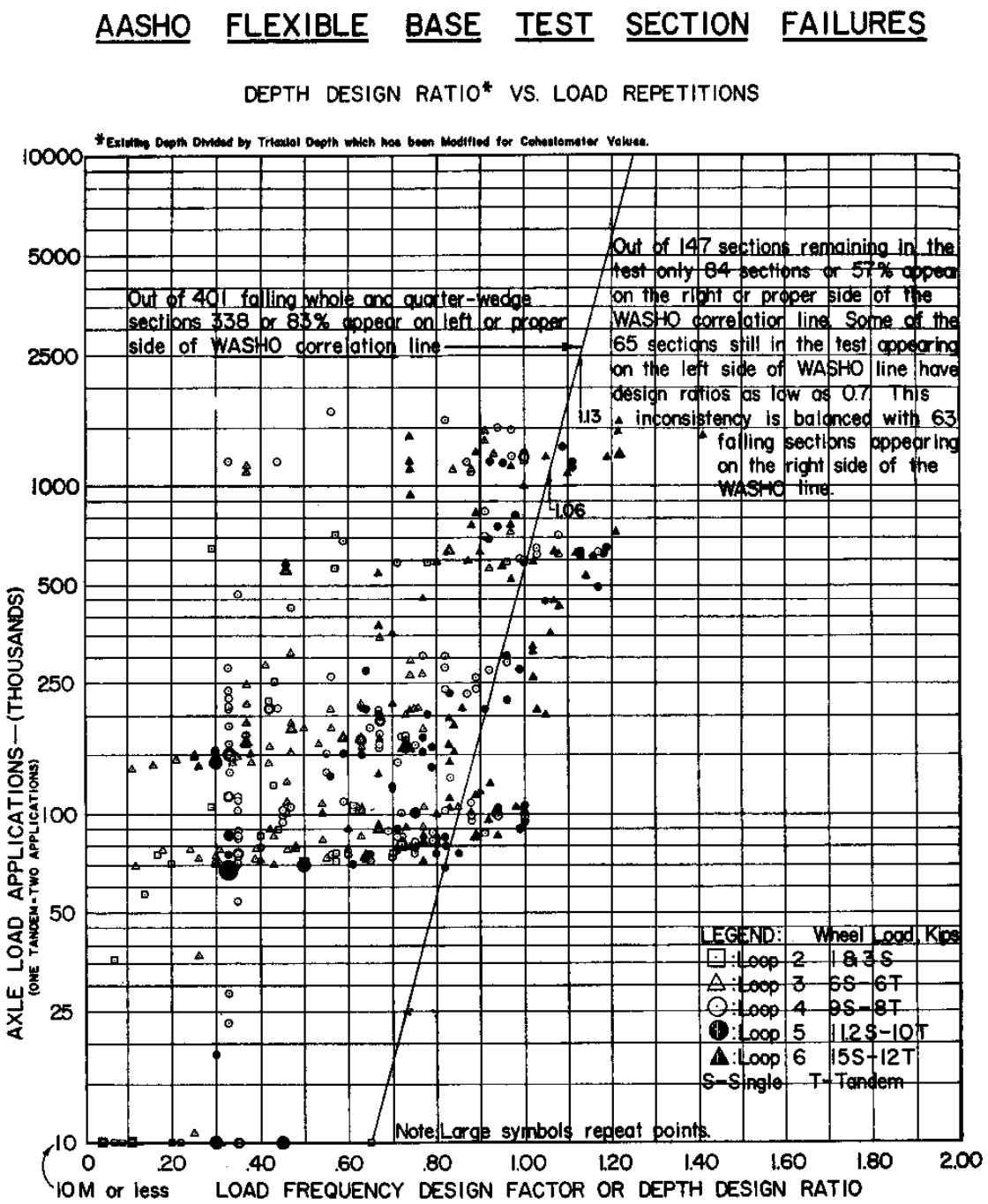

Figure 2.5. Verification of Load-Frequency Design Relationship with AASHO Road Test Data (McDowell, 1962).

by McDowell who summarized the findings on the chart based on the concurrence (or lack thereof) of the observed service lives to the WASHO correlation line (the same line that defines the load-frequency design factors). Note that the line is supposed to group the test sections into good-performing pavements (right of the line) and poorly performing

pavements (left of the line). The results, in terms of the numbers of correct and incorrect classifications are summarized on the chart. Based on the numbers shown, the authors are of the opinion that the results are mixed at best, depending on whether one views the results from the perspective of a glass being half-full or the same glass being half-empty.

Considering that the load-thickness design curves are based on a theoretical analysis of the required depth of cover to prevent overstressing the subgrade due to the application of one design wheel load, TxDOT's current practice of using FPS to design for repetitive loading and checking its result against the modified triaxial design method is, in the authors' opinion, a more appropriate application of the load-thickness design curves that is consistent with their original derivation. Since these curves form the central piece of the modified triaxial design method, researchers reviewed the literature to gain an understanding of how the curves were derived. The findings from this review are presented in the subsequent section. However, before proceeding with that discussion, the authors would like to note that the load-frequency design factors presented in Table 2.1 changed in the years after the AASHO road test. In a paper by McDowell (1962), he provided a hint as to the reason for the change. Specifically, since the initial development of the load-frequency design factors, he explained that a great deal of information on 18-kip ESALs had become available. Thus, he acknowledged that some type of substitution of 18-kip ESALs for the number of 8000 lb and higher wheel loads would be in order. However, information on how this change was made could not be obtained from the literature, although one could surmise that loadometer data might have been used to determine a relationship between the number of 18-kip ESALs and the corresponding number of wheel loads 8000 lb and higher.

LOAD-THICKNESS DESIGN CURVES

At the 23rd Annual Highway Short Course held at Texas A&M in 1949, McDowell presented a design table of thickness requirements for different triaxial classes, wheel loads, and base moduli. Table 2.2 reproduces this design table, which was also published in Highway Research Board Bulletin 8-R in 1949. It is interesting to observe that this table, which preceded the current load-thickness design curves, incorporated base modulus as a design variable. In a later paper, McDowell (1954) wrote that:

> *The depth of pavement table was revised and presented in graphical form in 1951 to avoid having to distinguish between high and low modulus base materials.*

Table 2.2. Initial Depth of Pavement Table for Texas Triaxial Design Method (Highway Research Board, 1949).

Class of Material	General Description of Material	Depth of Pavement (Base and Surfacing, in)					
		8,000 lb Wheel Load		12,000 lb Wheel Load		16,000 lb Wheel Load	
		High E* Base Course	Low E* Base Course	High E* Base Course	Low E* Base Course	High E* Base Course	Low E* Base Course
1	Good flexible base material	Good – light bituminous surfacing acceptable.					
2	Fair flexible base material	One to 4 inches of bituminous surfacing or a stable layer of Class 1 material covered with a good light surfacing.					
3	Borderline base and subbase materials	3-8	4-10	4-10	5-12	4-12	6-14
4	Fair to poor subgrade	8-13	10-16	10-15	12-20	12-18	14-23
5	Weak subgrade	13-17	16-21	16-21	20-26	18-24	23-30
6	Very weak subgrade	17+	21+	21+	26+	24+	30+

* E = Young's modulus. In these computations, high E was approximately 20,000 psi and low E was approximately 6,000 psi. The table is not strictly applicable to materials of considerably different characteristics. At stop signs, additional base depth of 2 to 4 inches plus heavy surfacing is indicated.

The reasons as to why base modulus was dropped as a design variable are not clear. Some inferences may be made from a report prepared by the Soils Section of the Texas Highway Department Materials and Tests Laboratory (1949), which noted the difficulty in characterizing modulus. In particular, the report noted:

> *We have found the various moduli of disturbed soils (including base and subbase materials) to be somewhat variable and therefore difficult to evaluate, whereas shearing strengths are more definite and can better be applied to this problem [of designing pavements].*

The fact that moduli are highly sensitive to minor variations of moisture, density, and lateral restraint, plus the fact that some soils have moduli in excess of some base course materials…..led us to seek other criteria in the design of flexible pavements. The fact is that some of the flexible base materials with good shearing strengths do not always have high moduli of elasticity; their moduli are independent of their shearing strengths. Such materials include a multitude of locally produced base and subbase materials which are widely used in construction and maintenance.

In view of the uncertainty of the previously mentioned factors, a design method based upon a comparison of reliable strength test data with suitable mathematical stress estimates, all correlated with service behavior, seems to be the logical procedure.

It would thus appear that limitations in test methods and equipment for characterizing modulus at that time made it impractical to develop a design method that required modulus testing in addition to triaxial tests to characterize pavement materials for design purposes. In addition, it would appear that THD soils engineers were concerned that a provision for modulus testing would preclude the use of certain local materials that have, from experience, shown good shear strengths but have low modulus of elasticity. Finally, eliminating modulus as a design variable suggests that assumptions on modular ratios would had to have been made to compute suitable mathematical stress estimates in developing the load-thickness design curves. In fact, in describing the design method, the report notes the application of a correction factor of 0.85 to account for the difference in stiffness between base and subgrade materials. The following excerpt from the THD report (1949) explains how this value was selected:

Experience indicates that this is the proper factor with the great majority of flexible base materials. If the base material is cemented, other stiffness ratios may be required, or possibly even an entirely different method.

While assumptions for computing wheel load stresses were presented, the report provided neither details nor examples on how wheel load stresses are to be calculated at various depths for comparisons with Mohr-Coulomb failure envelopes determined from

triaxial tests. The methodology for stress computation was later explained by McDowell (1955) in a paper he presented at the 34th Annual Meeting of the Highway Research Board. Following the methodology presented in this paper, researchers made an attempt to regenerate the existing load-thickness design curves of the modified Texas triaxial design method. The following discussion serves to illustrate the methodology established by McDowell and to verify the researchers' understanding of how the design curves given in Figure 2.6 were developed.

RE-CREATION OF LOAD-THICKNESS DESIGN CURVES

McDowell (1955) used one-layer elastic solutions to calculate vertical, radial, and shear stresses at different depths and lateral positions for different wheel loads. In his analysis, McDowell represented the wheel load as an area of uniform pressure applied on a circular footprint. Researchers note that McDowell modeled only a single wheel load in his stress analysis. Thus, while the design wheel load in Figure 2.6 is assumed to be distributed on a set of dual tires, the original derivation of the chart is based on a single wheel load of magnitude comparable to the load acting on a dual tire set.

In his analysis, McDowell modeled the subgrade as a semi-infinite, homogeneous, isotropic, elastic body. Since pavements comprise base material overlying the subgrade, McDowell applied corresponding shear stress correction factors to the shear stresses from one-layer elastic solutions to account for differences in base and subgrade moduli in a two-layer pavement system. Table 2.3 shows the shear stress correction factors F_s corresponding to the assumed variations of modular ratio E_2/E_1 with depth that McDowell used in his analysis. In this table, the modular ratio is the ratio of the subgrade modulus E_2 to the base modulus E_1. McDowell assumed that this ratio varies with depth z according to Table 2.3. Note that the table gives the shear stress correction factors as a function of the non-dimensional ratio z/a where a is the radius of the circularly loaded area of uniform pressure representing the wheel load. Using the calculated stresses for a given depth and wheel load, the Mohr's circles and the failure envelope corresponding to the predicted stresses are determined. The failure envelope is then used to determine the minimum triaxial class that would be required of a subgrade material to sustain the predicted stresses for the given depth and wheel load. This analysis thus identifies a point on the load-thickness design chart. Other points to generate the curves are then determined in a similar fashion.

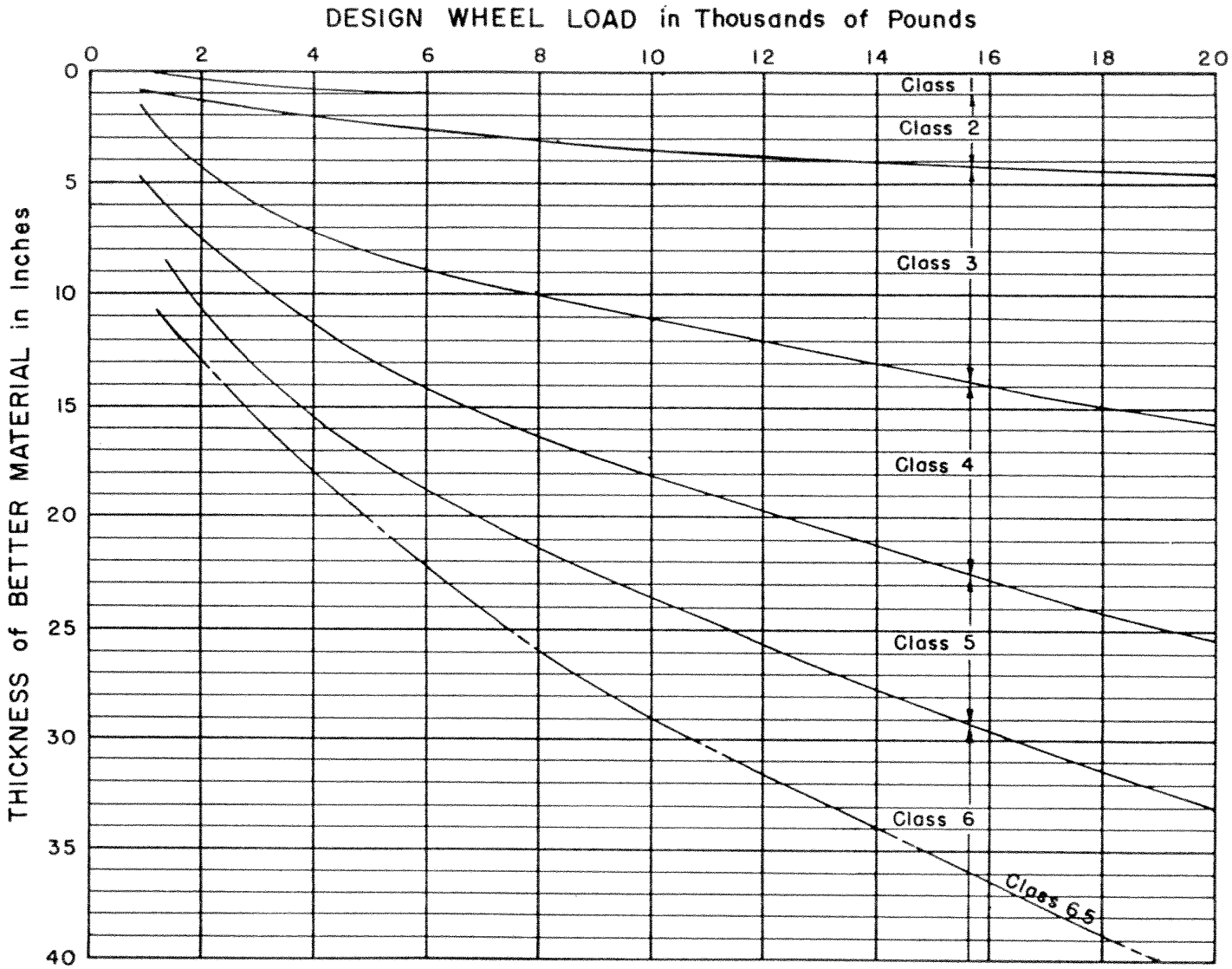

Figure 2.6. TxDOT Test Method Tex-117E Flexible Base Design Chart.

Table 2.3. Assumed Variation of Modular Ratios with Depth and Corresponding Shear Stress Correction Factors (McDowell, 1955).

z/a	E_2/E_1*	F_s
0.25	1.00	1.00
0.50	0.95	0.96
0.75	0.90	0.95
1.00	0.85	0.93
1.25	0.80	0.90
1.50	0.75	0.89
1.75	0.70	0.87
2.00	0.65	0.84
2.50	0.60	0.81
3.00	0.50	0.76
4.00	0.40	0.67
5.00	0.35	0.58

*According to McDowell (1955), these are empirical values based upon experience.

Prior to re-creating the thickness design curves using the above approach, researchers made a check of McDowell's elastic solutions by comparing his results with those determined from the layered elastic program BISAR (Bitumen Structures Analysis in Roads) by de Jong et al. (1973). For this check, researchers considered the results reported by McDowell (1955) from the analysis he made of the stresses at a 7-inch depth due to a wheel load acting on a circular area of 5.6-inch radius with a uniform pressure of 100 psi. This depth and radius corresponds to $z/a = 1.25$, for which McDowell assumed a modular ratio of 0.80 (see Table 2.3).

Given the above conditions, researchers used the BISAR program to compute the stresses at the top of the subgrade for a two-layer system consisting of a 7-inch base with a modulus of 10 ksi overlying a subgrade with a modulus of 8 ksi. The choice of a 10 ksi base modulus follows the example McDowell gave in his paper to explain the modular ratios he assumed (see Table 2.3). Figure 2.7 compares the stresses determined from BISAR with the corresponding stresses reported by McDowell (1955). For the runs made with BISAR, researchers determined the stresses at the same lateral offsets from the circular load that McDowell considered in his analysis. Figure 2.7 shows good agreement between the stresses obtained by McDowell and those from the BISAR program, particularly with the radial and

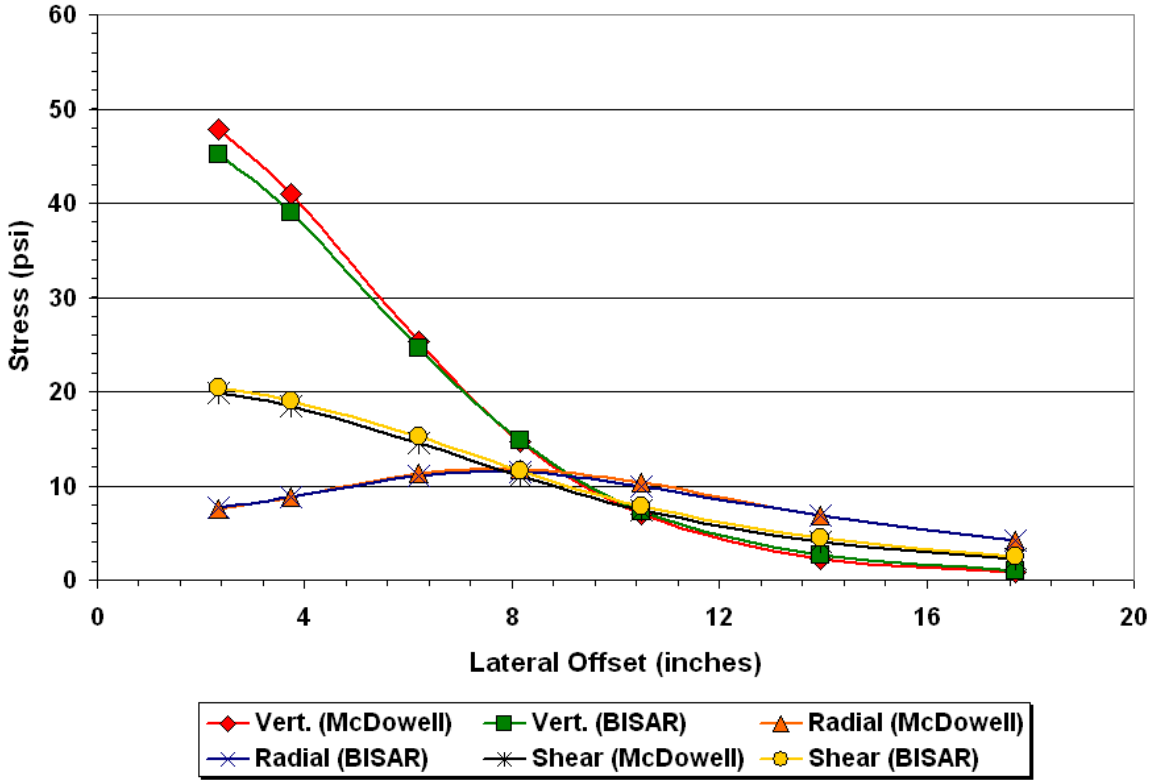

Figure 2.7. Comparison of Stresses from McDowell with Stresses from BISAR.

shear stresses. This result verifies the researchers' understanding of how McDowell conducted his stress analysis to develop the flexible base design chart in Figure 2.6.

Researchers then proceeded to re-create the load-thickness design curves using the following procedure:

- For a given wheel load and triaxial class, the required thickness of cover is determined from the flexible base design chart (Figure 2.6).
- The radial, vertical, and shear stresses at the required depth are determined using one-layer elastic theory at various lateral positions from the wheel load. The computed shear stresses are corrected using the factors F_s given in Table 2.3.
- The Mohr's circles corresponding to the stresses computed at different offsets from the wheel load are determined as well as the failure envelope.
- The failure envelope is then superimposed on the classification chart (Figure 2.8) to determine the minimum class required to sustain the predicted stresses for the given wheel load.

To illustrate the above procedure, consider a Class 4 subgrade. Assuming a wheel load of 14 kips, a required depth of cover of about 13 inches is determined from the existing design

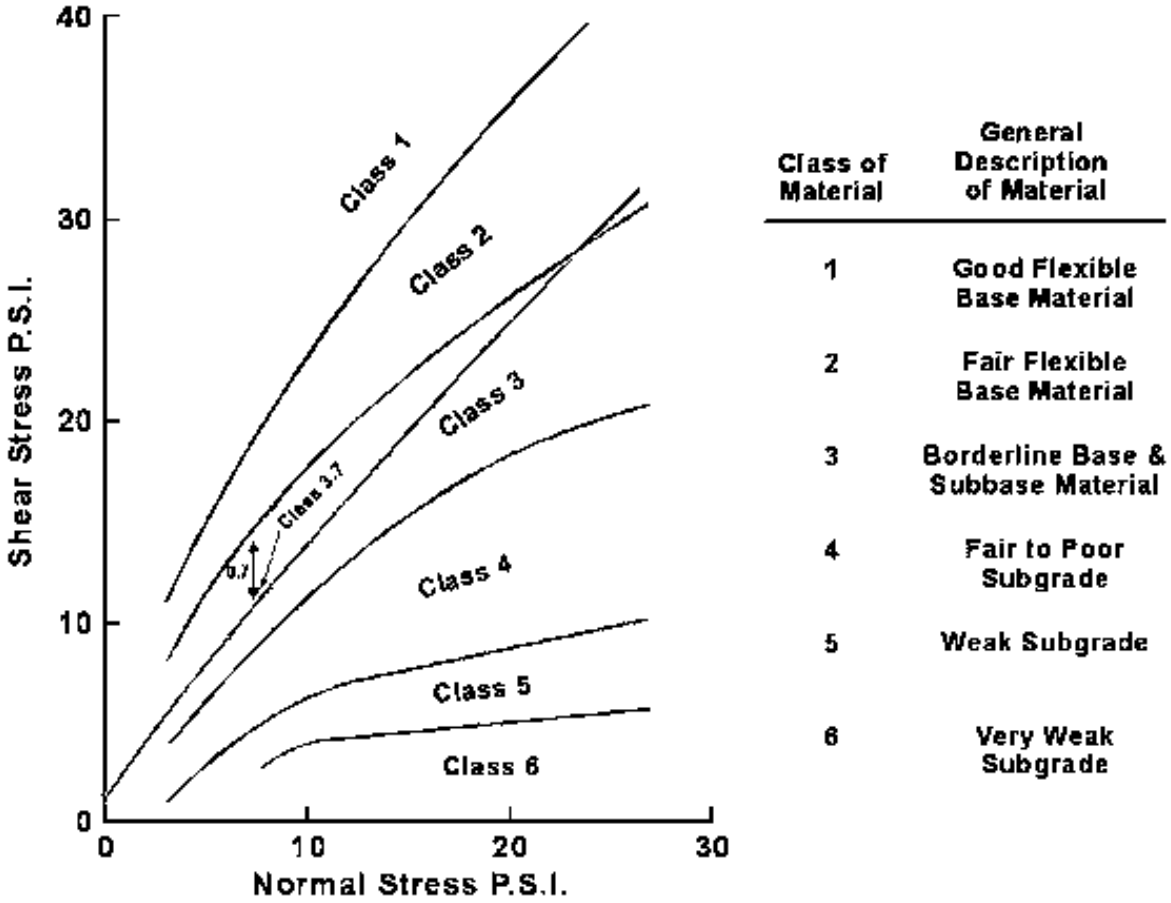

Figure 2.8. TxDOT Test Method Tex-117E Material Classification Chart.

chart (Figure 2.6). Assuming a contact pressure of 100 psi, the radius of the circular loaded area is determined to be 6.7 inches. Radial, vertical, and shear stresses at the 13-inch depth are then calculated at various lateral positions ranging from zero (underneath the center of the wheel load) to four times the radius of the loaded area. Researchers note that McDowell (1955) considered the effect of surcharge in predicting the stresses for cases where the required depths are more than 12 inches. Researchers also followed his approach for considering surcharge in re-creating the load-thickness design curves. Table 2.4 shows the stresses computed for this particular example.

Figure 2.9 presents the Mohr's circles corresponding to the computed stresses at 13-inch depth. If these circles are superimposed on the material classification chart presented in Figure 2.8, one finds that a minimum triaxial class of 4 is required to sustain the 14-kip wheel load without overstressing the subgrade. Thus, a point on the thickness design chart is

Table 2.4. Computed Stresses at 13-inch Depth for Various Lateral Offsets.

r/a[1]	Vertical Stress (psi)	Radial Stress (psi)	Maximum Shear Stress (psi)	
			Uncorrected	Corrected[2]
0.0	29.47	1.74	13.88	11.77
0.2	29.01	1.88	13.75	11.66
0.4	27.70	2.28	13.41	11.37
0.6	25.64	2.89	12.85	10.89
0.8	23.04	3.61	12.15	10.30
1.0	20.09	4.37	11.26	9.55
1.2	17.08	5.04	10.27	8.71
1.4	14.16	5.57	9.26	7.85
1.6	11.53	5.90	8.28	7.02
1.8	9.23	6.03	7.29	6.18
2.0	7.32	5.97	6.44	5.46
2.4	4.52	5.49	4.89	4.14
2.8	2.78	4.75	3.71	3.14
3.2	1.73	3.98	2.82	2.40
3.6	1.10	3.28	2.18	1.85
4.0	0.72	2.70	1.70	1.44

[1]Lateral offset r from center of circular wheel load as a multiple of the load radius a.
[2]Uncorrected maximum shear stress × F_s of 0.848 for z/a of 1.94.

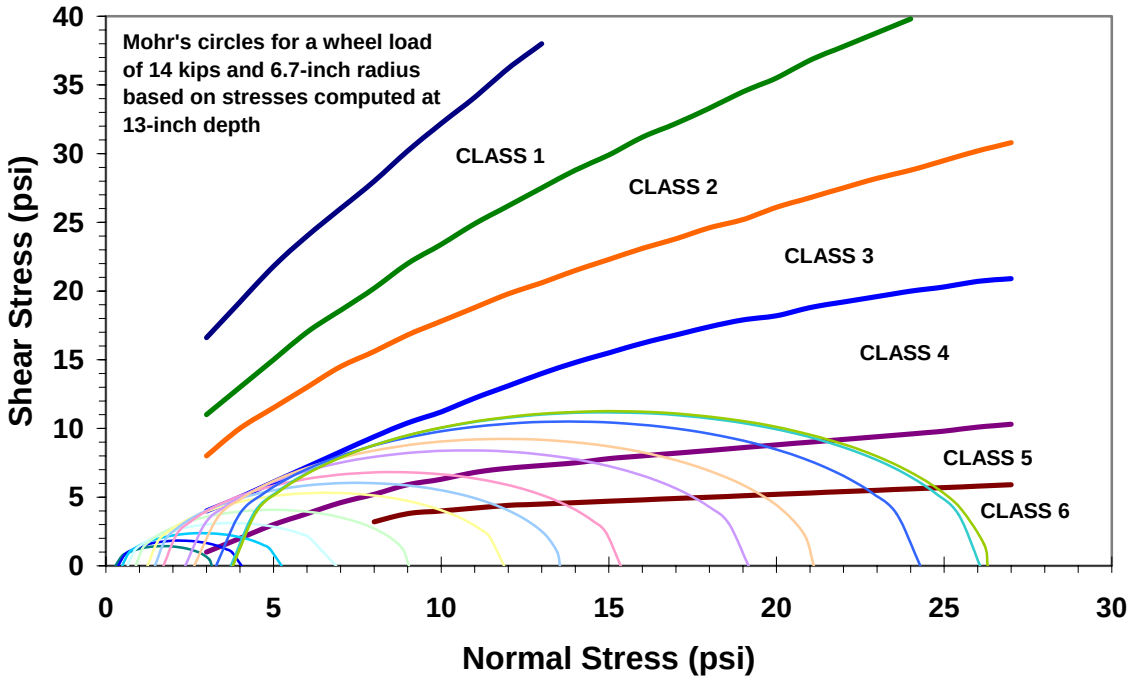

Figure 2.9. Determination of Required Triaxial Class from Computed Mohr's Circles.

determined. According to McDowell (1955), the following equation may be used to generate the curve for a given triaxial class once a point on the curve has been determined:

$$D_X = D_0\sqrt{\frac{P_X}{P_0}} \qquad (2.2)$$

where,

D_X = depth for wheel load P_X, and

D_0 = known depth for wheel load P_0.

Figure 2.10 verifies the above equation by comparing the existing curves (denoted by the solid lines) with corresponding curves generated using Eq. (2.2).

Researchers computed wheel load stresses corresponding to other points on the flexible base design chart and plotted the solutions determined against the existing load-thickness design curves. The solutions are identified by the yellow dots in Figure 2.11 along with a number for each point corresponding to the calculated minimum required class of subgrade from the analysis. It is observed that the solutions agree quite reasonably with the existing curves, thus, verifying the methodology McDowell used in their derivation.

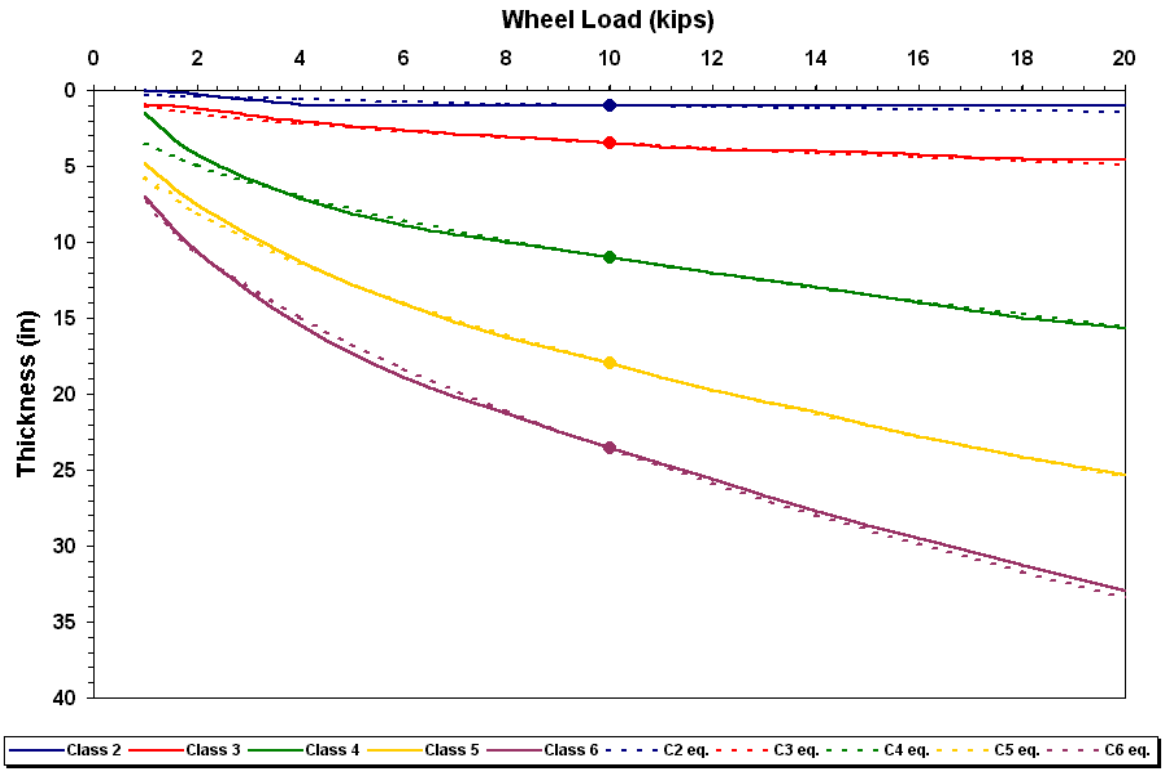

Figure 2.10. Comparison of Curves Determined Using Eq. (2.2) with Existing Load-Thickness Design Curves.

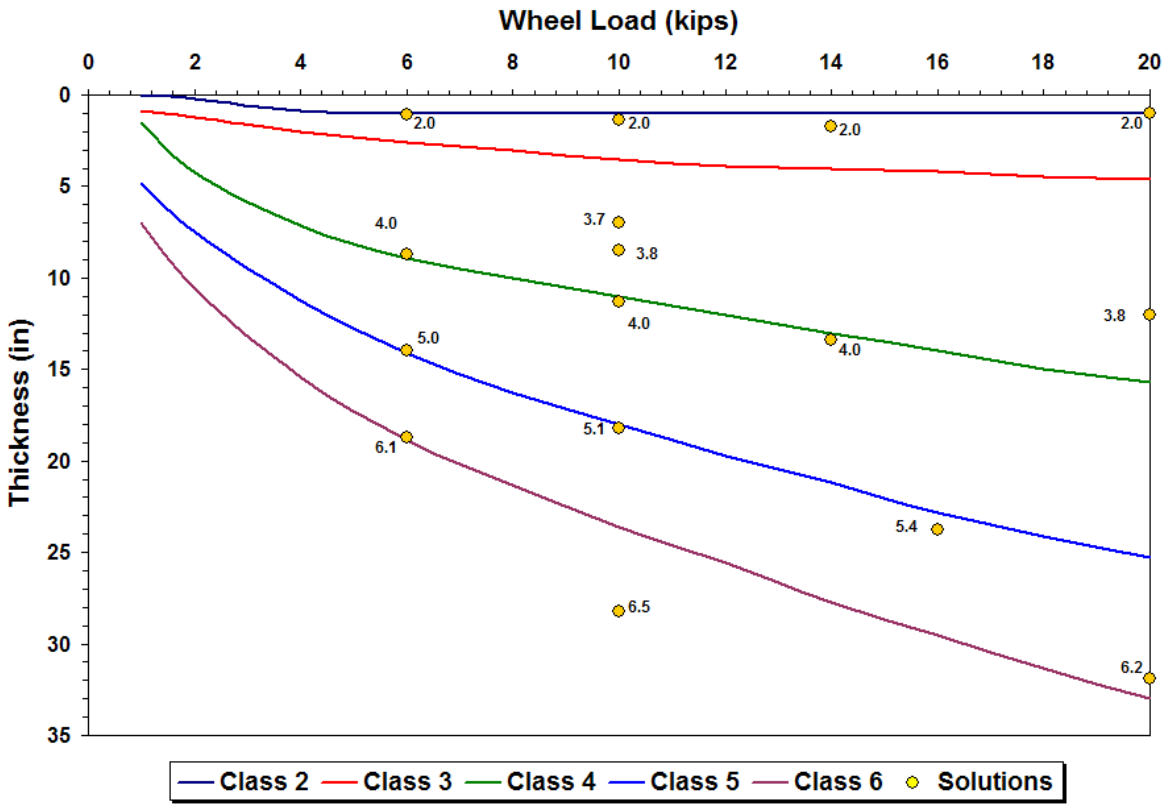

Figure 2.11. Solutions Determined from Re-Creation of Thickness Design Curves.

CONSIDERATION OF STABILIZED LAYERS

McDowell considered the design of pavements with stabilized layers by allowing for reductions in thickness that varied with the cohesiometer value of the stabilized material. The thickness reduction chart he proposed is based on the thickness design equation formulated by Hveem and Carmany (1948) for the California Division of Highways. This design equation is given by:

$$T = \frac{(K\ P\ \sqrt{a}\ \log r)\left(\frac{P_h}{P_v} - 0.10\right)}{\sqrt[5]{c}} \qquad (2.3)$$

where,

T = thickness of cover (inches),

K = constant (0.02 for design),

P = effective tire pressure (psi),

a = effective tire area (in^2),

r = number of load repetitions,

P_h = transmitted horizontal pressure from stabilometer test,

P_v = applied vertical pressure in stabilometer test, and

c = tensile strength of cover material from cohesiometer test (gm/in^2).

The cover material referred to in Eq. (2.3) relates to the thickness of better material placed to protect the subgrade. This material can be stabilized or unstabilized. Assuming a cohesiometer value of 100 for unstabilized materials, McDowell (1962) showed that reductions in thickness for stabilized materials vary with their cohesiometer values according to the dashed lines plotted in Figure 2.12. Note that the reductions based on Eq. (2.3) increase with higher cohesiometer values and that the linear relationships given by the dashed lines in the figure all originate from zero. In proposing the thickness reduction chart for the Texas triaxial design method, McDowell revised the linear relationships derived from Eq. (2.3) such that reductions are applied only for depths of cover of 8 inches or greater. Thus, according to McDowell (1962):

> *Lines for cohesiometer values of 200, 300, 500, 1000, and 2000, were curved so as to become tangent to a line originating at the 8-in. level and extending across the chart.*

The thickness reduction relationships proposed by McDowell are shown by the solid lines in Figure 2.12.

SUMMARY OF FINDINGS FROM LITERATURE REVIEW

Based on the literature review, the following major findings are noted:

- The modified Texas triaxial design method determines the depth of cover based on keeping the wheel load stresses in the subgrade within the Mohr-Coulomb failure envelope of the subgrade material.
- The computation of wheel load stresses for deriving the thickness design curves was done using layered elastic theory along with assumptions McDowell made regarding the variation of modular ratios with depth as given in Table 2.3.
- As originally developed, the mechanism of fatigue from repetitive loading was not included as a criterion in the determination of the thickness design curves. It was after the flexible base design chart was developed that McDowell came up with an approximate procedure to consider the effect of repetitive loading on the thickness design through the introduction of a load-frequency design factor. In this regard, McDowell evaluated the correlation between observed service lives of pavement test

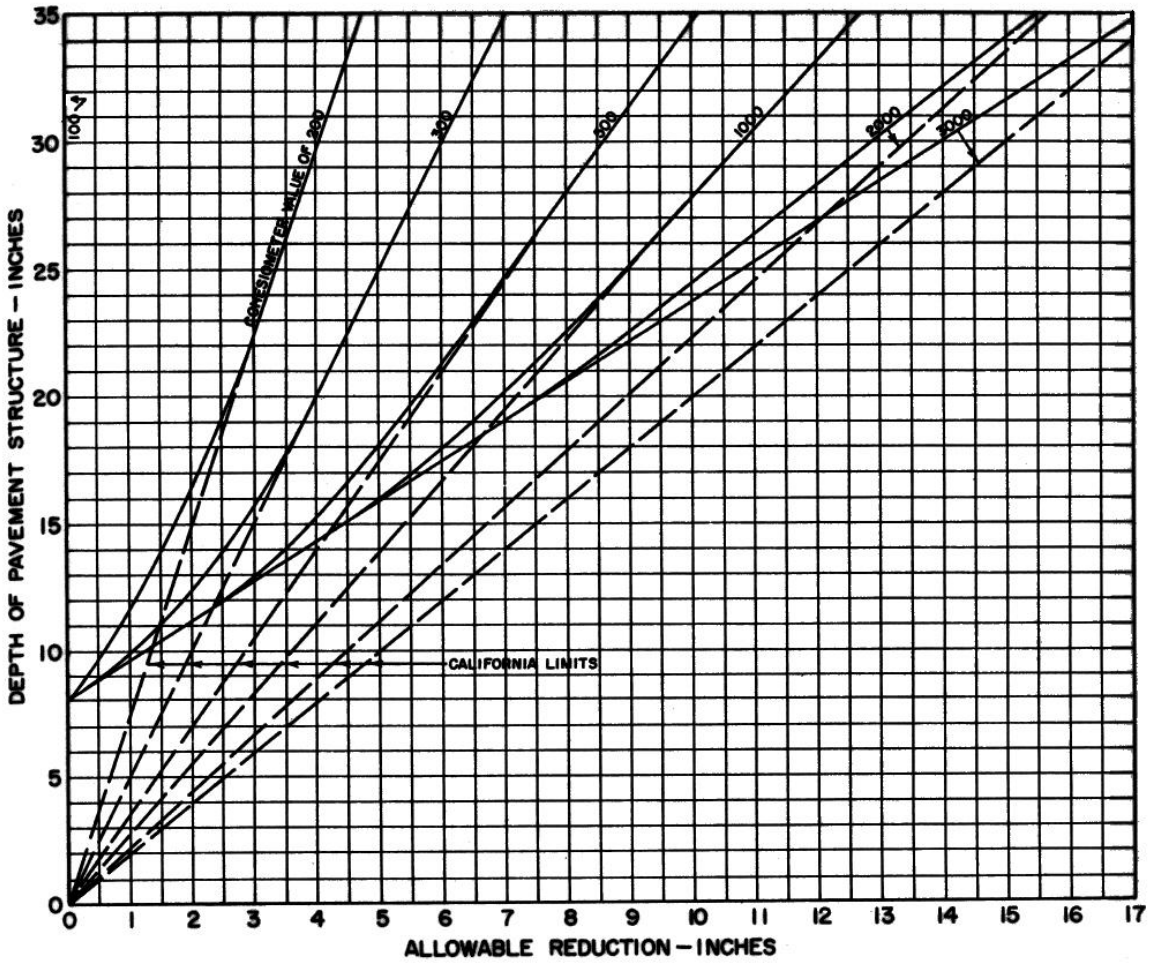

Figure 2.12. Thickness Reduction Chart for Stabilized Layers (McDowell, 1962).

sections and their depth design ratios. The correlations showed a fair amount of scatter in the data, and did not, in the authors' opinion, reasonably differentiate between good- versus poor-performing test sections.

- Considering that the load-thickness design curves are based on a theoretical analysis of the required depth of cover to keep the shear stresses in the subgrade within its Mohr-Coulomb failure envelope, TxDOT's current practice of using FPS to design for repetitive loading and checking its result against the modified triaxial design method is, in the authors' opinion, a more appropriate application of the load-thickness design curves that is consistent with their original derivation. This derivation is based on the predicted subgrade stresses due to one static application of a surface wheel load represented by a uniform pressure distribution acting on a

circular area. Repetitive loading was not considered in deriving the load-thickness design curves.

- After the thickness design curves were developed, McDowell modified the triaxial design method to consider the use of stabilized layers in pavement design. He introduced a chart that allowed for reduction in the required depth of cover based on the cohesiometer value of the stabilized material. The thickness reduction chart he developed is based on the thickness design equation formulated by Hveem and Carmany (1948) for the California Division of Highways. In developing the chart for the Texas triaxial design method, McDowell revised the linear relationships derived from Hveem and Carmany's equation such that reductions are applied only for depths of cover of 8 inches or greater.

CHAPTER III. FIELD AND LABORATORY TEST PROGRAM

Based on the findings from the literature review presented in the previous chapter, researchers established a field and laboratory test program to verify the load-thickness design curves in the modified Texas triaxial design method. Considering that the current method is based on a theoretical analysis of allowable wheel loads using layered elastic theory, researchers conducted plate bearing tests on full-scale field sections, given that the load configuration for this test most closely approximates the loading assumptions used in developing the existing design curves. A total of 30 full-scale pavement sections were constructed within the Riverside Campus of Texas A&M University for the purpose of conducting plate bearing tests. The construction was accomplished in two phases.

- Phase I. In FY 2004, twenty flexible base sections were constructed;
- Phase II. After testing the flexible base sections in FY 2004, 10 of the 20 flexible base sections were removed in FY 2005 and replaced by 10 stabilized base sections for testing in FY 2005.

PHASE I FULL-SCALE PAVEMENT TEST SECTIONS

In Phase I, twenty flexible base sections were constructed on two types of subgrades: clay and sand. Ten of the sections were built on an existing test track located beside Taxiway 7 of the Riverside Campus. The existing hot-mix asphalt and flexible base material on the test track were removed and the new test sections placed on the native clay subgrade. This site is hereafter referred to as the *clay site.* The other ten (identical) test sections were located near the entrance of the Riverside Campus on an existing native sandy subgrade. This site is hereafter referred to as the *sandy site.*

Each test section was 16 ft long and 12 ft wide. The plans called for placing five different flexible base materials at two thicknesses (6 and 12 inches) on two separate lanes at each site for a total of 20 test sections. The final riding surface of the test sections was a Grade 4 surface treatment. This pavement structure, consisting of native subgrade underlying a flexible base with a thin surface treatment, provides a close approximation to the two-layer pavement systems considered by McDowell (1955) in developing the load-thickness design curves. Table 3.1 identifies the flexible base sections constructed in Phase I.

Table 3.1. Phase I Flexible Base Sections.

Test Section Number	Section Identifier	Subgrade	Base Material
1	SSC_12	Clay	Sandstone
2	UGC_12	Clay	Untreated Uncrushed Gravel
3	CAC_12	Clay	Lime-Stabilized Caliche
4	G2C_12	Clay	Grade 2 Crushed Limestone
5	G1C_12	Clay	Grade 1 Crushed Limestone
6	SSC_6	Clay	Sandstone
7	UGC_6	Clay	Untreated Uncrushed Gravel
8	CAC_6	Clay	Lime-Stabilized Caliche
9	G2C_6	Clay	Grade 2 Crushed Limestone
10	G1C_6	Clay	Grade 1 Crushed Limestone
11	G1S_6	Sand	Grade 1 Crushed Limestone
12	G2S_6	Sand	Grade 2 Crushed Limestone
13	CAS_6	Sand	Lime-Stabilized Caliche
14	UGS_6	Sand	Untreated Uncrushed Gravel
15	SSS_6	Sand	Sandstone
16	G1S_12	Sand	Grade 1 Crushed Limestone
17	G2S_12	Sand	Grade 2 Crushed Limestone
18	CAS_12	Sand	Lime-Stabilized Caliche
19	UGS_12	Sand	Untreated Uncrushed Gravel
20	SSS_12	Sand	Sandstone

Subgrade Material Properties

A geotechnical investigation in the general area revealed that the sandy site is underlain by four distinct layers. The first layer is a 13-ft thick layer of silty sand followed by clean sand to a depth of 26 ft. The third layer consists of clayey sand extending to a depth of 41 ft underlain by hard clay (shale). The water table is about 25 ft below the surface. The

sandy site comprises a small pocket of sandy deposits within the Riverside Campus where the native soil is generally clay.

Results of Texas triaxial tests (TxDOT Test Method Tex-117E) on clay and sandy subgrade soil samples taken from each site gave the following properties:

Test Site	*Texas Triaxial Classification*	*Cohesion (psi)*	*Friction angle °*
Clay site	6.1	1.7	10.3
Sandy site	3.7	6.0	32.8

The cohesion and friction angle given above were determined from a linearization of the Tex-117E triaxial test data. Atterberg limits tests (Tex-104-E and Tex-106-E) on the soil from the sandy site indicated the soil was nonplastic. The clay site samples had a liquid limit of 48 and plasticity index (PI) of 31. Grading analyses of samples taken at the sandy site gave the following results:

Sieve Size	*Percent Passing*
No. 4	72
No. 10	51
No. 30	34
No. 40	31
No. 100	11

Optimum moisture density curves were performed for each subgrade material according to Test Method Tex-113E. The results from these tests are presented below:

Subgrade	*Optimum moisture content, %*	*Density (pcf)*
Clay	14	104.8
Sand	11	120.4

Selecting Flexible Base Materials

A total of five flexible base materials were selected for the test sections. Each base material was placed at two thicknesses and on the two different subgrades for a total of 20 test sections (5 base materials × 2 thicknesses × 2 subgrades). To aid in selecting the flexible base materials, researchers reviewed the survey results of all district laboratory

engineers/supervisors by Nazarian et al. (1996) in which they report the distribution of granular base materials used in the state, as follows:

- 50 percent limestone,
- 15 percent iron ore,
- 11 percent caliche,
- 7 percent gravel, and
- 16 percent other.

Based on this survey and updated information from the project director and Project Monitoring Committee, the following flexible base materials were selected:

- Grade 1, limestone;
- Grade 2, limestone;
- Caliche with 2 percent lime (2 percent lime is commonly added to this base in south Texas);
- Sandstone; and
- Gravel.

The survey identified the most commonly used granular base materials but did not distinguish which ones were treated with lime or cement. It is noted that both unstabilized and lime-treated uncrushed gravel sections were built and tested at the Riverside Campus during this project. Researchers worked closely with district laboratory engineers and supervisors to produce the material specifications (as used by the respective districts) for the purchase of these materials to construct the test sections. Appendix A of this report shows purchase requisition and material specifications used for test section construction.

Upon award of the construction project to a contractor, researchers worked closely with the districts to identify state approved stockpiled base materials (for all of the sources except the sandstone). District personnel then contacted aggregate pit managers to authorize the aggregate producer to sell the base materials from state designated stockpiles to the selected contractor. Materials and pit locations are listed in Table 3.2.

Researchers note that in the specifications of the purchase requisition given in Appendix A, specific pits are identified which do not match the pits shown in Table 3.2 for every source. The pit locations in the purchase requisition were provided to the contractor for cost estimating purposes only. However, once construction began, it was necessary to change some of the aggregate sources in order to find state designated/approved stockpiles of

base. The materials listed in Table 3.2 were those actually used for construction of the test sections.

Table 3.2. Base Material Types and Sources Used for Phase I Test Section Construction.

Flexible Base Description	Specification	Coordinating District	Pit Name and Location
Grade 1, Crushed Limestone	Item 247, Type A, Grade 1	Bryan	Texas Crushed Stone, Georgetown, Feld Pit, Bell County
Grade 2, Crushed Limestone	Item 247, Type A, Grade 2	Bryan	Vulcan Pit, Groesbeck, Freestone County
Caliche	*Item 247, Type D, Grade 6, with 2% lime added at construction site	Pharr	Lambert Pit, Hidalgo County
Sandstone	*Item 247, Type A, Grade 4	Paris	Martin Marietta, Sawyer Quarry, Sawyer, Oklahoma
Uncrushed Gravel	*Item 247, Type B, Grade 6	Yoakum	CW&A Materials, Welder Pit, Victoria County

*Additional specification requirements for these materials are shown in the purchase requisition in Appendix A.

PHASE II FULL-SCALE PAVEMENT TEST SECTIONS

After testing the Phase I flexible base sections, 10 of the 20 flexible base sections were reconstructed in FY 2005. All of the 6-inch thick sections were replaced with sections having stabilized layers – five on each subgrade. The following five test sections were placed on each of the two subgrades:

- 6 inches of plant-mixed cement-treated (3.0 percent) Grade 2 crushed limestone with a Grade 4 surface treatment;
- 6 inches of plant-mixed cement-treated (4.5 percent) Grade 2 crushed limestone with a Grade 4 surface treatment;
- 6 inches of uncrushed gravel treated with 2 percent lime with a Grade 4 surface treatment;
- 6 inches of Grade 1 crushed limestone, surface treatment, and 2.5 inches of Type D hot-mix asphaltic concrete (HMAC); and
- 6 inches of Grade 1 crushed limestone, surface treatment, and 4.5 inches of Type D HMAC.

Table 3.3 presents the stabilized sections built in Phase II of the project. The Grade 1 limestone, Grade 2 limestone, and uncrushed gravel used for the construction of the base sections in Phase II were obtained from the sources shown in Table 3.2. The cement contents for stabilization of the Grade 2 limestone were selected by the project director and Project Monitoring Committee to be 3.0 and 4.5 percent. The 3.0 percent content is representative of what is currently used around the state. Although 4.5 percent cement is generally higher than what TxDOT currently uses, it was selected because the design curves represented in Tex-117E are based upon cement-treated base materials with high unconfined compressive strength. Therefore, to satisfy the objectives of the research and to look forward into establishing values for use in today's stabilization procedures, the Project Monitoring Committee recommended using 3.0 and 4.5 percent cement for the two sections to be treated.

The uncrushed gravel section was treated with two percent lime which is typical for districts using this base. The other two sections consisted of Grade 1 crushed limestone surfaced with 2.5 and 4.5 inches of HMAC, respectively, to evaluate the effect of HMAC surfacings. The existing Tex-117E thickness design curves give different credits (by way of cohesiometer values) for different ranges of HMAC thicknesses. Details of the Phase II construction sequence and specifications are given in Appendix A.

Table 3.3. Phase II Stabilized Sections.

Test Section Number	Section Composition
6B	Grade 2 with 4.5 percent cement on clay
7B	Grade 2 with 3 percent cement on clay
8B	Uncrushed gravel with 2 percent lime on clay
9B	Thin Type D HMAC over Grade 1 on clay
10B	Thick Type D HMAC over Grade 1 on clay
11B	Thick Type D HMAC over Grade 1 on sandy subgrade
12B	Thin Type D HMAC over Grade 1 on sandy subgrade
13B	Uncrushed gravel with 2 percent lime on sandy subgrade
14B	Grade 2 with 3 percent cement on sandy subgrade
15B	Grade 2 with 4.5 percent cement on sandy subgrade

LABORATORY TESTING ON BASE MATERIALS

The five flexible base materials used for Phase I and Phase II construction were subjected to the laboratory tests listed in Table 3.4 to characterize the material properties for analyses of test data. Descriptions of the test procedures can be found in the applicable test

methods. Once base materials were purchased, delivered, and stockpiled at the Riverside Campus, researchers sampled the stockpiles and performed the laboratory tests identified in Table 3.4. Consistent with the current practice in the Pharr District, all of the laboratory tests on caliche were performed with 1 percent lime while the test sections were constructed with 2 percent lime. For uncrushed gravel, all laboratory data are based on testing untreated specimens. Appendix B presents the results from the tests performed on flexible base materials.

Table 3.4. Laboratory Tests Performed on Flexible Base Materials.

Laboratory Test	Test Method
Gradation	Tex-110E
Liquid limit	Tex-104E
Plasticity index	Tex-106E
Optimum moisture/density	Tex-113E
Triaxial (performed on capillary saturated specimens)	Tex-117E
Triaxial (performed at optimum moisture content)	Modified Tex-117E[1]
Triaxial (performed at optimum moisture content)	Tex-143E
Tube suction	Tex-145E
Soil suction	Filter paper (Bulut, R., R. L. Lytton, and W. K. Wray, 2001)
Resilient modulus (done at UTEP)	Modified AASHTO[2] T-307 (Nazarian, S. et al., 1996)

[1] Test method was modified by not subjecting the specimens to capillary saturation. Specimens were all tested at their respective optimum moisture contents.
[2] American Association of State Highway and Transportation Officials

In addition, samples of the same materials were sent to the University of Texas at El Paso (UTEP) for fabrication and testing of small-scale pavement models that are described in Chapter V of this report. Inasmuch as small-scale laboratory tests provide better control of test conditions and are less expensive to conduct compared to full-scale pavement tests, this project investigated the application of small-scale pavement models for verifying the existing triaxial design curves. Chapter V of this report documents the work done to establish the requirements for small-scale pavement testing and includes descriptions of the laboratory tests done at UTEP.

FIELD TESTS ON FULL-SCALE PAVEMENT SECTIONS

Researchers conducted tests on the full-scale pavement sections to check the uniformity of construction as well as to establish layer thickness and stiffness values for analyzing the plate bearing test data collected on the different sections. The following tests were conducted:

- ground penetrating radar (GPR),
- dynamic cone penetrometer (DCP),
- falling weight deflectometer (FWD), and
- portable seismic pavement analyzer (PSPA).

The following sections present the results from the tests conducted.

Tests to Determine Layer Thickness

Researchers used ground penetrating radar to determine the insitu layer thicknesses of the as-built sections. Dynamic cone penetrometer tests were also conducted to supplement the data from GPR testing, particularly on sections where the reflections from the layer interfaces could not be observed from the GPR traces. To illustrate, Figures 3.1 and 3.2 show the GPR data taken, respectively, on the 12- and 6-inch flexible base sections constructed on the clay subgrade. Figure 3.1 shows that only reflections from the bottom of the sandstone base can be seen in the data. On the other four flexible base sections constructed with uncrushed gravel, lime-stabilized caliche, Grade 2, and Grade 1 crushed limestone, the reflections from the bottom of the base layers cannot be seen. In contrast, Figure 3.2 shows that more reflections from the bottom of the base are observed from the GPR data taken on the 6-inch sections. However, no reflections are seen from the bottom of the caliche base.

As noted previously, researchers collected DCP data on the flexible base sections to complement the GPR data for the purpose of determining layer thicknesses. In particular, DCP data were used to estimate the base thicknesses on the flexible base sections constructed on sandy subgrade, where no reflections from the bottom of the base layers could be observed from the radar data on both the 12- and 6-inch sections. Tables C1 to C14 in Appendix C present the thicknesses determined from GPR and DCP testing. In addition, Figures C1 to C15 present the data from DCP testing and illustrate how researchers used the DCP data to estimate layer thickness.

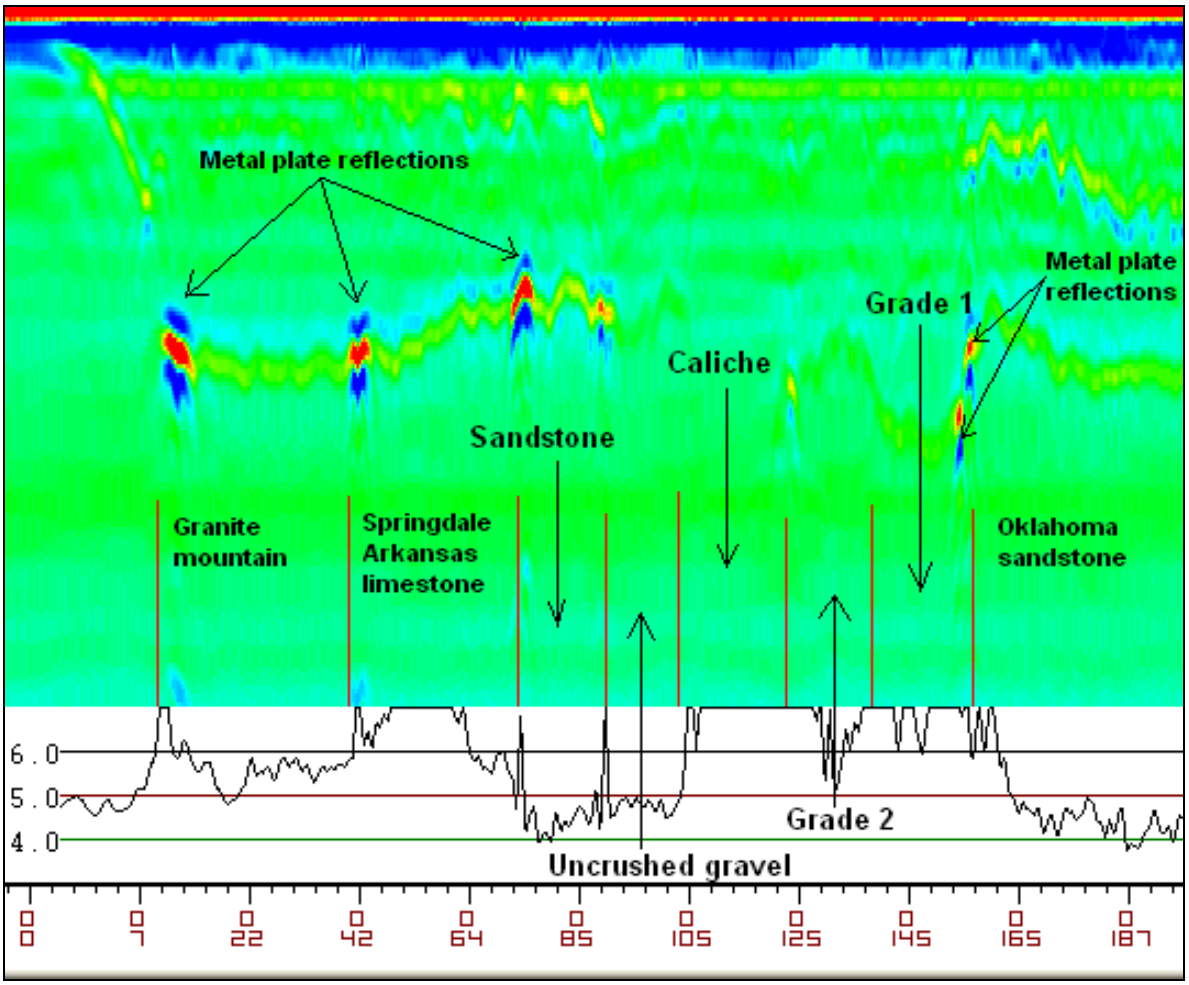

Figure 3.1. Graphical Display of GPR Data on 12-inch Flexible Base Sections Placed on Clay Subgrade.

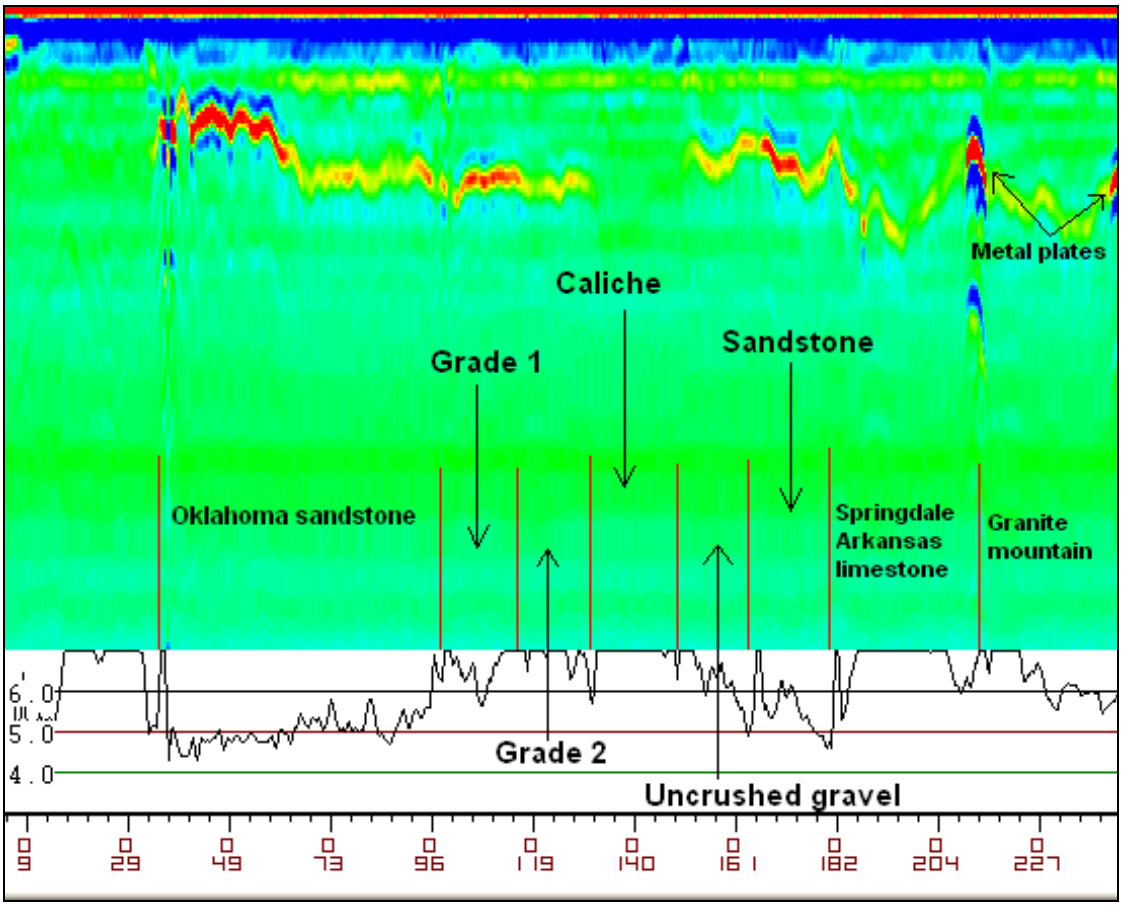

Figure 3.2. Graphical Display of GPR Data on 6-inch Flexible Base Sections Placed on Clay Subgrade.

The variability of the thickness estimates from the GPR data (as measured by their standard deviations) is generally comparable to the maximum aggregate size of the flexible base materials, indicating reasonable uniformity in the base thickness profiles. In addition, the standard deviations of the predicted thicknesses of the stabilized layers are generally smaller than the statistics determined for the flexible base sections indicating good uniformity in the stabilized thickness profiles.

Researchers note that Figures 3.1 and 3.2 show three other sections that bound the group of flexible base sections built on this project. These three sections, constructed with Granite mountain, Springdale limestone, and Oklahoma sandstone materials were built and tested on another TxDOT project to investigate premium base materials (Project 0-4358). The metal plate reflections shown in these figures are reflections from the metal plates placed on top of the clay subgrade at the boundaries of the Project 0-4358 test sections to locate the top of the subgrade for GPR data processing. However, it is noted that some shifting of the metal plates occurred during placement of the premium base materials on these test sections.

FWD Testing

Researchers collected FWD deflections to estimate the insitu layer stiffnesses for analyzing data from plate bearing tests done on each section. FWD tests were conducted at four locations along the longitudinal centerline of each section, with the loading plate positioned at ±2 and ±6 ft from the mid-point of the section. At each location, researchers positioned the FWD such that the front of the trailer faced towards the section mid-point. This setup insured that FWD deflections were collected within the interior of the section, away from the boundaries. Figure 3.3 shows a schematic of the FWD test layout.

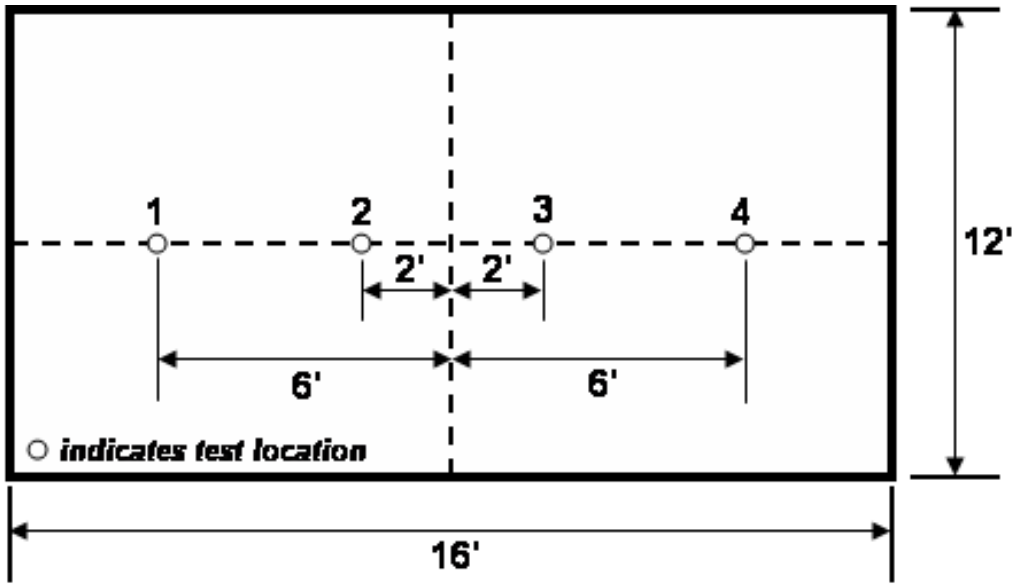

Figure 3.3. Schematic of FWD Test Layout.

Tables C15 to C17 in Appendix C present summaries of data obtained from the FWD tests conducted on the field sections. Surface deflections were measured from the FWD's seven geophones, with the first geophone located at the middle of the load plate and the remaining geophones positioned at 1 ft intervals on the geophone bar. Tables C15 to C17 present the measured deflections from geophones 1 and 7, the surface curvature indices (SCIs), and the layer moduli backcalculated from the measured deflection basins using the MODULUS program (Michalak and Scullion, 1995).

Examining the data obtained from the flexible base sections placed on the clay subgrade, it is observed that the deflections and backcalculated layer moduli within each section exhibit good uniformity. The coefficients of variation in the reported measurements are generally less than 10 percent on the clay subgrade sections. Looking at the data from the

flexible base sections placed on the sandy subgrade (Table C16), more variability is observed between the measurements within each section, particularly in the SCIs and base moduli. In most cases, the variability may be traced to a test location within a section where the data collected are quite different from the data taken at the other locations on the same section. If these extreme locations are ignored, the sections would appear more uniform. The sensor 7 deflections and the backcalculated subgrade moduli from the sand site show relatively less variability indicating a uniform sandy subgrade similar to the clay site.

Finally, examining the FWD data from the stabilized sections in Table C17 shows that these sections exhibit more uniformity than the flexible base sections placed on sandy subgrade but less uniformity compared to the clay subgrade sections. The stabilized sections exhibiting higher variability are the Grade 2 section on clay subgrade treated with 4.5 percent cement, the lime-treated uncrushed gravel section on sandy subgrade, and the Grade 2 section on the sandy subgrade treated with 3 percent cement. The other stabilized sections are fairly uniform in the opinion of the researchers.

The Portable Seismic Pavement Analyzer

Researchers used the portable seismic pavement analyzer to measure the seismic moduli of the pavement layers during construction, and to establish the uniformity of the test sections placed. Figure 3.4 shows a version of the PSPA for testing base and subgrade materials. This version is referred to as the dirt seismic property analyzer (DSPA). As shown in Figure 3.4, the DSPA consists of two transducers (accelerometers) and a source that are packaged into a hand-portable system for conducting high frequency seismic tests insitu (Baker et al., 1995). The source package is equipped with a transducer for triggering and advanced analysis purposes. The device is operated through a computer that handles all data acquisition and data reduction tasks. From the measurements collected, the average modulus of the exposed surface layer at the test location can be estimated within a few seconds in the field using the ultrasonic surface wave (USW) method described by Nazarian et al. (1993).

In the USW method, the modulus of the top pavement layer is directly determined without an inversion algorithm, since at wavelengths less than or equal to the thickness of the uppermost layer, the velocity of propagation is independent of wavelength. The modulus for the upper layer is calculated from the following equation:

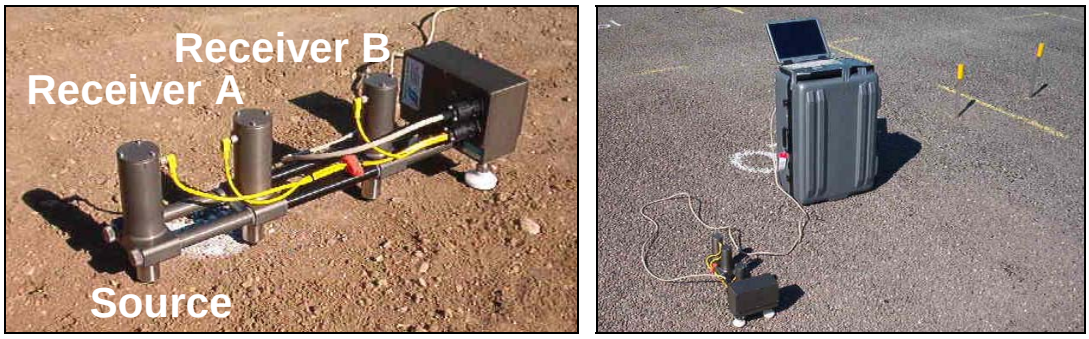

Figure 3.4. Dirt Seismic Property Analyzer.

$$E = 2\rho(1+\upsilon)\left[V_R(1.13-0.16\upsilon)\right]^2 \tag{3.1}$$

where V_R is the surface wave velocity, ρ the mass density, and υ the Poisson's ratio. Typical voltage outputs (time records) of the three accelerometers for a base material are shown in Figure 3.5a. The time records are then converted to a dispersion curve (variation in velocity with wavelength) as shown in Figure 3.5b. For practical reasons, dispersion curves are converted to moduli, with wavelength relabeled as depth. In that manner, the operator can get a qualitative feel for the variation in modulus with depth. To obtain the average modulus, the DSPA algorithm uses the dispersion curve down to approximately the nominal layer thickness.

The phase spectrum, which can be considered as an intermediate step between the time records and the dispersion curve (Figure 3.5b), is determined by conducting Fourier transform and spectral analysis on the time records from the two receivers. Two phase spectra are shown, one measured from the time records, and the best estimation of the phase when the effect of the body waves are removed. This best estimate is used to compute the dispersion curve as described in Desai and Nazarian (1993).

Seismic moduli need to be transformed to design moduli because seismic moduli are low-strain moduli whereas the design moduli close to the applied load correspond to high-strain moduli. Design modulus also depends on the thickness of the structure and on the state of stress under representative loads. The design modulus can be related to the seismic modulus through a nonlinear structural model proposed by Abdallah et al. (2002). In this regard, the material model adopted for raw base and subgrade materials is of the form:

$$E_{design} = E_{seis}\left(\frac{\sigma_{c\_ult}}{\sigma_{c\_init}}\right)^{k_2}\left(\frac{\sigma_{d\_ult}}{\sigma_{d\_init}}\right)^{k_3} \quad (3.2)$$

where E_{design} and E_{seis} (or k_1) are the design modulus and seismic modulus, respectively. Parameters σ_c and σ_d are, respectively, the confining pressure and deviatoric stress at the representative depth, and the subscripts "*ult*" and "*init*" correspond to the condition when the maximum truckload is applied to the pavement, and the free-field condition, respectively. Parameters k_2 and k_3 are regression parameters that are preferably determined from laboratory resilient modulus tests. Hilbrich and Scullion (2007) have shown that the design modulus of stabilized materials is about 70 percent of the seismic modulus. Due to their high stiffness, these materials experience strains that are in the linear elastic range.

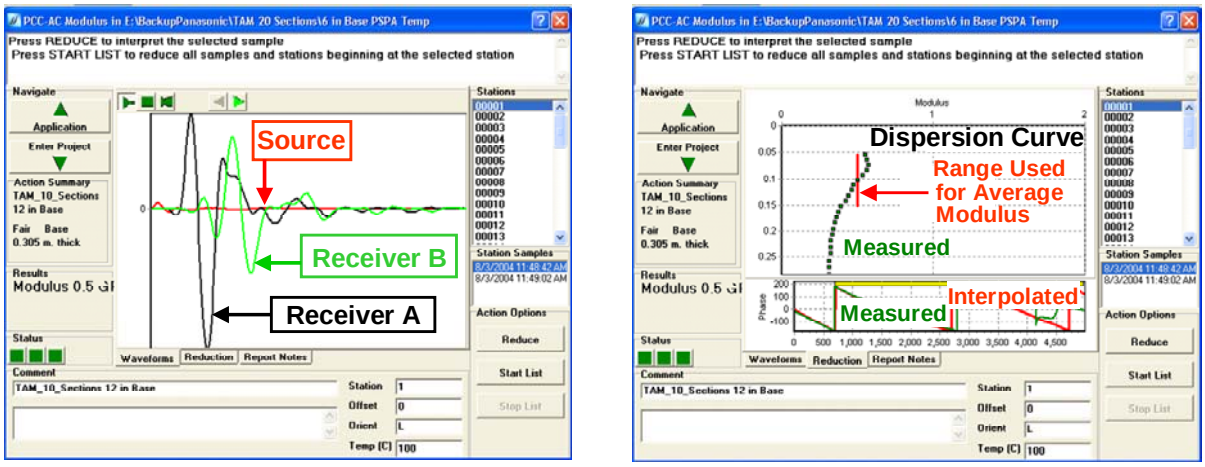

Figure 3.5. Typical DSPA Results.

Results from DSPA Testing

The variations in seismic modulus along the experimental full-scale sections are summarized in Figures C16 to C28 in Appendix C. On average, the seismic moduli of the ten flexible base sections on clay subgrade varied between 28 ksi and 37 ksi with an overall average of 33 ksi. Ignoring isolated points with very high and very low moduli, the coefficient of variation (COV) of the measured seismic moduli are typically less than 20 percent, indicating somewhat uniform clayey platform. The same pattern is evident for the sandy subgrade. However, some areas of low moduli can be observed near the edges of the platform at sections 12, 18, and 19. For the Phase II stabilized sections, only the clay subgrade was tested with the DSPA. The seismic moduli of the clay subgrade for the five

stabilized sections are more uniform with an average modulus of 31 ksi with a COV of about 20 percent. The field schedule did not permit a retest of the sandy subgrade.

Similar tests were carried out on the base materials. As anticipated, the seismic moduli varied significantly with the type of base used. In general, the trends are as anticipated, except for the seismic modulus of Grade 2 limestone being greater than the Grade 1 limestone for the flexible base sections on clay subgrade. The seismic moduli of the 6-inch thick base layers (Sections 6 through 10) are greater than those from the 12-inch sections (Sections 1 through 5). Higher variability in the modulus of some sections is observed perhaps because of the short length of the sections. For the bases placed on the sandy subgrade, the trends for measured seismic moduli are as anticipated. In almost all sections except for the Grade 1 limestone, the 6-inch thick sections (11 through 15) provided higher moduli as compared to the 12-inch thick sections. Again, due to the short length of the sections, some variability in the results is observed. The seismic moduli of the base from Phase II are significantly greater than those from Phase I because of the addition of the stabilizing agents. The Grade II limestone base with 4.5 percent cement yielded the highest seismic moduli for both the sandy and clay subgrade sections, followed by the same base with 3 percent cement. For the two sections with hot-mix asphalt surface, the seismic moduli exhibited the most uniformity. However, the seismic moduli of these sections placed on clay are higher than those on the sandy subgrade sections.

CHAPTER IV. CONSTRUCTION OF TEST SECTIONS

CONSTRUCTION OF PHASE I FULL-SCALE PAVEMENT TEST SECTIONS

Texas Transportation Institute (TTI) submitted a purchase requisition for construction of test sections on April 8, 2004. The plans and specifications for construction are shown in Appendix A of this report. As described in Chapter III, the Phase I test facility consisted of 20 full-scale pavement test sections identified in Table 3.1. The contract for construction of these test sections was awarded to Brazos Paving of Bryan, Texas. The five base materials placed on these sections were previously identified in Chapter III as follows:

- Sandstone (Martin Marietta, Sawyer, Oklahoma);
- Uncrushed gravel (CW&A Materials, Welder Pit, Victoria County);
- Caliche (with 2 percent lime) (Lambert Pit in Hidalgo County);
- Grade 2 crushed limestone (Vulcan Pit in Groesbeck); and
- Grade 1 crushed limestone (Texas Crushed Stone in Georgetown).

Researchers coordinated closely with the TxDOT districts that typically use these materials to ensure that materials used for construction met the 1993 TxDOT specifications. Brazos Paving sent trucks to each material source and hauled the materials back to the Riverside Campus. Four of the five base materials were obtained from state-approved stockpiles and researchers obtained copies of the state data for these materials. There were no state-approved stockpiles for the crushed sandstone. Thus, researchers relied primarily on gradation data obtained from belt samples as supplied by the plant laboratory.

Materials were delivered to the Riverside Campus and stockpiled along Taxiway 7 as shown in Figure 4.1. Once materials were delivered to the site, TTI sampled the stockpiles and determined the optimum moisture-density relationship for each base material and for the two types of subgrade materials. These results are presented in Appendix B.

Construction of Test Sections on Sandy Subgrade (Sections 11 through 20)

Construction of the test sections was performed during July and August of 2004. Weather caused some delays during construction but adequate drainage was provided at both sites to ensure that water flowed away from the test sections. Any placement, mixing, or densification problems that were experienced due to rainfall at the site were resolved such that the test sections met the density specifications. The subgrade was scarified to a depth of

Figure 4.1. Stockpiled Base Materials at Riverside Campus on Taxiway 7.

6 inches and compacted as described in the construction sequence given in Sheet 15 of the project plans in Appendix A. Scarification of the subgrade (see Figure 4.2) began on July 20, 2004. The contractor completed this work the following day, at which time the subgrade was ready for density testing (see Figure 4.3). Researchers set up a testing grid to be used for identification of testing locations. Each 12-ft by 16-ft test section was divided into nine testing locations as shown in Figure 4.4 where the test locations are numbered 1 through 9. Density tests were performed by TTI using a nuclear density gauge. Results of these tests are shown in Tables C18 to C27 in Appendix C.

After the subgrade was approved, the contractor began placement of base materials on the sand site. The contractor lightly sprinkled the subgrade with water prior to placement of base. Base materials were mixed with water at their stockpile locations (Figure 4.5) and then hauled to the sand site for placement. The contractor placed the base materials in 6-inch lifts (Figure 4.6).

The caliche was treated with 2 percent lime (in bags). To determine the correct quantity of lime to add, one bucket scoop of caliche was loaded onto a truck and its weight

Figure 4.2. Preparation of Sandy Subgrade.

Figure 4.3. Finished Subgrade at Sandy Site.

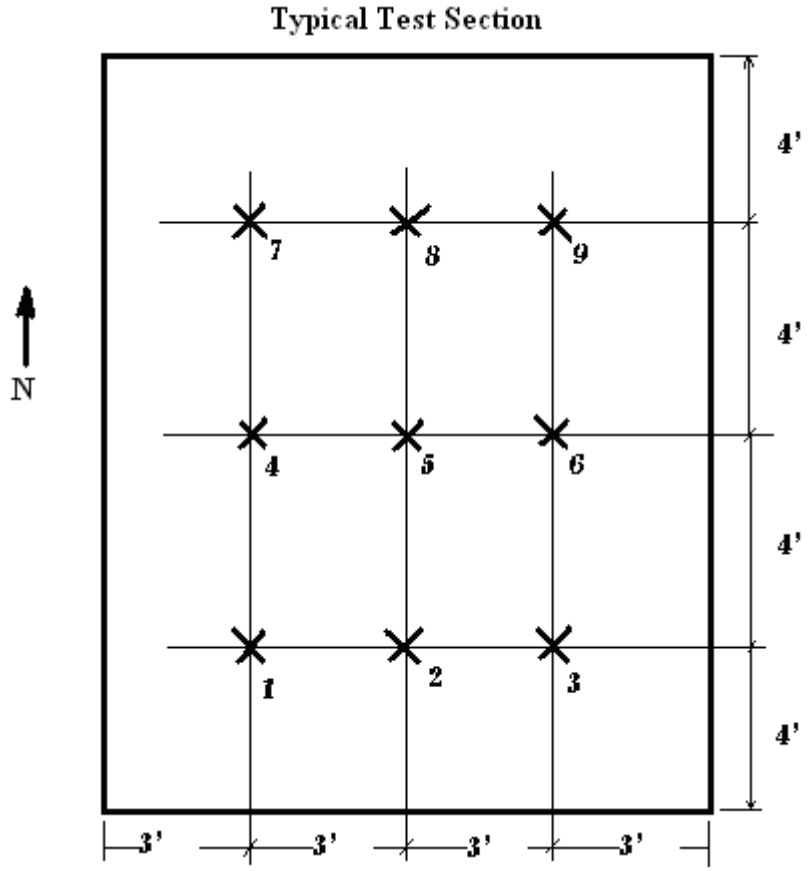

Figure 4.4. Diagram of Test Locations on each Section.

Figure 4.5. Checking Moisture Content of Base with Nuclear Gauge during the Mixing Process to Target Optimum Moisture Condition.

Figure 4.6. Placement of First 6-inch Lift (of 12-inch Thick Section) of Sandstone.

determined. From this measurement, the contractor found that one bucket scoop of caliche weighed 2800 lb. Four bucket scoops were mixed with 4½ bags of lime using a motor grader. The material was then hauled to the sand site location for placement.

Specifications required that the bases be compacted to 100 percent of maximum density. The contractor had difficulty achieving this target and brought out two different flat-wheel rollers and a pneumatic roller in an attempt to achieve the required compaction. Once the first lift of the 12-inch thick section was completed, researchers tested the layer for density and accepted the 6-inch layer based on the data presented in Table C19 of Appendix C. The top 6 inches of all base materials were then placed and compacted in a similar manner. Results of the density testing on the top 6 inches of all test sections are shown in Table C20. The contractor lightly sprayed an application of the prime to the test sections to somewhat seal the bases until the surface treatment could be applied to all 20 test sections (Figure 4.7).

Construction of Test Sections on Clay Subgrade (Sections 1 through 10)

The contractor began work on the clay site on August 11, 2004, by first removing the existing asphalt and base layers and then preparing the clay subgrade in the same manner as

Figure 4.7. Prime Coat Application to the Sandy Site Base Sections.

was described for the sand site. Once the subgrade was prepped and approved with respect to density testing, significant rainfall occurred. The contractor then completely reworked and recompacted the subgrade. After the subgrade was prepared and ready for testing, researchers performed density tests and approved the subgrade layer based on nuclear density data given Table C21. Results from DSPA tests performed on the subgrade and finished base sections are also presented in Appendix C. Figure 4.8 illustrates the finished clay subgrade.

The base materials were then placed in 6-inch lifts similar to the sandy site construction and were accepted based on the density test results given in Tables C22 and C23 of Appendix C. Figures 4.9 through 4.11 show different stages of the base construction at the clay site.

The contractor sprayed a prime coat of MC-30 to all 20 test sections and allowed it to cure for 48 hours prior to application of the surface treatment (Figures 4.12 and 4.13). The surface treatment consisted of hot asphalt cement (AC-20-5TR) and Grade 4 pre-coated limestone.

Figure 4.8. Prepared Clay Subgrade.

Figure 4.9. Placement of First Base Material on Clay Subgrade.

Figure 4.10. Placement of Second Base Material on Clay Subgrade.

Figure 4.11. Construction of Different Base Sections.

Figure 4.12. Application of Surface Treatment on Sandy Site.

Figure 4.13. Completed Surface Treatment on Sandy Site.

CONSTRUCTION OF PHASE II FULL-SCALE PAVEMENT TEST SECTIONS

After the Phase I tests were completed, 10 of the 20 flexible base sections were reconstructed in July and August of FY 2005 for testing stabilized materials as described in Chapter III. TTI submitted a purchase requisition for construction of the Phase II test sections in March 2005. This contract was awarded to Brazos Paving, the contractor for the Phase I construction. To achieve uniformity of construction and proper transition between the test sections constructed in Phase I, it was essential that the same contractor be used to construct all of the test sections.

Researchers again coordinated closely with TxDOT districts and obtained materials from state-approved stockpiles. Materials were delivered and stockpiled along Taxiway 7 as in the Phase I construction. Details of the Phase II construction sequence and specifications are shown in Appendix A.

The contractor began construction by removing the existing asphalt surface treatment and base materials for the 6-inch thick test sections to expose the subgrade. The existing clay and sandy subgrades were scarified to a depth of 6 inches over a width extending 4 ft beyond the outside longitudinal edge of the test sections. Density tests on the finished subgrades are presented in Tables C24 and C25 in Appendix C.

After researchers accepted the subgrade, the contractor began placing base materials beginning with the Grade 1 limestone base. The uncrushed gravel was mixed with 2 percent lime in the same manner as described for the caliche base in Phase I (Figures 4.14 and 4.15). The Grade 2 limestone sections were stabilized with two different cement contents: 3.0 and 4.5 percent. Mixing was done at the Scarmardo pugmill plant on August 1, 2005 (Figure 4.16) in Bryan, Texas. Prior to mixing the Grade 2 limestone material with cement, personnel from the Bryan District Laboratory supervised the calibration of the mixing plant on July 29, 2005, to ensure the accuracy of target cement contents (Figure 4.17).

The Grade 2 base materials that had been delivered to the Riverside Campus from the Vulcan Pit in Groesbeck were hauled by Brazos Paving to the pugmill mixing plant where it was stockpiled, as shown in Figure 4.18. The material was transferred to the hopper for mixing using a front-end loader. A TTI researcher supervised this operation to ensure minimal contamination from the sandy material under the stockpile shown in Figure 4.18.

Figure 4.14. Mixing Uncrushed Gravel with Lime on Concrete Pad.

Figure 4.15. Placement of Uncrushed Gravel Treated with 2 Percent Lime.

Figure 4.16. Scarmardo Pugmill Mixing Plant.

(a) Meter for Adjusting Amount of Cement Pumped to the Pugmill.

(b) Diverting Cement to Front-End Loader for Weighing.

Figure 4.17. Calibrating the Pugmill Mixing Plant.

Figure 4.18. Transferring Stockpiled Grade 2 into Pugmill Hopper with Front-End Loader.

The cement is metered into the pugmill where the base and cement are mixed. Water is then added to the blend and the material is transferred to dump trucks (Figure 4.19). The contractor then hauled the plant-mixed base material to the test sites where it was placed and compacted to maximum density (Figure 4.20). Tables C26 and C27 in Appendix C present the density test results on all ten of the finished base sections.

Base materials were then cured and primed as in the Phase I construction. The contractor then placed the surface treatment consisting of Grade 4 pre-coated limestone and AC-20-5TR hot asphalt cement. Finally, 2.5 inches of Item 340, Type D HMAC was placed on test sections 9B and 12B as described in the plans and specifications in Appendix A. A 4.5-inch thick layer of Type D HMAC was placed on Test Sections 10B and 11B.

Researchers ran plate bearing tests after construction of all the full-scale field sections to verify the load-thickness design curves in the modified triaxial design method. Chapter VI describes the plate bearing tests and presents the results from the verification effort.

Figure 4.19. Plant Mixed Grade 2 Base to be Hauled to Test Site.

Figure 4.20. Placement of Cement-Treated Grade 2 Base Material.

CHAPTER V. INVESTIGATION OF CORRESPONDENCE BETWEEN SMALL-SCALE AND FULL-SCALE PAVEMENT TESTS

INTRODUCTION

The main objectives of the small-scale studies were to simulate the variation in moisture content in base and subgrade and to evaluate the variation in load carrying capacity due to changes in moisture content. Small-scale tests provide better control of test conditions (moisture variations, loading rate, and load magnitudes) and are less expensive to conduct compared to full-scale pavement tests. Thus, researchers at the University of Texas at El Paso conducted small-scale pavement tests in the laboratory to supplement the data from full-scale pavement tests for verifying the existing triaxial design curves. To ensure that small-scale tests yield realistic results, and provide a "proof-of-concept" for the application of these models, UTEP researchers initially investigated the requirements for small-scale pavement testing during the first year of this project. This investigation included a comparative evaluation of pavement response data from two instrumented pavement sections at the Texas A&M Riverside Campus with corresponding data from small-scale pavement models fabricated at the field moisture contents and densities of the Riverside test sections, and using the same base and subgrade materials. UTEP researchers performed an extensive parametric study using the finite element method to obtain the best dimensions and address concerns about boundary condition effects related to small-scale experiments. Researchers also investigated the mechanistic behavior of the pavement models to establish transfer functions between small-scale and full-scale tests.

This chapter provides a background on the development of small-scale pavement models. It focuses on the experimental aspect of the research rather than the numerical modeling. As such, only some results from the numerical models are presented. Further details can be found in Amiri (2004).

LITERATURE REVIEW

Laboratory tests are usually performed on relatively small specimens that are assumed to be representative of a larger body of soil. Model tests usually attempt to reproduce the boundary conditions of a particular problem by subjecting a small-scale physical model of a full-scale prototype structure to loading. In some of the models,

principles of similitude are determined and satisfied. Rocha (1953 and 1957) made one of the most important contributions to the application of similitude to soil-mechanics model studies. The fundamental principle of model testing in soils that emerged from Rocha's work was first stated by Roscoe and Poorooshasb (1963). They showed that, to a close degree of approximation, the strain behaviors of two soil elements will only be identical when the elements are subjected to geometrically similar stress paths.

Dimensional analysis in relation to applied loads was carried out by Freitag (1965). Recently, Kim et al. (1998) conducted a study to explore the use of small-scale models of accelerated pavement testing devices to evaluate the performance of pavements in conjunction with full-scale tests. In their research, they considered thickness, mass density, and elastic properties of different layers, as well as the magnitude, area, and velocity of load as parameters that affect the behavior of moving traffic loads. When the same materials are used in full-scale and N-th scale model tests, the ratios of length, time rate of loading, and load should be 1/N, 1/N, and $1/N^2$, respectively, in order to get identical results between in-service pavements and small-scale models.

SMALL-SCALE PAVEMENT MODELS

Construction

Figure 5.1a shows a schematic of the small-scale pavement models used in this study. Three layers, consisting of pea gravel, subgrade, and base material, were placed layer-by-layer inside a tank. One consideration was the appropriate size of the tank to ensure that the interaction between the soil and the horizontal and vertical boundaries is minimal. Amiri (2004) established the appropriate dimensions through extensive finite element modeling. For a 6-inch diameter loading plate, a tank with a diameter of 36 inches and a height of 24 inches was deemed adequate.

The body of the tank was a 1-inch thick polyethylene pipe, reinforced with helical loops of the same material for minimizing the lateral deformation. A 0.5-inch thick acrylic sheet was glued to the bottom of the tank. The wall of the tank was smooth, but to further minimize friction, researchers attached a thin layer of plastic to the tank with axle grease.

A 0.75-inch PVC pipe was used at the bottom of the tank for introducing water to the specimen. Initially, researchers filled the tank with a 3-inch layer of pea gravel. Because of its high permeability, the pea gravel could be easily super-saturated allowing the moisture to

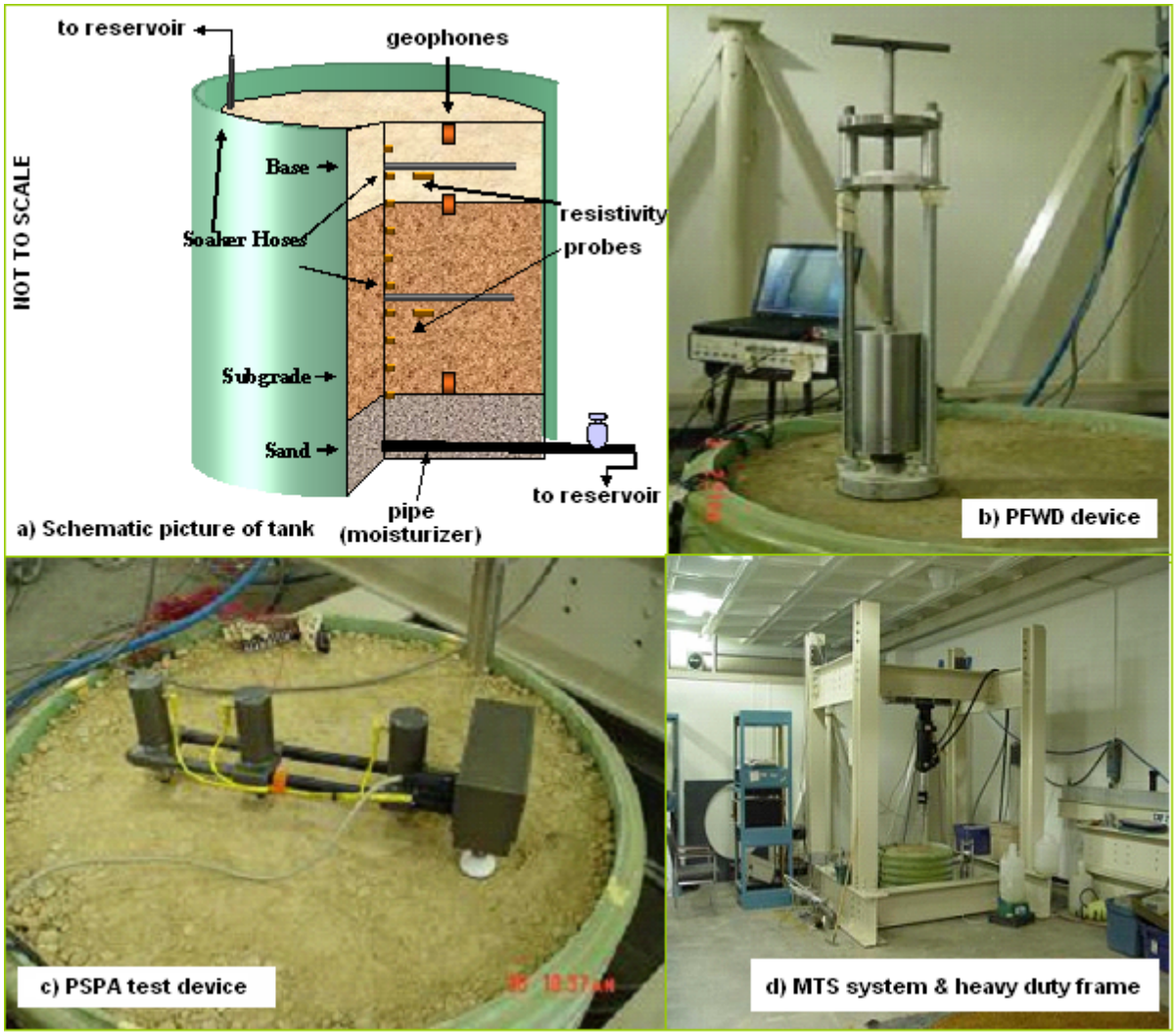

Figure 5.1. Small-Scale Model Illustration and Setup.

migrate to the subgrade and base due to capillary action. A 14-inch layer of subgrade soil was compacted on top of the pea gravel. This layer was placed in 2-inch lifts. For each lift, researchers calculated and mixed the amount of soil and water necessary to achieve the target moisture content and density. In order to reach a similar level of compaction, the target densities were chosen to equal the values obtained from corresponding field sections that researchers tested in this investigation. At pre-selected depths, researchers placed appropriate instrumentation in the tank. The top of each lift was scarified before the next layer was placed. A 5-inch layer of base at the desired density was placed on top of the subgrade following the procedure for the subgrade layer.

The wetting of each layer was carried out by introducing water to the gravel layer beneath the subgrade. Two sets of soaker hoses were placed in the middle of the base and

subgrade as an auxiliary device to saturate the soil in case the saturation could not be achieved through capillary suction. During testing, researchers found that increasing the head of the water introduced to the pea gravel was effective enough to moisture condition the soils. Thus, the soaker hoses were not actually used.

Instrumentation of Models

Researchers installed three types of instruments in the small-scale models. Six miniature geophones were embedded in two columns. The locations of the geophones are shown in Figure 5.1a. In each column, one geophone was at the bottom of the subgrade, another one between the base and subgrade, and the third one just under the surface. The embedded geophones were used to measure the vertical deflections under a portable FWD (PFWD) loading system for insitu material characterization (Figure 5.1b).

Researchers installed resistivity probes inside the models to monitor the moisture distribution. The probes were copper tubes (0.25 inches in both diameter and length) soldered to electrical terminal wires. One set of vertical probes, placed along a centered vertical column at 2-inch increments within the subgrade and base, was used to monitor the progression of moisture within the specimen. Two sets of horizontal probes were placed in the middle of the base and subgrade, respectively. The horizontal resistivity setup consisted of four probes at 3-inch spacing. The probes were offset from the center line of the tank by 6 inches so as not to interfere with the vertical probe at that level.

Testing of Small-Scale Models

The test program consisted of the following steps:

- moisture conditioning,
- material characterization, and
- loading of specimens.

Moisture Conditioning of Small-Scale Models

The major conditioning activity was to monitor the moisture content of the soil. During moisture conditioning of the model, researchers periodically measured the amount of water added to the soil so that the bulk moisture content of the soil in the tank could be calculated. To prevent moisture loss from the top of the specimen, researchers covered the surface of the specimen with a plastic sheet. The pea gravel layer was porous enough to

distribute water evenly at the bottom of the tank. Soil layers were also distributed and compacted uniformly and meticulously. These two factors created symmetry in the model, which assured sufficient uniformity of water distribution during moisture conditioning. Researchers tested the specimens on the following dates: (1) three days after fabrication of the model; (2) after moisture conditioning of the subgrade; and (3) after moisture conditioning of the base and subgrade.

Material Characterization

Shortly before loading the model, researchers performed tests with an impulse device and a portable seismic pavement analyzer. As shown in Figure 5.1b, the impulse device is a PFWD-type tester consisting of a 6-inch diameter plate with two rods on top that carry a falling weight load cushioned by a rubber bumper. The device worked by manually lifting and dropping a load onto the specimen surface. A load cell located directly under the bumper measured the applied load. The embedded geophones were used to measure the deformations due to the impulse. The models were tested at three locations, directly on top of the left column of geophones, in the middle of the two geophone columns and on the right column of geophones. At each location, researchers used three drop heights to apply nominal loads of 500, 1000, and 1500 lb. The time histories of the applied load and deflections of the geophones were recorded. The maximum deflection from each geophone was extracted and summarized for all cases. Researchers used the loads and deflections with a nonlinear finite element program to backcalculate the moduli of the layers.

The portable seismic pavement analyzer, shown in Figure 5.1c, was applied to perform tests on the base material. The device imparts an elastic disturbance within the layer by impacting the material with a small hammer and measures the surface waves propagating through the model. Comparing the waveforms received from the sensors, the velocity of the wave and thus, the shear modulus and Young's modulus of the material can be estimated. Researchers performed tests almost everyday, especially after introducing water to the model. The PSPA estimated very well the influence of water on the modulus of the material. However, only the modulus of the exposed layer (base in this case) could be measured.

Loading of Small-Scale Models

The small-scale model was built right under the frame of a 50-kip Materials Testing and Simulation (MTS) system. The heavy-duty frame, shown in Figure 5.1d, was designed

to minimize relative deformation within the loading frame. The MTS System provided the loading necessary for the test. However, the applied loads and resulting displacements were monitored, measured, digitized, and saved by a data acquisition system for further data analyses.

Figure 5.2 shows a sample of the load pattern and corresponding deflections. A cyclic ramp load was applied to the model using the MTS system. The ramp load was increased at a rate of 500 lb/minute to a peak load, maintained constant for 1 minute, and then decreased at the same rate of 500 lb/ minute. The maximum load was varied between 500 lb and 4500 lb (when possible) at 500-lb increments.

MATERIAL PROPERTIES

As mentioned previously, researchers fabricated and tested two models to verify the concept of small-scale pavement testing. For both models, a crushed limestone base was used. However, one model was prepared with a sandy gravel subgrade (providing strong support) while the other model had a highly plastic clay subgrade (representing a weak material). Each material was dried and then passed through a 1-inch sieve to exclude very coarse aggregates. The base and subgrade materials were retrieved from two existing pavement sections constructed previously at the Texas A&M Riverside Campus.

A series of laboratory tests were conducted on the materials that included index tests for Atterberg limits, resilient modulus tests, and triaxial tests. The liquid limit, plastic limit, and plasticity index were 21, 11, and 10, respectively, for the crushed limestone base. The corresponding index values for the sandy gravel subgrade were 20, 12, and 8, respectively. For the clay subgrade, the liquid limit was 35, the plastic limit 14, and the plasticity index 21.

The results from triaxial tests on the three materials are shown in Table 5.1. Researchers conducted triaxial tests on these materials using two test methods – the standard Texas triaxial test (Tex-117E), and the provisional Tex-143E. The seismic modulus, as measured with the free-free resonant column test (Nazarian et al., 2002), and the resilient modulus test results are also shown in Table 5.1. In general, the base and sandy gravel subgrade exhibit comparable moduli, while the clay subgrade is substantially softer.

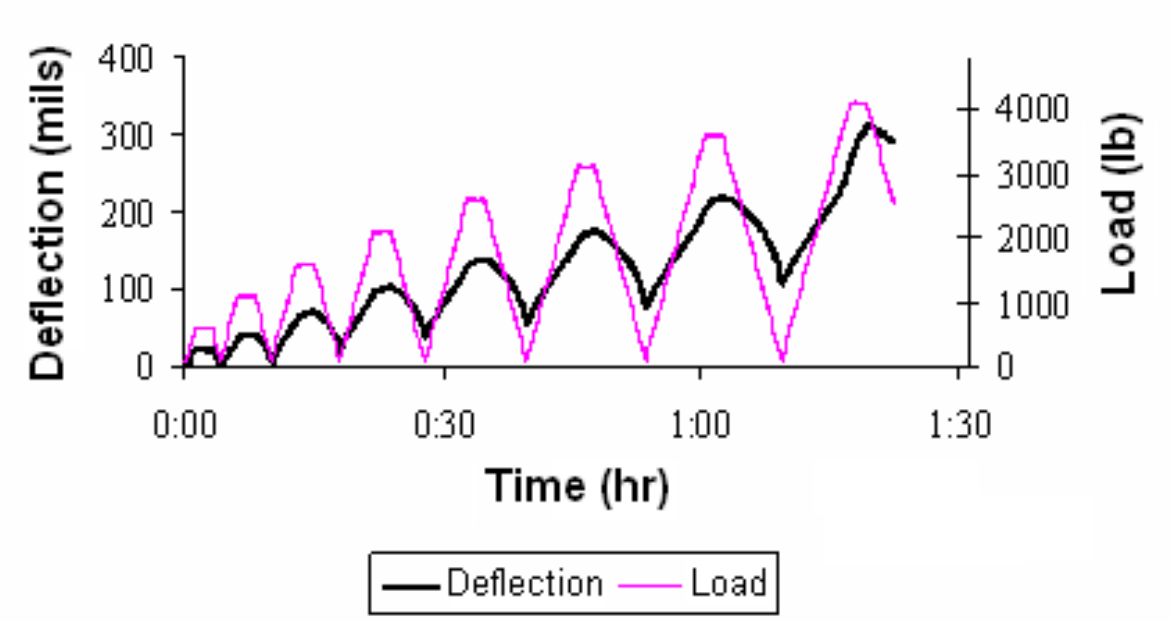

Figure 5.2. Typical Load Pattern and Corresponding Deflections.

Table 5.1. Properties of Base and Subgrade Materials from Verification Tests of Small-Scale Pavement Models.

Test \ Material			Crushed Limestone	Sandy Gravel	Clay
Atterberg limits	Liquid limit		20.7	20.4	35
	Plastic limit		11.3	12.5	14
	Plasticity index		9.4	7.9	21
Moisture susceptibility*	Initial modulus (ksi)		25	60	15.8
	Peak modulus (ksi)		450	280	4.1
	Peak to initial modulus ratio		18	4.67	3.85
	Residual modulus (ksi)		30	25	3
	Peak to residual modulus ratio		15	11.20	1.33
Tex-117E	Friction angle (°)		51.6	39.3	0.0
	Cohesion (psi)		6.4	4.9	6.1
	Classification		2.8	3.5	6.0
Tex-143E	Friction angle (°)		56.1	43.7	4.4
	Cohesion (psi)		3.3	3.5	6.8
	Classification		1.0	2.7	6.0
Resilient modulus**	Model parameters	k_1, ksi	23	22	7
		k_2	0.24	0.25	0.02
		k_3	-0.10	-0.14	-0.49
		R^2	0.87	0.94	0.97
	Resilient modulus (ksi)		57	65	24

*From seismic tests

**$M_R = K_1 \sigma_c^{k2} \sigma_d^{k3}$, where σ_c is the confining pressure and σ_d is the deviatoric stress.

SMALL-SCALE MODEL TEST RESULTS

In order to be concise, this section focuses on the results of tests on the sandy gravel subgrade model. For comprehensive results on the clay subgrade model, please refer to Amiri (2004).

The sandy gravel model was constructed to target moisture contents and densities representative of insitu values of the Riverside Campus field sections where the materials were taken. These sections were built on a TxDOT project conducted in the early to mid-1990s to evaluate pavement response under tire loads representative of superheavy load moves. The moisture contents of the crushed limestone base and sandy gravel subgrade were 6.0 and 5.5, respectively. The target densities were 137 pcf and 141 pcf for the two materials.

The subgrade for the small-scale pavement model was placed in a denser state than the base to be consistent with the measured densities of the full-scale test sections. Approximate bulk moisture contents of the model were 5.6, 12, and 13 percent for insitu, subgrade moisture conditioned, and base and subgrade moisture conditioned states, respectively. The bulk moisture content of the model approximately doubled after the first moisture conditioning (from 5.6 to 12 percent) while after the second conditioning, it increased by only 1 percent. The effects of water level on the electrical resistance and modulus of the soils in the sandy-gravel model are shown in Figure 5.3. The resistance values of the base and subgrade (Figures 5.3a and 5.3b) dropped after the first moisture conditioning indicating movement of water into the layers. After the second conditioning, the resistance in the base decreased further from about 100 Ω to 80 Ω while in the subgrade, the resistance hardly changed. This observation indicates that during the first phase, the subgrade had been fully wetted. Vertical probes used to monitor the progression of the water front gave consistent results as the horizontal probes.

The results in Figure 5.3c were obtained from tests done with the PSPA. The seismic modulus of the base decreased from about 180 ksi to about 80 ksi after the first moisture conditioning. After the second conditioning, the base modulus further decreased to about 50 ksi. These observations indicate that, even during the first moisture conditioning, the modulus of the base was affected as a result of capillary flow. After the second conditioning, the modulus of the base material did not change as much. The slight increase in modulus

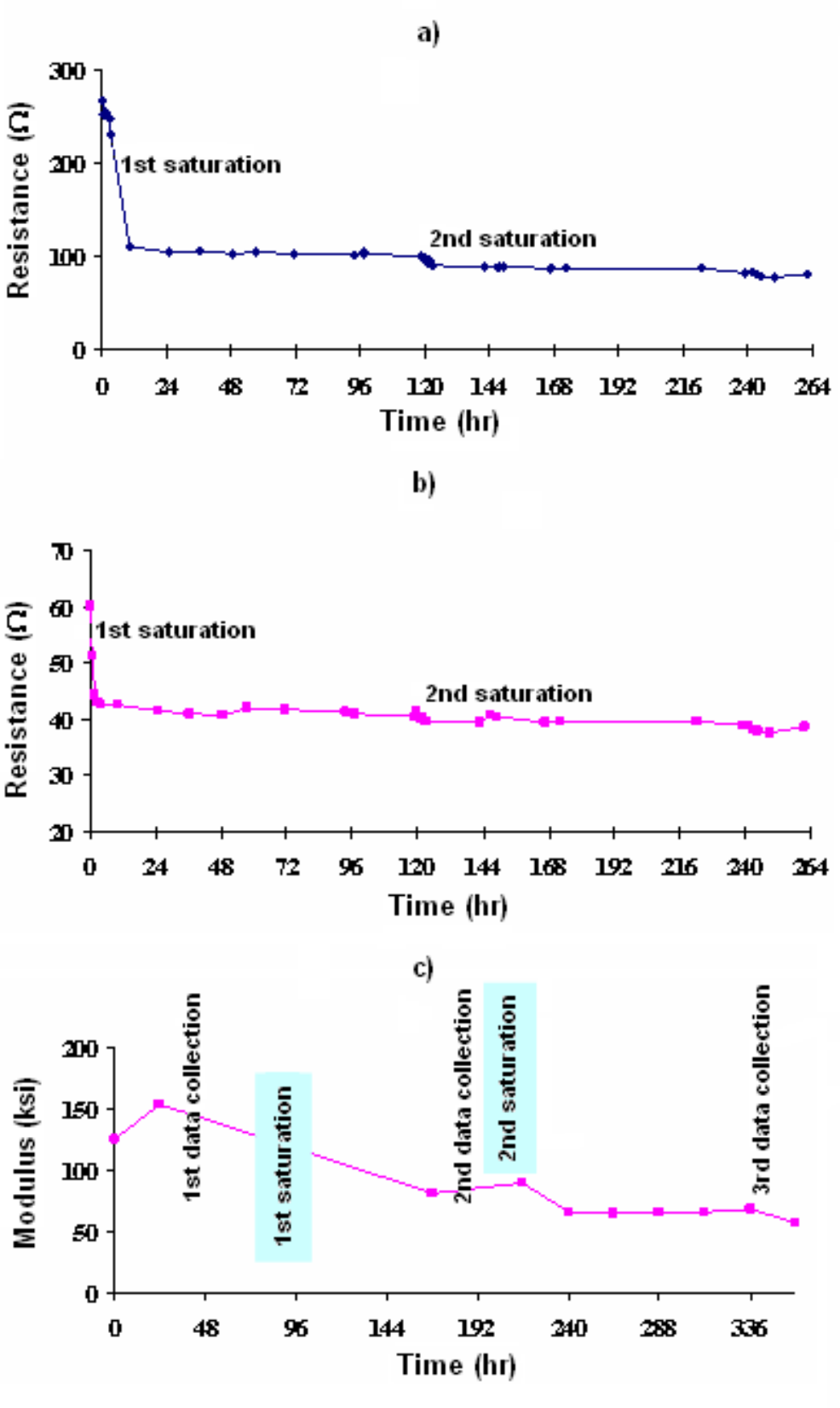

Figure 5.3. Temporal Measurements of a) Resistance in Base Material; b) Resistance in Subgrade Material; and c) Modulus of Base Material.

between the two conditioning stages may be due to disconnection of the water reservoir from the tank during the days that data collection was in progress.

The deflections measured with the portable impulse device were used in backcalculating the moduli of the base and subgrade materials. The deflections were incorporated into a numerical model considering nonlinear parameters of the materials to backcalculate the moduli. The average moduli of the sandy gravel material were 46, 31, and 19 ksi for dry, subgrade moisture conditioned, and base/subgrade moisture conditioned states, respectively. The corresponding values for the crushed limestone base were 35 ksi, 19 ksi, and 12 ksi, respectively. Similarly, the average moduli of the clay subgrade were 35, 27, and 17 ksi for the dry, subgrade moisture conditioned, and base/subgrade moisture conditioned states, respectively. The corresponding values for the crushed limestone base placed on top of the clay subgrade were 20, 6, and 5 ksi, respectively. It is observed that the base exhibits a lower modulus for the clay model compared to the corresponding value for the sandy gravel model. This observation may reflect different levels of compaction of the base materials in the two models.

The variation of deflection with load for the three cases is shown in Figure 5.4. Little permanent deformation was observed under the dry condition for the sandy gravel model. The maximum deformation under a load of 4500 lb (equivalent to about an 18-kip wheel load) was about 40 mils. When the subgrade was moisture conditioned, the maximum deformation was less than 100 mils, while a permanent deformation of about 40 mils was observed. In the last stage, when the base and subgrade were both moisture conditioned, the maximum deflection of about 320 mils occurred at a load of 3500 lb, with a permanent deformation of about 290 mils. When the load was increased to more than 4000 lb, the deflection increased to over 400 mils since the model failed. Figure 5.4 also shows the backbone curve of each stage, which is the curve connecting the maximum load/deflection points.

The backbone curves for the sandy gravel and clay subgrade models under the three moisture conditions are compared in Figure 5.5. For both specimens, the maximum deformations become progressively greater as the wetting of the layers progresses. A fundamental difference in the load-deflection curves between the two models can also be

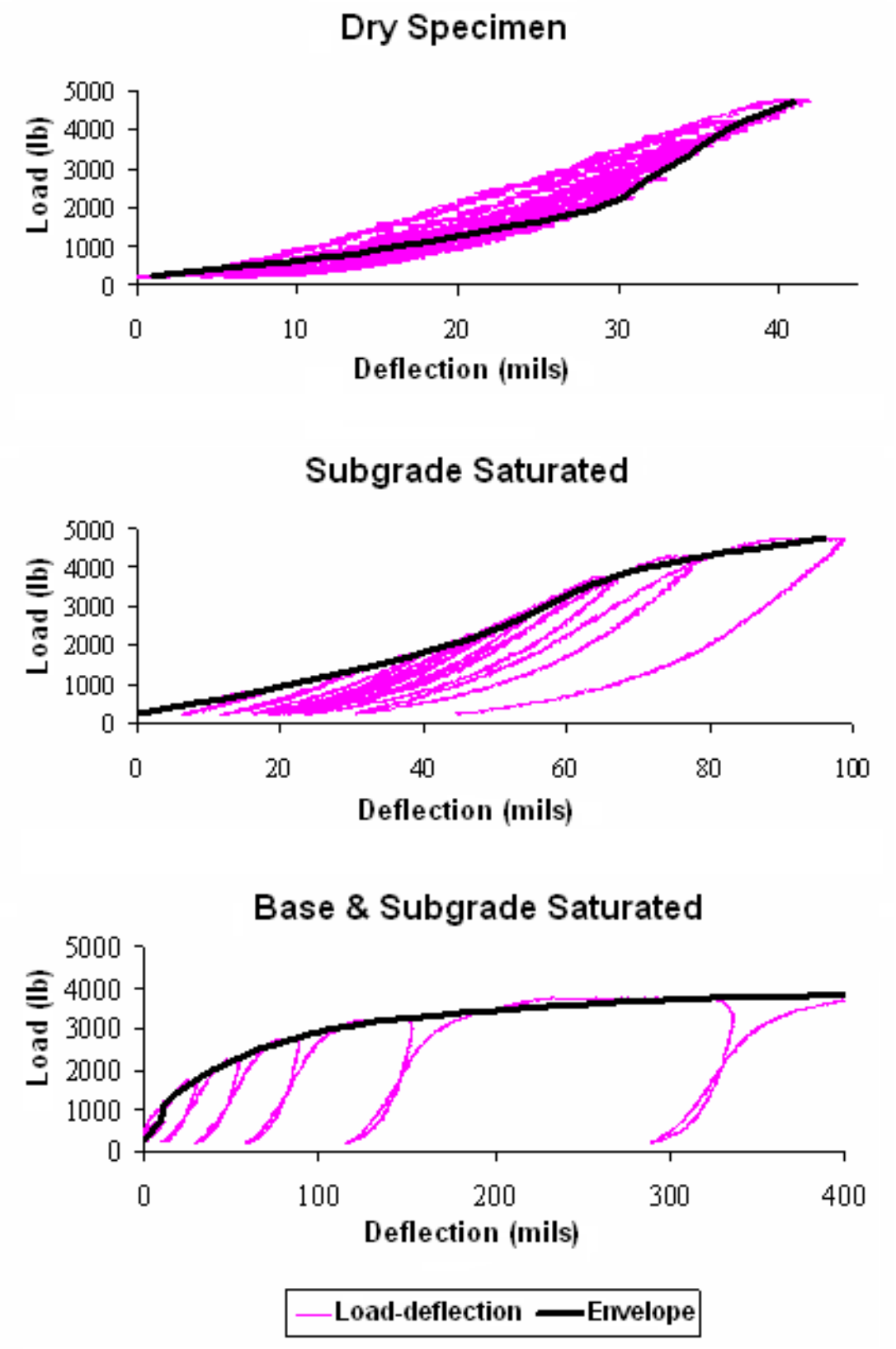

Figure 5.4. Variation of Deflection with Load from Plate Load Tests of Sandy Gravel Model.

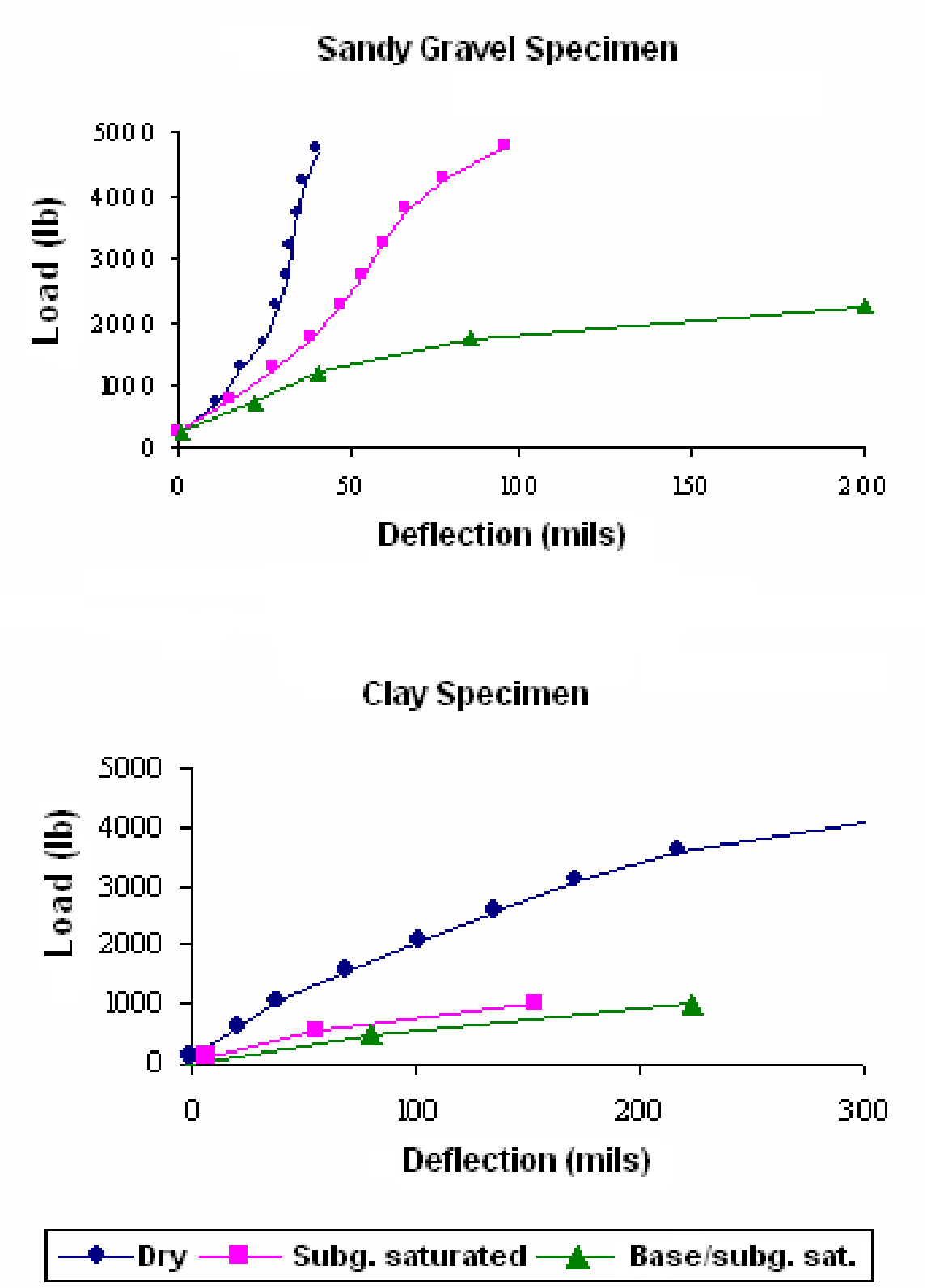

Figure 5.5. Comparison of Backbone Curves from Three Stages of Plate Load Tests.

seen. In the sandy gravel case, an initial settlement is observed while in the clay model, this phenomenon is not observed.

FULL-SCALE TEST RESULTS

TTI researchers conducted field tests on two full-scale pavement sections built with the same base and subgrade materials as the small-scale pavement models tested at UTEP. The hot-mix asphalt and base layers at both field sections were nominally 1 inch and 10 inches thick, respectively. To measure the deformations of the base and subgrade, TTI researchers instrumented both sections with multi-depth deflectometers (MDDs). Each MDD had three linear variable differential transducers (LVDTs) positioned close to the top of the base, bottom of the base, and 12 inches into the subgrade.

A plate bearing test was carried out at each section. A plate with a radius of 6.6 inches was loaded monotonically up to 30 kips while the deflections of the load plate and the embedded LVDTs were measured. The average deflection of the three LVDTs on the load plate was reported as the deflection of the plate. The load-deflection curves for the pavement section on the sandy gravel subgrade are shown in Figure 5.6a. A careful inspection of this figure indicates that a significant amount of initial seating settlement (about 15 mils) occurs. From the load-deformation curves determined from the MDD, only 3 mils of the initial seating settlement (out of 15 mils) are related to the subgrade and the rest occurs inside the base and the hot-mix layers. Even though not shown here, this initial seating settlement is equal to the total permanent deflection of the load plate, and was treated as a settlement deflection in the analysis of the results. Out of 64 mils of total deformation measured at a load of 30 kips, 42 percent (27 mils) occurred in the subgrade and 34 percent (22 mils) in the base. By way of contrast, for the pavement section on the clay subgrade (Figure 5.6b), the majority of the deformation occurred in the subgrade. Out of 255 mils total deflection, 185 mils (73 percent) were from the subgrade and 52 mils (20 percent) from the base.

The FWD tests were performed shortly before the plate load tests. For both sections, the modulus of the Type D mix was about 300 ksi. For the sandy subgrade section, the moduli of the base and subgrade were 80 and 97 ksi, respectively, with an apparent depth to bedrock of 76 in. For the clay subgrade section, the moduli of the base and subgrade were

32 and 8 ksi, respectively, with an apparent depth to bedrock about the same as the other section. A shallow stiff layer is not anticipated at either site given the geology of the region.

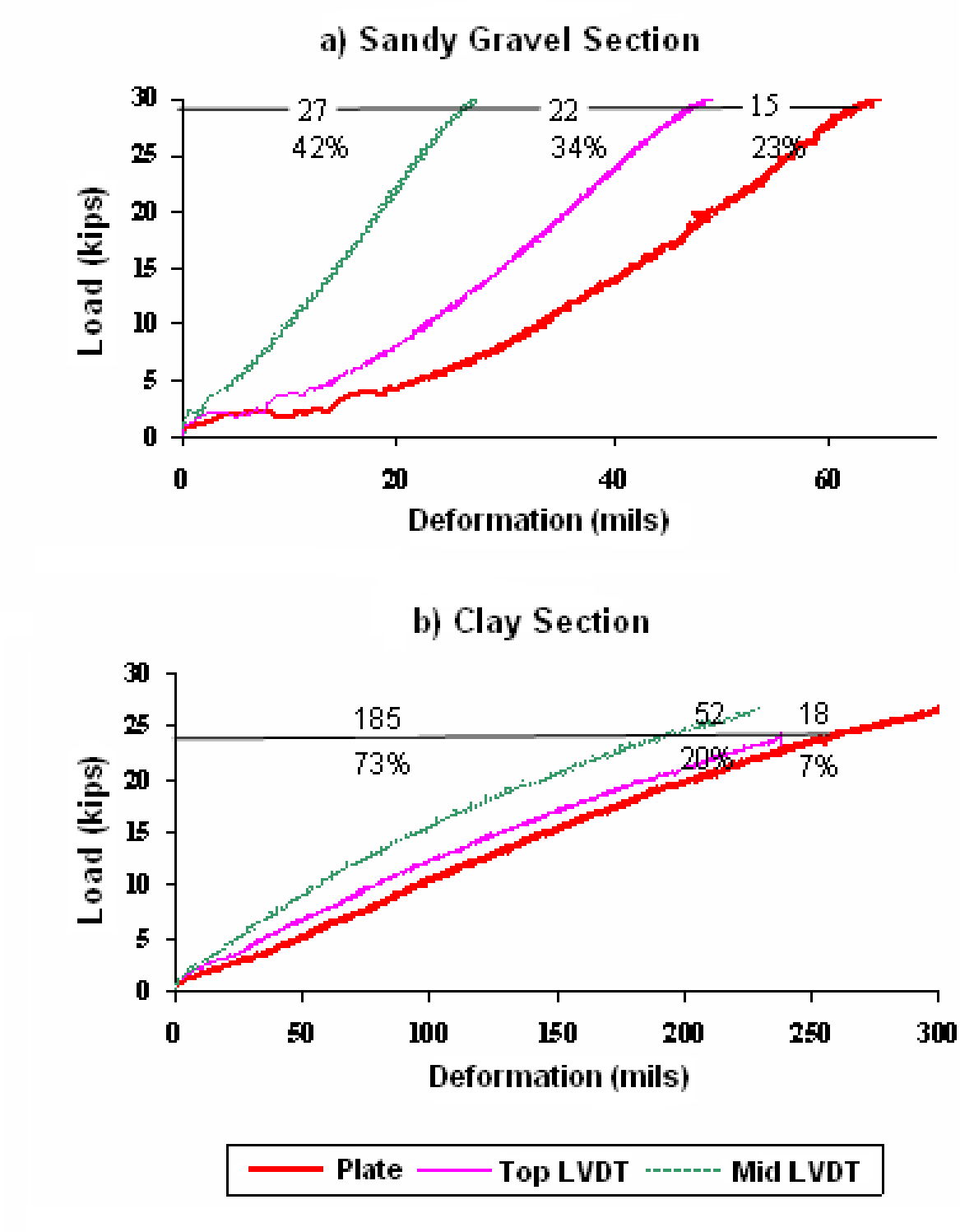

Figure 5.6. Load-Deflection Data from Plate Load Tests on Full-Scale Sections (percents show the ratio of deflection from each layer to the total deflection).

FINITE ELEMENT MODELING

To numerically analyze the results, finite element models were developed using the ABAQUS software (see Amiri, 2004, for details). UTEP researchers implemented a nonlinear model using the parameters given in Table 5.1 that were determined from the resilient modulus tests done on soil samples. Nonlinear models were used to predict the soil behavior more precisely, especially for the saturated condition.

The small-scale models comprised the soil, tank, and load plate. The elements for the geo-materials were defined as quadrilateral, which is a 4-node bilinear axisymmetric continuum element. The elements of the tank body were 3-node, bilinear, axisymmetric, continuum elements. The elements along the axis of symmetry were restrained from radial movement while the elements at the bottom of the mesh were restricted from radial and vertical movements.

Researchers modeled the full-scale pavement section using three-dimensional (3D) finite elements. For this analysis, infinite elements were used instead of classic boundary conditions since the region of interest is small in size compared to the surrounding medium. Researchers modeled a section of pavement with a width of 72 inches and a length of 160 inches.

ANALYSIS OF RESULTS

For each set of materials, the results of the small-scale and full-scale tests under similar moisture and density conditions were compared to find the relationship between the full-scale and small-scale test results. Figure 5.7a compares the load-deflection curve from the small-scale test with corresponding results from full-scale testing of the sandy gravel section. For compatibility, the loads obtained from the small-scale tests were multiplied by the ratio of the areas of the full-scale and small-scale plates (based on similitude rules). Some initial deformations with a small increase in loads are apparent from both tests, perhaps due to the seating of the load plate mechanism. At a given load, the deflection from the small-scale test falls in between the deflections measured on the load plate and from the top LVDT. This occurs because of the absence of the hot-mix layer in the small-scale models. Since the small-scale models are roughly the half-scale models of the field, it was practically impossible to place a hot-mix layer on these laboratory models. Based on the numerical

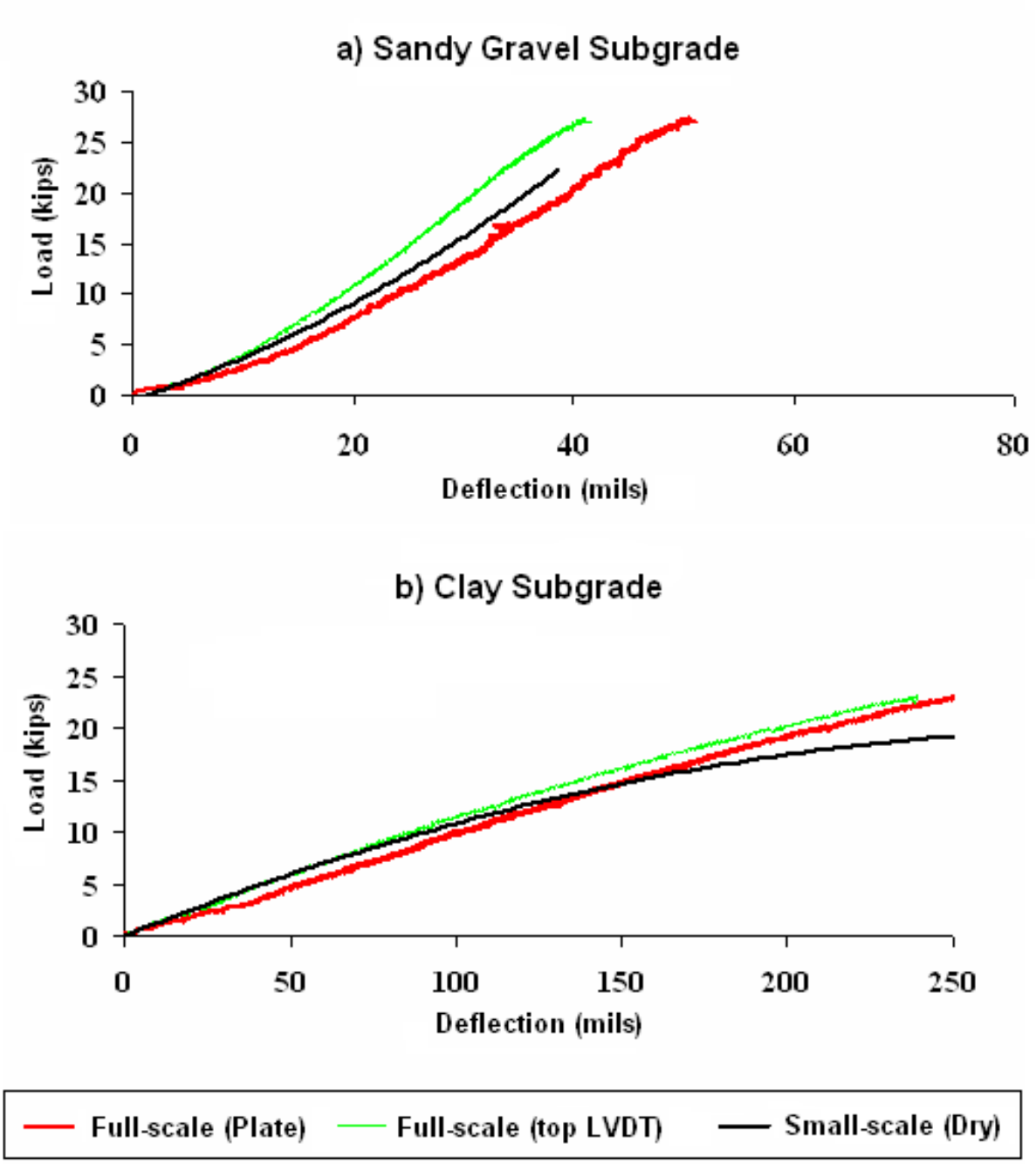

Figure 5.7. Comparison of Small-Scale and Full-Scale Experimental Results.

analysis, less than 4 percent of the deformation is attributed to the asphalt layer for this sandy gravel subgrade site.

Figure 5.7b compares the deflections of the load plate and the top LVDT from the full-scale test with the deflections of the load plate on the small-scale specimen for the clay subgrade. For deflections less than 130 mils, the deformations of the small-scale specimen

are smaller than those of the full-scale test. For deformations greater than 130 mils, the small-scale specimen experiences greater deformations. This change in pattern might be because of the cracks that were created around the load plate that finally led to a puncture failure of the small-scale specimen.

The second aspect of the analyses consisted of comparing the results from the numerical and experimental models. The load-deflection curves from the finite element models are compared with those from the small-scale experiments using the sandy gravel subgrade in Figure 5.8a. Since the finite element models do not consider the permanent deflections, the net deflections from the experimental tests were used. Some initial seating settlements (deformations of the load plate with no appreciable load) had also occurred during the plate load tests. These settlements, which were approximately equal to 8 mils, 10 mils and 17 mils for the dry, subgrade moisture conditioned and base and subgrade-moisture conditioned states, respectively, were subtracted from the total settlements to obtain the net settlements. The experimental deflections are greater than those from the finite element models. This difference is even more pronounced for the moisture conditioned cases.

The measured deflections for all three moisture conditions, as shown by Amiri (2004), were systematically 1.96 times greater than the calculated values. The sources of differences between the experimental and numerical results can be attributed to problems with the accuracy of the finite element (FE) models, problems with the determination of the moduli of the layers, or the simplifications associated with the constitutive models. Since the patterns are similar, the numerical models can be calibrated with appropriate experimental models.

Figure 5.8c compares the load-deflection curves from the finite element models with the net deflections from the experimental tests for the clay subgrade specimens. In this case, the permanent deflections were noticeable even for the dry model. Similar to the sandy gravel model, the experimental deflections are greater than those from the finite element models. The measured deflections are almost systematically 2.1 times greater than the calculated values independent of the moisture condition. Once again, problems with the accuracy of the FE models, the uncertainties in the backcalculated moduli of the layers, or the simplifications associated with the constitutive models, are plausible reasons for the differences.

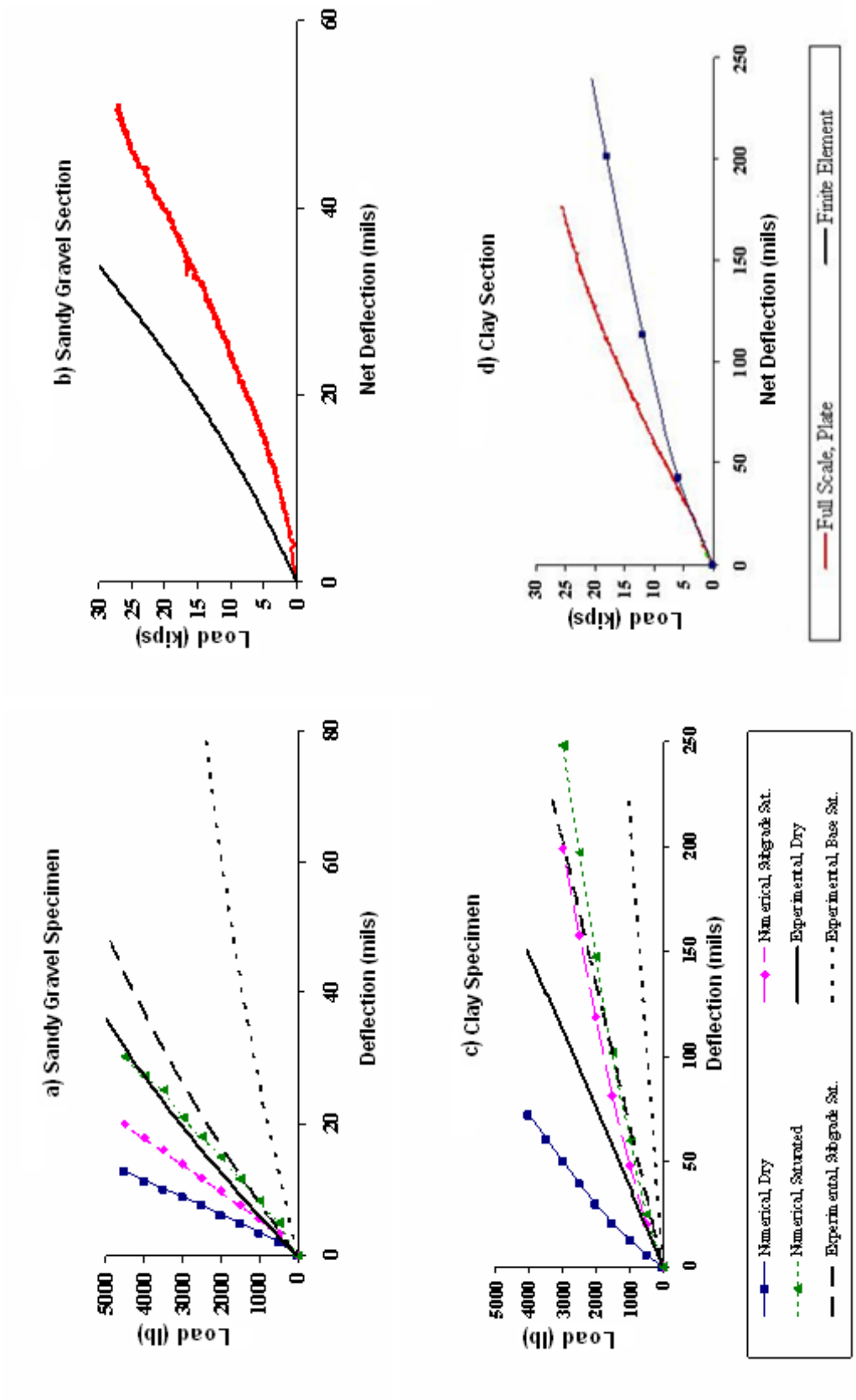

Figure 5.8. Comparison of Numerical and Experimental Results.

An interesting observation in the results is worth mentioning. The small-scale models were constructed with similar densities to the corresponding field sections as an approximate criterion to attain the same modulus for each material. The backcalculated moduli of the sandy gravel subgrade and crushed limestone base in the small-scale specimens were 46 and 35 ksi, respectively, while in the field, they were 97 and 80 ksi. Considerable engineering judgment had to be used in the backcalculation of the results from the small-scale models. Also, the sandy gravel test section has been in place since the mid-1990s. Thus, the differences in the backcalculated layer moduli may reflect the effects of varying degrees of consolidation within the sandy gravel subgrade for the field test section. The impact of the apparent depth to the rigid layer of 76 inches in the field is also of interest. The depth to the rigid layer may be interpreted as an apparent depth that reflects the stress sensitivity of the subgrade. The moduli from seismic tests performed on the base materials in the small-scale tests and at the Riverside Campus test site were within 20 percent of one another. Unfortunately, seismic tests on the subgrade are not available to judge the closeness of their moduli.

Figures 5.8b and 5.8d compare the load deflection curves from the finite element models with the net deflections from field tests on the sandy gravel and clay subgrade sections, respectively. As shown in Figure 5.8b, the patterns between the experimental and numerical results are quite similar. However, the experimental deflections are on the average 1.6 times greater than the numerical ones for the sandy gravel section. Figure 5.8d shows that the experimental deflections are initially close to the corresponding numerical estimates. However, for deflections greater than 50 mils, the numerical results are greater than the net deflections from the field test. One reason for this difference could be the different loading pattern between the plate load tests (static) vs. the FWD tests (dynamic) used for backcalculation of the moduli. Even though not shown in the figures, the deflections measured with the first sensor of the FWD at a given load were roughly 60 percent to 75 percent of the deflections measured under the static loads.

SUMMARY

In this chapter, the feasibility of understanding the behavior of actual pavement sections with small-scale models in the laboratory was investigated. When the small-scale models are carefully constructed to achieve approximate densities and moisture contents as existing pavement sections, the predicted deformation responses from numerical models

exhibit trends similar to the observed results but with magnitudes that differ by about a factor of 2 from the test data. The differences appear to be systematic indicating that numerical models can be properly calibrated using small-scale test results. In addition, researchers found reasonable agreement between the load-deformation responses of corresponding small-scale models and full-scale pavement sections after adjusting for scale effects based on similitude rules. In the researchers' opinion, these findings demonstrate that small-scale tests can be effectively used along with full-scale experiments to verify existing models or design procedures under different conditions.

Small-scale tests carried out under different moisture conditions for the base and subgrade materials tested in this chapter demonstrated the detrimental impact of moisture on the deformation response of small-scale pavement models. A similar observation was noted from results of small-scale tests conducted on models fabricated with the same base and subgrade materials used for construction of full-scale pavement sections at the Riverside Campus. The succeeding chapter presents findings from the full-scale and small-scale pavement tests conducted by researchers to verify the existing triaxial design curves.

A one-to-one comparison of the experimental results from the small-scale and full-scale tests conducted on the flexible base sections in Phase I was not feasible since the laboratory and field tests were carried out in parallel at different moisture levels and densities. Furthermore, the main goal of the full-scale tests was to verify the existing Texas triaxial design curves, whereas the goal of the small-scale tests was to establish the impact of moisture on the load-bearing capacity of pavement sections. To further evaluate the appropriateness of the small-scale tests, the results from the numerical models and experimental results for all base materials on the two subgrades are compared in Figure 5.9. To develop the figure, the loads obtained from the experimental results are compared with the loads from the corresponding FE models for each specimen at increments of 50 mils until failure. The slope of the best fit line is an indication of the transfer function between the experimental and numerical results. On average, the transfer function is about two, which is comparable to the values reported herein for the validation specimens. Even though more one-to-one comparisons between the full-scale and small-scale tests would be beneficial, this study has demonstrated, in the authors' opinion, the value of small-scale pavement tests in supplementing the results from full-scale tests. Based on the experience gained from

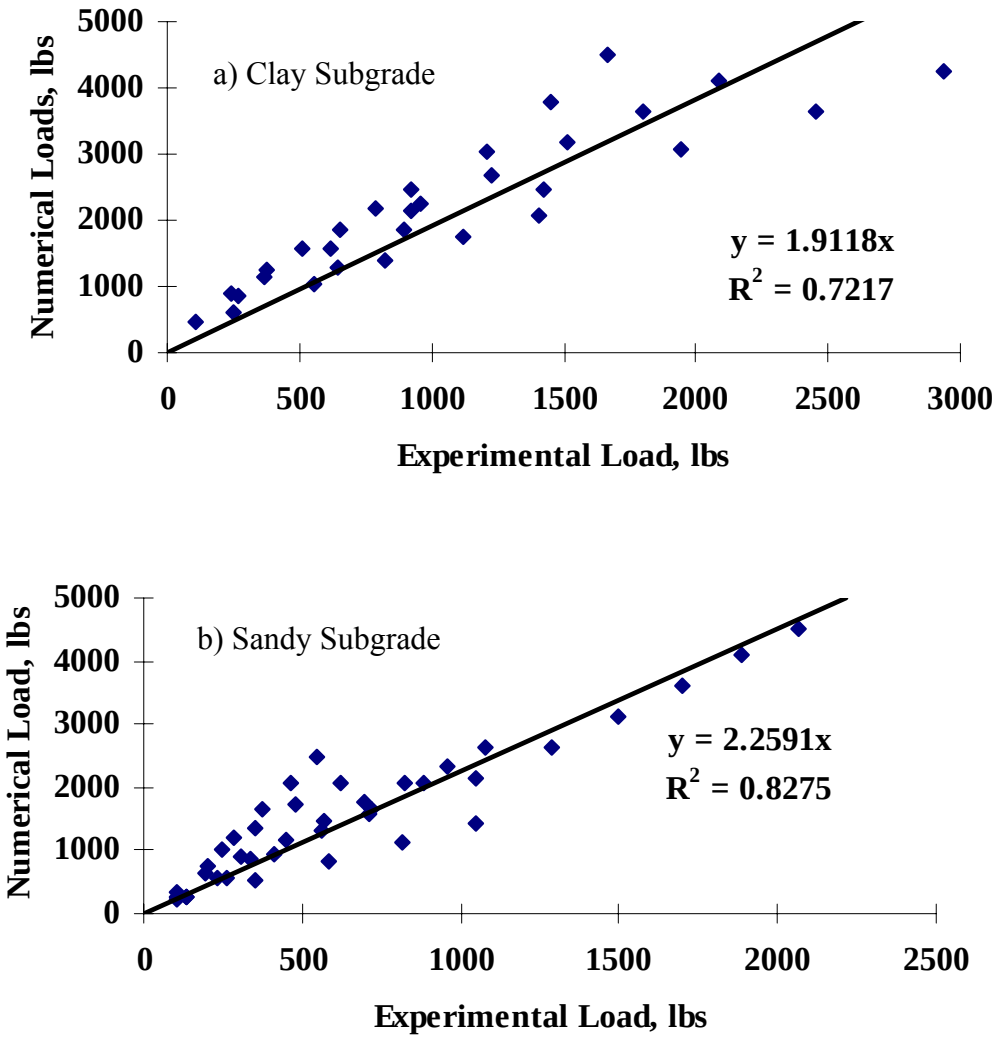

Figure 5.9. Comparison of Experimental and Numerical Results from Small-Scale Tests of Flexible Base Materials.

small-scale tests, it seems that these tests are quite feasible and economical for parametric studies under well-controlled conditions to understand the impact of different structural and environmental parameters that impact pavement structural design.

Small-scale tests carried out under different moisture conditions for the base and subgrade materials tested in this chapter demonstrated the detrimental impact of moisture on the deformation response of small-scale pavement models. A similar observation was noted from results of small-scale tests conducted on models fabricated with the same base and subgrade materials used for construction of full-scale pavement sections at the Riverside Campus. The succeeding chapter presents findings from the full-scale and small-scale pavement tests conducted by researchers to verify the existing triaxial design curves.

CHAPTER VI. VERIFICATION OF EXISTING DESIGN CURVES

From the literature review presented in Chapter II, researchers verified the method used by McDowell (1955) to develop the existing triaxial design curves. This method is based on a stress analysis to establish the depth of cover required to keep the load induced stresses in the subgrade within the material's failure envelope (as defined by its Texas triaxial class). Researchers demonstrated the methodology by re-creating the existing load-thickness design curves. To go one step further, researchers conducted plate bearing tests on laboratory specimens and on full-scale field sections to verify the load bearing capacity estimates from the triaxial design curves. This verification compared the allowable wheel loads determined from the curves with the corresponding wheel loads established from test data. The findings from this investigation are presented in this chapter.

FIELD PLATE BEARING TESTS

Plate bearing tests were conducted on full-scale pavement sections built with different flexible base materials, stabilized layers, and thickness, and placed on two different subgrades. Each test section was 16 ft long and 12 ft wide. The sections were constructed and tested in two phases as documented in Chapter III of this report. In Phase I, ten flexible base sections were built on native clay subgrade, while another 10 were founded on sand subgrade. Table 6.1 identifies the different flexible base sections tested in Phase I. Also given in the table are the measured base thickness on each section as established from ground penetrating radar and dynamic cone penetrometer measurements, and the estimated base and subgrade moduli from FWD measurements. Table 6.2 presents similar information for the stabilized sections built in Phase II of the research project.

Researchers performed plate bearing tests on the full-scale pavement sections using ASTM D 1196 as a guide. Figure 6.1 illustrates the test setup. Load was applied to the pavement through a 12-inch diameter rigid steel plate with a 55-ton hydraulic jack that reacted against the tractor-trailer shown in Figure 6.2. Researchers placed and strapped concrete blocks above the trailer axles to provide the reaction required for the test. In addition, a couple of heavy I-beams were bolted to the trailer frame along its mid-span in order to minimize the sag of the trailer as the pavement is loaded during the test. With the

Table 6.1. Flexible Base Sections Tested in Phase I.

Section Identifier	Subgrade	Base Material	Backcalculated Modulus (ksi)[1]		Base Thickness (inches)[2]
			Base	Subgrade	
SSC_12	Clay	Sandstone	17.5	7.4	13
UGC_12	Clay	Uncrushed Gravel	38.6	10.3	12
CAC_12	Clay	Lime-Stabilized Caliche	18.0	8.6	12
G2C_12	Clay	Grade 2 Crushed Limestone	20.9	8.3	12
G1C_12	Clay	Grade 1 Crushed Limestone	20.3	9.6	12
SSC_6	Clay	Sandstone	22.4	9.1	6.5
UGC_6	Clay	Uncrushed Gravel	27.5	9.3	7.2
CAC_6	Clay	Lime-Stabilized Caliche	22.8	10.4	6.5
G2C_6	Clay	Grade 2 Crushed Limestone	40.9	11.4	6.7
G1C_6	Clay	Grade 1 Crushed Limestone	33.0	12.3	7
G1S_6	Sand	Grade 1 Crushed Limestone	64.6	11.2	6
G2S_6	Sand	Grade 2 Crushed Limestone	47.7	12.4	6
CAS_6	Sand	Lime-Stabilized Caliche	62.4	11.2	5
UGS_6	Sand	Uncrushed Gravel	64.9	12.0	6.8
SSS_6	Sand	Sandstone	101.5	12.5	6.6
G1S_12	Sand	Grade 1 Crushed Limestone	104.8	16.2	11
G2S_12	Sand	Grade 2 Crushed Limestone	28.0	15.5	11.8
CAS_12	Sand	Lime-Stabilized Caliche	70.6	14.8	11.5
UGS_12	Sand	Uncrushed Gravel	24.0	13.3	11
SSS_12	Sand	Sandstone	46.7	15.0	11.2

[1]Based on average of backcalculated moduli determined at FWD stations 2 and 3 in the middle area of each section where plate bearing tests were conducted.
[2]Based on average thickness in middle area of each section within FWD stations 2 and 3.

Table 6.2. Stabilized Sections Tested in Phase II.

Section Identifier	Section Composition	Backcalculated Modulus (ksi)			Thickness (in)	
		Stabilized Material	Base*	Subgrade	Stabilized Material	Base*
6B	Grade 2 with 4.5% cement on clay	580.0		14.5	5.8	
7B	Grade 2 with 3% cement on clay	272.6		13.2	6.4	
8B	Uncrushed gravel with 2% lime on clay	28.2		9.0	6.3	
9B	Thin Type D HMAC over Grade 1 on clay	132.6	25.0	8.8	3.2	7.0
10B	Thick Type D HMAC over Grade 1 on clay	101.7	25.6	9.6	5.1	6.3
11B	Thick Type D HMAC over Grade 1 on sand	200.0	38.3	12.7	3.7	7.9
12B	Thin Type D HMAC over Grade 1 on sand	200.0	54.8	13.4	2.7	6.3
13B	Uncrushed gravel with 2% lime on sand	88.9		12.0	6.2	
14B	Grade 2 with 3% cement on sand	314.0		12.3	6.1	
15B	Grade 2 with 4.5% cement on sand	540.0		12.2	6.6	

* Shaded cells indicate sections where the stabilized material is the base layer.

Figure 6.1. Plate Bearing Test Setup.

Figure 6.2. Tractor-Trailer Used for Plate Bearing Test.

loads shown in Figure 6.2, the trailer weighed 80,100 lb (40,700 lb on the drive axle, and 39,400 lb on the trailer axle). Researchers used three linear variable differential transducers positioned at 120° intervals around the load plate to measure its displacements during the test. The transducers were mounted on deflection beams (Figure 6.1) that rested on supports located a minimum of 8 ft from the load plate or the nearest tire of the test vehicle.

Two sets of tests were conducted for the purpose of verifying the existing triaxial design curves. These tests were conducted in the mid-area of each section, within the vicinity of FWD stations 2 and 3 along the section's longitudinal centerline as illustrated in Figure 3.3. In the first set, researchers ran the plate bearing test under monotonic loading until the test area failed (as evidenced by excessive deformations under the load plate and/or reduction in the test load), or until the maximum safe load was reached, whichever came first. Figure 6.3 illustrates the displacement history from a monotonic loading test. Note that displacement measurements continued after failure occurred to establish how much of the total deformation was recovered after unloading and how much of it was permanent. The second set of tests was conducted under step loading on a different area of the pavement section. In this test, researchers applied a series of step loads to the section, of magnitudes below the peak load registered from the monotonic loading test. Figure 6.4 illustrates the displacement history from a step loading test. As shown, researchers monitored the displacements during the loading and unloading portions of each step to collect data for evaluating relationships between permanent deformation and applied load. These relationships provided a basis for defining pavement bearing capacity in terms of an allowable permanent deformation criterion due to one wheel load application.

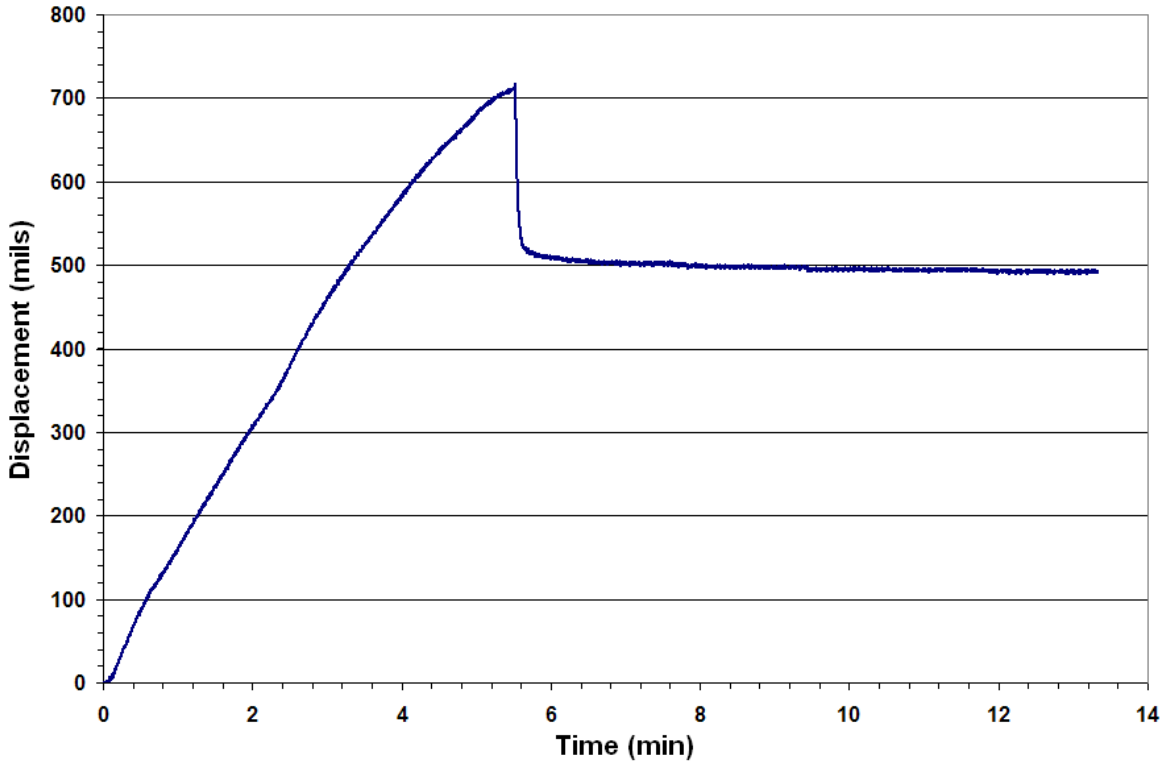

Figure 6.3. Displacement History from Monotonic Loading Test.

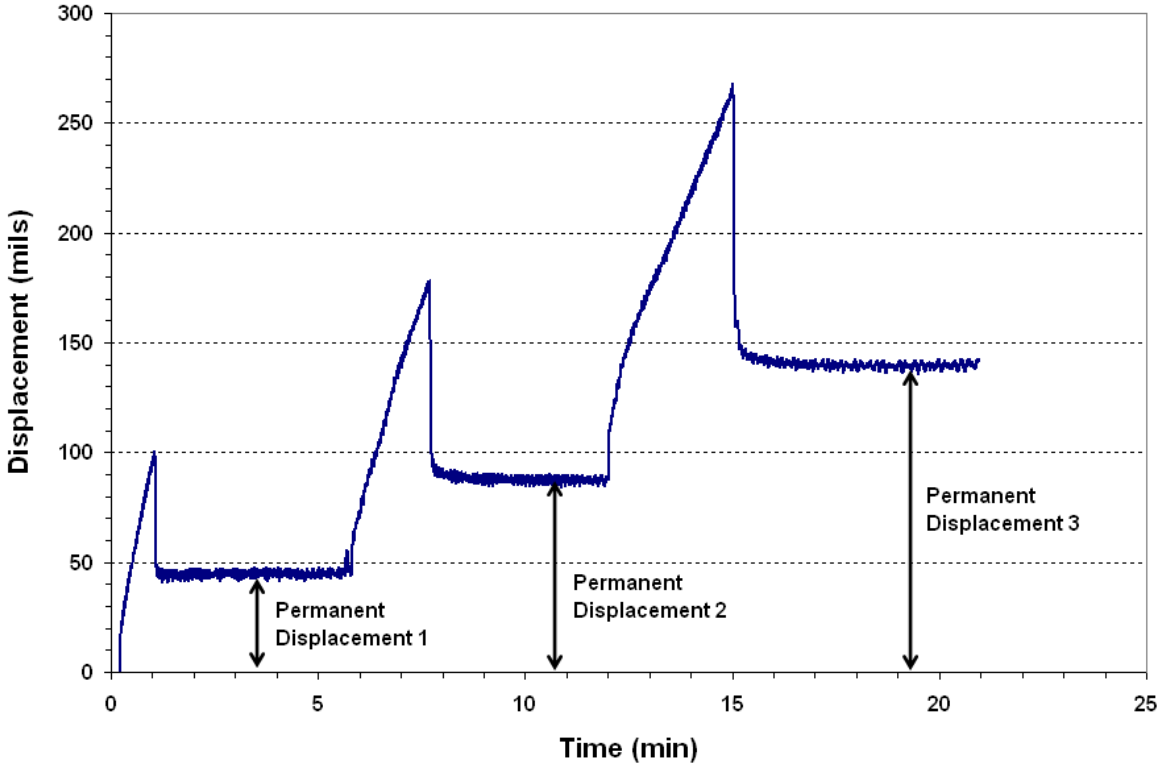

Figure 6.4. Displacement History from Step Loading Test.

Appendix D presents load-displacement curves from plate bearing tests conducted on the flexible base and stabilized sections. The load-displacement curves from tests on sections built on clay generally exhibit an initial linear phase followed by a nonlinear phase where the slope of the tangent to the curve diminishes with increasing displacement until the peak or ultimate load is reached. From that point, a reduction in load is observed with increasing displacements. In contrast, test data from sections built on sand generally exhibit a proportional relationship between load and displacement up to the peak load. In addition, tests conducted on the sand sections yielded smaller displacements compared to the measured displacements on corresponding clay sections.

ANALYSIS OF PLATE BEARING TEST DATA ON FLEXIBLE BASE SECTIONS

Figure 6.5 compares the relationships between permanent displacement and applied load from tests conducted on the thin Grade 1 crushed limestone base sections. This figure shows higher permanent deformations on the clay subgrade section, reflecting the weaker support provided by this material (as reflected in its Texas triaxial class of 6.1) compared to the sand subgrade, which has a Texas triaxial class of 3.7. Relationships such as those illustrated in Figure 6.5 provide a basis for defining allowable wheel loads based on a tolerable level of permanent displacement for one load application. Proceeding with this approach, researchers evaluated the permanent deformation behavior of the sections tested using the following permanent deformation model proposed by Tseng and Lytton (1989):

$$\delta_a = \sum_{i=1}^{n} \left[\frac{\varepsilon_{0i}}{\varepsilon_{ri}} e^{-\left(\frac{\rho_i}{N}\right)^{\beta_i}} \times \varepsilon_{vi}(h_i) \right] \qquad (6.1)$$

where,

δ_a = total permanent displacement,

$\frac{\varepsilon_{0_i}}{\varepsilon_{r_i}}, \rho_i, \beta_i$ = permanent deformation parameters for the ith pavement layer,

ε_{vi} = vertical compressive strain at a given depth within ith pavement layer,

h_i = layer thickness, and

N = number of load applications.

In the application of Eq. (6.1), the pavement is first subdivided into a total of n sublayers. Knowing the permanent deformation properties of the pavement materials and the computed

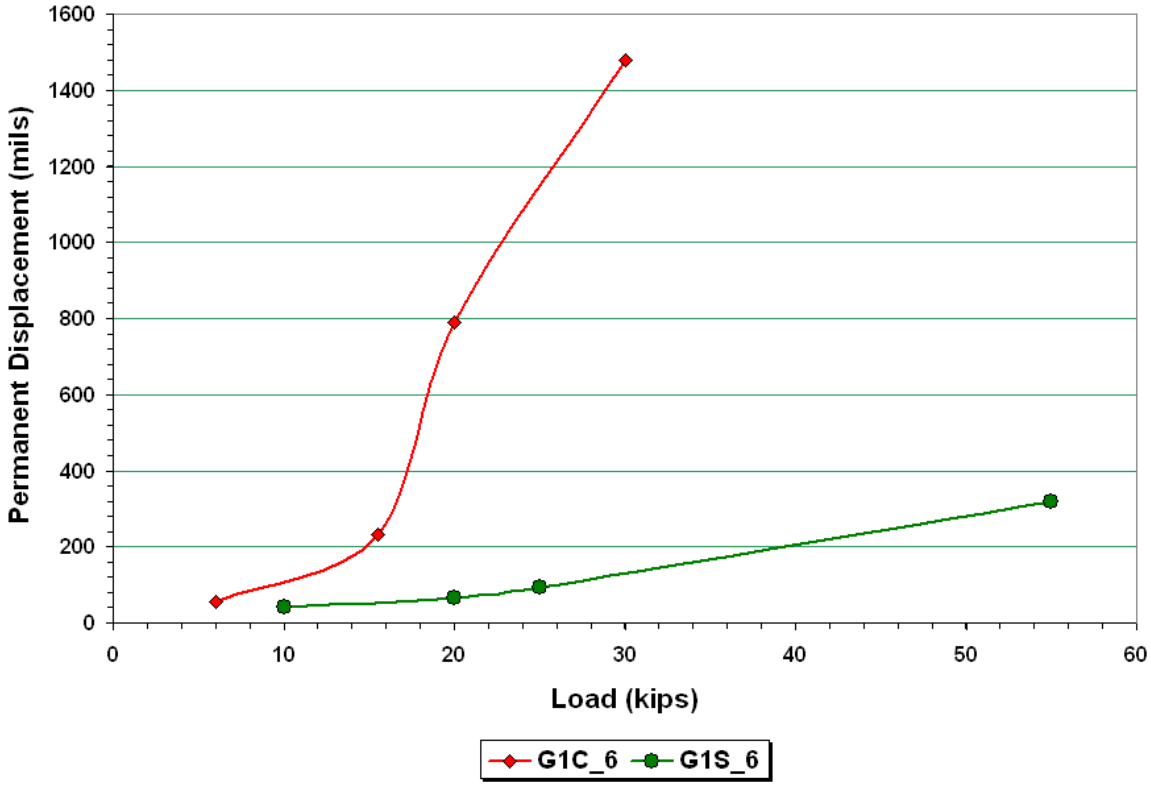

Figure 6.5. Relationships between Permanent Displacement and Load Level for Thin Grade 1 Crushed Limestone Sections on Clay and Sandy Subgrades.

vertical compressive strains at the sublayer depths underneath the load, the permanent deformation of each sublayer is then predicted and the resulting estimates are summed to determine the total permanent displacement in accordance with Eq. (6.1). Researchers used the above model with Excel's™ equation solver to backcalculate the permanent deformation parameters of the base and subgrade materials from the plate bearing test data obtained from the different sections. In this analysis, the permanent deformation properties are adjusted iteratively to minimize the sum of squared errors between the permanent displacements predicted from Eq. (6.1) at $N = 1$ and the corresponding measured values at the different load levels at which plate bearing tests were conducted. In this way, researchers evaluated the relationships between permanent deformation and load level.

Figures 6.6 and 6.7 illustrate the relationships determined for the thin flexible base sections at the clay and sandy subgrade sites, respectively. In these figures, the solid lines represent the relationships based on fitting Eq. (6.1) to the plate bearing test data, which are denoted by symbols on the charts. The results are color coded, with the fitted curve and corresponding plate bearing test data plotted with the same color for a given section.

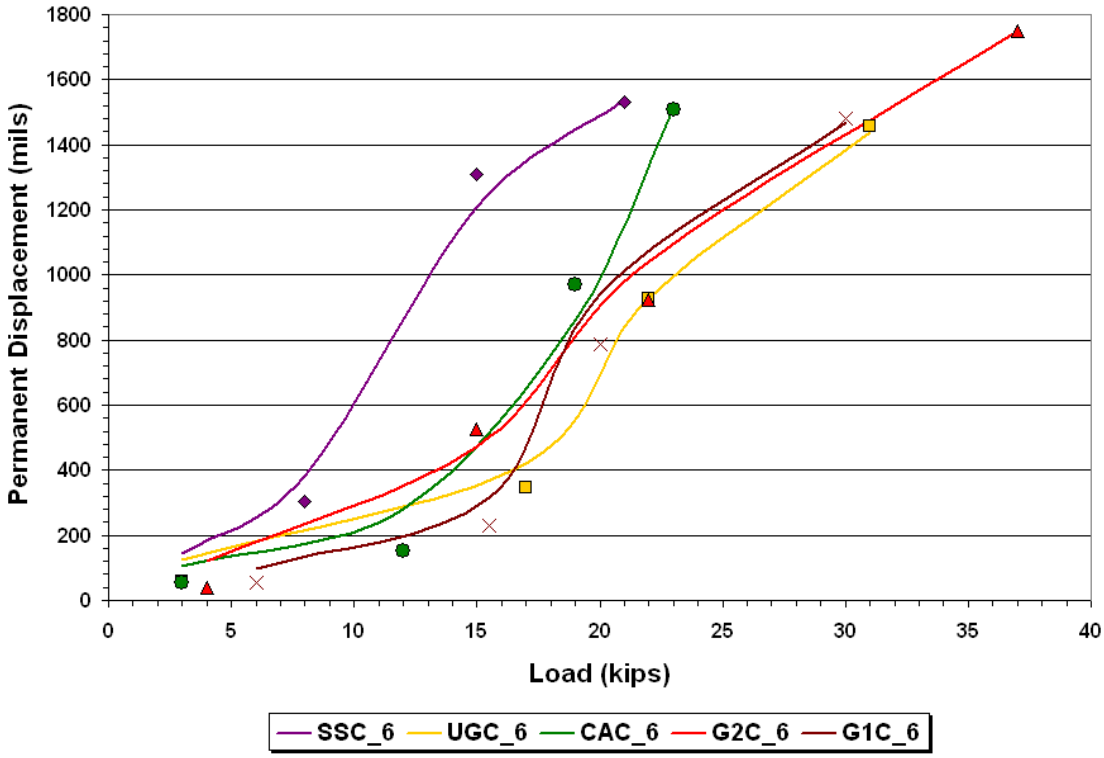

Figure 6.6. Relationships between Permanent Displacement and Load Level for Thin Flexible Base Sections on Clay Subgrade.

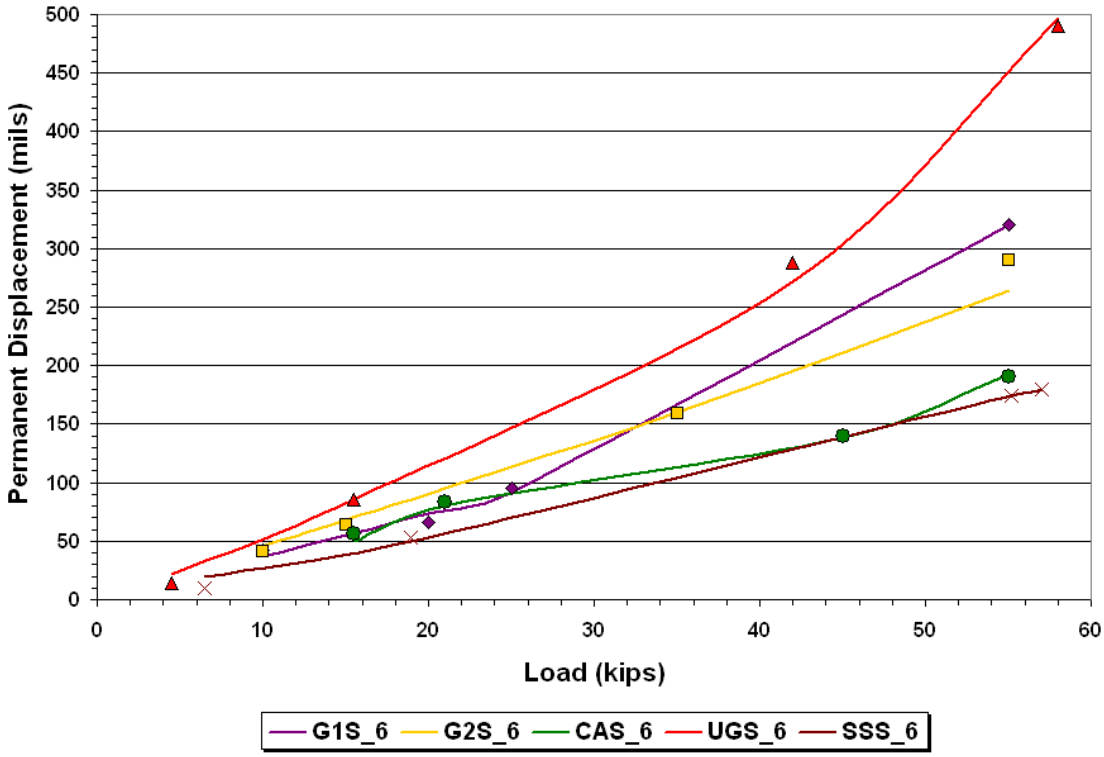

Figure 6.7. Relationships between Permanent Displacement and Load Level for Thin Flexible Base Sections on Sandy Subgrade.

To examine goodness-of-fit, the predicted permanent displacements are compared with the corresponding measurements in Figures 6.8 to 6.10. In these figures, the *x*-axis refers to the permanent displacements determined from the data on the unloading portion of the step loading test. The *y*-axis corresponds to the predictions using Eq. (6.1) with the permanent deformation properties determined from the model fitting. In the authors' opinion, the predictions compare quite favorably with the test values, particularly for the sand sections. Researchers determined the regression relationship between the predicted and measured values to quantify the agreement based on the coefficient of determination (R^2) and the root-mean-square error (RMSE). Figures 6.8 to 6.10 show these statistics. For all sections, researchers found the coefficients of determination to be close to unity. The sand sections, however, show a lower root-mean-square error of 8 mils compared to the clay sections, for which the RMSE is 56 mils.

ASSESSMENT OF TEX-117E DESIGN CURVES AGAINST PLATE BEARING TEST DATA ON FLEXIBLE BASE SECTIONS

Knowing the Texas triaxial classifications of the clay and sandy subgrade materials, and the base thickness of each section tested, researchers used the existing load-thickness design curves in TxDOT Test Method Tex-117E to determine the load bearing capacity of each pavement section. Table 6.3 presents the allowable loads determined from this calculation. Researchers note that the term "allowable load" as used herein refers to a wheel load characterized by a circular footprint of uniform pressure and of load magnitude such that the subgrade shear stresses induced under load are within the Mohr-Coulomb failure envelope of the subgrade material. The term "allowable load" is not necessarily equivalent to the "design wheel load" that refers to the wheel load used for the thickness design of a given pavement. In terms of current practice, the design wheel load shown on the *x*-axis of the flexible base design chart (Figure 2.6) refers to one of the following:

- the average of the ten heaviest wheel loads daily if the percent of tandem axles characterizing the traffic for the given design problem is less than 50 percent, or
- the ATHWLD multiplied by a load adjustment factor of 1.3 if the percent of tandem axles is equal to or greater than 50 percent.

While the allowable load and the design wheel load as used herein are based on the shear strength of the subgrade material as determined by its Mohr-Coulomb failure envelope, the difference in terminology relates to the context in which the terms are used. The design

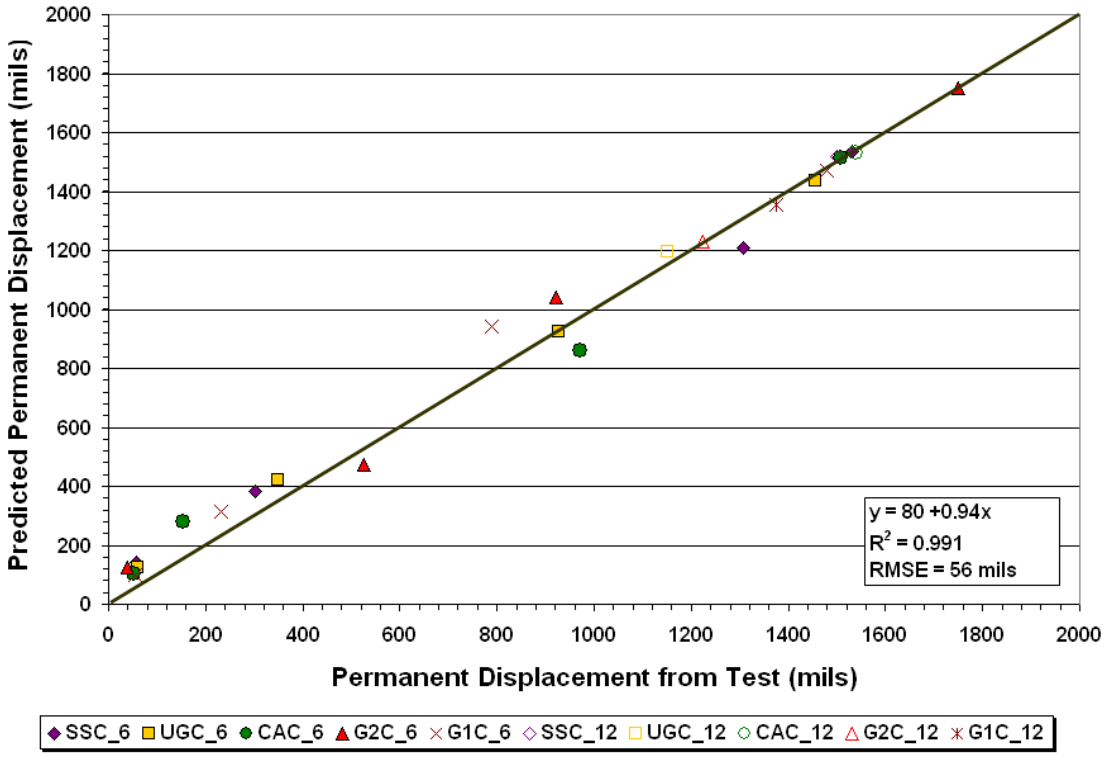

Figure 6.8. Comparison of Predicted and Measured Permanent Displacements for Flexible Base Sections on Clay.

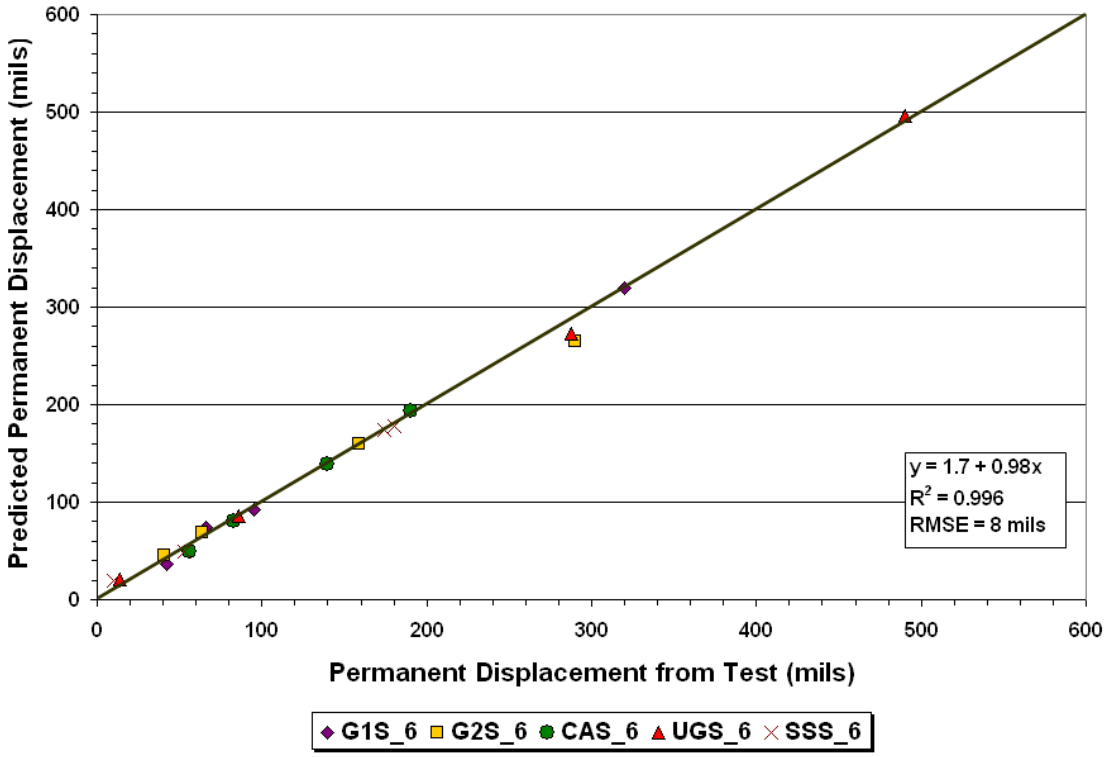

Figure 6.9. Comparison of Predicted and Measured Permanent Displacements for Thin Flexible Base Sections on Sandy Subgrade.

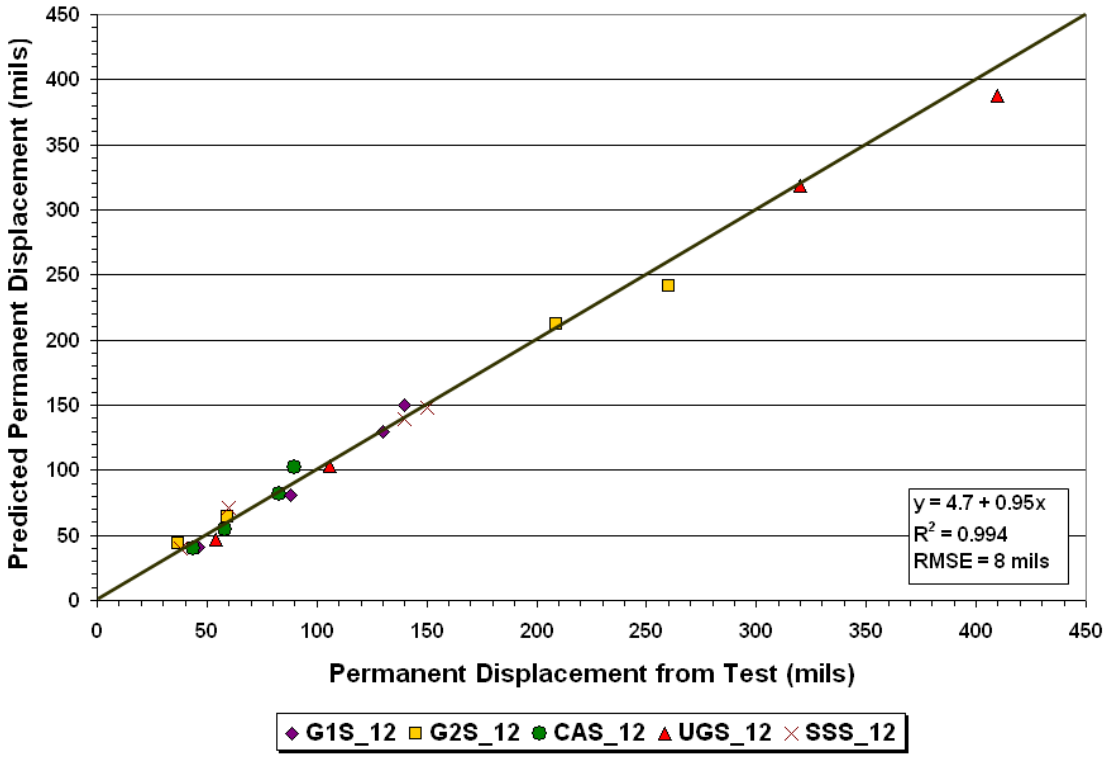

Figure 6.10. Comparison of Predicted and Measured Permanent Displacements for Thick Flexible Base Sections on Sandy Subgrade.

Table 6.3. Allowable Wheel Loads on Flexible Base Sections Based on Tex-117E Design Curves.

Clay		Sand	
Section Identifier	Tex-117E Allowable Wheel Load (kips)	Section Identifier	Tex-117E Allowable Wheel Load (kips)
SSC_6	1	SSS_6	4.6
UGC_6	1	UGS_6	4.6
CAC_6	1	CAS_6	4.6
G2C_6	1	G2S_6	4.6
G1C_6	1	G1S_6	4.6
SSC_12	2.5	SSS_12	18.2
UGC_12	2.5	UGS_12	18.2
CAC_12	2.5	CAS_12	18.2
G2C_12	2.5	G2S_12	18.2
G1C_12	2.5	G1S_12	18.2

wheel load refers to the wheel load that the engineer specifies to come up with a thickness design. On the other hand, the term "allowable load" refers to the wheel load that a given pavement can structurally support without overstressing the subgrade based on its Mohr-Coulomb failure envelope. In this report, researchers use the term "allowable load" to quantify the load bearing capacity of the sections tested in this project. This load is determined from analyzing test data collected on a given section. Given this distinction, the results from this analysis should not be misinterpreted as loads used for designing the test sections.

To verify the bearing capacity estimates from the existing design curves, researchers found it necessary to first define what constitutes failure due to one wheel load application. For example, on the thin clay sections where the Tex-117E allowable wheel load is 1 kip, what criterion does one use to determine whether or not the pavement failed due to one application of that load? In the analysis, therefore, of plate bearing test data, researchers sought to establish a realistic approach with which to verify the triaxial design curves based on the measured deformation response from the plate bearing tests done on each section. Since the design method checks the structural adequacy of a given pavement to sustain one application of the design load given by the ATHWLD, the primary failure mechanism of interest is load-associated permanent deformation, i.e., will the pavement rut under one application of the ATHWLD for the assumed condition of subgrade strength and base thickness? To answer this question, researchers used the plate bearing test results to estimate the permanent deformations associated with the allowable wheel loads given in Table 6.3. Figures 6.11 and 6.12 plot these estimates for the sections tested along with the allowable wheel loads from the current triaxial design curves. In these figures, the bars denote the Tex-117E allowable loads shown on the primary *y*-axis, while the dots connected by the dashed line denote the permanent deformation estimates shown on the secondary *y*-axis. Researchers determined the permanent deformation estimates (labeled PD_117E in the figure legends) using Eq. (6.1) with the corresponding permanent deformation properties determined from model fitting.

Given the magnitudes of the permanent deformations estimated from test data on each section, Figures 6.11 and 6.12 show that no discernable or visible rut depths are expected under the allowable loads determined from the existing Tex-117E flexible base design chart.

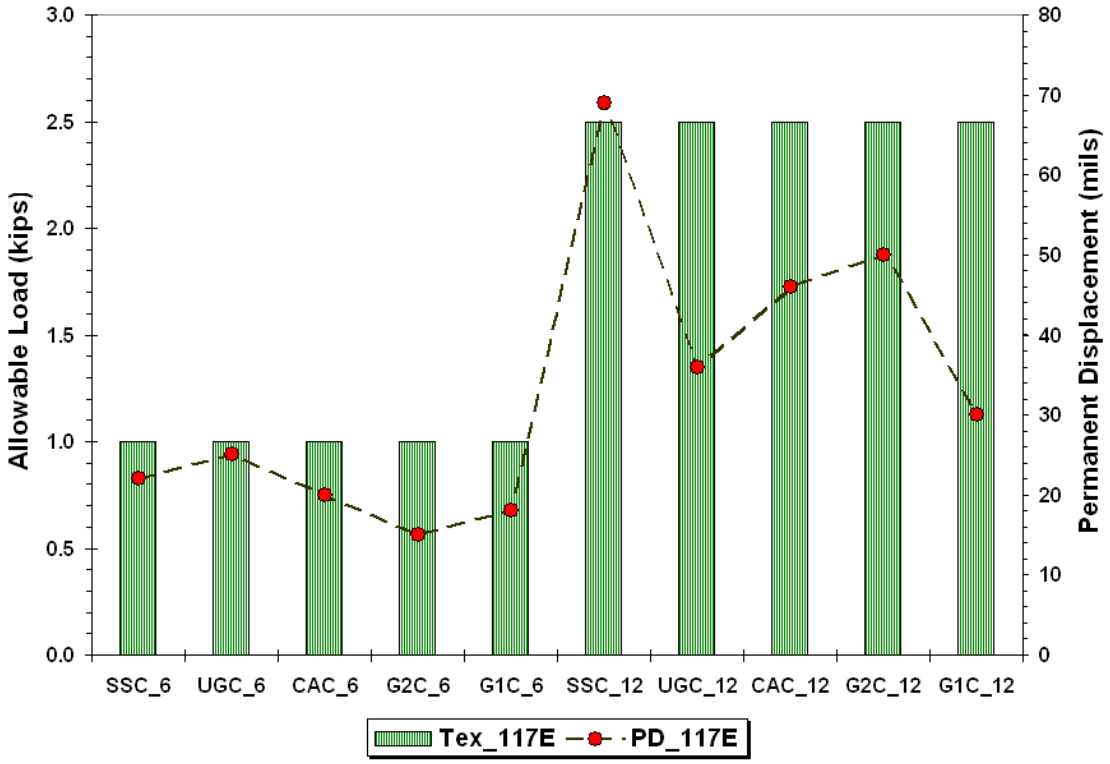

Figure 6.11. Permanent Deformations Corresponding to Tex-117E Allowable Wheel Loads for Flexible Base Sections on Clay Subgrade.

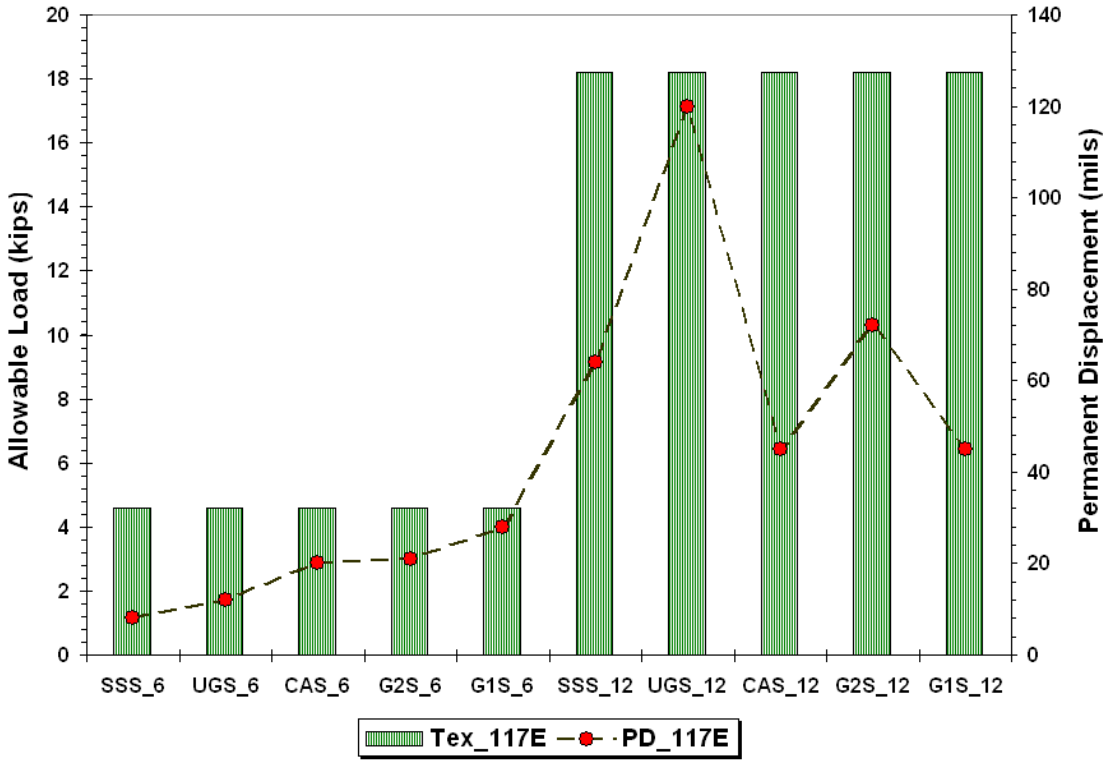

Figure 6.12. Permanent Deformations Corresponding to Tex-117E Allowable Wheel Loads for Flexible Base Sections on Sandy Subgrade.

Note that all permanent deformation estimates are below the limiting level of 0.5 inch (500 mils) typically used as a criterion to decide on the need for pavement rehabilitation based on condition survey data collected to support pavement management activities. The permanent deformations corresponding to the Tex-117E allowable wheel loads ranged from 15 to 69 mils for the flexible base sections on clay, and from 8 to 120 mils for similar sections built on sandy subgrade. These magnitudes would be hard to discern with the naked eye. From this perspective, it appears that the current triaxial design curves are rather conservative as the magnitudes of the permanent deformations are quite a bit smaller than rut depths typically used as failure criteria. The conservatism becomes more apparent when one considers that the allowable wheel loads do not include the 1.3 load adjustment factor applied to the ATHWLD when the projected truck traffic has more than 50 percent tandem axles.

Note that the permanent deformations plotted on the secondary *y*-axis in Figures 6.11 and 6.12 vary across sections with the same allowable wheel loads. This observation suggests that other factors besides the subgrade triaxial class influence the response of pavements under traffic loading. While the permanent deformations are generally under 50 mils, there are four sections (SSC_12, SSS_12, UGS_12, and G2S_12) where the estimated permanent deformations corresponding to the Tex-117E allowable loads are greater than 50 mils. Given this observation, another perspective with which to assess the current design method is to compare the allowable wheel loads from the existing triaxial design curves with the corresponding permissible loads that would produce the same level of damage on the sections tested. Figures 6.13 and 6.14 show this comparison assuming a permissible permanent displacement of 50 mils. In the charts shown, the bars with the dotted patterns denote the allowable loads based on this 50-mil criterion. Also shown are the estimated permanent deformation estimates (plotted on the secondary *y*-axis) corresponding to the Tex-117E allowable loads.

For a 50-mil permanent displacement, researchers determined the allowable wheel loads based on the relationships between permanent displacement and applied load evaluated from the plate bearing test data. From this analysis, the allowable wheel loads for SSC_12, SSS_12, UGS_12, and G2S_12 reduce to 2.0, 12.3, 6.5, and 12.5 kips, respectively, compared with the Tex-117E loads of 2.5 kips for SSC_12, and 18.2 kips for the other three sections. In the researchers' opinion, this approach of using a limiting level of permanent

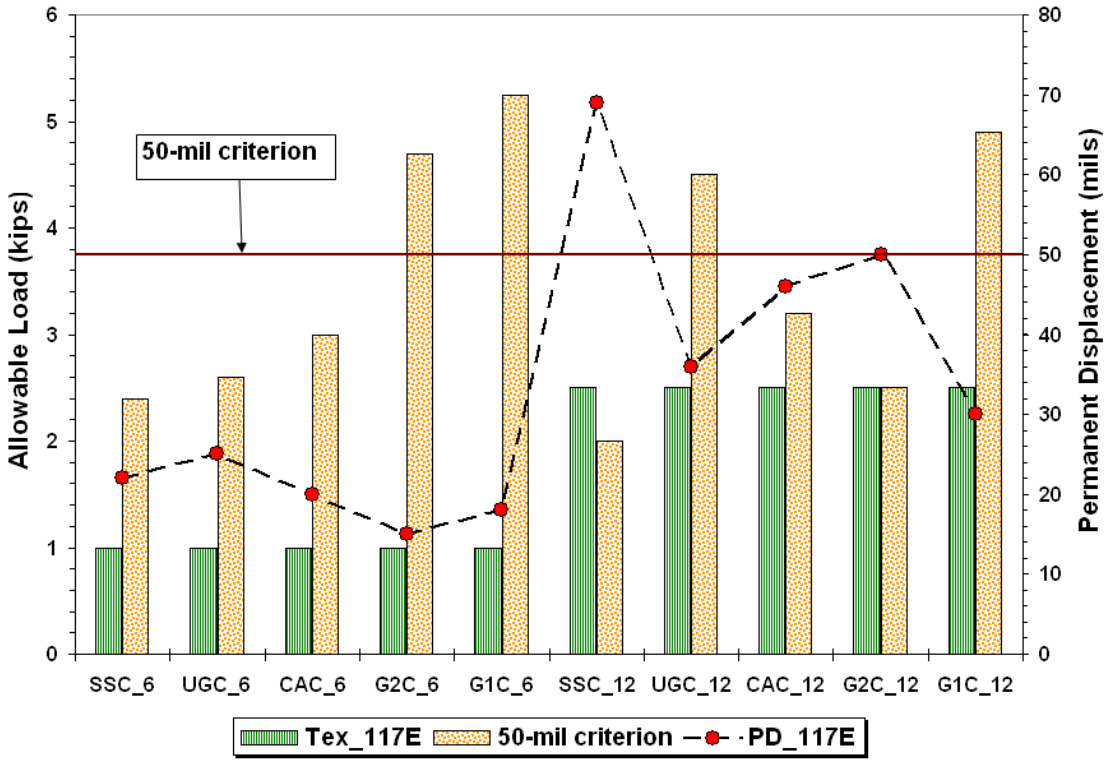

Figure 6.13. Comparison of Tex-117E Allowable Wheel Loads on Clay Sections with Corresponding Estimates based on 50-mil Limiting Permanent Displacement Criterion.

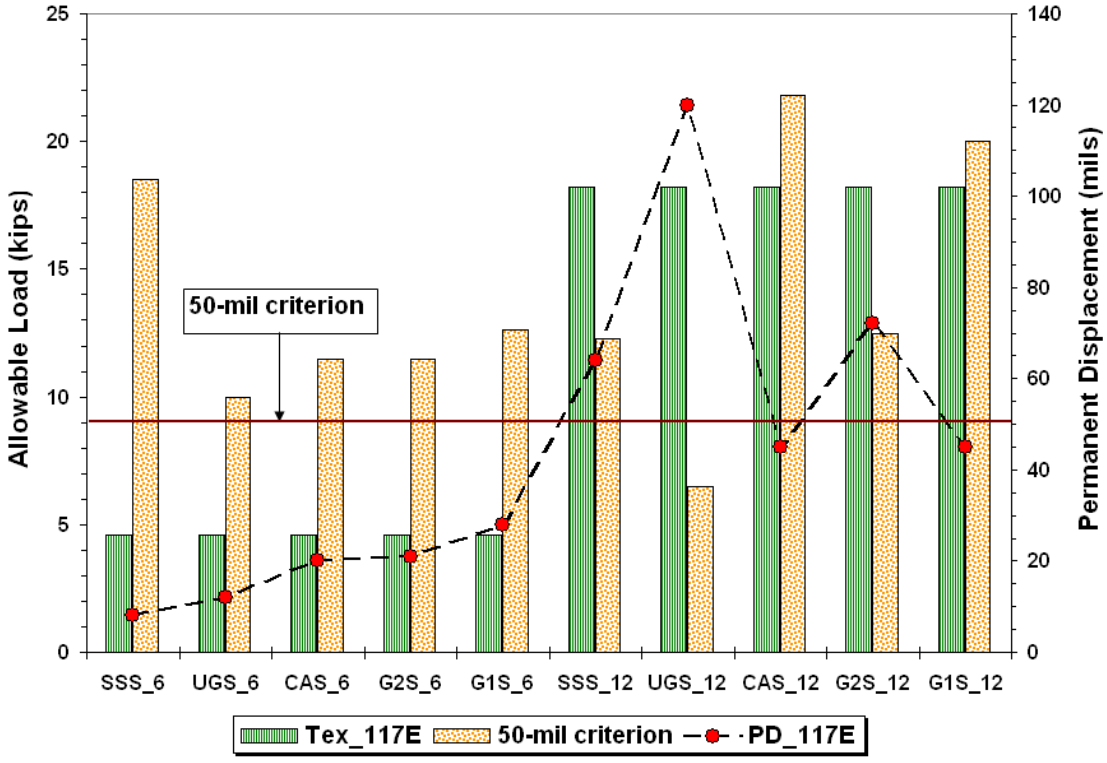

Figure 6.14. Comparison of Tex-117E Allowable Wheel Loads on Sandy Sections with Corresponding Estimates based on 50-mil Limiting Permanent Displacement Criterion.

displacement to establish pavement bearing capacity estimates presents a rational alternative to the current triaxial design method.

Researchers note that a deformation of 50 mils is hard to discern with the naked eye, and is within the range of macro-texture of pavement surfaces. For the purpose of checking whether a pavement design will fail due to one static application of the design wheel load, a 50-mil permanent displacement certainly does not amount to a "failure" condition. Researchers recognize that this approach does not consider the accumulation of permanent deformation due to repetitive loading. However, the issue of repetitive loading is outside the scope of this project, which aims to verify the existing triaxial design method that checks against subgrade shear failure due to one static application of the design wheel load. In terms of current practice, TxDOT engineers use the FPS program to design pavements for repetitive loading.

RESULTS FROM TESTS ON STABILIZED SECTIONS

Table 6.2 identifies stabilized sections on which researchers conducted plate bearing tests in Phase II of this TxDOT project. These sections replaced the thin flexible base sections placed on the clay and sandy subgrades and comprised the following stabilized materials:

- lime-stabilized uncrushed gravel (UG) base,
- cement-treated base (CTB) consisting of Grade 2 crushed limestone at two cement contents (3 percent and 4.5 percent), and
- Type D HMAC over Grade 1 crushed limestone base at two thickness levels.

Figure 6.15 illustrates the beneficial effect of lime-stabilization on pavement bearing capacity from tests conducted on untreated and lime-stabilized uncrushed gravel aggregate. The permanent displacements on the stabilized section are significantly lower than on the untreated section. Figures 6.16 and 6.17 show the relationships between permanent displacement and load level from plate bearing test data collected on stabilized sections. The sections on clay experienced more permanent displacements than the sections on sand. Similar to the evaluation done on the flexible base sections, researchers used the plate bearing test data to estimate pavement bearing capacity based on a limiting permanent displacement of 50 mils. The results from this evaluation are presented in Figure 6.18, which compare the allowable loads based on this criterion with the corresponding loads based on

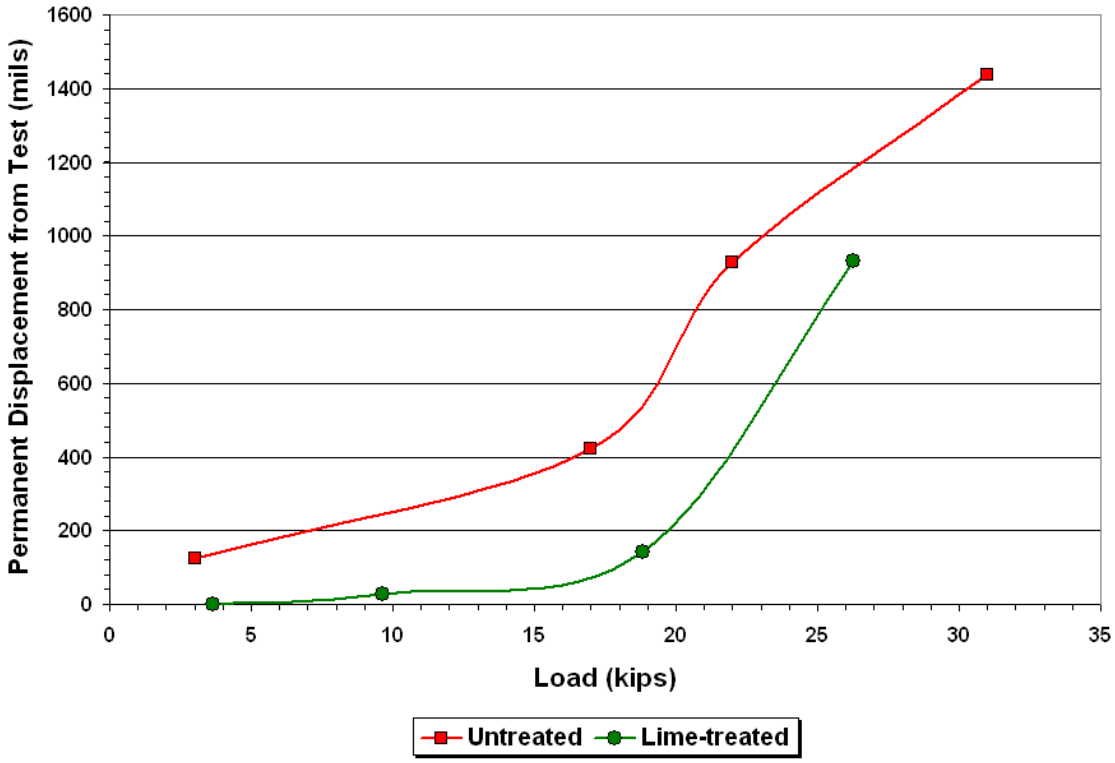

Figure 6.15. Effect of Lime Stabilization on Pavement Bearing Capacity of Sections with Uncrushed Gravel Base on Clay Subgrade.

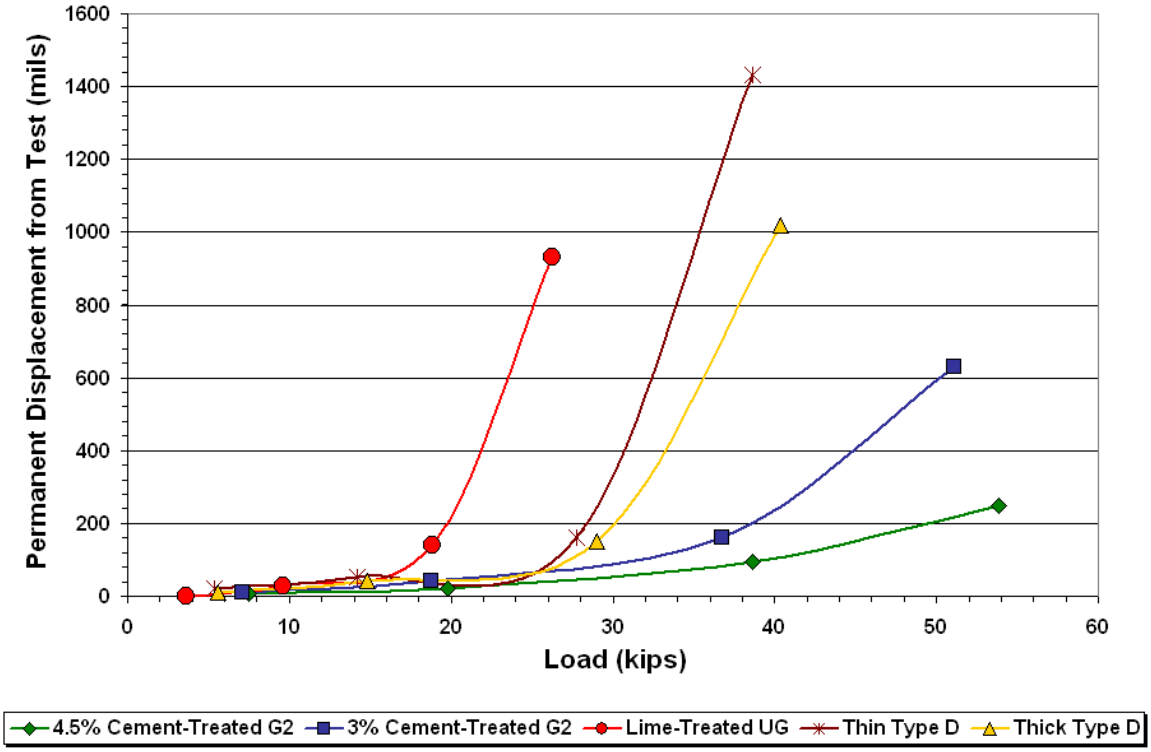

Figure 6.16. Relationships between Permanent Displacement and Load for Stabilized Sections on Clay Subgrade.

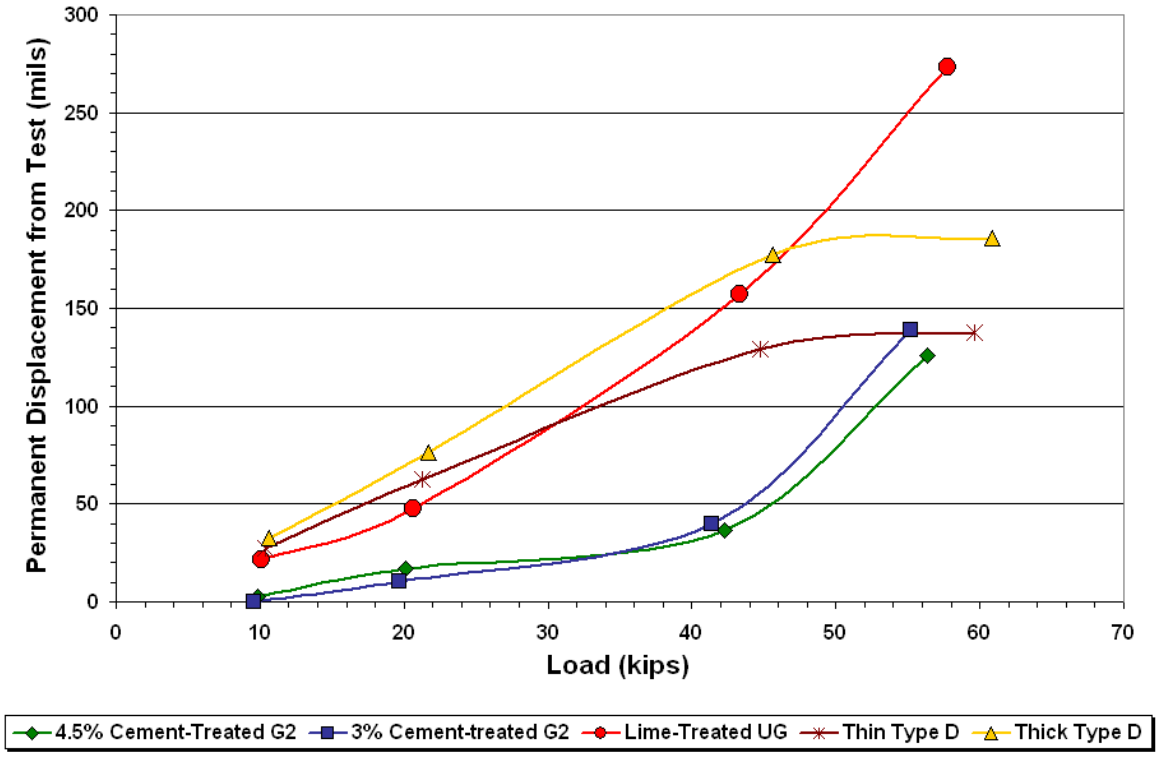

Figure 6.17. Relationships between Permanent Displacement and Load for Stabilized Sections on Sandy Subgrade.

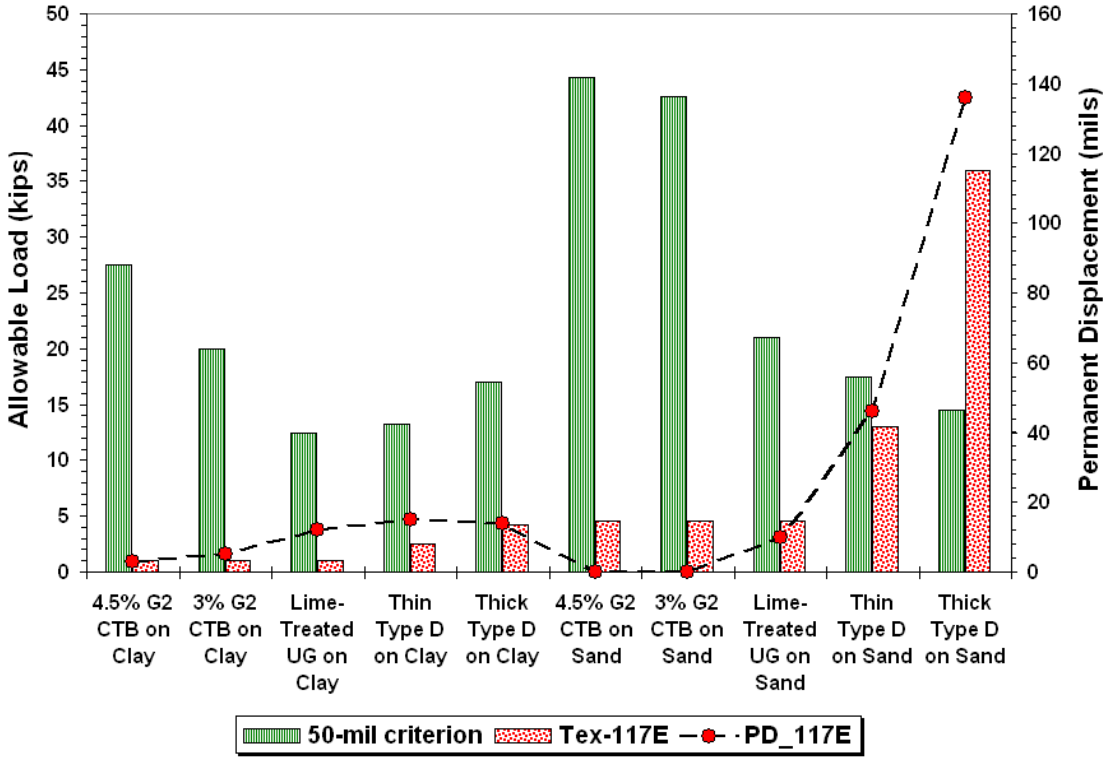

Figure 6.18. Allowable Loads from Test Data on Stabilized Sections (50-mil Limiting Permanent Displacement Criterion).

Tex-117E. For comparison, the permanent deformations (PD_117E) corresponding to the Tex-117E allowable loads are also shown on the secondary *y*-axis. In determining the allowable loads based on the existing triaxial design method, researchers considered the thickness reductions for stabilized materials as described by Fernando, Oh, Ryu, and Nazarian (2008). Except for the HMAC sections, no thickness reductions were applied for the other stabilized sections, which have base thicknesses of less than 8 inches. Researchers note that the Tex-117E thickness reduction chart does not provide reductions for depths of cover below 8 inches.

Figure 6.18 shows that the existing design method is generally too conservative for the stabilized sections tested in this project, with the exception of the thick HMAC section on the sandy subgrade, where the allowable load based on the modified triaxial design method is significantly higher than the allowable load based on a limiting permanent displacement of 50 mils. Except for the HMAC sections placed on sandy subgrade, the predicted permanent deformations corresponding to the Tex-117E allowable loads are all within 20 mils.

RESULTS FROM LABORATORY PLATE BEARING TESTS ON SMALL-SCALE PAVEMENT MODELS

The University of Texas at El Paso carried out laboratory plate bearing tests on small-scale pavement models. UTEP researchers conducted these tests on models fabricated with the same base and subgrade materials used for construction of full-scale pavement sections at the Riverside Campus. The fabrication of these models and the setup used for plate bearing tests were discussed earlier in Chapter V. Thus, only the test results are presented here. Small-scale pavement tests provided researchers the opportunity to study the effects of moisture on load bearing capacity under controlled laboratory conditions. Tables 6.4 and 6.5 show the moisture contents of the small-scale models as determined by UTEP from their tests. It is observed that the clay and caliche materials exhibited significant changes in moisture content as the models underwent moisture conditioning as compared to the other materials.

Test data conducted under different moisture conditions demonstrated the detrimental effect of moisture on the deformation response of the materials tested. This observation is illustrated in Figures 6.19 and 6.20, which show the relationships between permanent displacement and load level for Grade 2 crushed limestone specimens tested at three different moisture conditions. Similar to the analysis of data from full-scale plate bearing tests, researchers determined the loads corresponding to a permanent displacement of 50 mils using

Table 6.4. Measured Moisture Contents of Subgrade Soils from Tests on Small-Scale Pavement Models.

Small-Scale Pavement Model		Subgrade Soil Moisture Content (%)	
Subgrade Material	Base Material	Optimum	After Moisture Conditioning
Sandy	Caliche	10.6	14.7
	Grade 1 Crushed Limestone	11.6	14.8
	Grade 2 Crushed Limestone	10.7	15.2
	Sandstone	10.1	14.7
	Uncrushed Gravel	11.3	13.5
Clay	Caliche	18.3	32.7
	Grade 1 Crushed Limestone	20.5	29.4
	Grade 2 Crushed Limestone	16.9	28.9
	Sandstone	15.0	32.9
	Uncrushed Gravel	17.4	26.6

Table 6.5. Measured Moisture Contents of Base Materials from Tests on Small-Scale Pavement Models.

Subgrade Material	Model Condition	Base Moisture Content (%)				
		Caliche	Crushed Limestone		Sandstone	Uncrushed Gravel
			Grade 1	Grade 2		
Sandy	Optimum	13.2	7.5	6.1	6.1	7.0
	Moisture-Conditioned Subgrade	19.0	9.8	6.4	6.2	8.1
	Moisture-Conditioned Base/Subgrade	21.1	10.7	7.3	7.6	9.2
Clay	Optimum	11.6	7.7	7.7	6.2	6.1
	Moisture-Conditioned Subgrade	19.0	9.4	8.7	7.4	6.3
	Moisture-Conditioned Base/Subgrade.	21.3	9.9	8.9	9.5	8.8

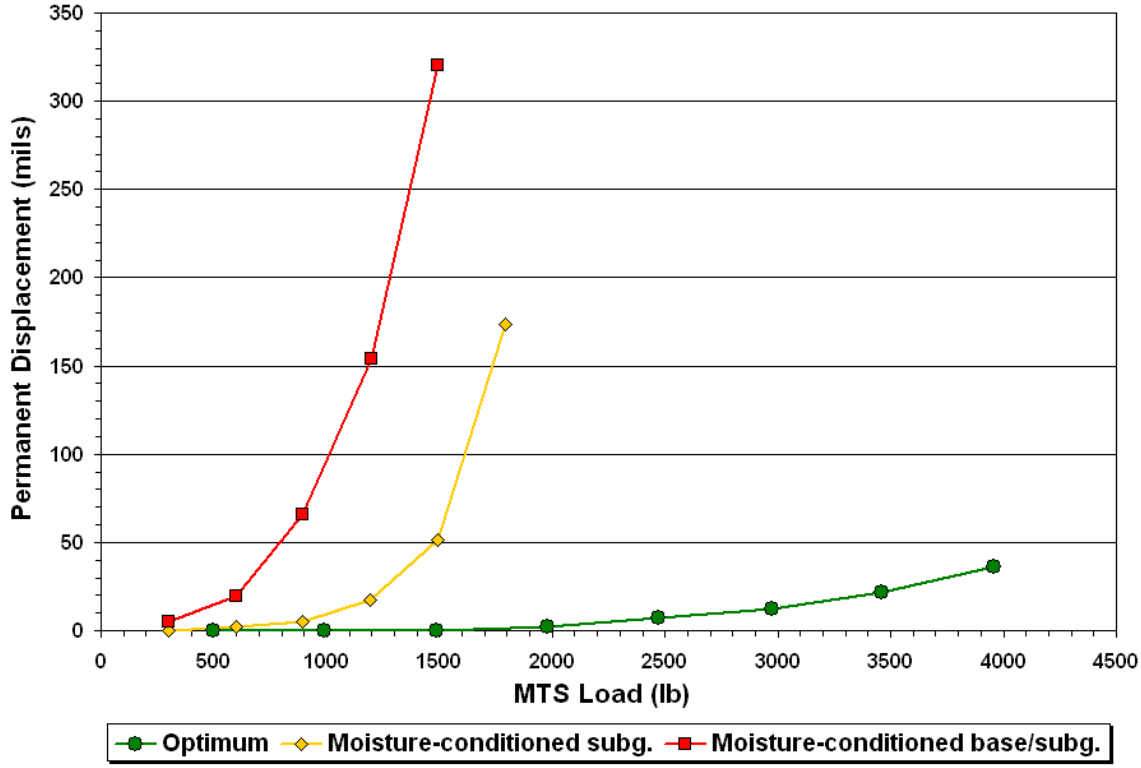

Figure 6.19. Relationships between Permanent Displacement and Load Level for Different Moisture Conditions (Grade 2 Crushed Limestone on Clay Model).

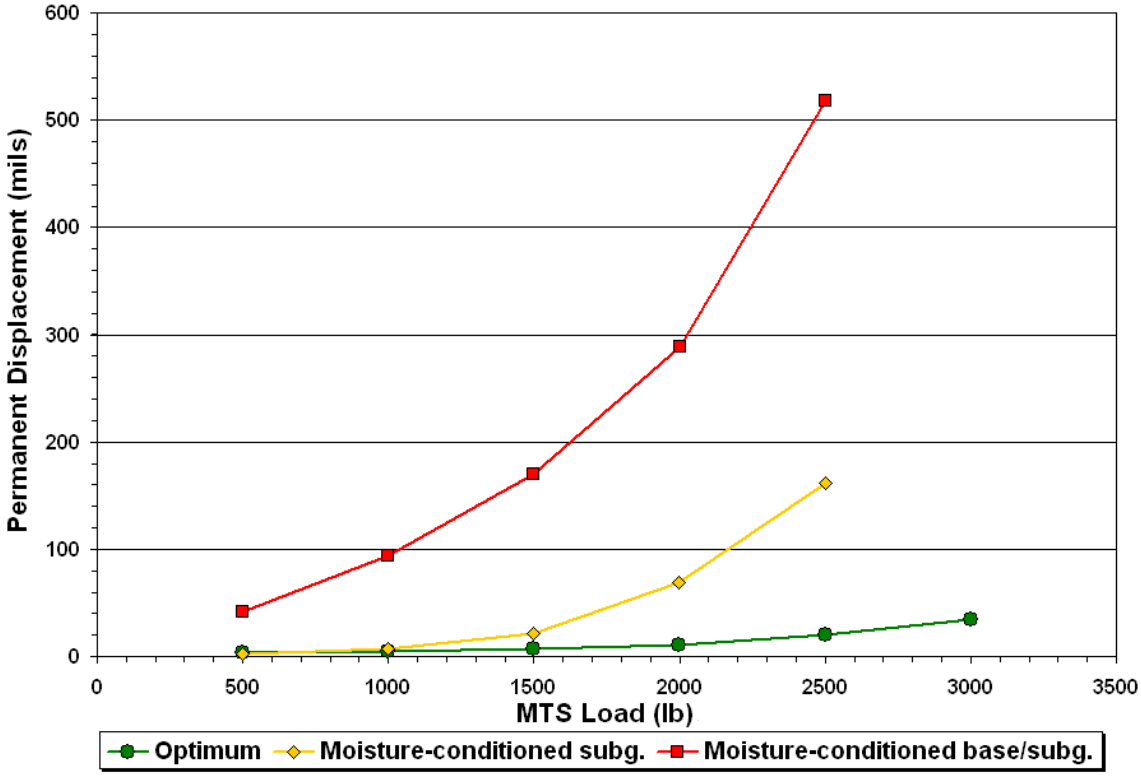

Figure 6.20. Relationships between Permanent Displacement and Load Level for Different Moisture Conditions (Grade 2 Crushed Limestone on Sand Model).

the data from small-scale pavement tests conducted at UTEP. Figures 6.21 and 6.22 show the results from these calculations. For comparison, laboratory equivalent values of allowable loads based on the current triaxial design curves are also shown on the charts. These values were determined by dividing the Tex-117E allowable loads by 4 corresponding to the ratio of the loaded areas between full-scale and small-scale testing, following similitude rules.

Figure 6.21 shows drastic reductions in load bearing capacity between optimum moisture and after moisture conditioning of the subgrade for small-scale models where the base materials are placed on clay. On the sand specimens, the reductions in load bearing capacity are not as dramatic (Figure 6.22), reflecting lesser susceptibility to moisture in the sandy subgrade material compared to the clay. The results shown in Figures 6.21 and 6.22 suggest that the best use of premium base materials is on subgrades that exhibit less moisture susceptibility and better strength properties as characterized by the subgrade triaxial class or the shear failure envelope. It is also of interest to note that the laboratory equivalent Tex-117E loads are more comparable with the results from tests after moisture conditioning of the base and subgrade materials, particularly for the small-scale models where clay was used as the subgrade. This observation reflects the high degree of conservatism in the current test method. In the authors' opinion, the observed differences in the load bearing capacities at various moisture conditions suggest the need to properly account for these effects in the existing triaxial design method, considering the range of climatic and soil conditions found across the state. Modifications made by researchers to account for moisture effects in the existing method for checking FPS-generated flexible pavement designs are documented in the companion report to this project by Fernando, Oh, Ryu, and Nazarian (2008).

OBSERVATIONS FROM TRENCHING FULL-SCALE PAVEMENT SECTIONS

Researchers cut trenches on the flexible base sections after completion of plate bearing tests to identify the layer in which failure originated. This determination was accomplished by examining the pavement cross-sections underneath the plate bearing test locations at which trenches were cut. Figure 6.23 shows a picture of the pavement cross-section taken at the uncrushed gravel base trench. This figure indicates that failure started in the clay subgrade as evident in the bowl-shaped deformation of the clay soil underneath the tested area.

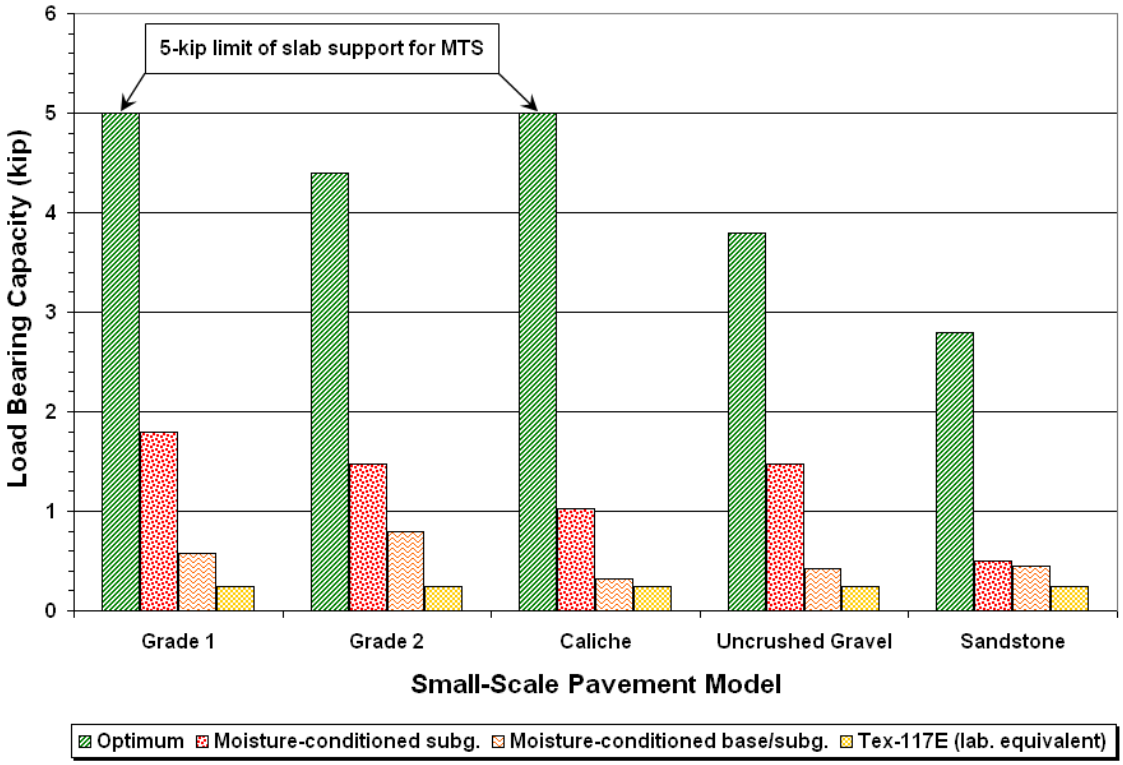

Figure 6.21. Variation of Load Bearing Capacity with Moisture Condition from Small-Scale Tests of Models with Base Materials on Clay.

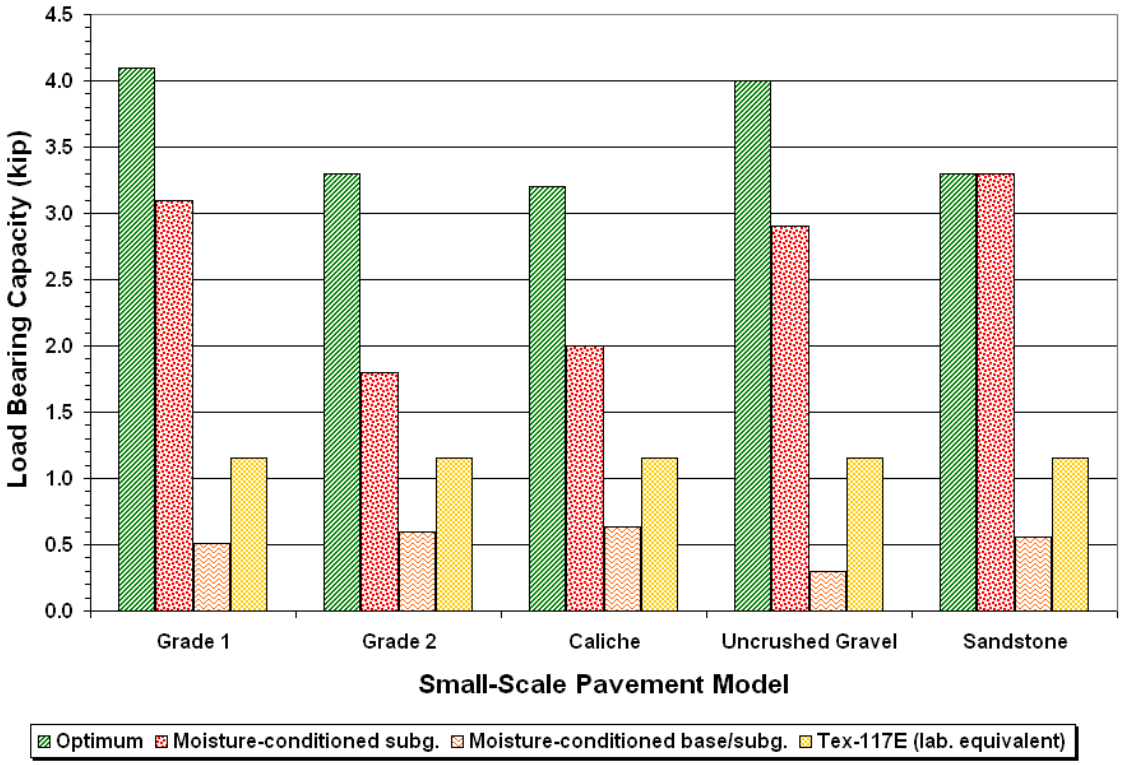

Figure 6.22. Variation of Load Bearing Capacity with Moisture Condition from Small-Scale Tests of Models with Base Materials on Sandy Subgrade.

Figure 6.23. View of Pavement Cross-Section at the Uncrushed Gravel Base Trench.

To establish the cross-sectional profiles, researchers laid out a straightedge across the width of the trench and took elevation measurements as illustrated in Figure 6.23. The resulting cross-sectional profiles from these measurements are given in Figures C29 to C38 in Appendix C. The shaded oval-shaped area on each chart in the appendix indicates the location of the plate bearing test. From examination of the cross-sectional profiles, one observes a noticeable bowl-shaped deformation at the top of the clay subgrade on each tested section. These observations suggest that failure originated from the subgrade for tests done on flexible base sections at the clay site. In the authors' opinion, this finding is consistent with the existing triaxial design method in the sense that it implies the need to minimize stresses in the subgrade as a criterion for pavement design, which is the philosophy behind the development of the existing Tex-117E flexible base design chart.

Researchers also made similar efforts to trench the sand sections to establish where failure originated, as was done at the clay site. However, for the sand sections, it was difficult to distinguish the base/subgrade interface due to the smearing that occurs as the trench is cut and because the sandy material blends in with the flexible base and does not provide a sharp contrast unlike the clay subgrade. Thus, it was not possible to establish whether failure originated on the sandy subgrade for these sections.

CHAPTER VII. SUMMARY OF FINDINGS AND RECOMMENDATIONS

A major objective of this project was to verify the load-thickness design chart in Test Method Tex-117E that is used by TxDOT engineers to check flexible pavement designs from the Department's FPS program. To carry out this investigation, researchers executed a comprehensive work plan that included:

- a literature review of the modified triaxial design method,
- development and execution of a plan to verify the load-thickness design curves based on testing full-scale field sections and small-scale pavement specimens,
- investigation of the correspondence between small-scale and full-scale pavement test results,
- analysis of plate bearing test data to evaluate the deformation response of field sections and small-scale laboratory specimens, and
- assessment of the existing load-thickness design curves against plate bearing test results.

Based on the research conducted, the following findings are noted:

- From the literature review, researchers verified the method used by McDowell to develop the existing triaxial design curves. This method is based on a stress analysis to establish the depth of cover required to keep the load induced stresses in the subgrade within the material's failure envelope (as defined by its Texas triaxial class). The computation of wheel load stresses for deriving the thickness design curves was done using layered elastic theory along with certain assumptions McDowell made regarding the variation of modular ratios with depth. Researchers demonstrated the methodology by re-creating the existing load-thickness design curves in this report.
- As originally developed, the mechanism of fatigue from repetitive loading was not included as a criterion in the determination of the thickness design curves. It was after the development of the flexible base design chart that McDowell came up with an approximate procedure to consider the effect of repetitive loading on the thickness design through the introduction of a load-frequency design factor. In this regard, McDowell evaluated the correlation between observed service lives of pavement test sections and their depth design ratios. The correlations showed a fair amount of

scatter in the data, and did not, in the authors' opinion, reasonably differentiate between good- versus poor-performing test sections. Considering that the load-thickness design curves are based on a theoretical analysis of the required depth of cover to prevent subgrade shear failure due to the static application of one design wheel load, TxDOT's current practice of using FPS to design for repetitive loading and using Tex-117E as a design check on FPS without the load-frequency adjustment is, in the researchers' opinion, a more appropriate application of the load-thickness design curves that is consistent with their original derivation.

- The thickness reduction chart for stabilized layers is based on the design equation formulated by Hveem and Carmany (1948) for the California Division of Highways. In developing the chart for the Texas triaxial design method, McDowell revised the linear relationships derived from Hveem and Carmany's equation such that reductions are applied only for depths of cover of 8 inches or greater.

Based on the findings from the literature review, researchers established a field and laboratory test program to verify the load-thickness design curves in the modified Texas triaxial design method. Considering that the current method is based on a theoretical analysis of allowable wheel loads using layered elastic theory, researchers conducted plate bearing tests on full-scale field sections, given that the load configuration for this test most closely approximates the assumptions used in developing the existing design curves. A total of 30 full-scale pavement sections were constructed within the Riverside Campus of Texas A&M University for the purpose of conducting plate bearing tests. In addition, UTEP researchers conducted laboratory tests on small-scale pavement models fabricated with the same base and subgrade materials used on the full-scale field sections. Based on the analyses of data derived from these tests, the authors note the following findings:

- When the small-scale specimens are carefully constructed to achieve approximate densities and moisture contents as existing pavement sections, the predicted deformation responses from numerical models exhibit trends similar to the observed results but with magnitudes that differ by about a factor of 2 from the test data. The differences appear to be systematic indicating that numerical models can be properly calibrated using small-scale test results. In addition, researchers found reasonable agreement between the load-deformation responses of corresponding small-scale specimens and full-scale pavement sections after adjusting for scale effects based on

similitude rules. In the researchers' opinion, these findings demonstrate that small-scale tests can be effectively used along with full-scale experiments to verify existing models or design procedures under different conditions.

- Small-scale tests carried out under different moisture conditions demonstrated the detrimental impact of moisture on the deformation response of small-scale pavement models fabricated with the same base and subgrade materials used on the full-scale pavement sections tested in this project. In particular, test results showed drastic reductions in load bearing capacity between optimum moisture and subgrade saturated conditions for specimens with base materials placed on clay. On the sand specimens, the reductions in load bearing capacity were not as dramatic, reflecting lesser susceptibility to moisture in the sandy subgrade material compared to the clay. The small-scale test results suggest that the best use of premium base materials is on subgrades that exhibit less moisture susceptibility and better strength properties as characterized by the subgrade triaxial class or the shear failure envelope. The authors also note that the laboratory equivalent Tex-117E loads were more comparable with the results from tests where both base and subgrade are moisture-conditioned, particularly for the clay subgrade models. This observation reflects the high degree of conservatism in the current test method.
- Researchers used the existing triaxial design curves in TxDOT Test Method Tex-117E to determine the load bearing capacity of each pavement section tested at the Texas A&M Riverside Campus. To verify the bearing capacity estimates from the existing design curves, researchers used the plate bearing test results to estimate the permanent deformations associated with the allowable wheel loads from Tex-117E. The permanent deformations determined from this analysis range from 15 to 69 mils for the flexible base sections on clay, and from 8 to 120 mils for similar sections built on sandy subgrade. These magnitudes would be hard to discern with the naked eye, and are all below the the limiting level of 0.5 inch (500 mils) typically used as a criterion to decide on the need for pavement rehabilitation based on condition survey data collected to support pavement management activities. From this perspective, it appears that the current triaxial design curves are rather conservative as used for the purpose of checking the structural adequacy of a given pavement to sustain one application of the design load. The conservatism becomes more apparent when one

considers that the allowable wheel loads do not include the 1.3 load adjustment factor applied to the ATHWLD when the projected truck traffic has more than 50 percent tandem axles.

- The data analysis also showed that permanent deformations vary across sections with the same allowable wheel loads based on the current triaxial design curves. This finding reflects the fact that the base material is not directly considered as a design variable in the existing method. Indeed, the literature review revealed that the load-thickness design relationships originally included base modulus as a design variable. However, for the possible reasons cited in Chapter II of this report, it was later removed as a factor in the load-thickness design curves. In its place, McDowell assumed modular ratios that varied with depth in developing the existing triaxial design chart. The design curves are therefore tied to these assumptions, which do not vary with base type.
- Test data obtained from the uncrushed gravel base sections showed the beneficial effect of lime stabilization on pavement bearing capacity. The permanent displacements on the stabilized section were significantly lower than on the untreated section. The data analysis showed that the existing design method is generally too conservative for the stabilized sections tested in this project, with the exception of the thick HMAC section on the sandy subgrade, where the allowable load based on the modified triaxial design method is significantly higher than the allowable load based on a limiting permanent displacement of 50 mils. Except for the HMAC sections placed on sandy subgrade, the predicted permanent deformations corresponding to the Tex-117E allowable loads are all within 20 mils.
- The cross-sectional profiles determined from trenches dug at the clay sections showed a noticeable bowl-shaped deformation of the clay subgrade after testing. These observations suggest that failure originated from the subgrade for tests done on flexible base sections at the clay site. In the authors' opinion, this finding is consistent with the existing triaxial design method in the sense that it implies the need to minimize stresses in the subgrade as a criterion for pavement design, which is the philosophy behind the development of the existing load-thickness design chart. For the sand sections, it was difficult to distinguish the base/subgrade interface due to the smearing that occurs as the trench is cut and because the sandy material blends in with

the flexible base and does not provide a sharp contrast unlike the clay subgrade. Thus, it was not possible to establish whether failure originated on the sandy subgrade for these sections.

Considering the findings from the verification of the triaxial design curves presented in this report, researchers offer the following recommendations to improve the triaxial design check presently implemented under Tex-117E:

- The stress analysis McDowell did to develop the existing triaxial design chart can now be made with more sophisticated computer programs that permit engineers to model more realistically the actual materials comprising a given pavement, or the materials that the engineer considers using for a given design. In view of the advances in pavement analysis tools since the time the triaxial design curves were originally developed, researchers recommend that the stress analysis embedded in the existing triaxial design method be implemented in a layered elastic computer program. In this regard, the modified triaxial (MTRX) program developed by Fernando et al. (2001) offers a suitable starting point for developing this computerized stress-based procedure. This work would require modifications to MTRX to incoporate the findings from this research project.
- The findings from field and laboratory tests conducted in this project verified the conservatism in the existing design method that has been previously recognized by TxDOT engineers. For the near term, researchers recommend that TxDOT consider dropping the load adjustment factor of 1.3 from the existing design method. If an analysis of wheel load stresses under tandem axles is required in the design check, such an analysis can be accomplished more realistically with the computerized stress-based analysis procedure proposed by researchers. Additionally, TxDOT's current practice of using FPS to design for repetitive loading and using Tex-117E as a design check on FPS without the load-frequency adjustment should be continued (for the near term).
- The observed differences in load bearing capacities at various moisture conditions from tests done on small-scale pavement specimens suggest the need to properly account for moisture effects and differences in moisture susceptibilities between different soils. This change in the existing triaxial design method should consider the range of climatic and soil conditions found across Texas and provide TxDOT

engineers the option to conduct the triaxial design check for other than the worst moisture condition. Recognizing the regional variations in soils and moisture conditions across Texas can help TxDOT engineers establish cost-effective pavement designs for the given local conditions.

The recommendations presented are addressed by researchers in the companion report by Fernando, Oh, Ryu, and Nazarian (2008) that documents the work done to improve the existing design method based on the findings presented in this report. This work led to the development of a computer program for checking flexible pavement designs from FPS that uses the same approach followed by McDowell in developing the original design curves but provides engineers with greater versatility in modeling flexible pavement systems and axle configurations in the stress analysis. This computer program also includes a database of soil properties covering each of the 254 Texas counties for evaluating the effects of moisture changes on soil strength properties and to account for effects of differences in moisture susceptibilities among soils in the triaxial design check. The computer program *LoadGage* is described in the *LoadGage User's Manual* prepared by Fernando, Oh, and Liu (2007).

REFERENCES

AASHO Road Test: Report 5 – Pavement Research. Highway Research Board Special Report 61E, 1962.

Abdallah, I., A. Meshkani, D. Yuan, and S. Nazarian. *Design Program Using Seismic Moduli*. Research Report 1780-4, Center for Highway Materials Research, The University of Texas at El Paso, El Paso, Tex., 2002.

Amiri, H. *Impact of Moisture Variation on Stiffness Response of Pavements through Small Scale Models*. M.S. Thesis, The University of Texas at El Paso, El Paso, Tex., 2004.

Baker, M. R., K. Crain, and S. Nazarian. *Determination of Pavement Thickness with a New Ultrasonic Device*. Research Report 1966-1, Center for Highway Materials Research, The University of Texas at El Paso, El Paso, Tex., 1995.

Bulut, R., R. L. Lytton, and W. K. Wray. *Suction Measurements by Filter Paper*. Expansive Clay Soils and Vegetative Influence on Shallow Foundations, ASCE Geotechnical Special Publication No. 115 (eds. C. Vipulanandan, M. B. Addison, and M. Hasen), American Society of Civil Engineers, Reston, Va., pp. 243-261, 2001.

De Jong, D. L., M. G. F. Peutz, and A. R. Korswagen. *Computer Program BISAR*. External Report, Koninklijke/Shell-Laboratorium, The Netherlands, 1973.

Desai, M., and S. Nazarian. *Automated Surface Wave Method: Field Testing*. Journal of Geotechnical Engineering, American Society of Civil Engineers, Vol. 119, No. 7, pp 1094-1111, 1993.

Fernando, E. G., D. R. Luhr, and H. N. Saxena. *The Development of a Procedure for Analyzing Load Limits on Low-Volume Roads*. Fourth International Conference on Low-Volume Roads, Vol. 1, Transportation Research Record 1106, Transportation Research Board, Washington, D.C., 1987, pp. 145-156.

Fernando, E. G., W. Liu, T. Lee, and T. Scullion. *The Texas Modified Triaxial (MTRX) Design Program*. Research Report 1869-3, Texas Transportation Institute, The Texas A&M University System, College Station, Tex., 2001.

Fernando, E. G., J. Oh, and W. Liu. *LoadGage User's Manual*. Product 0-4519-P3, Texas Transportation Institute, The Texas A&M University System, College Station, Tex., 2007.

Fernando, E. G., J. Oh, D. Ryu, and S. Nazarian. *Consideration of Regional Variations in Climatic and Soil Conditions in the Modified Triaxial Design Method*. Research Report 0-4519-2, Texas Transportation Institute, The Texas A&M University System, College Station, Tex., 2008.

Flexible Pavement Design Correlation Study. Bulletin 133, Highway Research Board, Washington, D.C., 1956.

Freitag, D. R. *A Dimensional Analysis of the Performance of Pneumatic Tires on Soft Soils*. Ph.D. Thesis, Auburn University, Auburn, Ala., 1965.

Gardner, W. R. *Some Steady State Solutions of the Unsaturated Moisture Flow Equation with Application of Evaporation from a Water Table*. Soil Science, Vol. 85, pp. 223-232, 1958.

Highway Research Board. *Current Road Problems: Thickness of Flexible Pavements*. Bulletin No. 8-R, Highway Research Board, Washington, D.C., 1949.

Hilbrich, S., and T. Scullion. *A Rapid Alternative for Lab Determination of Resilient Modulus Input Values for the AASHTO M-E Design Guide*. Paper presented at the Transportation Research Board Annual Meeting, Washington, D.C., 2007.

Hveem, F. N., and R. M. Carmany. *The Factors Underlying the Rational Design of Pavements*. Proceedings, 28th Annual Meeting of the Highway Research Board, Washington, D.C., pp. 101-136, 1948.

Kim, S. M., F. Hugo, and J. M. Roesset. *Small-scale Accelerated Pavement Testing*. Journal of Transportation Engineering, Vol. 124, Issue 2, pp. 117-122, 1998.

Lytton, R. L., D. E. Pufahl, C. H. Michalak, H. S. Liang, and B. J. Dempsey. *An Integrated Model of the Climatic Effects on Pavement*. Report No. FHWA-RD-90-033, Texas Transportation Institute, The Texas A&M University System, College Station, Tex., 1990.

McDowell, C. *Adaptation of Triaxial Testing to Flexible Pavements and Bridge Foundatons*. 23rd Annual Highway Short Course, College Station, Tex., 1949.

McDowell, C. *Triaxial Tests in Analysis of Flexible Pavements*. Research Report 16-B, Highway Research Board, Washington, D.C., 1954, pp. 1-28.

McDowell, C. *Wheel-Load-Stress Computations Related to Flexible Pavement Design*. Bulletin 114, Highway Research Board, Washington, D.C., 1955, pp. 1-20.

McDowell, C. *Road Test Findings Utilized in Analysis of Texas Triaxial Method of Pavement Design*. Highway Research Board Special Report 73, The AASHO Road Test: Proceedings of a Conference held May 16-18, 1962, St. Louis, Mo., pp. 314-386.

Michalak, C. H., and T. Scullion. *MODULUS 5.0: User's Manual*. Research Report 1987-1, Texas Transportation Institute, The Texas A&M University System, College Station, Tex., 1995.

Nazarian, S., M. R. Baker, and K. Crain. *Fabrication and Testing of a Seismic Pavement Analyzer*. SHRP Report H-375, Strategic Highway Research Program, National Research Council, Washington, D.C., 1993.

Nazarian, S., R. Pezo, B. Melarkodi, and M. Picornell. *Testing Methodology for Resilient Modulus of Base Materials*. Transportation Research Record 1547, Transportation Research Board, Washington, D. C., pp. 46-52, 1996.

Nazarian S., D. Yuan, V. Tandon, and M. Arellano. *Quality Management of Flexible Pavement Layers with Seismic Methods*. Research Report 1735-3F, Center for Highway Materials Research, The University of Texas at El Paso, Tex., 2002.

Rocha, M. *Similarity Conditions in Model Studies of Soil Mechanics Problems*. Laboratoria Nacional de Engenharia, Publication No. 35, Lisbon, Portugal, 1953.

Rocha, M. *The Possibility of Solving Soil Mechanics Problems by the Use of Models*. Proceedings of the 4th International Conference on Soil Mechanics, London, 1957.

Roscoe, K. H., and H. B. Poorooshasb. *A Fundamental Principle of Similarity in Model Tests for Earth Pressure Problems*. Proceedings of 2nd Asian Conference on Soil Mechanics, Tokyo, 1963.

Triaxial Testing: Its Adaptation and Application to Highway Materials. Soils Section, Materials and Tests Laboratory, Texas Highway Department, 1949.

Tseng, K-H., and R. L. Lytton. *Prediction of Permanent Deformation in Flexible Pavement Materials*. Implication of Aggregates in the Design, Construction, and Performance of Flexible Pavements, ASTM STP 1016, American Society for Testing and Materials, Philadelphia, Pa., pp. 154-172, 1989.

Uzan, J. *Granular Material Characterization*. Transportation Research Record 1022, Transportation Research Board, Washington, D.C., pp. 52-59, 1985.

APPENDIX A. PLANS AND SPECIFICATIONS FOR PHASE I AND PHASE II FIELD TEST CONSTRUCTION

PHASE I SPECIFICATIONS GOVERNING THE INSTALLATION OF TxDOT RESEARCH PROJECT 0-4519 TEST FACILITY

I. INTRODUCTION

The following specifications and attached plans describe the construction of a proposed test facility consisting of 20 full-scale pavement test sections within the Riverside Campus of Texas A&M University. Twenty flexible base sections are proposed. Ten sections will be built over an existing test track located beside Taxiway 7. The existing hot-mix asphalt and flexible base material on the existing test track must be removed and the new test sections placed on the existing native clay subgrade. This site is hereafter referred to as the clay site. The other ten sections will be located near the entrance of the Riverside Campus as shown on the plans. Topsoil must be removed at this location and test sections placed directly on existing native sand subgrade. This site is hereafter referred to as the sand site.

Each test section will be 16 ft long and 12 ft wide. Five different flexible base materials at two thicknesses (6 and 12 inches) are proposed at the clay site and the sand site for a total of 20 test sections. The final riding surface of the test sections will be a Grade 4 surface treatment.

II. PAYMENT

Payment for construction of the proposed facility will be made at the single, lump sum bid price upon completion of the work. No direct compensation will be made for the individual items listed below as this is considered in the total bid price. Payment is considered to be full compensation for furnishing labor, equipment, tools, materials, water, and other incidentals necessary to complete all work items. Work should be completed within 45 days of start of construction.

III. MAINTENANCE OF TRAFFIC AT THE CONSTRUCTION SITES

The safety of the public and the convenience of traffic shall be regarded as of prime importance. The Contractor shall be responsible for keeping the taxiways and access roads near the proposed test sections open and accessible to traffic. The Contractor shall have sole responsibility for providing, installing, moving, replacing,

maintaining, cleaning, and removing, upon completion of work, all barricades, warning signs, barriers, cones, lights, signals, and other such devices necessary for safe passage of traffic at the vicinity of the construction site.

IV. CONSTRUCTION SEQUENCE

Note: Construction shall not begin until all base materials have been delivered.

Clay Site *(Refer to construction sequence shown on page 14 of project plans.)*

1. Remove existing asphalt pavement and base materials to expose clay subgrade as shown on plans.
2. Scarify clay subgrade to a uniform depth of 6 inches for a width of 33 ft as shown on sheet 14 of the plans. Compact to maximum density as described in Item VII of this document.
3. Excavate 6 inches of the subgrade for half of the roadway (sections 6 through 10) as shown on sheet 14 of the plans. Scarify subgrade to a uniform depth of 6 inches for sections 6 through 10. Compact to maximum density as described in Item VII of this document.
4. Bring all five base materials to moisture content directed by Engineer and compact to maximum density to achieve 6-inch thick layer for sections 6 through 10 as shown in plans.
5. Place and compact all five base materials to achieve final grade for sections 1 through 10.
6. Place and compact top soil adjacent to sections to achieve adequate drainage.
7. Cure base as directed to at least 2 percentage points below optimum. Apply prime coat and allow to cure as directed.
8. Apply surface treatment.

Sand Site *(Refer to construction sequence shown on page 15 of project plans.)*

1. Remove existing top soil to expose sandy subgrade as shown on plans.
2. Scarify sand subgrade to a uniform depth of 6 inches for a width of 33 ft as shown on sheet 15 of the plans. Compact to maximum density as described in Item VII of this document.

3. Excavate 6 inches of the subgrade for half of the roadway (sections 16 through 20) as shown on sheet 15 of the plans. Scarify subgrade to a uniform depth of 6 inches for sections 16 through 20. Compact to maximum density as described in Item VII of this document.
4. Bring all five base materials to moisture content directed by Engineer and compact to maximum density to achieve 6-inch thick layer for sections 16 through 20 as shown in plans.
5. Place and compact all five base materials to achieve final grade for sections 11 through 20.
6. Place and compact top soil or crushed limestone as directed on the plans adjacent to sections to achieve adequate drainage.
7. Cure base as directed to at least 2 percentage points below optimum. Apply prime coat and allow to cure as directed.
8. Apply surface treatment.

V. REMOVAL OF EXISTING ASPHALT PAVEMENT AND BASE MATERIALS

The Contractor shall remove the existing asphalt pavement and base materials located at the clay site. These salvaged materials must be removed from the site and will be the property of the Contractor.

VI. SITE CLEARING AND GRUBBING

The Contractor shall clear and grub the sand site in accordance with Item 100 of the 1993 Standard Specifications for Construction of Highways, Streets and Bridges published by the Texas Department of Transportation (TxDOT). This publication will hereafter be referred to as the Standard Specifications. The area covered by the test facility, as shown in the plans, shall be cleared. This shall include the removal of top soil (approximately 6 to 8 inches) to expose the native sand. The top soil shall be stockpiled adjacent to the site and used as needed to adjust the grade on either side of test facility to achieve adequate drainage.

VII. PREPARATION OF SUBGRADE MATERIALS

The Contractor shall compact the native subgrade materials to at least 95 percent of the optimum density determined using Test Method Tex-113E. The subgrade shall be scarified and compacted as described in Item IV of this document and as shown on sheets 14 and 15 of the plans. Prior to and in conjunction with the rolling operation, the subgrade shall be brought to the moisture content necessary to obtain the required density and shall be kept level with suitable equipment to ensure uniform compaction. If additional material is needed to bring subgrade to final required elevation, it shall be excavated from subgrade area adjacent to test sections. Any excavated areas outside the test sections should be filled to original grade using select fill. Clods or lumps of subgrade shall be broken and material shall be mixed by blading, harrowing, disking, or similar methods to achieve uniformity. The optimum density and moisture content will be determined in the laboratory by the Texas Transportation Institute using samples of subgrade taken from the site. Field density and moisture content determination for compaction control will be conducted by a representative of TTI. The compacted subgrade shall conform to the lines, grade, and cross-section shown on the plans.

VIII. BASE COURSE MATERIALS

Five different types of base course materials shall be provided for construction of the test sections according to the following specifications or as approved by the Engineer:

Test Sections 1, 6, 11, and 16

Test sections 1, 6, 11, and 16 as shown on plans shall be constructed with a crushed limestone (TxDOT Standard Specifications Item 247, Type A, Grade 1) from Texas Crushed Stone in Georgetown.

Test Sections 2, 7, 12, and 17

Test Sections 2, 7, 12, and 17 as shown on plans shall be constructed with a crushed limestone (TxDOT Standard Specifications Item 247, Type A, Grade 2) from Texas Crushed Stone in Georgetown.

Test Sections 3, 8, 13, and 18

Test Sections 3, 8, 13, and 18 as shown on plans shall be constructed with a caliche base (TxDOT Standard Specifications Item 247, Type D, Grade 6, with 2 percent lime added) from the Vannoy Pit in Linn. The caliche base shall conform to the following requirements.

Before lime is added:

Sieve Size	*Percent Retained*
2-inch	0
1/2-inch	20 - 60
No. 4	40 - 75
No. 40	70 - 90
Max PI	15
Max. Wet Ball PI	15
Wet Ball Mill Max. Amount	50
Min. Compressive Strength, psi	150 at 15 psi lateral pressure

Compressive strength is determined using Test Method Tex-117E. However, capillary saturation is limited to 24 hours. The Wet Ball Test (Tex-116E) shall be run and the plasticity index (PI) of the material passing the No. 40 sieve shall be determined (wet ball PI).

After 1% lime (laboratory) is added to unlimed material:

Max PI	12
Min. Compressive Strength, psi (Tex-121-E)	180 at 15 psi lateral pressure

Two percent lime (by weight) will be incorporated into the caliche flexible base in accordance with the provisions of Standard Specification Items 263 and 264.

Test Sections 4, 9, 14, and 19

Test Sections 4, 9, 14, and 19 as shown on plans shall be constructed with an uncrushed gravel base (TxDOT Standard Specifications Item 247, Type B, Grade 6) from

CW&A Materials in Victoria. The uncrushed gravel base shall also conform to the following requirements.

Sieve Size	*Percent Retained*
2 1/2-inch	0
1 3/4-inch	0 - 10
3/8-inch	20- 35
No. 4	30 - 40
No. 40	60 - 80
PI	6 - 16

Test Sections 5, 10, 15, and 20

Test Sections 5, 10, 15, and 20 as shown on plans shall be constructed with a crushed sandstone base (TxDOT Standard Specifications Item Type A, Grade 4) from the Martin Marietta Pit in Apple, Oklahoma. The crushed sandstone base shall also conform to the following requirements:

- Wet Ball Mill, maximum of 40 percent
- Max. Increase in passing No. 40: 20 percent

Other Base Material Requirements

The contractor shall also provide an additional 2 cubic yards of each base material to be used for research laboratory testing. The contractor shall provide the Engineer with recent test data (as described in the physical requirements of Item 247 of the Standard Specifications) from the proposed base sources. Data may be obtained from recent construction projects. These data will be used by the Engineer to aid in approving the proposed base sources.

IX. COMPACTED BASE COURSE

Base materials will be placed within the limits of the test facilities shown in the plans. After placing the base materials, the existing soil surface shall be leveled and brought to the elevation profile necessary for the finished, primed surface to be at the same elevation as the adjacent taxiway for the clay site. At the sand site, the existing soil

surface shall be leveled and brought to the elevation profile necessary for the finished, primed surface to be above grade so that adequate drainage is achieved.

The base materials shall be mixed with water to the moisture content directed by the Engineer. Desired moisture content of the base material shall be achieved prior to placement in the test sections. The Contractor will compact the base materials to at least 100 percent of the optimum density determined using Test Method Tex-113E. The Contractor shall furnish, at no cost, samples of the base materials for determination of optimum density in the laboratory. This determination shall be made by TTI.

The 6-inch base materials shown in the plans shall be compacted in a single lift while the 12-inch base materials shall be compacted in two 6-inch lifts. Field density determination for compaction control will be made by a representative of TTI using Test Method Tex-115E, Part II (nuclear method). Field density tests will be taken on each lift. The bases shall conform to the lines, grade, and cross-section shown in the plans. The thicknesses of the compacted bases shall be checked by TTI using Test Method Tex-140-E, ground penetrating radar, or other method determined by the Engineer at locations specified by the Engineer. The average measurement at each location should be within ± ½ inch of the corresponding design thicknesses. Areas that are out of tolerance will be corrected by the Contractor at his or her own expense. After testing, the Contractor shall fill and recompact all holes where thickness measurements were made.

X. CURING THE BASE

Cure the base sections until the moisture content is at least 2 percentage points below optimum prior to application of prime material.

XI. PRIMING THE BASE

A prime coat shall be applied to the completed base course according to Item 310 of the Standard Specifications. The asphaltic material used for the prime coat shall be an MC-30 meeting the requirements of Item 300 of the Standard Specifications applied at a rate of 0.12 gal/yd^2. Excess water shall not be applied to the base prior to application of prime. Allow prime coat to cure for at least 7 days prior to application of surface treatment.

XII. SURFACE TREATMENT

A surface treatment (Item 316, Standard Specifications) shall be applied to the primed base. A sprayed-on application of HFRS-2p shall be applied according to Item 316 of the Standard Specifications. The HFRS-2p shall meet the requirements of Standard Specification Item 300, "Asphalts, Oils and Emulsions." The application rate should be about 0.40 gal/yd^2. Standard Specification Item 302, Grade 4 stone should be spread at a rate of about 1 yd^3/125 yd^2. A pneumatic roller should be used to seat the stone. The binder application rate may need to be adjusted for the different base materials.

XIII. ACCESS PAD AT SAND SITE

A 6-inch thick layer of crushed limestone or other approved material should be placed adjacent to test sections 11 through 20 as shown on Sheet 3 of project plans. Materials excavated and removed from existing test sections at the clay site may be used for this purpose. The access pad shall serve as a means to facilitate access to the test sections with test equipment. The access pad shall remain unsurfaced (no prime coat or surface treatment).

XIV. FINAL CLEAN-UP

Upon completion of the work and before acceptance and payment is made, the Contractor shall clean and remove rubbish, stockpiled materials, and temporary structures at and around the vicinity of the constructed test facilities. The Contractor shall restore in an acceptable manner all the property that has been damaged during the prosecution of the work and leave the construction site in a neat and presentable condition throughout. Unused materials cannot be dumped or deposited within the Texas A&M Riverside Campus and should be properly disposed of by the Contractor elsewhere.

XV. ADDITIONAL GUIDELINES

A. Conformity with Plans, Specifications, and Special Provisions

All work performed and all materials furnished shall be in reasonably close conformity with the lines, grades, cross-sections, dimensions, details, gradations, physical, and chemical characteristics of materials in accordance with tolerances shown

on the plans or indicated in the specifications and special provisions. The limits establishing reasonably close conformity will be as defined in the respective items of the contract or if not defined, as determined by the Engineer.

In the event the Engineer finds that the work performed or the materials used are not within reasonably close conformity with the plans, specifications, and special provisions, the affected material or product shall be removed and replaced or otherwise satisfactorily corrected by and at the expense of the contractor. Any deviations from the plans and approved working drawings will be made only with the approval of the Engineer.

B. Measurement of Quantities

All work completed under contract will be measured by the Engineer or his designated representative according to U.S. standard measures unless otherwise specified. All longitudinal measurements for surface area will be made along the actual surface of the roadway unless otherwise specified. For all transverse measurements for areas of base courses, surface courses, and pavements, the dimensions to be used in calculating the pay areas will be the neat dimensions and shall not exceed those shown in the plans or ordered in writing by the Engineer. All materials which are specified for measurement by the cubic yard shall be hauled in approved vehicles and measured therein at the point of delivery on the roadway. Vehicles for this purpose may be of any type or size satisfactory to the Engineer provided that the body is of such type that the actual contents may be readily and accurately determined.

C. Scope of Payment

The Contractor shall accept the compensation, as provided in the contract, as full payment for furnishing all materials, supplies, labor, tools, and equipment necessary to complete the work under the contract; for any loss or damage which may arise from the nature of the work or from the action of the elements; for any infringement of patent, trademark or copyright; and for completing the work according to the plans and specifications. The payment of any current or partial estimate shall in no way affect the obligation of the Contractor, at his or her expense, to repair or renew any defective parts of the construction, or to replace any defective materials used in the construction and to

be responsible for all damages due to such defects if such defects or damages are discovered on or before the final inspection and acceptance of the work.

D. Responsibility for Damage Claims

The Contractor agrees to indemnify and save harmless the State, its agents, and employees from all suits, actions, or claims, and from all liability and damages for any and all injuries or damages sustained by any person or property in consequence of any neglect in the performance of the contract by the Contractor from any claims or amounts arising or recovered under the "Workers' Compensation Laws," Chapter 101, Texas Civil Practice and Remedies Code (Texas Tort Claims Act), or any other laws. He or she shall further so indemnify and be responsible for all damages or injury to property of any character occurring during the prosecution of the work resulting from any act, omission, neglect, or misconduct on his or her part in the manner or method of executing the work, or from failure to properly execute the work, or from defective work or materials.

E. Authority and Duties of Inspectors

Inspectors will be authorized to inspect all work done and all materials furnished. Such inspection may extend to all or to any part of the work and to the preparation or manufacture of the materials to be used. An Inspector will be assigned to the work by the Engineer and will report to the Engineer as to the progress of the work and the manner in which the work is being performed; also, to report whenever it appears that the materials furnished and the work performed by the Contractor fail to fulfill the requirements of the specifications and contract and to call the attention of the Contractor to any such failure or other infringement. Such inspection will not relieve the Contractor from any obligation to perform the work in accordance with the requirements of the specifications. In case of any dispute arising between the Contractor and the Inspector as to materials furnished or the manner of performing the work, the Inspector will have the authority to reject materials, or suspend work on the operation or materials in dispute until the question at issue can be referred to and decided by the Engineer. The Inspector is not authorized to revoke, alter, enlarge, or release any requirement of the plans and specifications, or to approve or accept any portion of work, or to issue instructions

contrary to the plans and specifications. The Inspector will in no case act as foreman or perform other duties for the Contractor nor interfere with the management of the work. The Contractor shall furnish the Engineer and Inspector safe access to the work during construction and with every reasonable facility for ascertaining whether or not the work as performed is in accordance with the requirements of the contract.

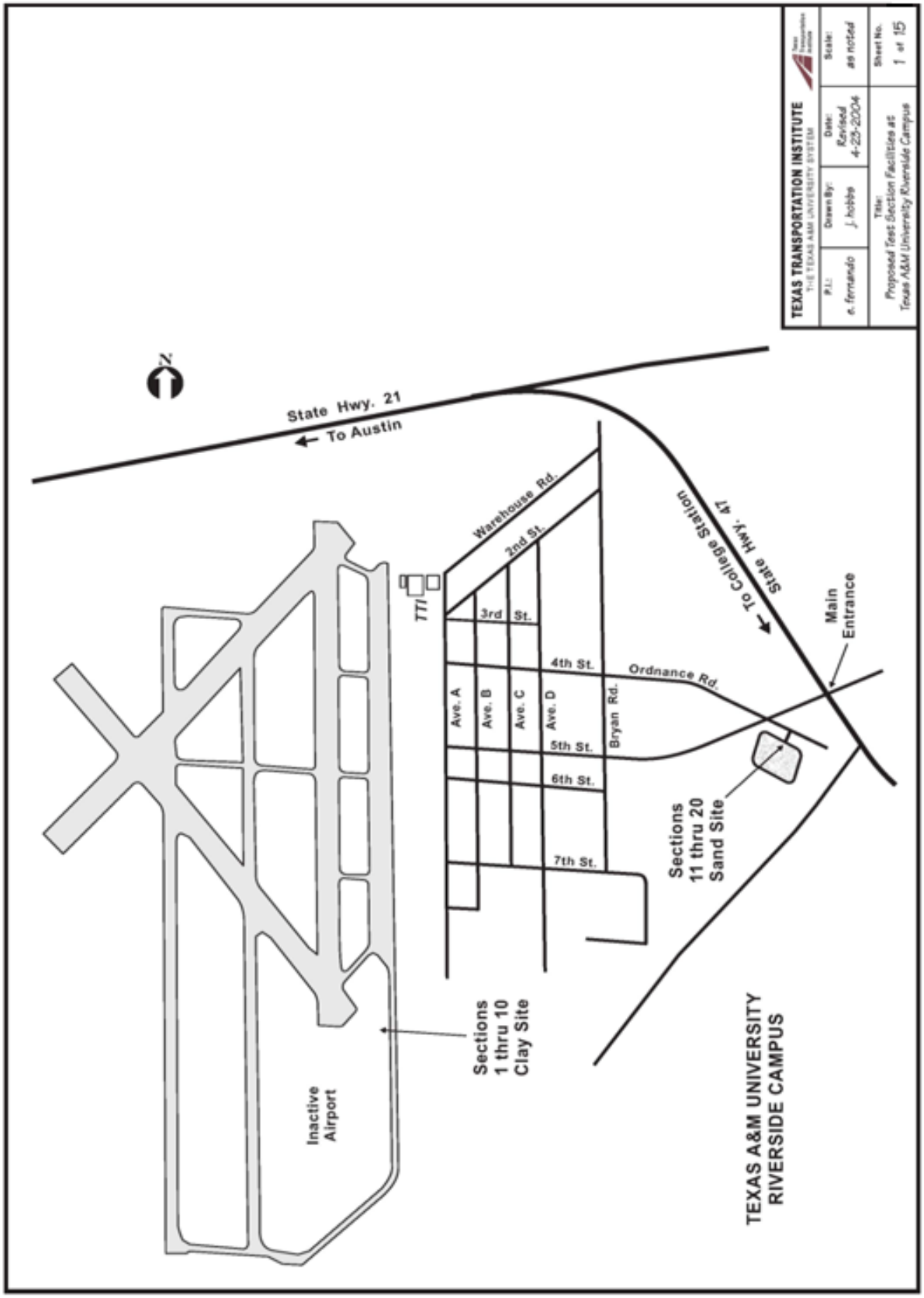

Figure A1. Map Showing Locations of Test Sections.

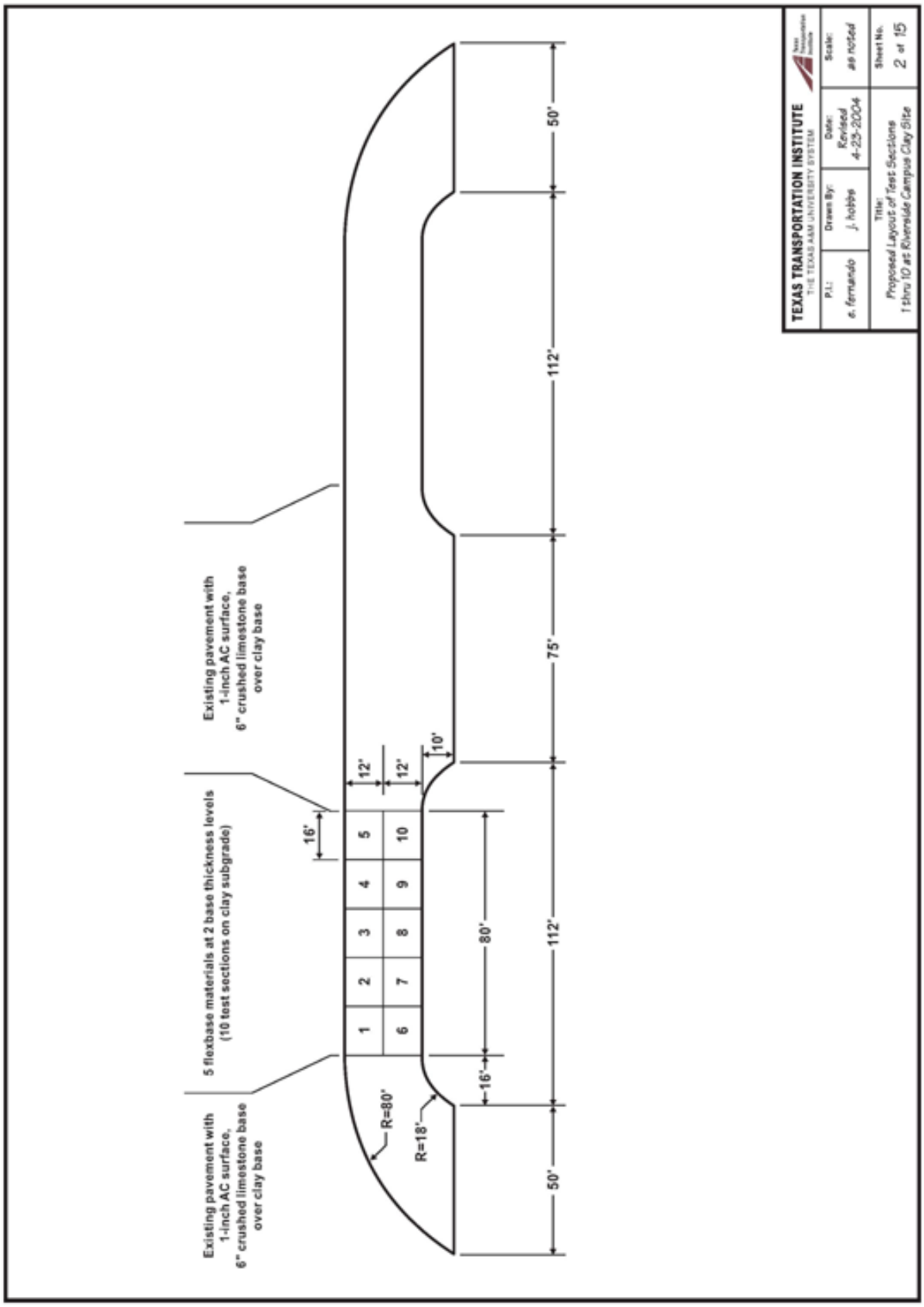

Figure A2. Layout of Flexible Base Sections on Clay Subgrade.

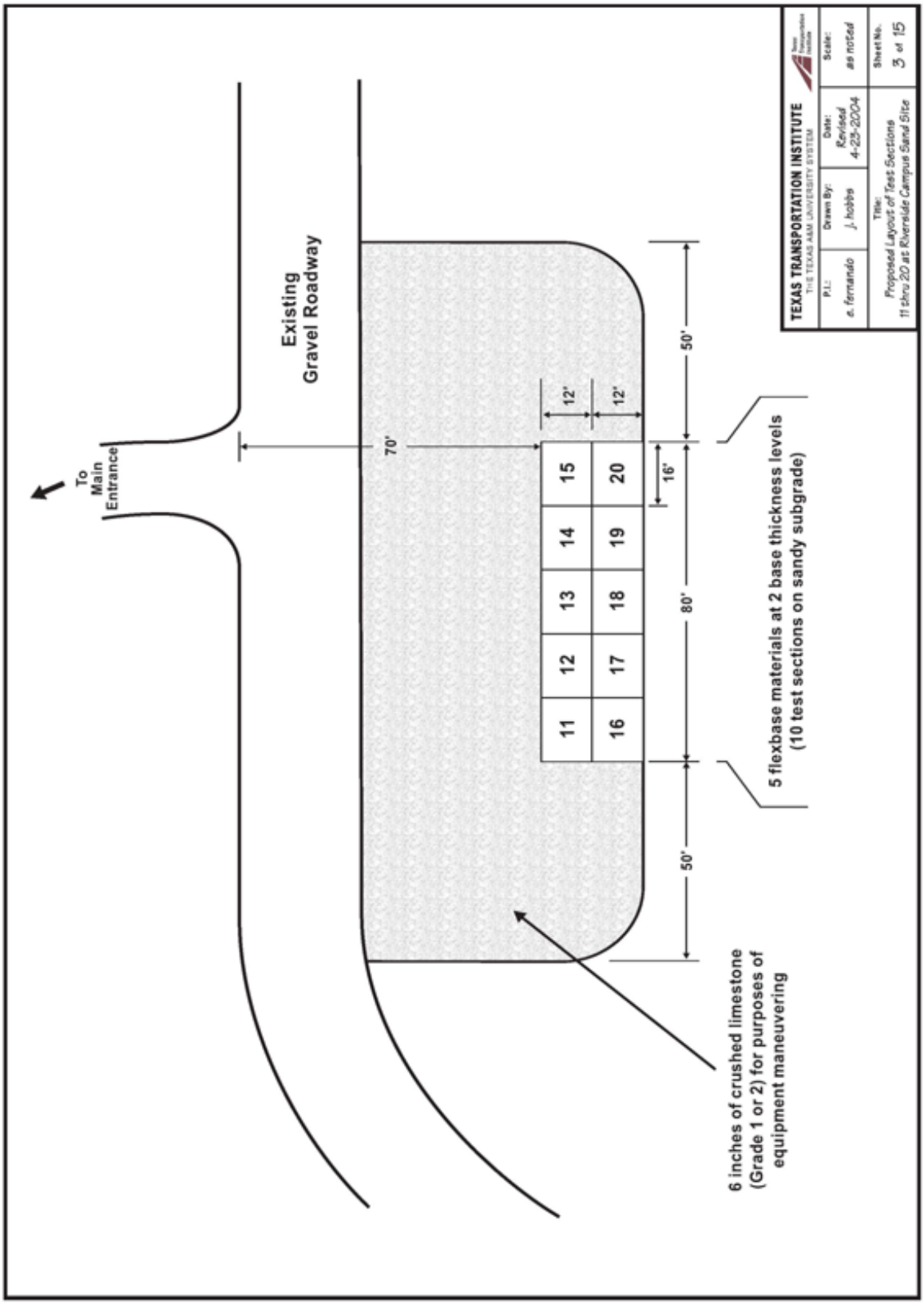

Figure A3. Layout of Flexible Base Sections on Sandy Subgrade.

Figure A4. Existing and Proposed Cross-Sections for Sections 1 and 6.

Figure A5. Existing and Proposed Cross-Sections for Sections 2 and 7.

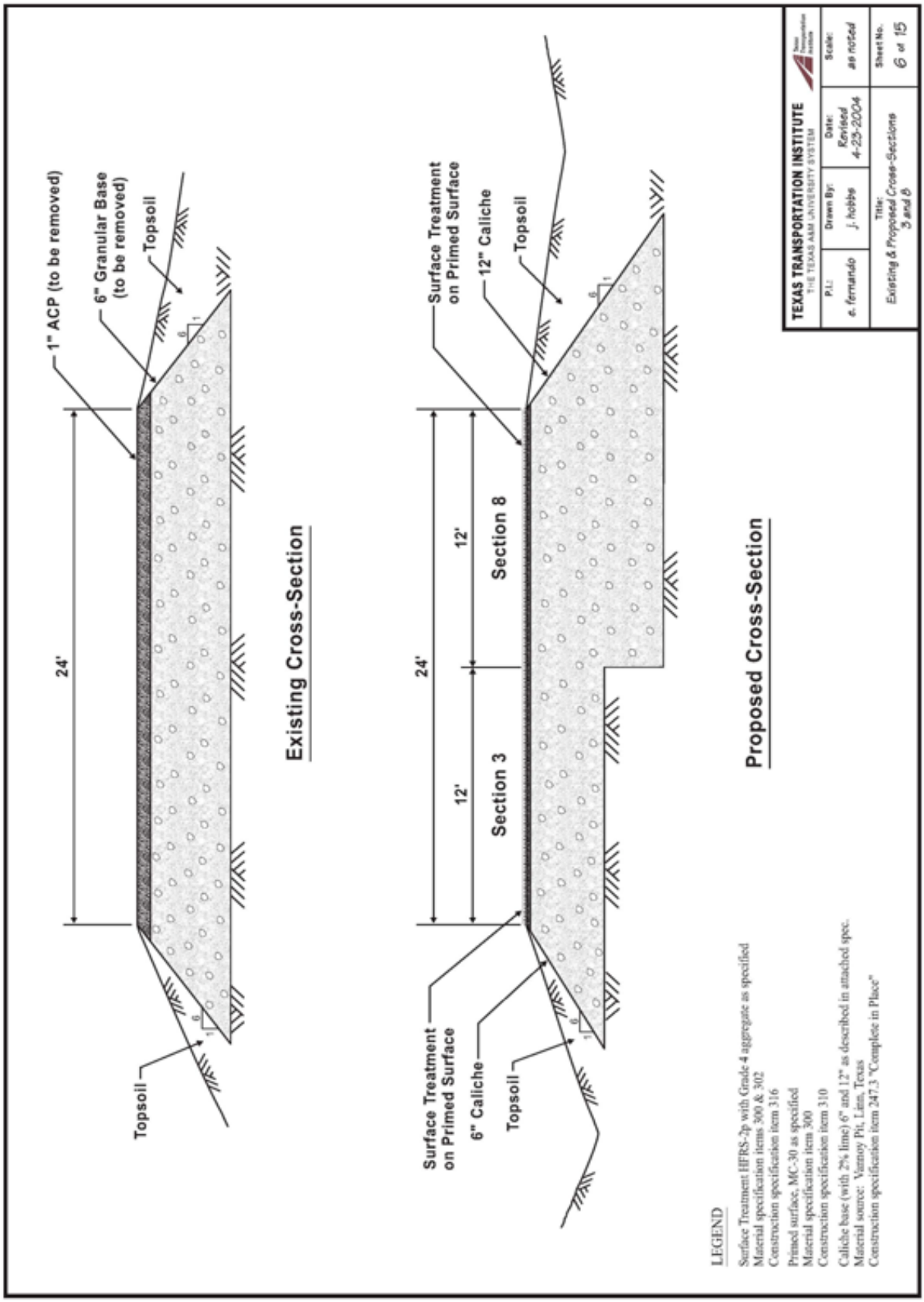

Figure A6. Existing and Proposed Cross-Sections for Sections 3 and 8.

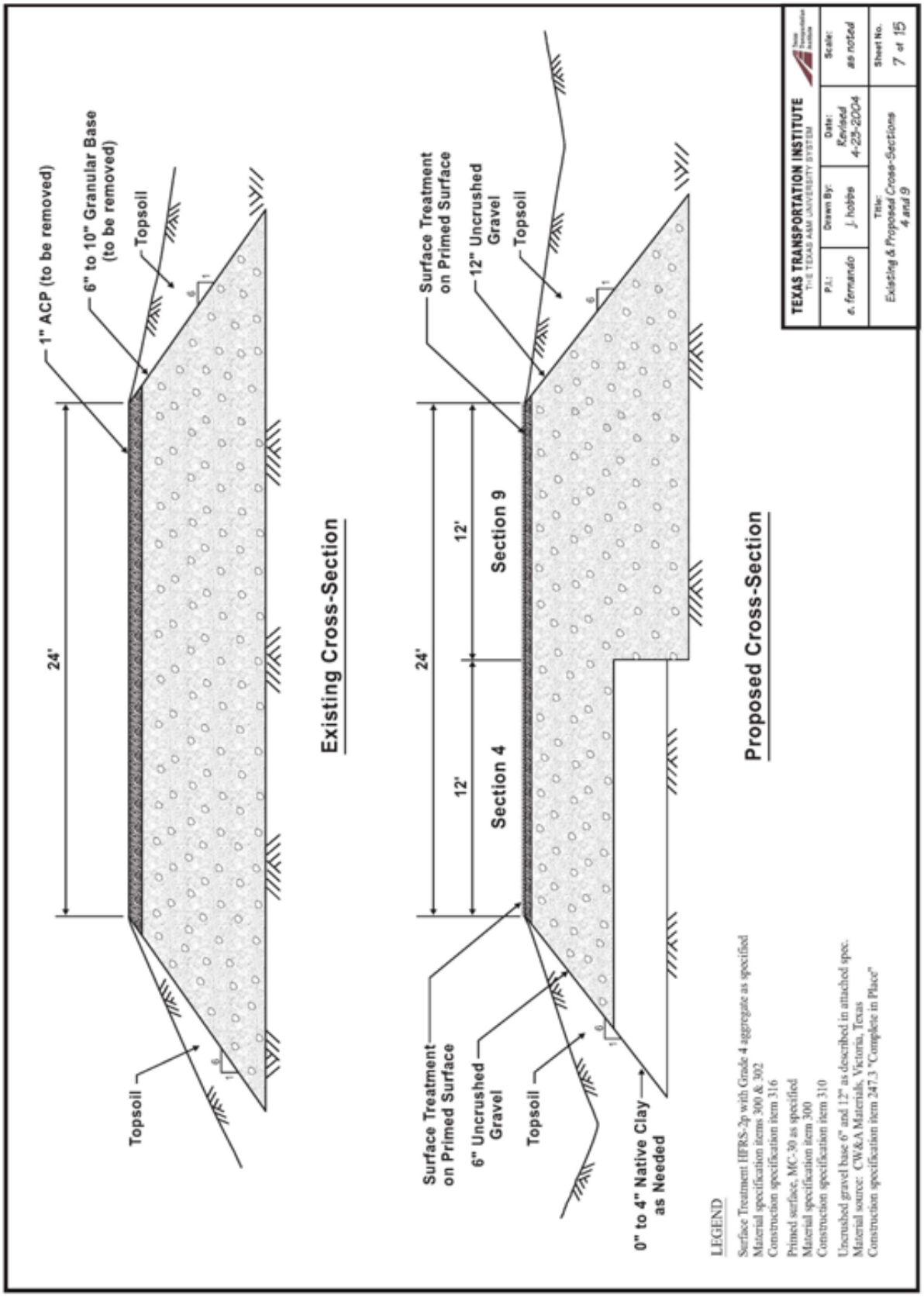

Figure A7. Existing and Proposed Cross-Sections for Sections 4 and 9.

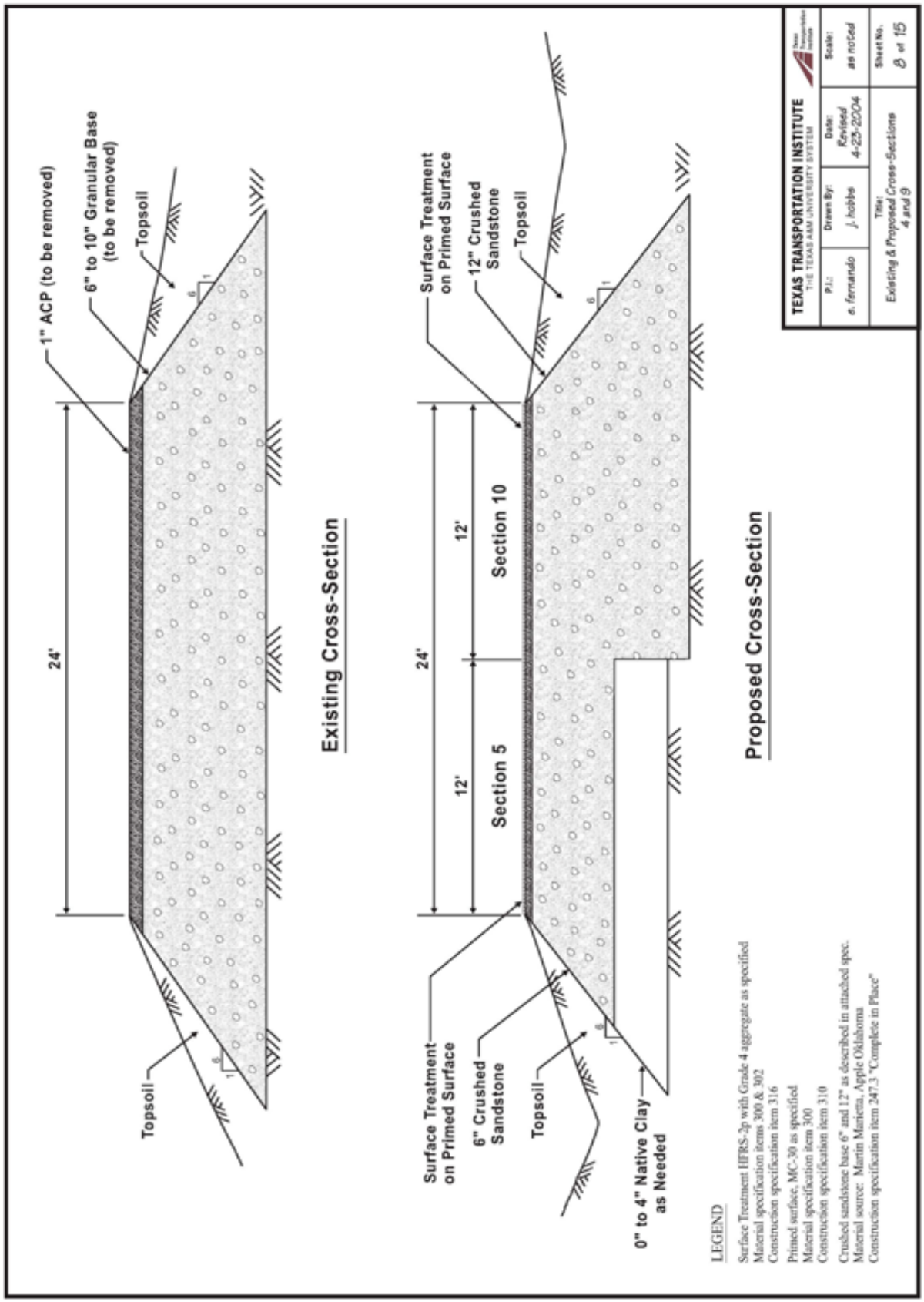

Figure A8. Existing and Proposed Cross-Sections for Sections 5 and 10.

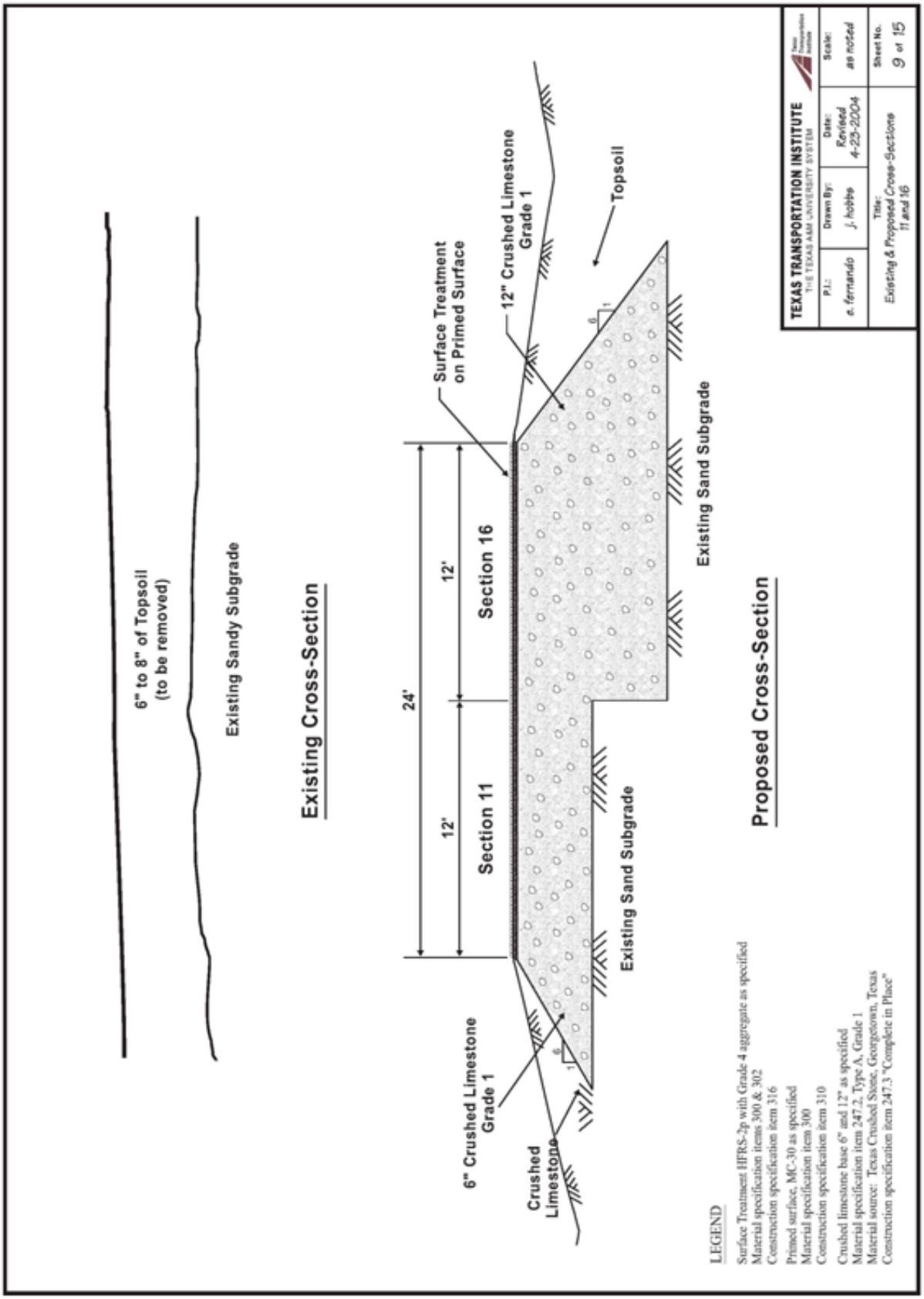

Figure A9. Existing and Proposed Cross-Sections for Sections 11 and 16.

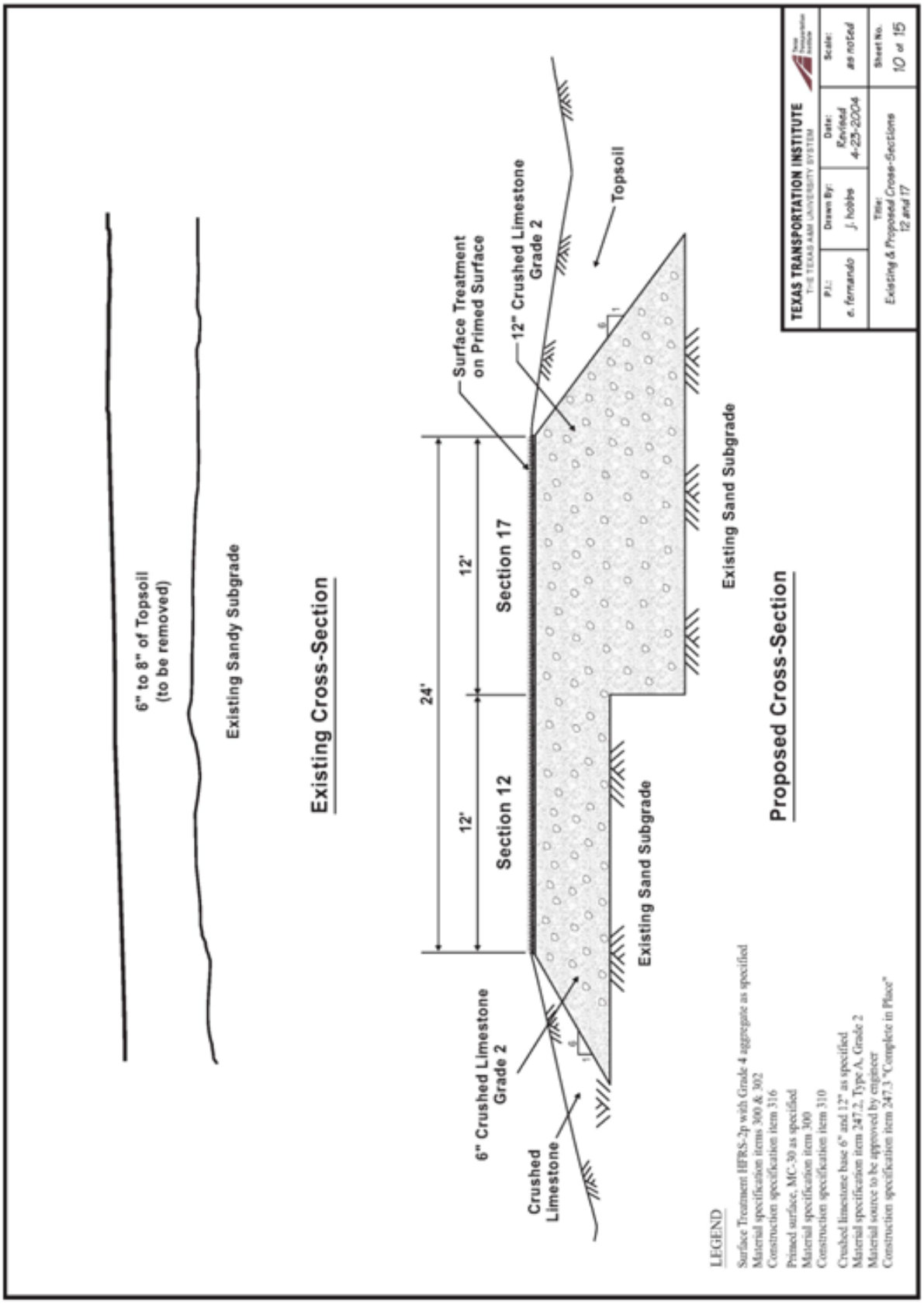

Figure A10. Existing and Proposed Cross-Sections for Sections 12 and 17.

Figure A11. Existing and Proposed Cross-Sections for Sections 13 and 18.

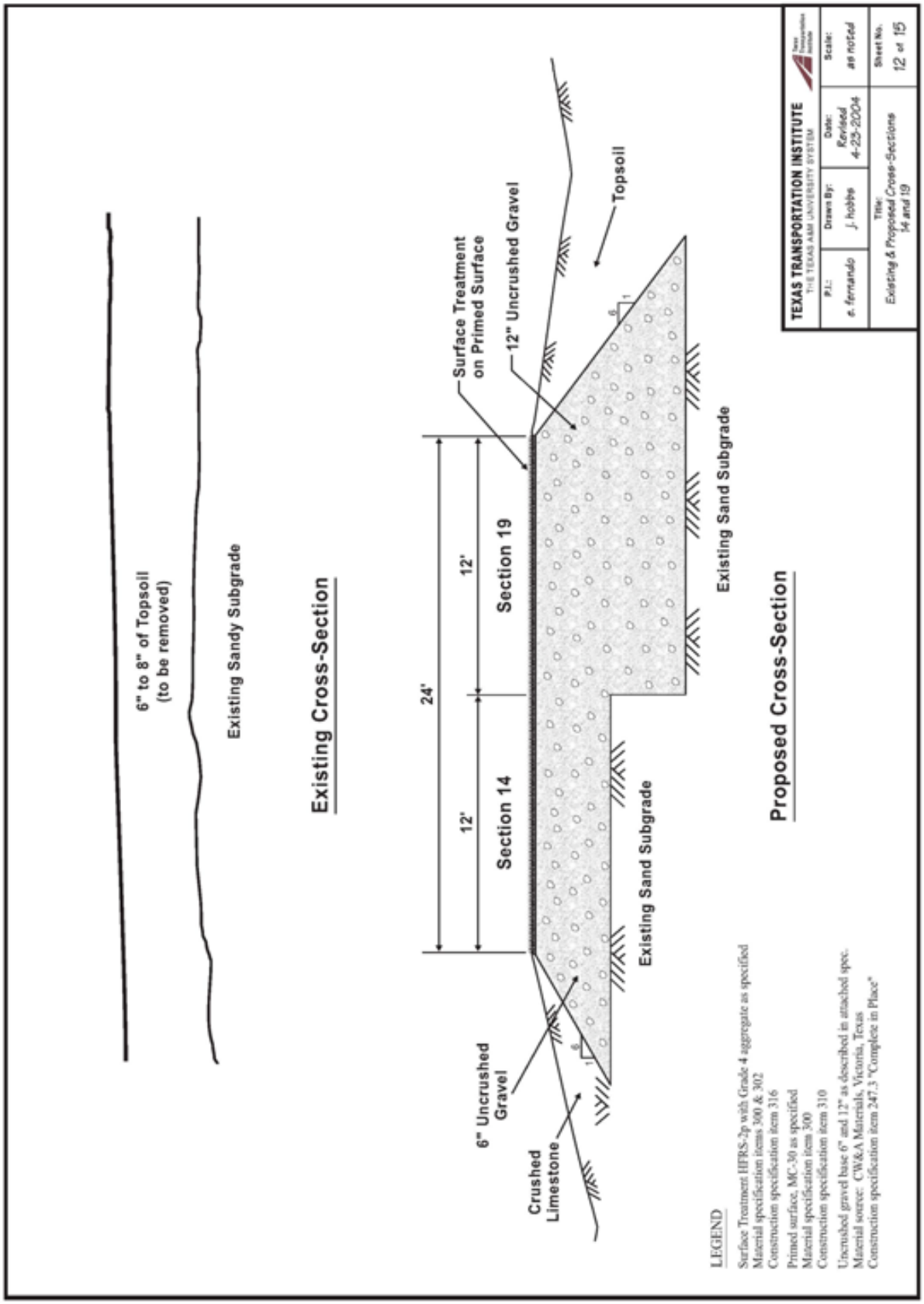

Figure A12. Existing and Proposed Cross-Sections for Sections 14 and 19.

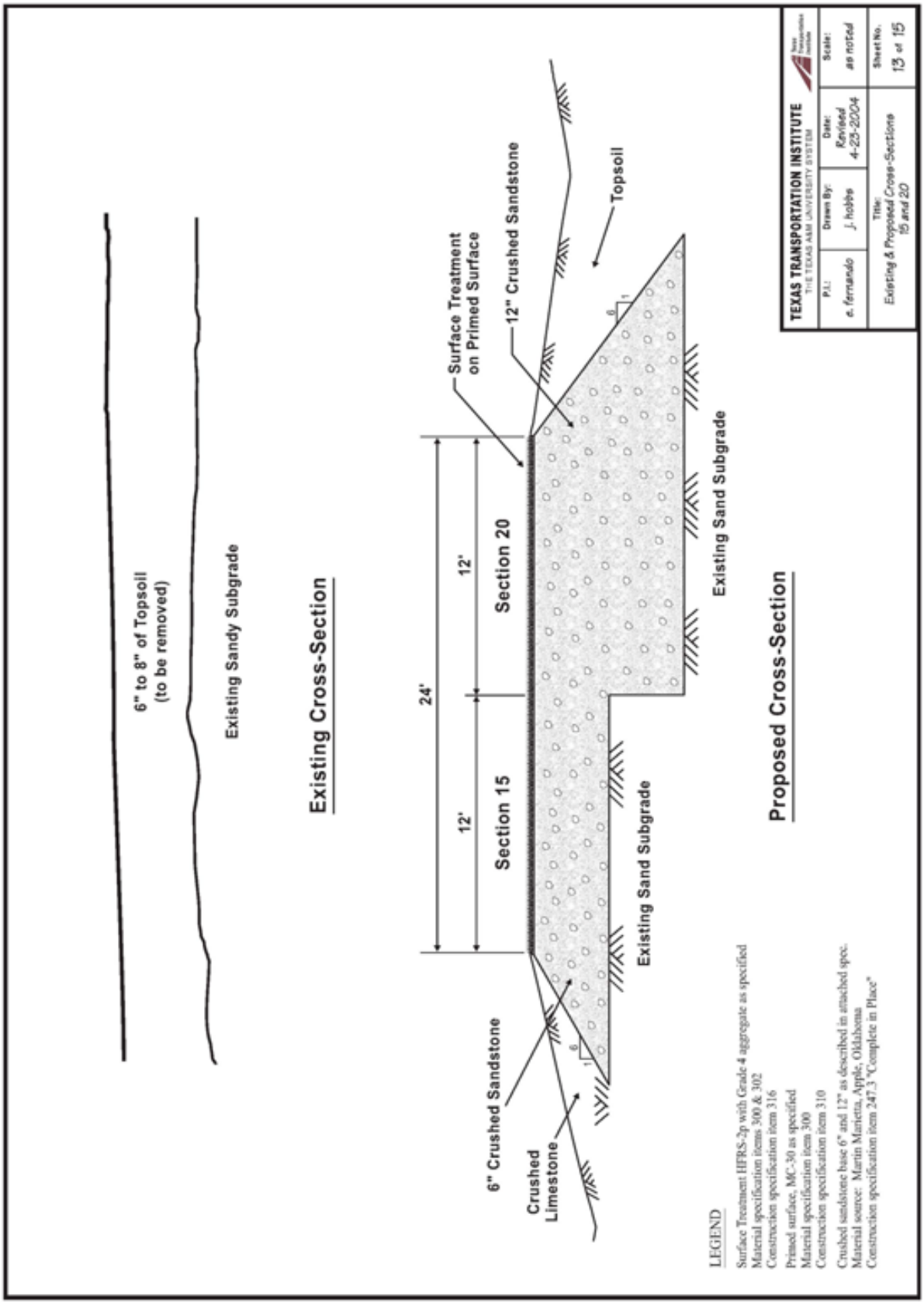

Figure A13. Existing and Proposed Cross-Sections for Sections 15 and 20.

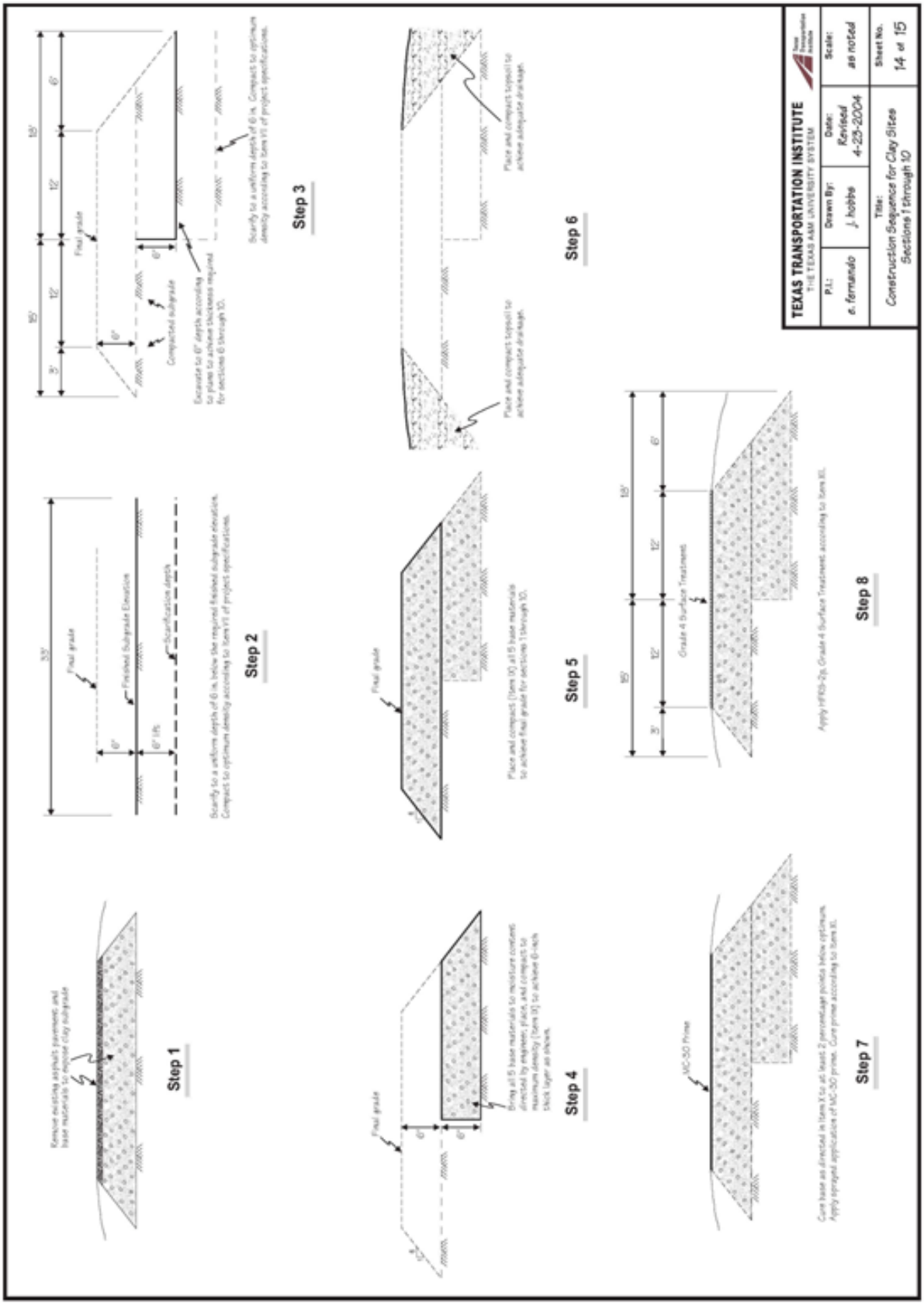

Figure A14. Construction Sequence for Flexible Base Sections on Clay Subgrade.

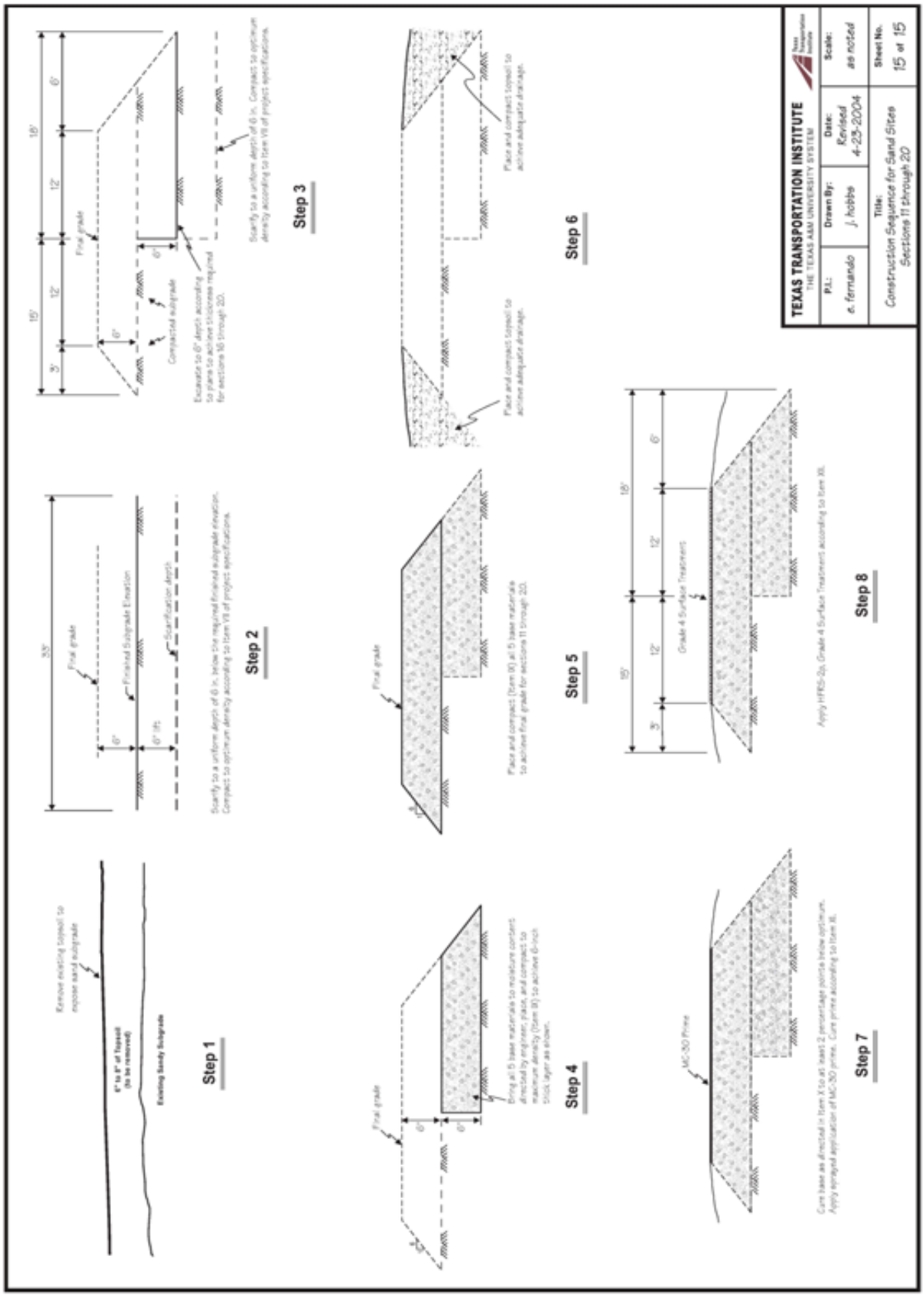

Figure A15. Construction Sequence for Flexible Base Sections on Sandy Subgrade.

PHASE II SPECIFICATIONS GOVERNING THE RECONSTRUCTION OF TEST SECTIONS FOR TxDOT RESEARCH PROJECT 0-4519

I. INTRODUCTION

The following specifications and attached plans describe the reconstruction of 10 full-scale pavement test sections within the Riverside Campus of Texas A&M University. The work proposed is described below.

- Two sections will require removing existing 6-inch sections of crushed sandstone, compacting subgrade, placing 6-inch layer of plant-mixed cement treated (4.5 percent) Grade 2 crushed limestone, applying prime, applying surface treatment.
- Two sections will require removing existing 6-inch sections of uncrushed gravel, compacting subgrade, placing 6-inch layer of plant-mixed cement treated (3.0 percent) Grade 2 crushed limestone, applying prime, applying surface treatment.
- Two sections will require removing existing 6-inch sections of caliche, compacting subgrade, placing 6-inch layer of plant-mixed lime treated (2 percent) uncrushed gravel, applying prime, applying surface treatment.
- Two sections will require removing existing 6-inch section of Grade 2 limestone, compacting subgrade, placing 6-inch layer of Grade 1 crushed limestone, applying prime, applying surface treatment, applying 2.5 inches of hot-mix asphalt concrete.
- Two sections will require applying 4.5 inches of hot-mix asphalt concrete to existing surface treatment.

Each test section will be 16 ft long and 12 ft wide. Five of the test sections will be placed near Taxiway 7 on an existing native clay subgrade. This site is hereafter referred to as the *clay site*. The other five sections will be placed on an existing native sand subgrade located near the entrance of the Riverside Campus as shown on the attached plans. This site is hereafter referred to as the *sand site.*

II. PAYMENT

Payment for construction of the proposed facility will be made at the single, lump sum bid price upon completion of the work. No direct compensation will be made for the individual items listed below as this is considered in the total bid price. Payment is considered to be full compensation for furnishing labor, equipment, tools, materials, water,

and other incidentals necessary to complete all work items. Work should be completed within 30 days of start of construction.

III. MAINTENANCE OF TRAFFIC AT THE CONSTRUCTION SITES

The safety of the public and the convenience of traffic shall be regarded as of prime importance. The Contractor shall be responsible for keeping the taxiways and access roads near the proposed test sections open and accessible to traffic. The Contractor shall have sole responsibility for providing, installing, moving, replacing, maintaining, cleaning, and removing, upon completion of work, all barricades, warning signs, barriers, cones, lights, signals, and other such devices necessary for safe passage of traffic at the vicinity of the construction site.

IV. CONSTRUCTION SEQUENCE

Note: Construction shall not begin until all base materials have been delivered to an approved location. The base materials at the sand site shall be placed and compacted prior to beginning construction at the clay site.

Sand Site

1. Remove existing asphalt surface treatment and base materials to expose sand subgrade as shown on plans. Care should be taken to not damage existing adjacent test sections which are not part of this reconstruction.
2. Scarify sand subgrade to a uniform depth of 6 inches and a width extending 4 ft beyond the outside longitudinal edge of the test sections. Compact to maximum density as described in Item VI of this document.
3. All four base materials shall be mixed and compacted to maximum density as described in Items VIII, IX, and X of this document to achieve a 6-inch thick layer for sections 12B through 15B as shown in plans.
4. Base materials for sections 12B through 15B shall be placed and compacted in the same day to achieve final grade.
5. Place and compact crushed limestone adjacent to sections to achieve adequate drainage.
6. Cure bases as directed in Item XI of this document.
7. Apply prime coat and allow to cure as directed in Item XII.

8. Apply surface treatment.
9. Apply dense-graded hot-mix asphalt to test sections 11B and 12B as directed.

Clay Site

1. Remove existing asphalt surface treatment and base materials to expose clay subgrade as shown on plans. Care should be taken to not damage existing adjacent test sections which are not part of this reconstruction.
2. Scarify clay subgrade to a uniform depth of 6 inches and a width extending 4 ft beyond the outside longitudinal edge of the test sections. Compact to maximum density as described in Item VI of this document.
3. All four base materials shall be mixed and compacted to maximum density as described in Items VIII, IX, and X of this document to achieve a 6-inch thick layer for sections 6B through 9B as shown in plans.
4. Base materials for sections 6B through 9B shall be placed and compacted in the same day to achieve final grade.
5. Place and compact top soil adjacent to sections to achieve adequate drainage.
6. Cure base as directed to at least 2 percentage points below optimum. Apply prime coat and allow to cure as directed.
7. Apply surface treatment.
8. Apply dense-graded hot-mix asphalt to the test sections as shown in the plans.

V. REMOVAL OF EXISTING BASE MATERIALS

The Contractor shall remove the existing surface treatment and base materials located at the clay and sand site. These salvaged materials must be removed from the site and will be the property of the Contractor.

VI. PREPARATION OF SUBGRADE MATERIALS

The Contractor shall compact the native subgrade materials to at least 95 percent of the optimum density determined using Test Method Tex-113E. The subgrade shall be scarified and compacted as described in Item IV of this document and as shown on sheets 14 and 15 of the plans. Prior to and in conjunction with the rolling operation, the subgrade shall be brought to the moisture content necessary to obtain the required density and shall be kept level with suitable equipment to ensure uniform compaction. If additional material is needed

to bring subgrade to final required elevation, it shall be excavated from subgrade area adjacent to test sections. Any excavated areas outside the test sections should be filled to original grade using select fill. Clods or lumps of subgrade shall be broken and material shall be mixed by blading, harrowing, disking, or similar methods to achieve uniformity. The optimum density and moisture content will be determined in the laboratory by the Texas Transportation Institute using samples of subgrade taken from the site. Field density and moisture content determination for compaction control will be conducted by a representative of TTI. The compacted subgrade shall conform to the lines, grade, and cross section shown on the plans.

VII. BASE COURSE MATERIALS

Five different types of base course materials shall be provided for construction of the test sections according to the following specifications. All base materials shall come from TxDOT approved stockpiles as determined by TTI engineers.

Test Sections 6B and 15B

Test sections 6B and 15B as shown on plans shall be constructed with a crushed limestone (TxDOT Standard Specifications Item 247, Type A, Grade 2) from Vulcan Materials in Groesbeck. The crushed limestone shall be plant-mixed with 4.5 percent cement according to TxDOT Standard Specification Item 276. The Contractor may assume this section will have 4.5 percent cement but the final value to use for construction may differ, depending on results from laboratory tests done on samples molded with different cement contents using the Grade 2 crushed limestone samples to be placed during construction. It is not expected that the cement content will be greater than 4.5 percent for each of these test sections.

Test Sections 7B and 14B

Test sections 7B and 14B as shown on plans shall be constructed with a crushed limestone (TxDOT Standard Specifications Item 247, Type A, Grade 2) from Vulcan Materials in Groesbeck. The crushed limestone shall be plant-mixed with 3.0 percent cement according to TxDOT Standard Specification Item 276. The Contractor may assume this section will have 3.0 percent cement but the final value to use for construction may differ, depending on results from laboratory tests done on samples molded with different cement contents using the Grade 2 crushed limestone samples to be placed during construction. It is

not expected that the cement content will be greater than 3.0 percent for each of these test sections.

Test Sections 8B and 13B

Test Sections 8B and 13B as shown on plans shall be constructed with an uncrushed gravel base (TxDOT Standard Specifications Item 247, Type B, Grade 6) from CW&A Materials in Victoria. The uncrushed gravel base shall also conform to the following requirements.

Sieve Size	*Percent Retained*
2 1/2-inch	0
1 3/4-inch	0 - 10
3/8-inch	20 - 50
No. 4	30 - 75
No. 40	60 - 80
Liquid Limit	Max 35
PI	6 - 16

The uncrushed gravel shall be plant-mixed with 2.0 percent lime according to TxDOT Standard Specification Item 263.

Test Sections 9B and 12B

Test Sections 9B and 12B as shown on plans shall be constructed with a crushed limestone (TxDOT Standard Specifications Item 247, Type A, Grade 1) from Texas Crushed Stone in Georgetown.

Other Base Material Requirements

The Contractor shall also provide an additional 2 cubic yards of each base material to be used for research laboratory testing. Base materials will be placed within the limits of the test facilities shown in the plans. After placing the base materials, the existing soil surface shall be leveled and brought to the elevation profile necessary for the finished, primed surface to be at the same elevation as the adjacent taxiway for the clay site. At the sand site, the existing soil surface shall be leveled and brought to the elevation profile necessary for the finished, primed surface to be above grade so that adequate drainage is achieved.

VIII. CEMENT TREATMENT (PLANT-MIXED)

The cement treated base materials shall be mixed, compacted, and finished according to TxDOT Standard Specification Item 276. Mix designs will be performed by Texas Transportation Institute to determine the target cement contents. Materials shall be mixed at optimum moisture content as determined by TTI. No water shall be added to the mixture after mixing is complete unless directed.

The 6-inch base materials shown in the plans shall be compacted in a single lift and compacted to 95 percent of the maximum density as determined with Tex-120E. Field density determination for compaction control will be made by a representative of TTI using Test Method Tex-115E, Part II (nuclear method). Three density tests will be taken on each test section and all three density tests must meet the required density.

The bases shall conform to the lines, grade, and cross-section shown in the plans. The thicknesses of the compacted bases shall be checked by TTI using Test Method Tex-140E, ground penetrating radar, or other method determined by the Engineer at locations specified by the Engineer. The average measurement at each location should be within ±1/2 inch of the corresponding design thicknesses. Areas that are out of tolerance will be corrected by the Contractor at his or her own expense. After testing, the Contractor shall fill and recompact all holes where thickness measurements were made.

IX. LIME TREATMENT (PLANT-MIXED)

The lime treated base materials shall be mixed, compacted, and finished according to TxDOT Standard Specification Item 263. Target lime content is 2.0 percent and no mix designs will be performed. Materials shall be mixed at optimum moisture content as determined by TTI. No water shall be added to the mixture after mixing is complete unless directed.

The 6-inch base materials shown in the plans shall be compacted in a single lift and compacted to 98 percent of the maximum density as determined with Tex-121E. Field density determination for compaction control will be made by a representative of TTI using Test Method Tex-115E, Part II (nuclear method). Three density tests will be taken on each test section and all three density tests must meet the required density.

The bases shall conform to the lines, grade, and cross-section shown in the plans. The thicknesses of the compacted bases shall be checked by TTI using Test Method Tex-140E, ground penetrating radar, or other method determined by the Engineer at locations

specified by the Engineer. The average measurement at each location should be within ±1/2 inch of the corresponding design thicknesses. Areas that are out of tolerance will be corrected by the Contractor at his or her own expense. After testing, the Contractor shall fill and recompact all holes where thickness measurements were made.

X. FLEXIBLE BASE

The flexible base sections shall be mixed, compacted, and finished according to TxDOT Standard Specification Item 247. Base material shall be mixed with water to the optimum moisture content as determined by TTI. Optimum moisture content of the base material shall be achieved prior to placement in the test sections.

The 6-inch base materials shown in the plans shall be compacted in a single lift and compacted to 100 percent of the maximum density as determined by Tex-113E. Field density determination for compaction control will be made by a representative of TTI using Test Method Tex-115E, Part II (nuclear method). Three density tests will be taken on each test section and all three density tests must meet the required density.

The bases shall conform to the lines, grade, and cross-section shown in the plans. The thicknesses of the compacted bases shall be checked by TTI using Test Method Tex-140E, ground penetrating radar, or other method determined by the Engineer at locations specified by the Engineer. The average measurement at each location should be within ±1/2 inch of the corresponding design thicknesses. Areas that are out of tolerance will be corrected by the Contractor at his or her own expense. After testing, the Contractor shall fill and recompact all holes where thickness measurements were made.

XI. CURING THE BASE

The flexible base sections shall be cured until the moisture content is at least 2 percentage points below optimum prior to applying a prime coat as directed in Item 247.4. The cement and lime treated base sections shall be cured a minimum of 7 days prior to application of prime.

XII. PRIMING THE BASE

A prime coat shall be applied to the completed base course according to Item 310 of the Standard Specifications. The asphaltic material used for the prime coat shall be an MC-30 meeting the requirements of Item 300 of the Standard Specifications applied at a rate

of 0.12 gal/yd^2. Allow prime coat to cure for at least 7 days prior to application of surface treatment.

XIII. SURFACE TREATMENT

A surface treatment (Item 316, Standard Specifications) shall be applied to the primed base. A sprayed-on application of AC-15P or AC-20-5TR (or other binder as approved by TTI) shall be applied according to Item 316 of the Standard Specifications. The binder shall meet the requirements of Standard Specification Item 300, "Asphalts, Oils and Emulsions." The application rate should be about 0.40 gal/yd^2. Standard Specification Item 302, Grade 4 stone should be spread at a rate of about 1 yd^3/125 yd^2. A pneumatic roller should be used to seat the stone. The binder application rate may need to be adjusted for the different base materials. The surface treatment shall be applied within 14 days of final compaction.

XIV. DENSE-GRADED HOT-MIX ASPHALT

Hot-mix asphalt concrete shall be placed on four of the test sections as shown in the plans. The HMAC shall be designed, produced, stored, transported, placed, and compacted in accordance with the requirements of TxDOT Standard Specification Item 340, Type D. The HMAC shall be compacted to contain from 5 percent to 9 percent air voids as determined in accordance with Tex-207-F. TTI will perform three density tests per test section and all three tests shall meet the required density.

XV. FINAL CLEAN-UP

Upon completion of the work and before acceptance and payment is made, the Contractor shall clean and remove rubbish, stockpiled materials, and temporary structures at and around the vicinity of the constructed test facilities. The Contractor shall restore in an acceptable manner all the property which has been damaged during the prosecution of the work and leave the construction site in a neat and presentable condition throughout. Unused materials cannot be dumped or deposited within the Texas A&M Riverside Campus and should be properly disposed of by the Contractor elsewhere.

XVI. ADDITIONAL GUIDELINES

A. Conformity with Plans, Specifications, and Special Provisions

All work performed and all materials furnished shall be in reasonably close conformity with the lines, grades, cross-sections, dimensions, details, gradations, physical, and chemical characteristics of materials in accordance with tolerances shown on the plans or indicated in the specifications and special provisions. The limits establishing reasonably close conformity will be as defined in the respective items of the contract or if not defined, as determined by the Engineer.

In the event the Engineer finds that the work performed or the materials used are not within reasonably close conformity with the plans, specifications, and special provisions, the affected material or product shall be removed and replaced or otherwise satisfactorily corrected by and at the expense of the contractor. Any deviations from the plans and approved working drawings will be made only with the approval of the Engineer.

B. Measurement of Quantities

All work completed under contract will be measured by the Engineer or his designated representative according to U.S. standard measures unless otherwise specified. All longitudinal measurements for surface area will be made along the actual surface of the roadway unless otherwise specified. For all transverse measurements for areas of base courses, surface courses, and pavements, the dimensions to be used in calculating the pay areas will be the neat dimensions and shall not exceed those shown in the plans or ordered in writing by the Engineer. All materials which are specified for measurement by the cubic yard shall be hauled in approved vehicles and measured therein at the point of delivery on the roadway. Vehicles for this purpose may be of any type or size satisfactory to the Engineer provided that the body is of such type that the actual contents may be readily and accurately determined.

C. Scope of Payment

The Contractor shall accept the compensation, as provided in the contract, as full payment for furnishing all materials, supplies, labor, tools, and equipment necessary to complete the work under the contract; for any loss or damage which may arise from the nature of the work or from the action of the elements; for any infringement of patent, trademark, or copyright; and for completing the work according to the plans and

specifications. The payment of any current or partial estimate shall in no way affect the obligation of the Contractor, at his or her expense, to repair or renew any defective parts of the construction, or to replace any defective materials used in the construction, and to be responsible for all damages due to such defects if such defects or damages are discovered on or before the final inspection and acceptance of the work.

D. Responsibility for Damage Claims

The Contractor agrees to indemnify and save harmless the State, its agents, and employees from all suits, actions or claims, and from all liability and damages for any and all injuries or damages sustained by any person or property in consequence of any neglect in the performance of the contract by the Contractor from any claims or amounts arising or recovered under the "Workers' Compensation Laws," Chapter 101, Texas Civil Practice and Remedies Code (Texas Tort Claims Act), or any other laws. He or she shall further so indemnify and be responsible for all damages or injury to property of any character occurring during the prosecution of the work resulting from any act, omission, neglect or misconduct on his or her part in the manner or method of executing the work; or from failure to properly execute the work; or from defective work or materials.

E. Authority and Duties of Inspectors

Inspectors will be authorized to inspect all work done and all materials furnished. Such inspection may extend to all or to any part of the work and to the preparation or manufacture of the materials to be used. An Inspector will be assigned to the work by the Engineer and will report to the Engineer as to the progress of the work and the manner in which the work is being performed; also to report whenever it appears that the materials furnished and the work performed by the Contractor fail to fulfill the requirements of the specifications and contract and to call the attention of the Contractor to any such failure or other infringement. Such inspection will not relieve the Contractor from any obligation to perform the work in accordance with the requirements of the specifications. In case of any dispute arising between the Contractor and the Inspector as to materials furnished, or the manner of performing the work, the Inspector will have the authority to reject materials or suspend work on the operation or materials in dispute until the question at issue can be referred to and decided by the Engineer. The Inspector is not authorized to revoke, alter, enlarge, or release any requirement of the plans and specifications, or to approve or accept

any portion of work, or to issue instructions contrary to the plans and specifications. The Inspector will in no case act as foreman or perform other duties for the Contractor nor interfere with the management of the work.

The Contractor shall furnish the Engineer and Inspector safe access to the work during construction and with every reasonable facility for ascertaining whether or not the work as performed is in accordance with the requirements of the contract.

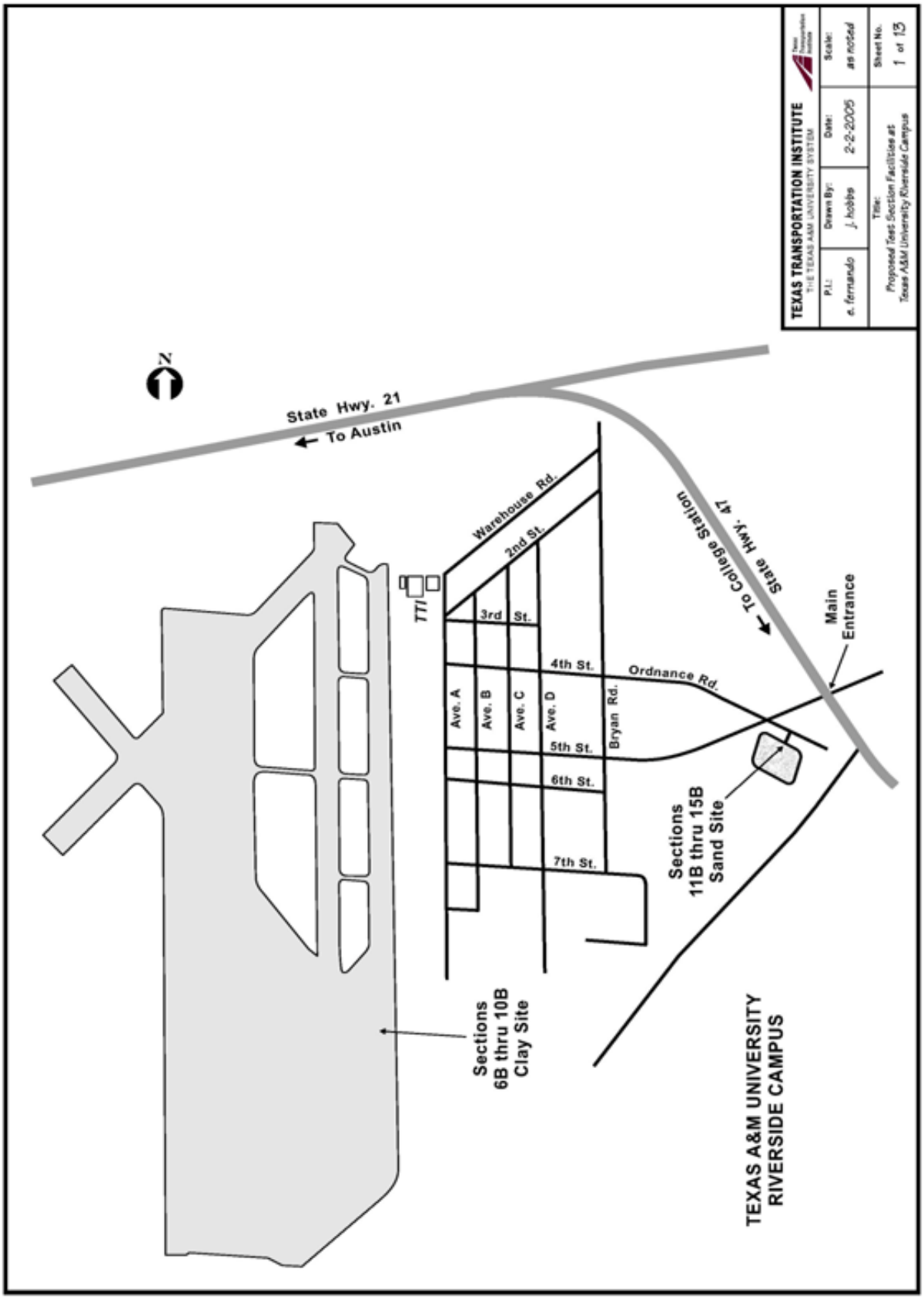

Figure A16. Map Showing Locations of Stabilized Test Sections.

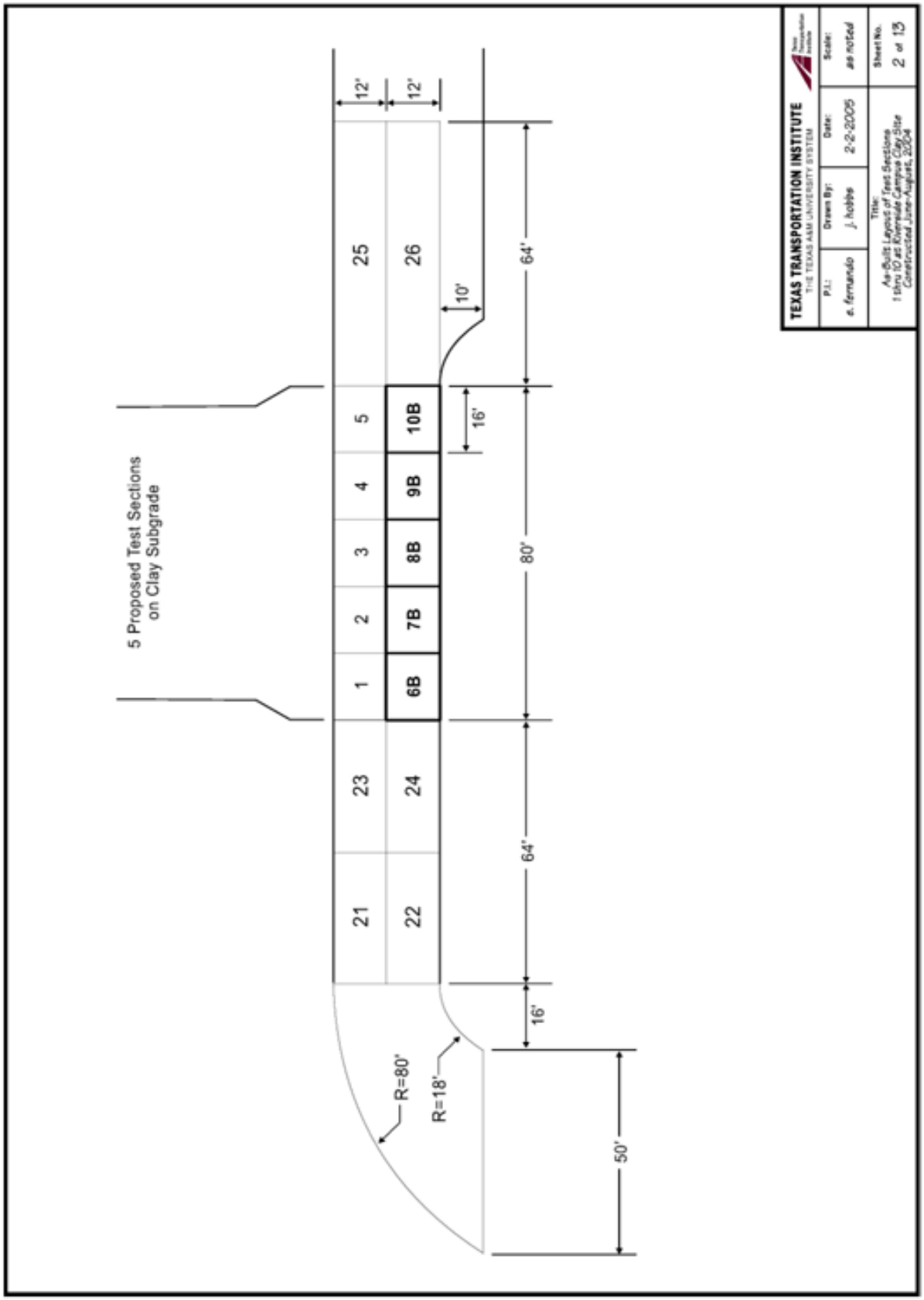

Figure A17. Layout of Stabilized Sections on Clay Subgrade.

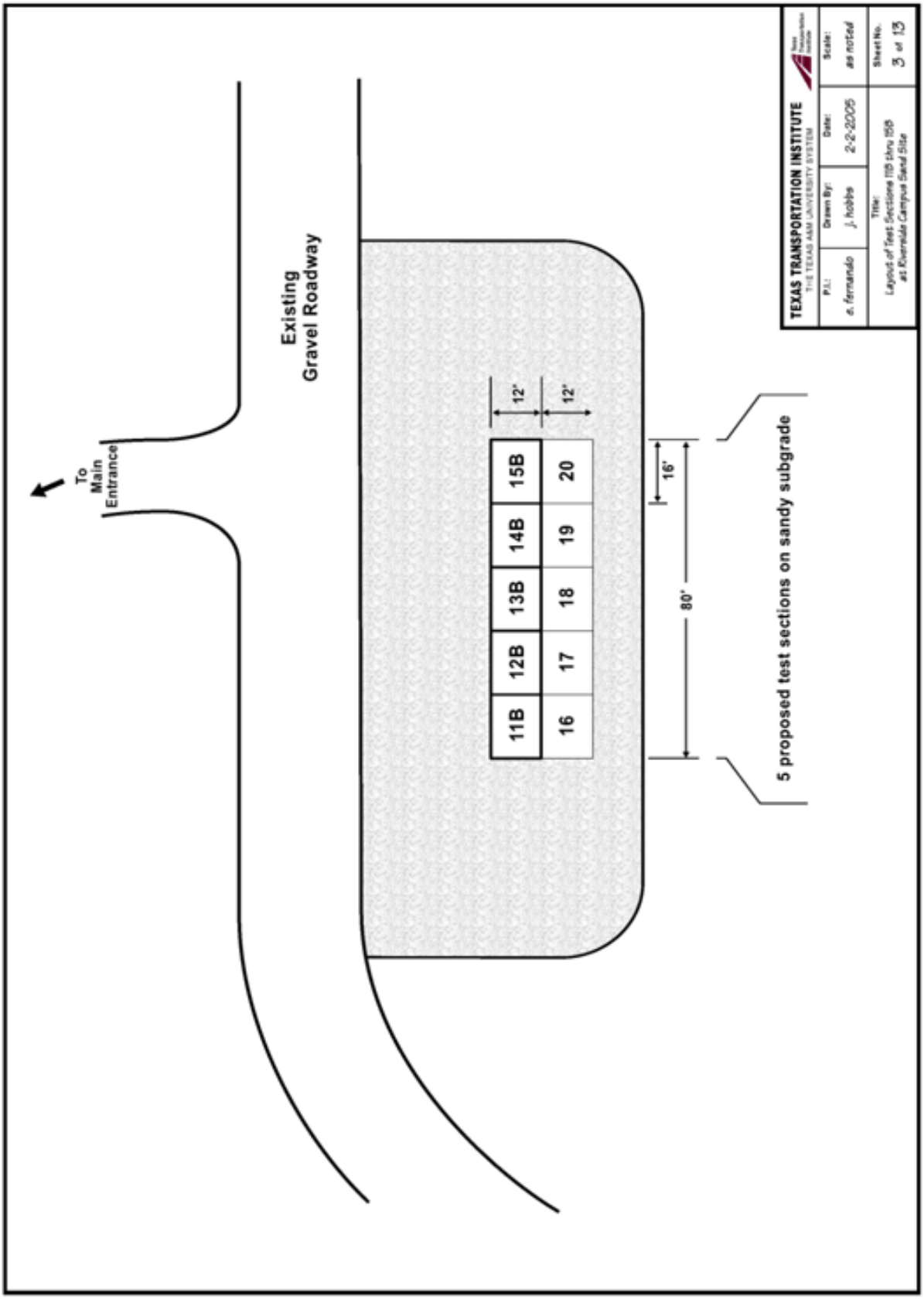

Figure A18. Layout of Stabilized Sections on Sandy Subgrade.

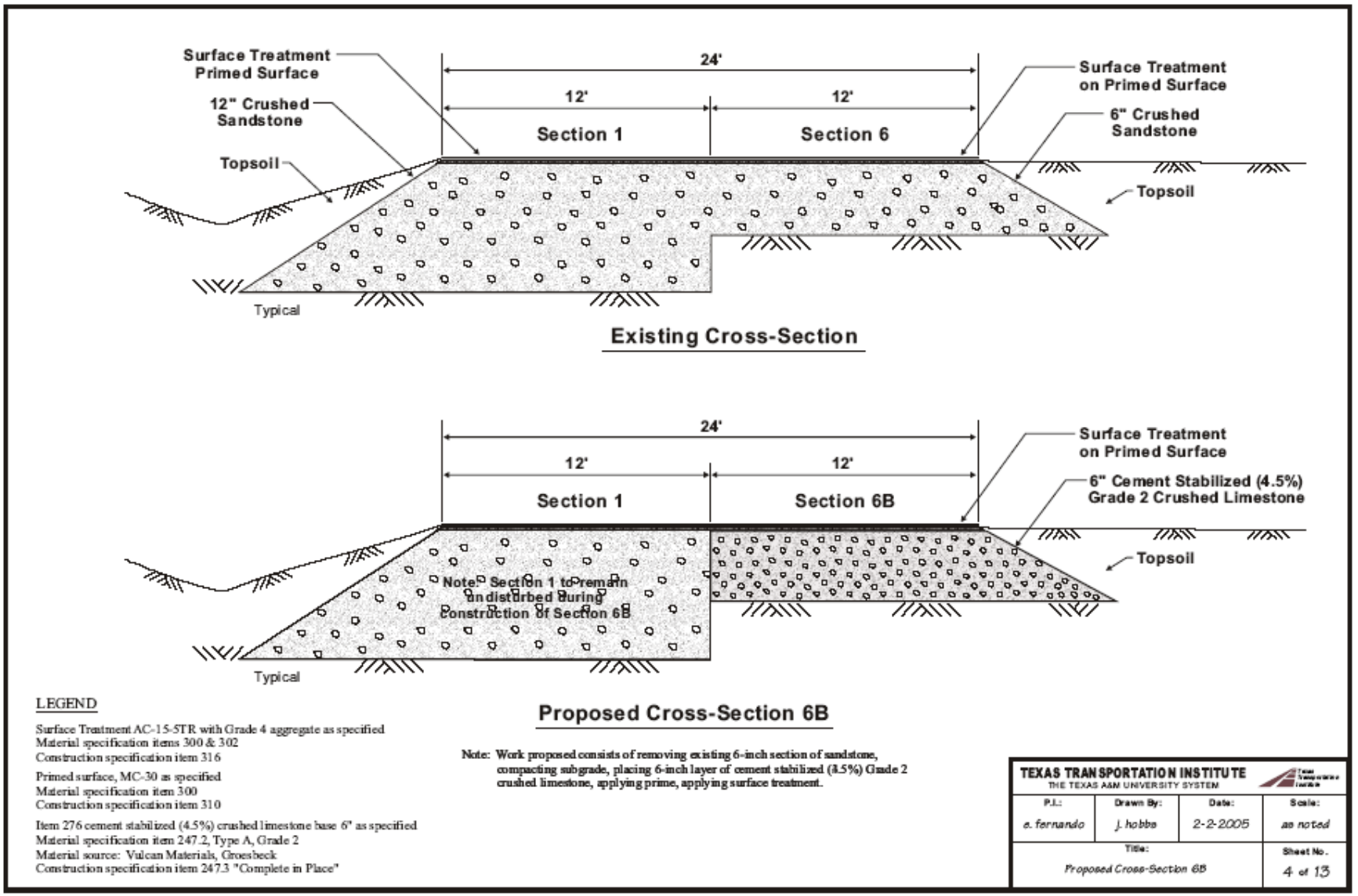

Figure A19. Proposed Cross-Section for Section 6B.

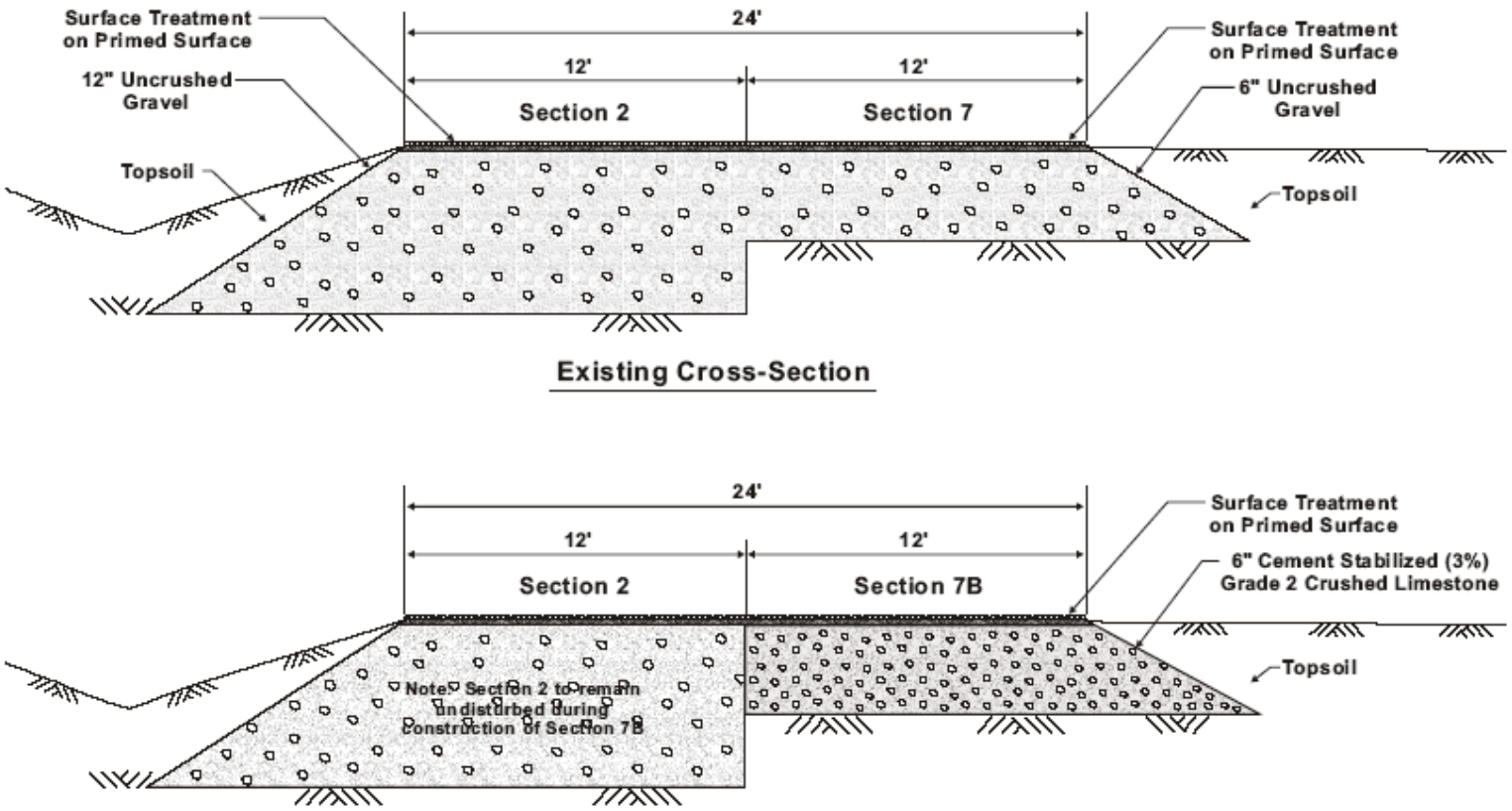

LEGEND

Surface Treatment AC-15-5TR with Grade 4 aggregate as specified
Material specification items 300 & 302
Construction specification item 316

Primed surface, MC-30 as specified
Material specification item 300
Construction specification item 310

Item 276 cement stabilized (3%) crushed limestone base 6" as specified
Material specification item 247.2, Type A, Grade 2
Material source: Vulcan Materials, Groesbeck
Construction specification item 247.3 "Complete in Place"

Note: Work proposed consists of removing existing 6-inch section of uncrushed gravel, compacting subgrade, placing 6-inch layer of cement stabilized (3%) Grade 2 crushed limestone, applying prime, applying surface treatment.

TEXAS TRANSPORTATION INSTITUTE THE TEXAS A&M UNIVERSITY SYSTEM			
P.I.:	Drawn By:	Date:	Scale:
a. fernando	j. hobbs	2-2-2005	as noted
Title: Proposed Cross-Section 7B			Sheet No.: 5 of 13

Figure A20. Proposed Cross-Section for Section 7B.

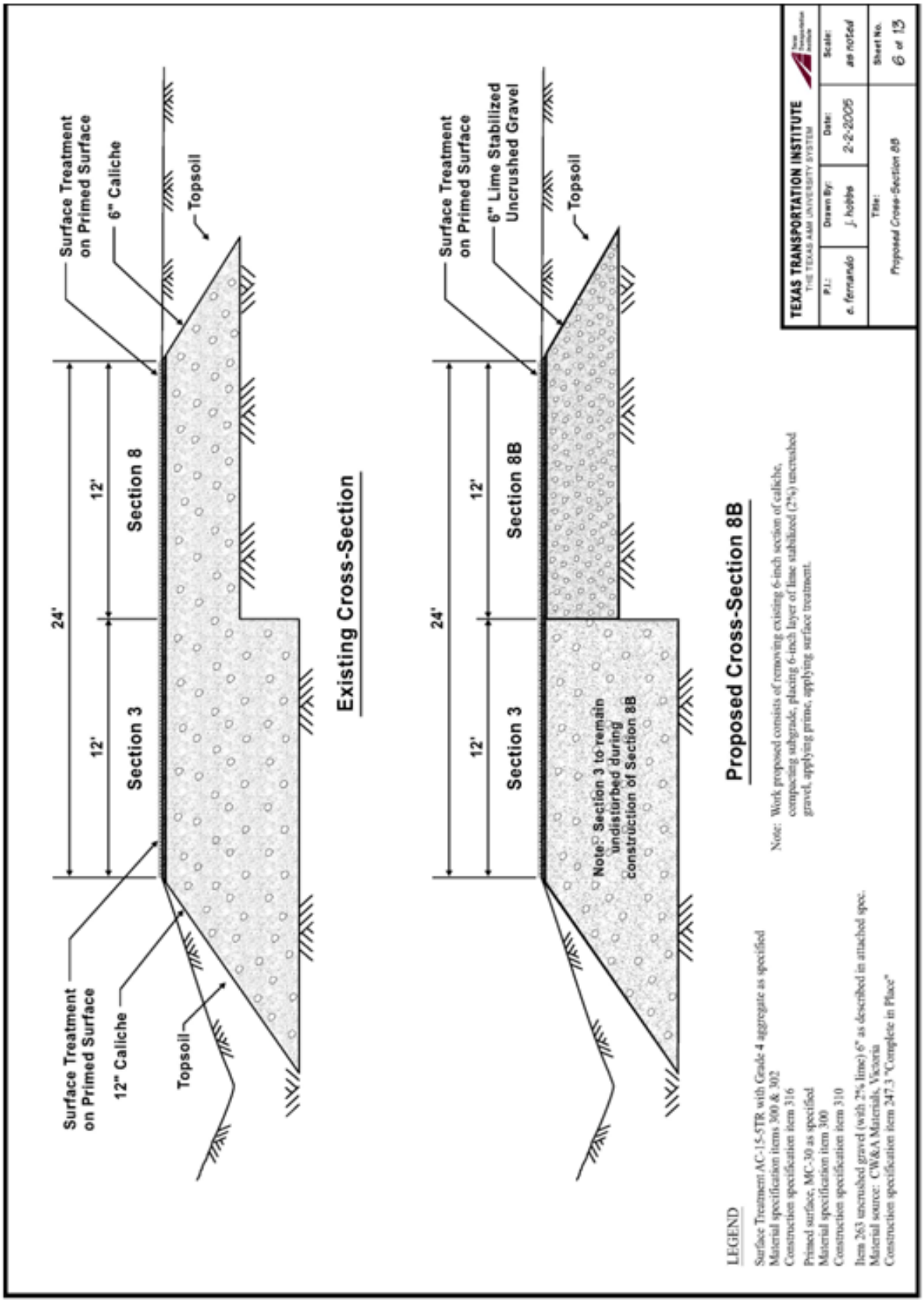

Figure A21. Proposed Cross-Section for Section 8B.

Figure A22. Proposed Cross-Section for Section 9B.

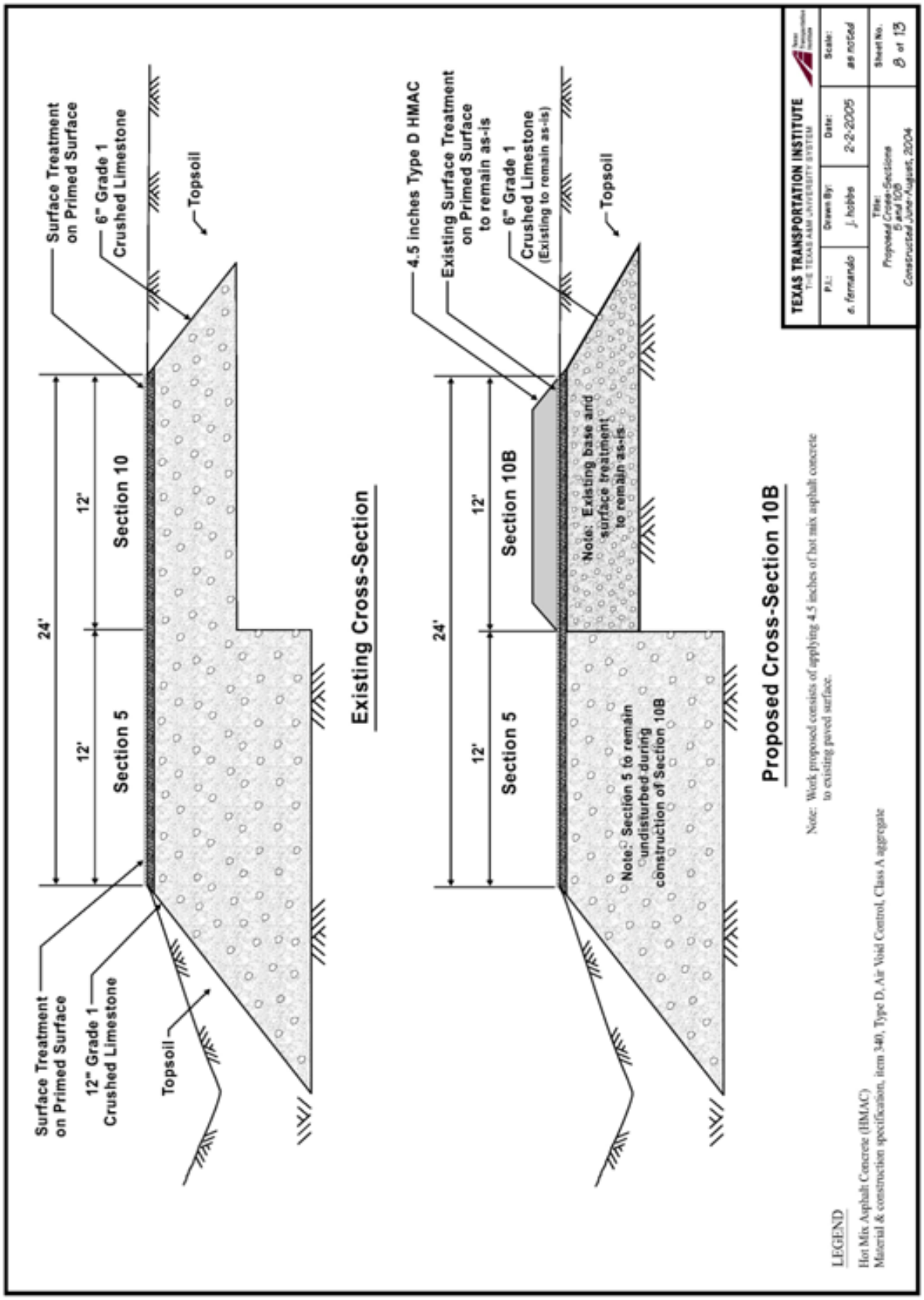

Figure A23. Proposed Cross-Section for Section 10B.

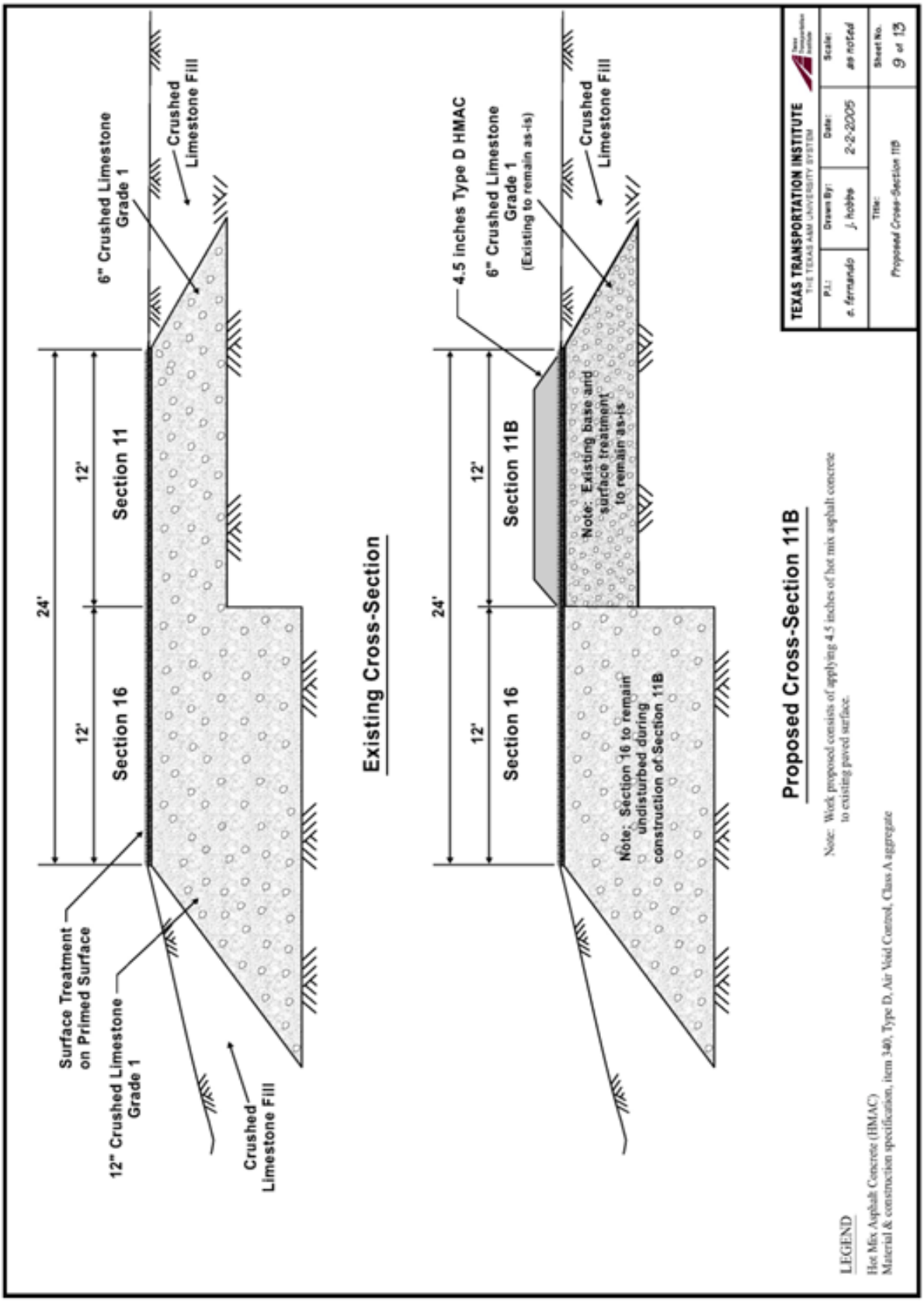

Figure A24. Proposed Cross-Section for Section 11B.

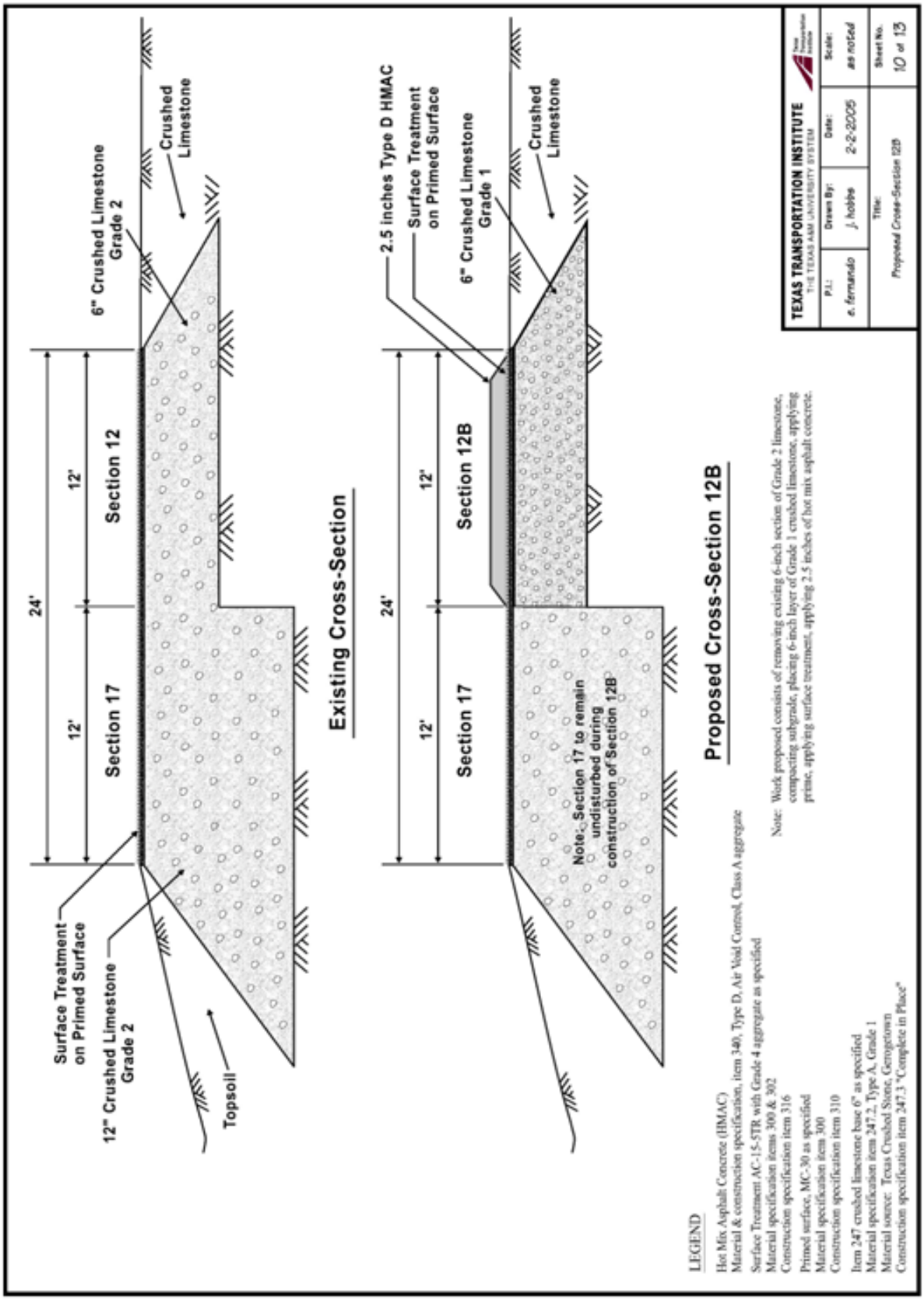

Figure A25. Proposed Cross-Section for Section 12B.

Figure A26. Proposed Cross-Section for Section 13B.

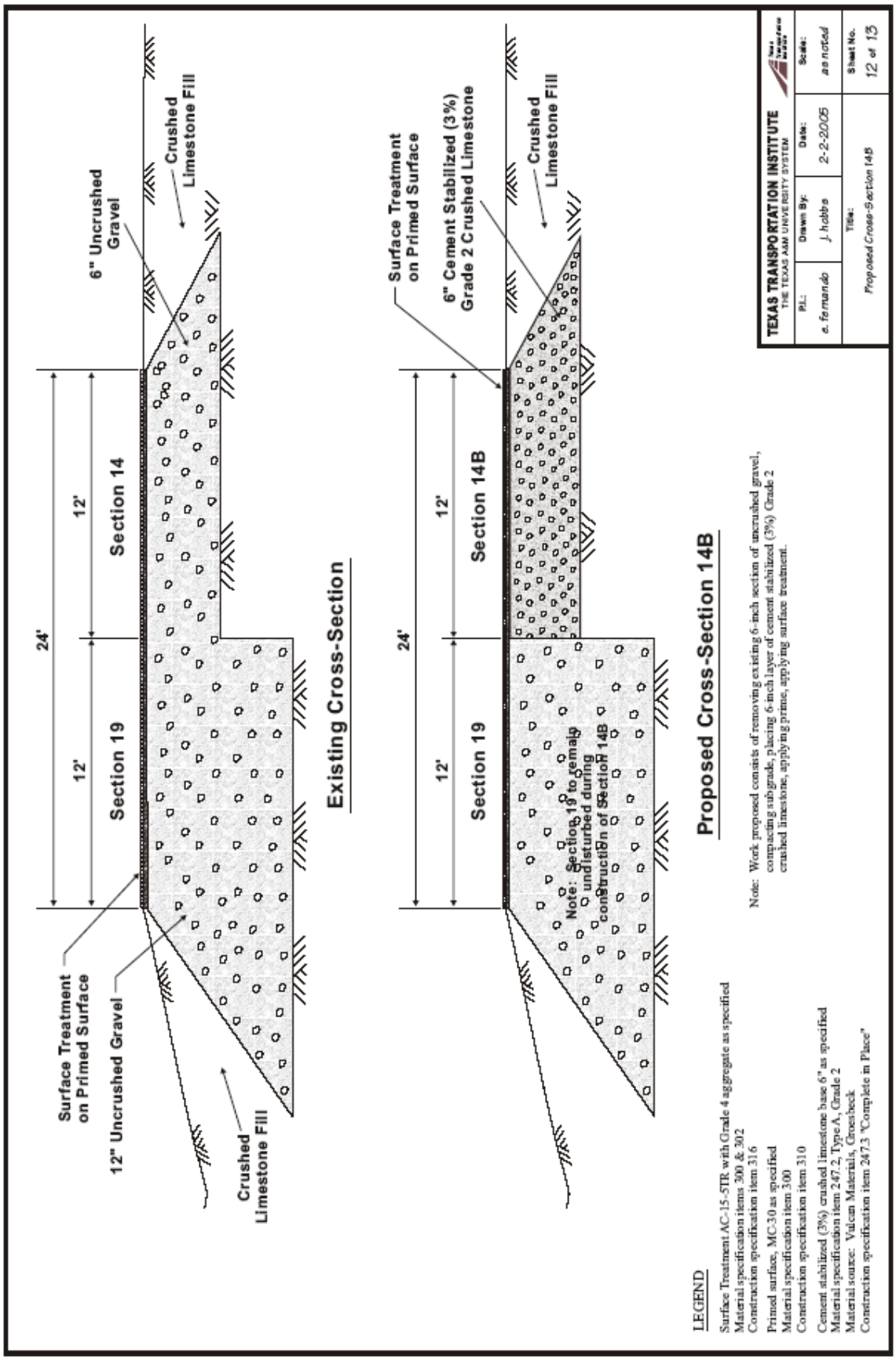

Figure A27. Proposed Cross-Section for Section 14B.

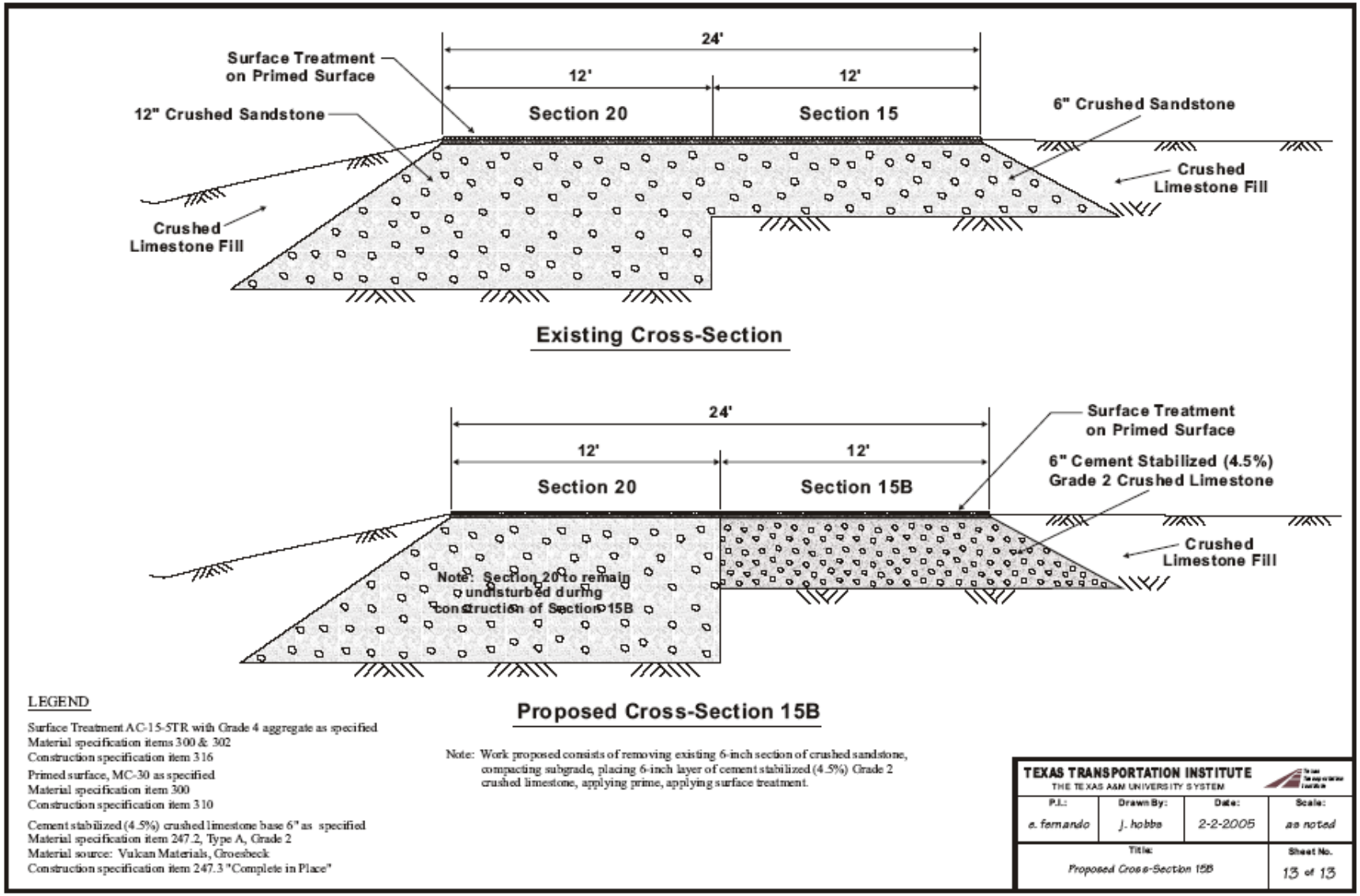

Figure A28. Proposed Cross-Section for Section 15B.

APPENDIX B. LABORATORY TEST RESULTS

Table B1. Gradation and Atterberg Limit Results for Base Materials.

Property	Base Material				
Master Gradation Sieve Size (% retained)	Grade 1 Limestone	Grade 2 Limestone	Caliche	Sandstone	Gravel
2-1/2 in	0	0	0	0	0
1-3/4 in	0	0	0	0	0
7/8 in	18.1	33.7	9.6	14.0	15.3
3/8 in	35.3	55.8	28.9	40.5	37.1
No. 4	49.7	70.0	48.1	59.2	56.4
No. 40	76.3	88.4	79.3	79.2	83.2
No. 100	86.4	94.7	94.1	89.4	95.8
No. 200	92.0	98.9	97.8	95.2	98.9
Liquid Limit, %	15	19	27	16	22
Plasticity Index	2	6	9	6	14

Table B2. Optimum Moisture Density Data for Base Materials.

Materials	Optimum Moisture Content	Optimum Density
Grade 1 Limestone (Phase I and II)	134.7	8.3
Grade 2 Limestone (Phase I and II) w/ 4.5 percent cement (Phase II)	134.1 133.8	7.7 7.3
Caliche (Phase I)	109.8	15.6
Sandstone (Phase I)	135.4	7.3
Gravel (Phase I and II)	137.2	6.3

Table B3. Triaxial Test Results for Base Materials.

Grade 1 Limestone					
Tex-117E		Modified Tex-117E		Tex-143*	
σ_3 (psi)	σ_1 (psi)	σ_3 (psi)	σ_1 (psi)	σ_3 (psi)	σ_1 (psi)
0	41.8	0	67.0	3	50.0
3	131.9	3	135.9	7	112.2
5	135.5	5	140.6	10	145.7
10	145.6	10	148.0		
15	169.4	15	191.1		
20	187.9	20	237.7		
TTC**	1.0	1.0		1.0	
c (psi)	15.9	23.0		4.3	
$\phi°$	49.8	46.3		59.5	

* Tex-143 tests done only at confining pressures of 0, 3, and 5 psi.

** Texas triaxial class

Table B3. Triaxial Test Results for Base Materials (continued).

Grade 2 Limestone					
Tex-117E		Modified Tex-117E		Tex-143	
σ_3 (psi)	σ_1 (psi)	σ_3 (psi)	σ_1 (psi)	σ_3 (psi)	σ_1 (psi)
0	25.4	0	40.7	3	66.3
3	85.9	3	88.8	7	124.4
5	98.7	5	99.0	10	155.0
10	146.4	10	187.3		
15	184.7	15	208.4		
20	194.5	20	245.9		
TTC	2.3	1.0		1.0	
c (psi)	8.0	19.0		6.0	
$\phi°$	55.7	50.7		57.0	
Caliche					
Tex-117E		Modified Tex-117E		Tex-143	
σ_3 (psi)	σ_1 (psi)	σ_3 (psi)	σ_1 (psi)	σ_3 (psi)	σ_1 (psi)
0	47.8	0	76.6	3	67.7
3	146.4	3	151.3	7	131.9
5	156.7	5	157.1	10	156.4
10	162.9	10	195.7		
15	218.3	15	246.0		
20	231.9	20	255.3		
TTC	1.0	1.0		1.0	
c (psi)	17.4	32.5		10.0	
$\phi°$	52.5	45.8		56.0	
Sandstone					
Tex-117E		Modified Tex-117E		Tex-143	
σ_3 (psi)	σ_1 (psi)	σ_3 (psi)	σ_1 (psi)	σ_3 (psi)	σ_1 (psi)
0	38.8	0	62.1	3	95.6
3	53.7	3	76.1	7	147.3
5	106.2	5	126.5	10	177.1
10	145.4	10	198.8		
15	198.5	15	224.1		
20	212.0	20	268.1		
TTC	2.1	1.0		1.0	
c (psi)	9.4	17.0		12.0	
$\phi°$	56.4	56.0		56.8	

Table B3. Triaxial Test Results for Base Materials (continued).

Uncrushed Gravel					
Tex-117E		Modified Tex-117E		Tex-143	
σ_3 (psi)	σ_1 (psi)	σ_3 (psi)	σ_1 (psi)	σ_3 (psi)	σ_1 (psi)
0	10.9	0	30.8	3	30.5
3	33.7	3	87.1	7	47.6
5	56.1	5	98.7	10	73.5
10	75.8	10	106.4		
15	89.5	15	157.4		
20	110.9	20	178.1		
TTC	2.5	2.3		3.0	
c (psi)	9.3	14.0		3.2	
$\phi°$	48.3	47.0		45.7	

Table B4. Triaxial Test Results for Subgrade Materials.

Clay							
Tex-117E		Modified Tex-117E		Tex-143		Tex-143 at field moisture content*	
σ_3 (psi)	σ_1 (psi)	σ_3 (psi)	σ_1 (psi)	σ_3 (psi)	σ_1 (psi)	σ_3 (psi)	σ_1 (psi)
0	4.2	0	100.1	3	73.8	3	25.3
3	10.1	3	101.3	7	84.2	7	28.8
5	11.2	5	114.4	10	95.9	10	33.5
10	17.1	10	136.4				
15	24.9	15	150.7				
20	32.5	20	180.0				
TTC	6.1	2.8		2.9		5.0	
c (psi)	1.7	24.7		18.0		11.4	
$\phi°$	10.3	35.0		31.0		1.0	
Sandy Soil							
Tex-117E		Modified Tex-117E		Tex-143		Tex-143 at field moisture content*	
σ_3 (psi)	σ_1 (psi)	σ_3 (psi)	σ_1 (psi)	σ_3 (psi)	σ_1 (psi)	σ_3 (psi)	σ_1 (psi)
0	18.2	0	32.9	3	20.2	3	19.4
3	35.8	3	41.0	7	41.1	7	37.1
5	39.4	5	50.0	10	53.5	10	48.2
10	69.9	10	73.0				
15	72.7	15	80.5				
20	87.9	20	98.9				
TTC	3.7	3.5		3.8		4.0	
c (psi)	6.0	8.4		5.2		2.0	
$\phi°$	32.8	30.5		35.0		38.0	

*Specimens tested at average field moisture content (clay = 22% and sand = 7%).

Table B5. Tube Suction Test Results.

Test Parameter	Grade 1 Limestone	Grade 2 Limestone	Caliche	Sandstone	Gravel
Dielectric Value	18.3	20.6	23.2	11.7	20.2
Moisture Susceptibility Rating	Poor	Poor	Poor	Marginal	Poor

Table B6. Resilient Modulus Parameters*.

Material		Caliche	Limestone		Sandstone	Uncrushed Gravel	Sand	Clay
			Grade 1	Grade 2				
Optimum	K_1	2434	3423	657	1901	669	919	1927
	K_2	-0.2	0.35	0.7	0.35	0.7	0.60	0.0
	K_3	-0.2	-0.2	-0.3	-0.1	-0.6	0.0	-0.1
	R^2	0.91	0.89	0.94	0.91	0.91	0.86	0.97
Saturated	K_1	281	1699	367	2196	490	437	2916
	K_2	0.5	0.20	0.5	0.0	1.0	1.0	0.9
	K_3	-0.4	-0.11	-0.3	0.2	-0.5	-0.24	0.8
	R^2	0.99	0.97	0.90	0.96	0.94	0.81	0.93

* Based on the following nonlinear resilient modulus equation by Uzan (1985):

$$M_R = K_1 P_a \left(\frac{I_1}{P_a} \right)^{K_2} \left(\frac{\tau_{oct}}{P_a} \right)^{K_3} \quad \text{(B1)}$$

where,

M_R = resilient modulus,

P_a = atmospheric pressure (14.5 psi),

I_1 = first stress invariant,

τ_{oct} = octahedral shear stress, and

K_1, K_2, K_3 = stress-dependent material constants.

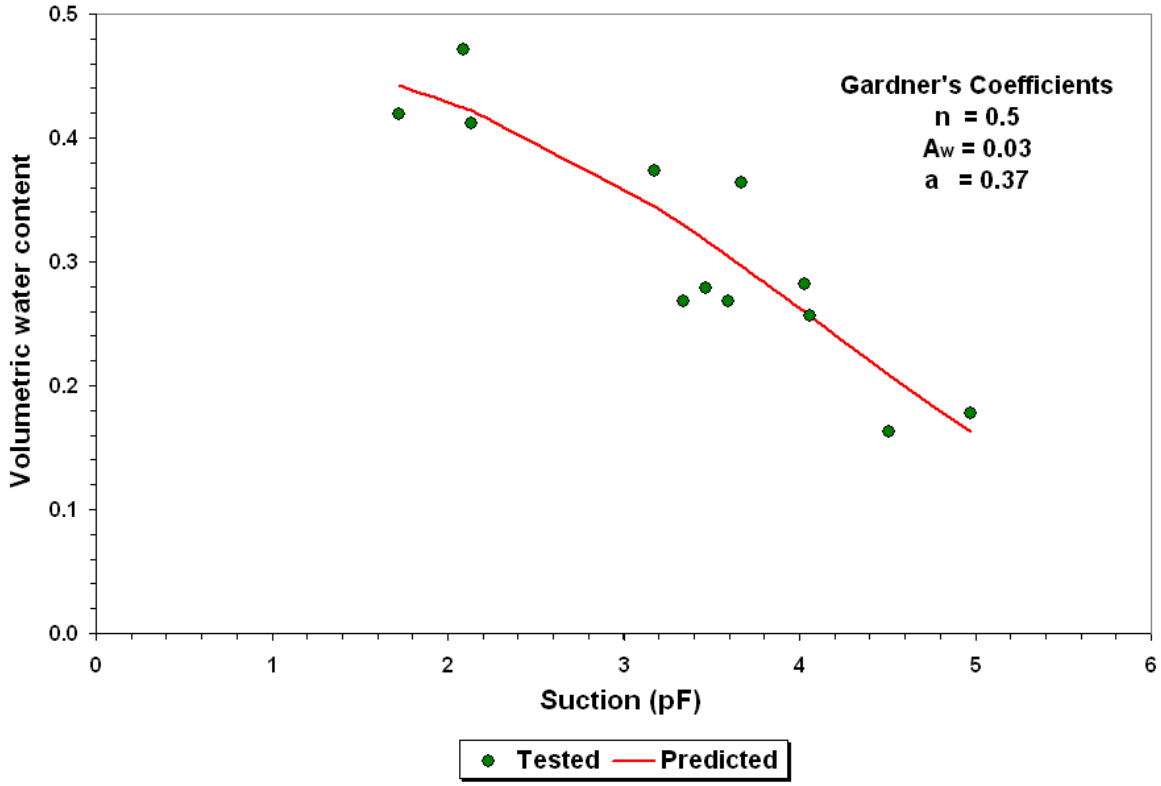

Figure B1. Results from Soil Suction Tests on Clay Subgrade.

Note: Soil suction tests were made using the filter paper method described by Bulut, Lytton, and Wray (2001). The fitted curve and the coefficients of Gardner's equation for the clay subgrade are shown in Figure B1. These coefficients relate the volumetric water content to the measured soil suction according to the following equation by Gardner (1958):

$$\theta_u = \frac{n}{A_w |h|^a + 1} \qquad \text{(B2)}$$

where,

θ_u = unsaturated volumetric moisture content,

n = porosity,

A_w, a = model coefficients, and

h = soil suction in cm of water head.

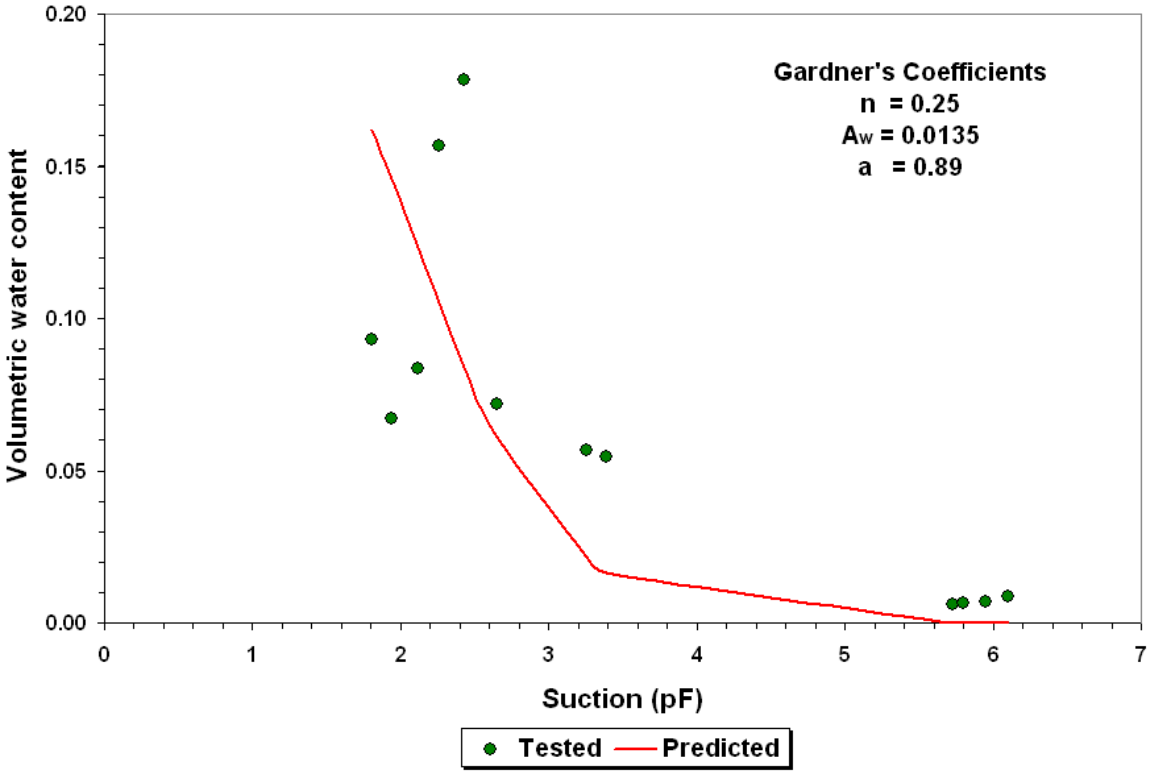

Figure B2. Results from Soil Suction Tests on Sandy Subgrade.

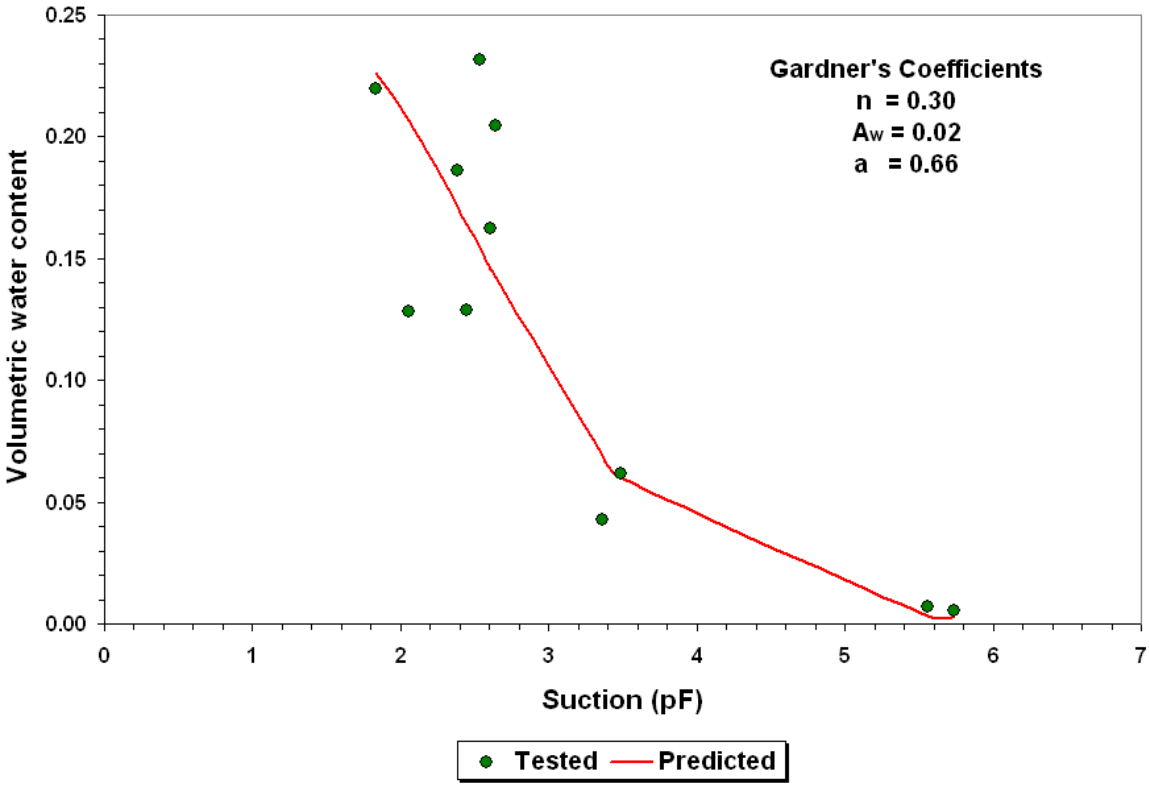

Figure B3. Results from Soil Suction Tests on Grade 1 Crushed Limestone.

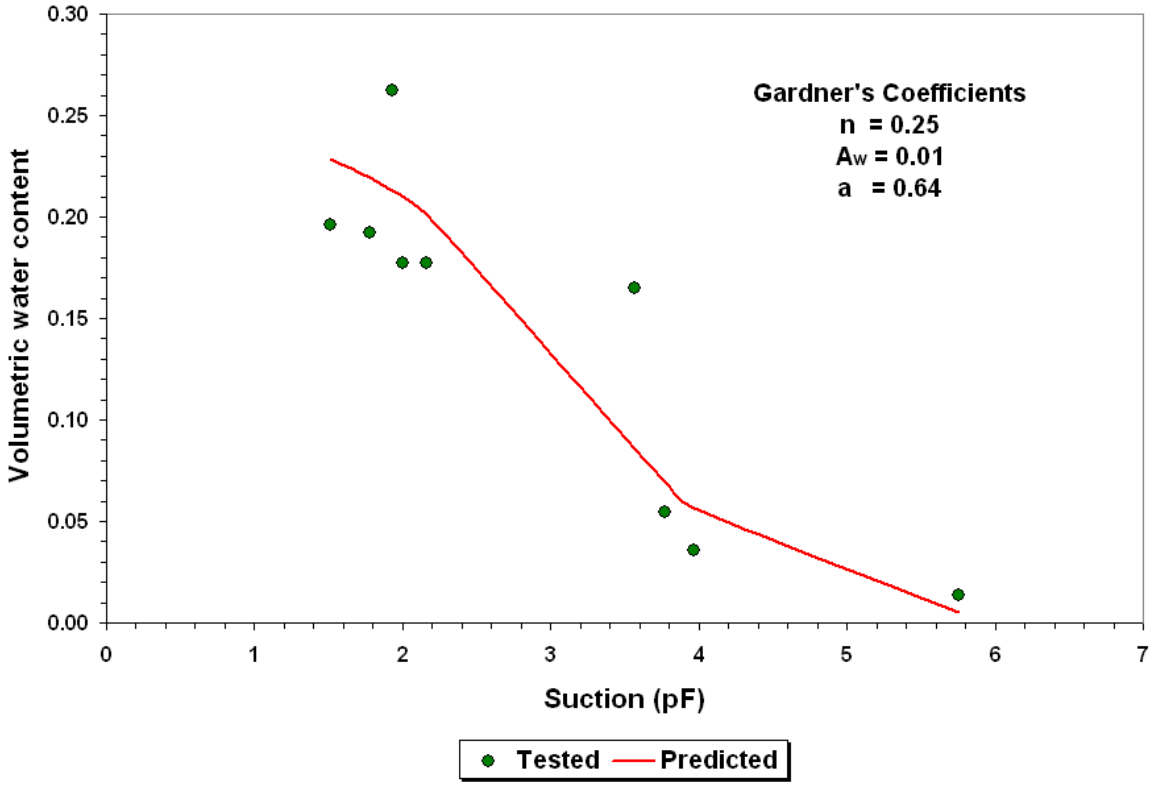

Figure B4. Results from Soil Suction Tests on Grade 2 Crushed Limestone.

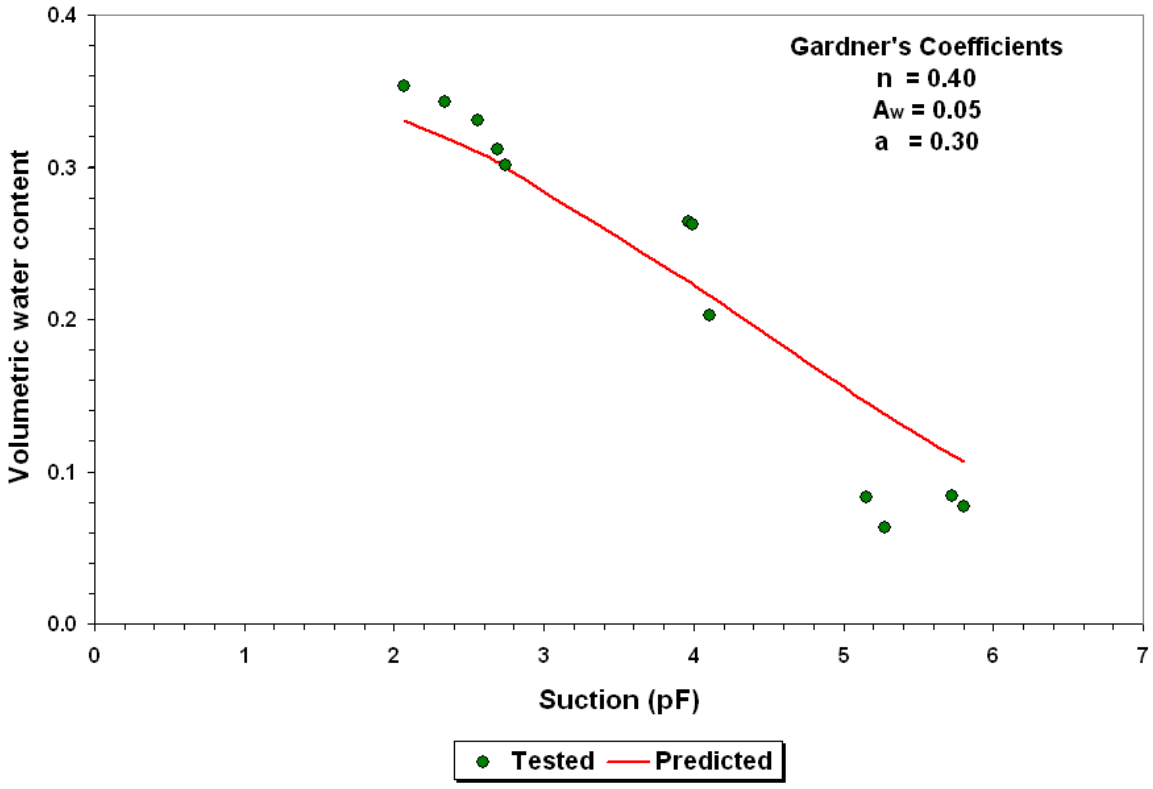

Figure B5. Results from Soil Suction Tests on Caliche.

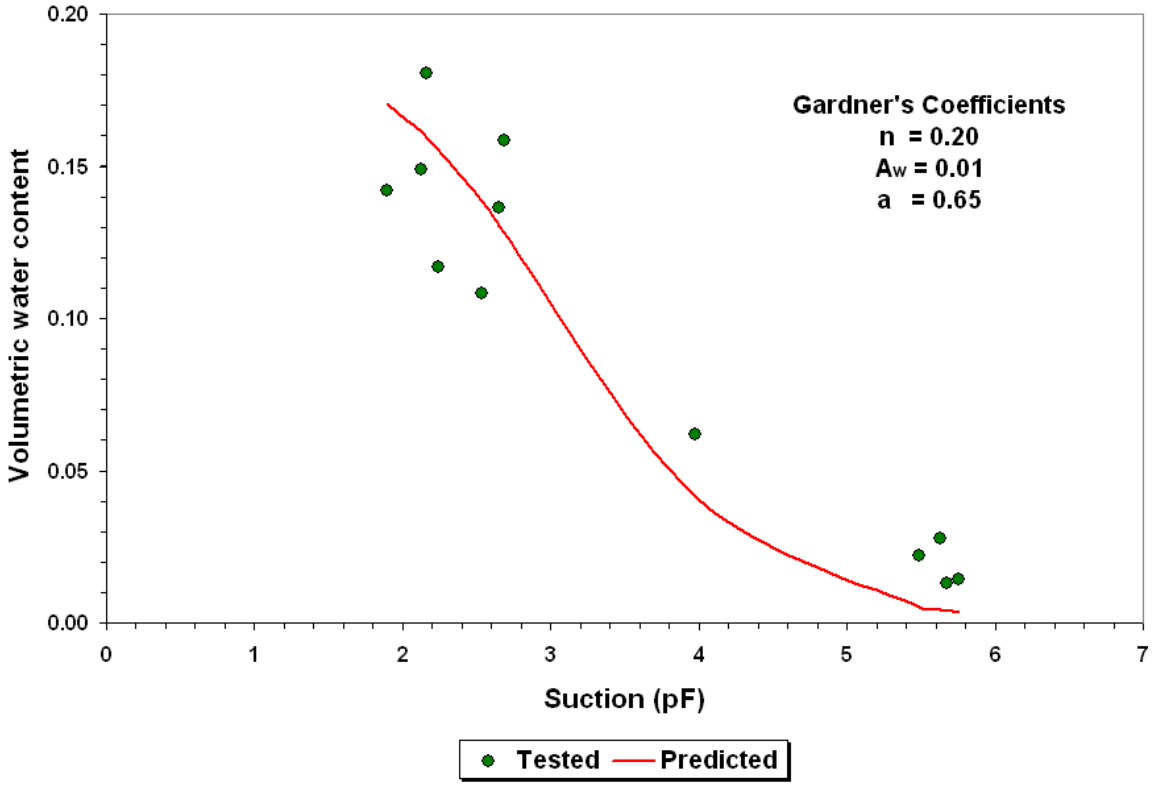

Figure B6. Results from Soil Suction Tests on Uncrushed Gravel.

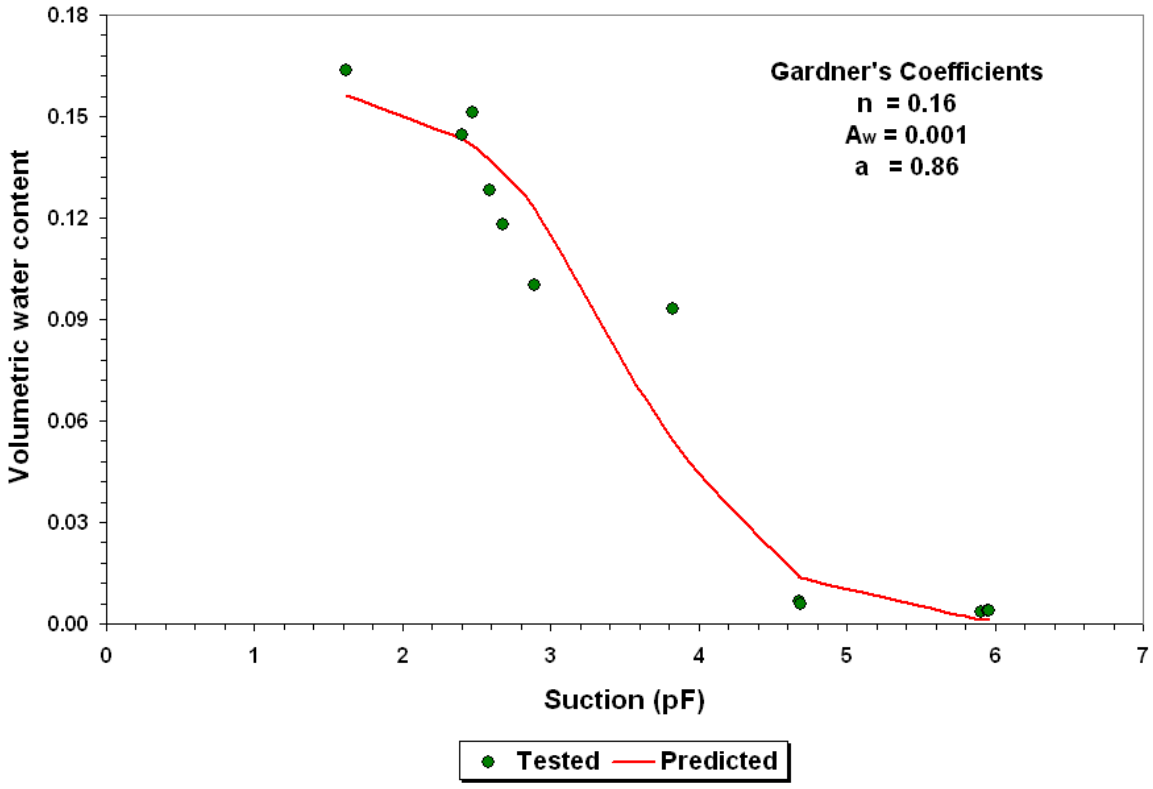

Figure B7. Results from Soil Suction Tests on Sandstone.

APPENDIX C. DATA FROM TESTS CONDUCTED DURING AND AFTER CONSTRUCTION OF FULL-SCALE PAVEMENT SECTIONS

Table C1. Base Thickness Estimates from GPR Data on Thin Sandstone Section on Clay Subgrade.

Distance (feet)	Thickness (inches)
0.00	6.1
0.33	6.0
0.67	5.7
1.00	4.9
1.50	4.8
2.00	5.2
2.33	5.7
2.67	5.9
3.00	5.9
3.50	6.0
4.00	6.2
4.50	6.4
5.00	6.5
5.50	6.6
6.00	6.5
6.33	6.3
6.67	6.4
7.00	6.5
7.50	6.5
8.00	6.4
8.33	6.4
8.67	6.4
9.00	6.5
9.50	6.6
10.00	7.1
10.50	7.3
11.00	7.4
11.33	7.7
11.67	7.6
12.00	7.6
12.50	7.6
13.00	7.5
13.33	7.5
13.67	7.4
14.00	7.6
14.50	7.4
15.00	7.4
15.50	7.1
16.00	7.0
Average (inches)	6.6
Standard Deviation (inches)	0.77

Table C2. Base Thickness Estimates from GPR Data on Thin Uncrushed Gravel Section on Clay Subgrade.

Distance (feet)	Thickness (inches)
0.00	6.4
0.50	5.4
1.00	4.7
1.50	4.9
2.00	6.0
2.50	6.0
3.00	6.1
3.50	6.1
4.00	6.2
4.50	6.4
5.00	6.5
5.33	6.7
5.67	7.1
6.00	7.3
6.50	7.4
6.83	7.2
7.17	7.1
7.50	7.2
8.00	7.4
8.50	7.4
9.00	7.1
9.50	6.9
10.00	7.0
10.50	7.2
10.83	7.1
11.17	7.1
11.50	6.9
12.00	6.9
12.50	6.8
13.00	6.6
13.50	6.6
14.00	6.5
14.50	6.6
15.00	6.9
Average (inches)	6.6
Standard Deviation (inches)	0.67

Table C3. Base Thickness Estimates from GPR Data on Thin Grade 2 Crushed Limestone Section on Clay Subgrade.

Distance (feet)	Thickness (inches)
0.00	6.2
0.50	5.4
0.83	5.0
1.17	6.2
1.50	7.3
2.00	7.0
2.50	6.9
3.00	6.8
3.50	6.7
4.00	6.9
4.50	6.9
4.83	6.7
5.17	6.7
5.50	7.0
6.00	6.9
6.50	6.4
7.00	6.4
7.50	6.5
7.83	6.5
8.17	6.8
8.50	7.0
9.00	7.0
9.50	6.8
10.00	6.6
10.50	6.9
10.83	7.2
11.17	7.2
11.50	7.1
12.00	6.9
12.50	6.5
13.00	6.6
13.50	6.9
13.83	6.9
14.17	7.1
14.50	7.3
Average (inches)	6.7
Standard Deviation (inches)	0.47

Table C4. Base Thickness Estimates from GPR Data on Thin Grade 1 Crushed Limestone Section on Clay Subgrade.

Distance (feet)	Thickness (inches)
0.00	7.1
0.50	6.3
1.00	5.6
1.50	5.1
1.83	5.7
2.17	7.1
2.50	7.3
3.00	7.3
3.50	7.3
4.00	7.2
4.50	7.1
5.00	7.0
5.50	7.0
6.00	6.8
6.50	6.7
7.00	6.7
7.50	6.7
7.83	7.0
8.17	7.1
8.50	7.3
9.00	7.4
9.50	7.2
10.00	7.1
10.50	6.9
10.83	6.8
11.17	6.7
11.50	6.6
12.00	6.6
12.50	6.5
13.00	6.4
13.50	6.4
14.00	6.5
14.50	6.5
14.83	6.3
15.17	6.2
15.50	6.1
16.00	6.1
Average (inches)	6.7
Standard Deviation (inches)	0.53

Table C5. Base Thickness Estimates from GPR Data on Thick Sandstone Section on Clay Subgrade.

Distance (feet)	Thickness (inches)
0.00	10.3
0.50	10.7
0.83	12.9
1.17	13.0
1.50	12.5
2.00	12.5
2.50	12.7
3.00	13.2
3.50	14.1
3.83	14.2
4.17	14.0
4.50	14.0
5.00	14.3
5.50	14.7
6.00	14.7
6.50	14.0
6.83	13.1
7.17	12.9
7.50	13.1
8.00	13.1
8.50	12.5
8.83	12.4
9.17	12.6
9.50	12.6
10.00	12.6
10.50	12.4
11.00	12.3
11.50	12.3
11.83	12.4
12.17	12.7
12.50	13.2
13.00	13.7
13.50	13.9
13.83	13.5
14.17	12.7
14.50	12.7
15.00	13.8
15.50	13.4
16.00	11.3
Average (inches)	13.0
Standard Deviation (inches)	0.95

Table C6. Base Thickness Estimates from GPR Data on Cement-Treated Sections on Clay Subgrade*.

Section	Distance (feet)	Thickness (inches)
Grade 2 with 4.5% cement	2	5.4
	6	6.3
	8	5.7
	Average (inches)	5.8
	Standard Deviation (inches)	0.46
Grade 2 with 3.0% cement	3	6.4
	7	6.5
	9	6.5
	11	6.3
	12	6.6
	15	6.1
	16	6.4
	Average (inches)	6.4
	Standard Deviation (inches)	0.16

*Hard to see bottom of base for many of the traces collected.

Table C7. Base Thickness Estimates from GPR Data on Stabilized Uncrushed Gravel Section on Clay Subgrade.

Distance (feet)	Thickness (inches)
0	5.6
1	5.6
2	6.9
3	5.5
4	6.1
5	6.2
6	6.0
7	6.1
8	6.4
9	6.6
10	6.4
11	6.6
12	6.2
13	6.6
14	7.5
15	7.0
16	7.0
Average (inches)	6.4
Standard Deviation (inches)	0.56

Table C8. Thickness Estimates from GPR Data on Thin HMAC Section on Clay Subgrade.

Distance (feet)	Thickness (inches)	
	Type D HMAC	Grade 1 Base
0	2.6	6.0
1	2.4	6.6
2	2.5	7.1
3	2.5	3.5
4	2.7	6.7
5	2.5	6.0
6	2.8	5.9
7	3.3	7.6
8	3.3	7.8
9	3.3	7.1
10	3.3	6.6
11	3.4	6.0
12	3.1	6.0
13	3.0	6.4
Average (inches)	2.9	6.4
Standard Deviation (inches)	0.37	1.03

Table C9. Thickness Estimates from GPR Data on Thick HMAC Section on Clay Subgrade.

Distance (feet)	Thickness (inches)	
	Type D HMAC	Grade 1 Base
0	4.9	7.9
1	4.9	7.0
2	4.9	6.6
3	4.9	6.8
4	4.7	6.8
5	4.5	6.7
6	4.7	6.6
7	5.2	6.3
8	5.1	6.2
9	5.1	6.3
10	5.3	6.2
11	5.1	6.0
12	5.5	5.4
13	5.2	5.5
14	5.2	5.9
15	5.0	8.4
Average (inches)	5.0	6.5
Standard Deviation (inches)	0.28	0.80

Table C10. Thickness Estimates from GPR Data on Thick HMAC Section on Sandy Subgrade.

Distance (feet)	Thickness (inches)	
	Type D HMAC	Grade 1 Base
0	4.1	8.3
1	3.8	7.3
2	3.8	7.3
3	3.8	7.3
4	3.8	7.1
5	3.8	7.2
6	3.6	7.6
7	3.7	7.5
8	3.8	7.5
9	3.9	7.9
10	3.8	8.0
11	3.7	8.3
12	3.6	8.3
13	3.5	8.6
14	3.7	8.3
15	3.2	10.3
Average (inches)	3.7	7.9
Standard Deviation (inches)	0.20	0.80

Table C11. Thickness Estimates from GPR Data on Thin HMAC Section on Sandy Subgrade.

Distance (feet)	Thickness (inches)	
	Type D HMAC	Grade 1 Base
0	2.7	6.7
1	2.7	6.3
2	2.7	6.0
3	2.8	5.7
4	2.9	6.1
5	2.8	6.3
6	2.7	5.7
7	2.9	5.9
8	2.7	6.3
9	2.8	6.7
10	2.6	6.6
11	2.6	7.0
12	2.7	6.5
13	2.6	6.1
14	2.5	6.4
Average (inches)	2.7	6.3
Standard Deviation (inches)	0.10	0.38

Table C12. Base Thickness Estimates from GPR Data on Stabilized Uncrushed Gravel Section on Sandy Subgrade.

Distance (feet)	Thickness (inches)
4	5.6
5	6.3
7	6.4
8	6.3
9	6.1
10	6.1
11	6.3
12	6.4
Average (inches)	6.2
Standard Deviation (inches)	0.26

Table C13. Base Thickness Estimates from GPR Data on Cement-Treated Sections on Sandy Subgrade*.

Section	Distance (feet)	Thickness (inches)
Grade 2 with 3.0% cement	1	6.4
	2	6.3
	5	5.7
	9	5.1
	11	5.2
	14	6.5
	15	6.6
	16	6.6
	Average (inches)	6.1
	Standard Deviation (inches)	0.63
Grade 2 with 4.5% cement	7	6.6
	8	6.7
	9	6.4
	Average (inches)	6.6
	Standard Deviation (inches)	0.15

*Hard to see bottom of base for many of the traces collected.

Table C14. Base Thickness Estimates from DCP Data.

Section Identifier	Subgrade	Base Material	Base Thickness (inches)
UGC_12	Clay	Uncrushed Gravel	12
CAC_12	Clay	Lime-Stabilized Caliche	12
G2C_12	Clay	Grade 2 Crushed Limestone	12
G1C_12	Clay	Grade 1 Crushed Limestone	12
CAC_6	Clay	Lime-Stabilized Caliche	6.5
G1S_6	Sand	Grade 1 Crushed Limestone	6
G2S_6	Sand	Grade 2 Crushed Limestone	6
CAS_6	Sand	Lime-Stabilized Caliche	5
UGS_6	Sand	Uncrushed Gravel	6.8
SSS_6	Sand	Sandstone	6.6
G1S_12	Sand	Grade 1 Crushed Limestone	11
G2S_12	Sand	Grade 2 Crushed Limestone	11.8
CAS_12	Sand	Lime-Stabilized Caliche	11.5
UGS_12	Sand	Uncrushed Gravel	11
SSS_12	Sand	Sandstone	11.2

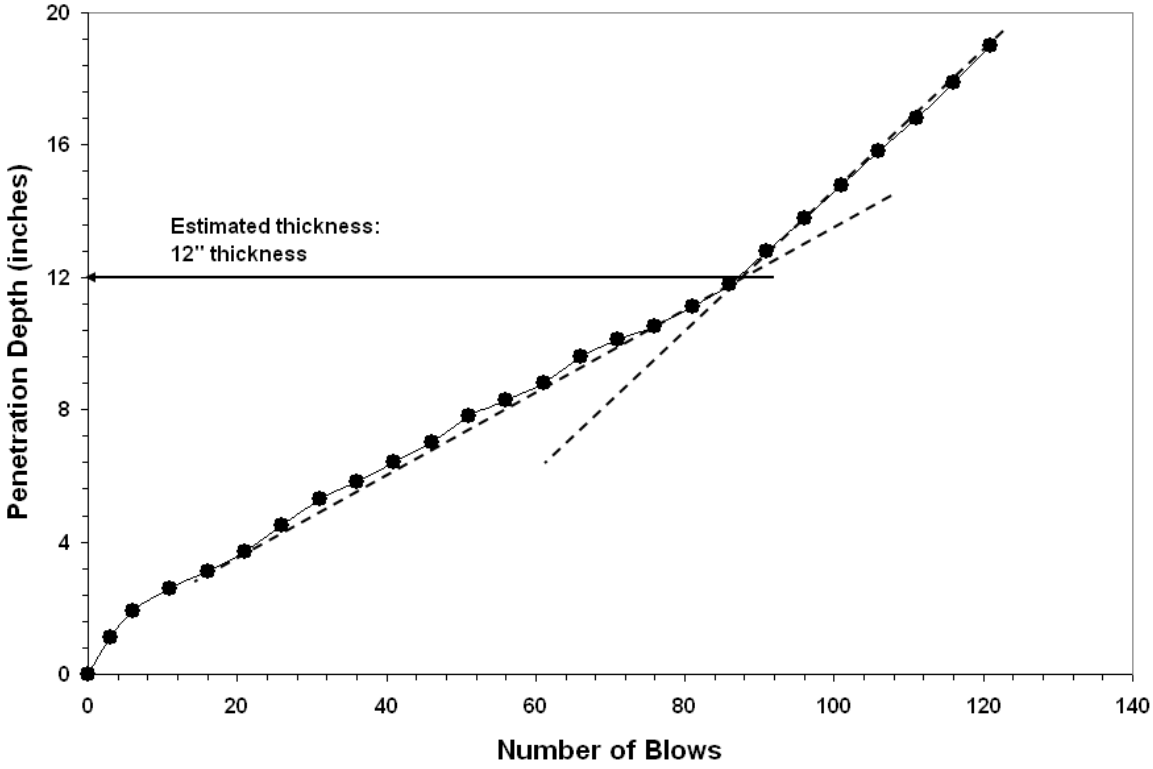

Figure C1. Estimating Base Thickness from DCP Data on Section UGC_12.

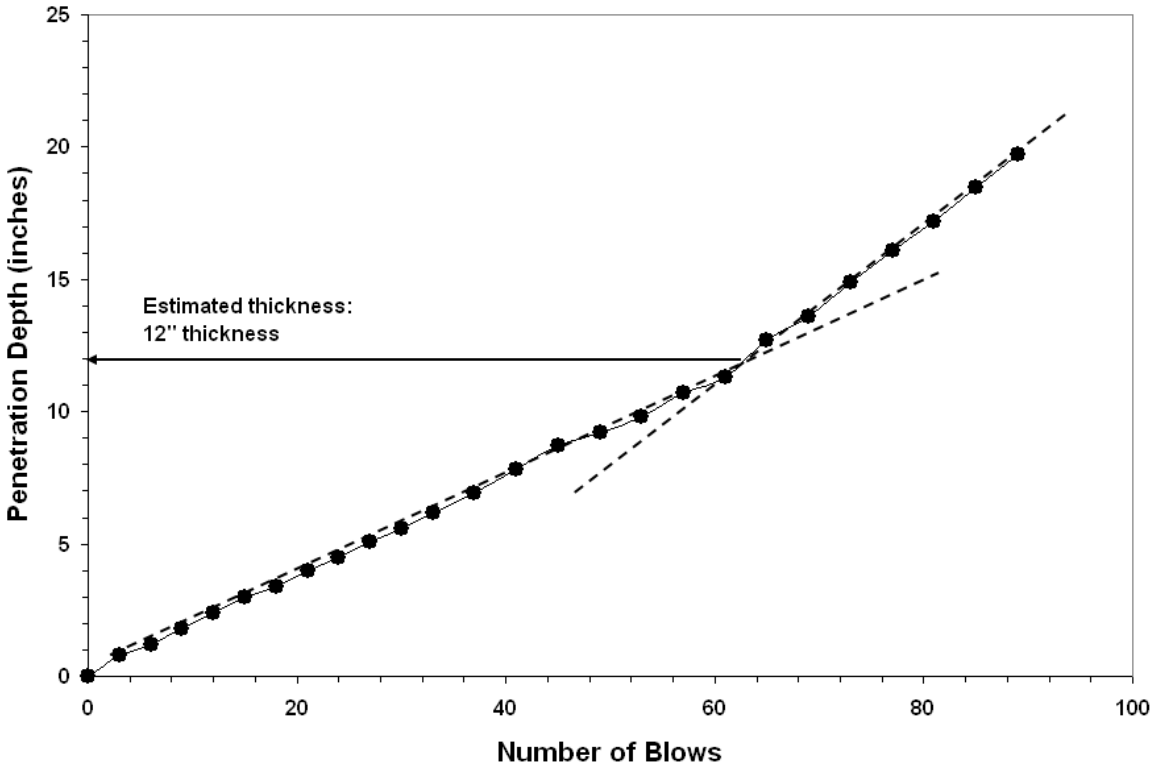

Figure C2. Estimating Base Thickness from DCP Data on Section CAC_12.

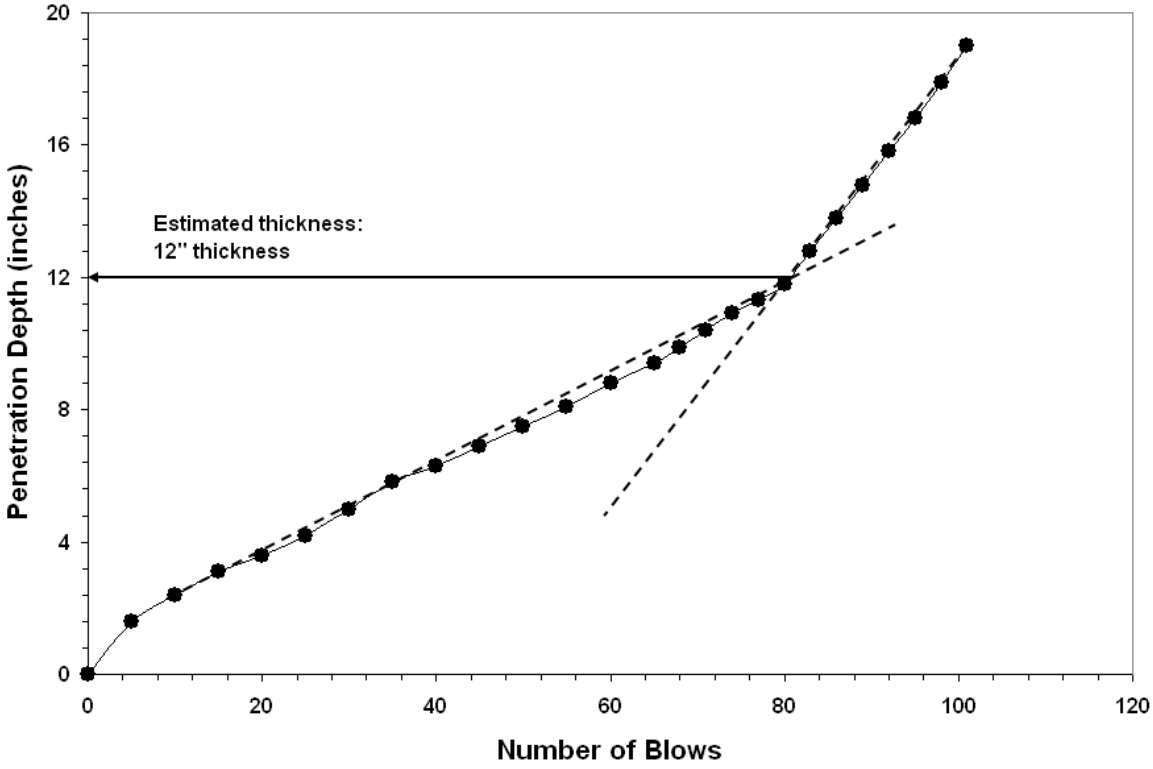

Figure C3. Estimating Base Thickness from DCP Data on Section G2C_12.

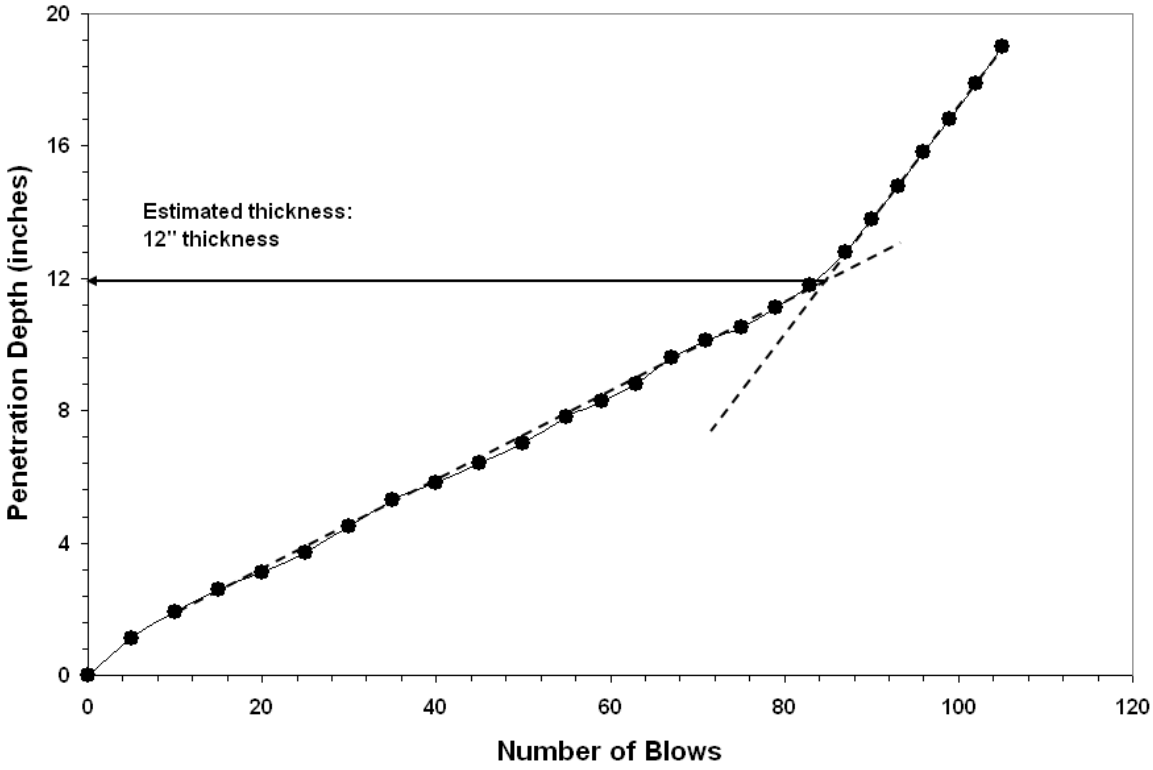

Figure C4. Estimating Base Thickness from DCP Data on Section G1C_12.

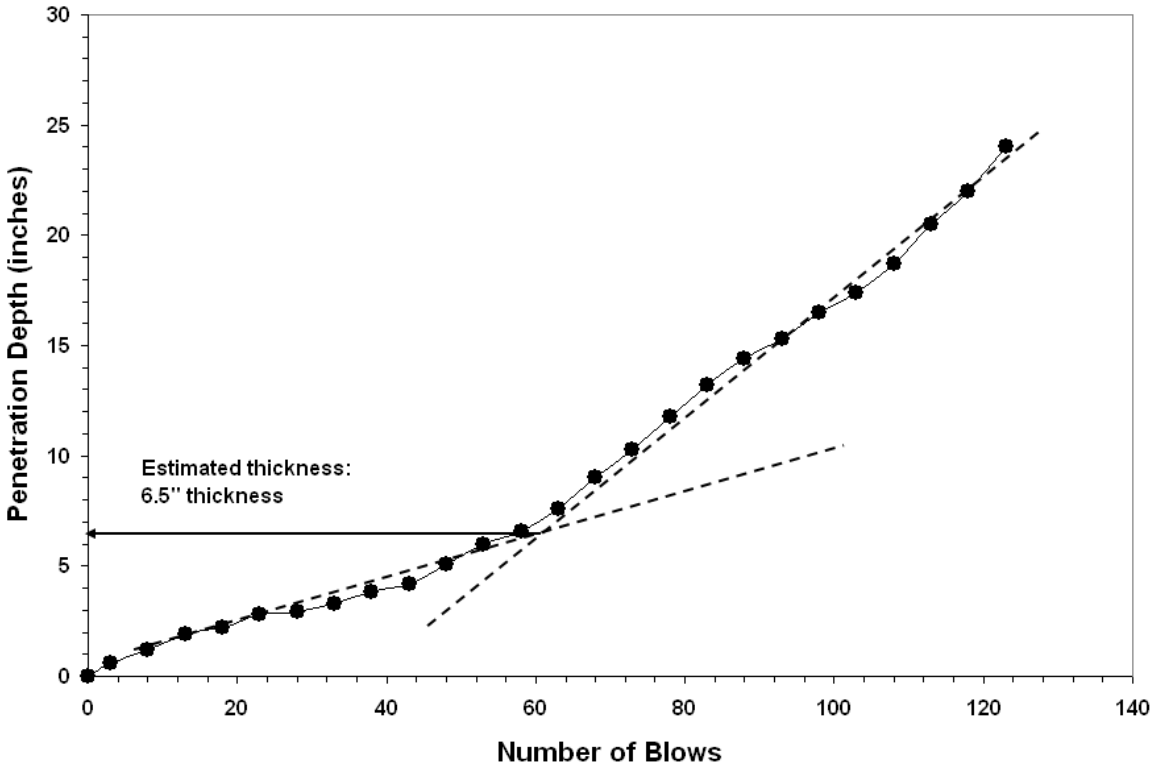

Figure C5. Estimating Base Thickness from DCP Data on Section CAC_6.

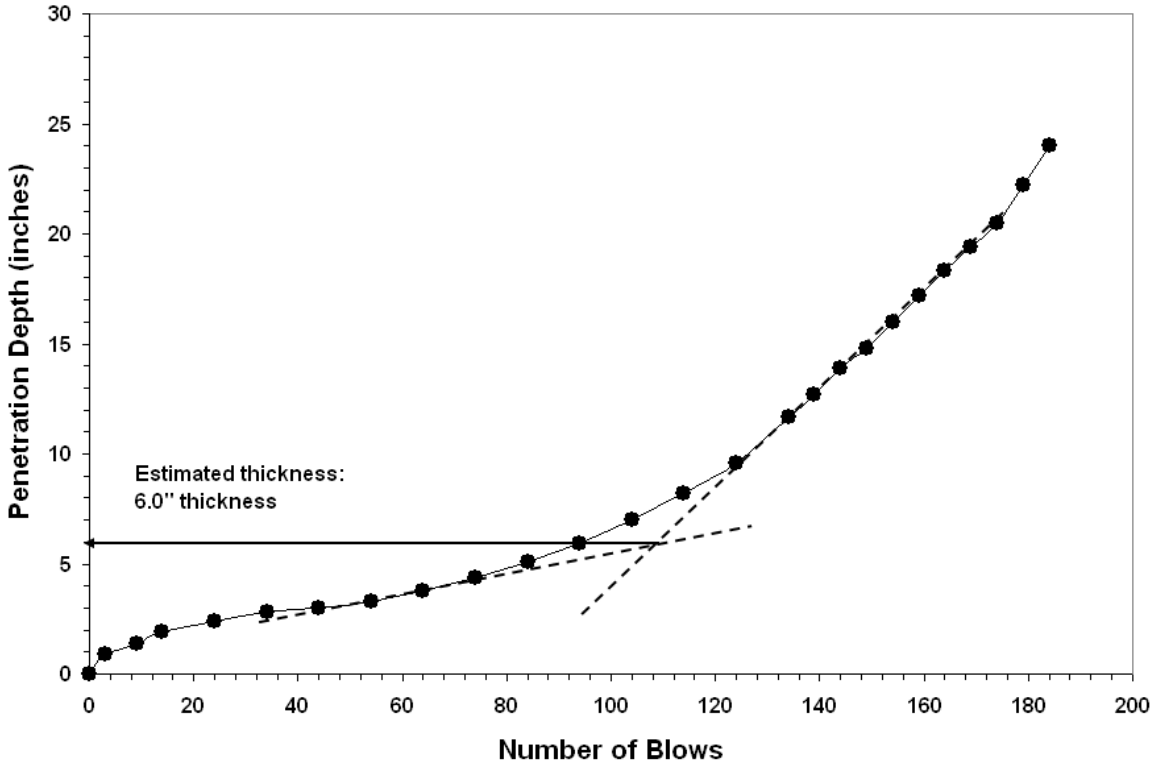

Figure C6. Estimating Base Thickness from DCP Data on Section G1S_6.

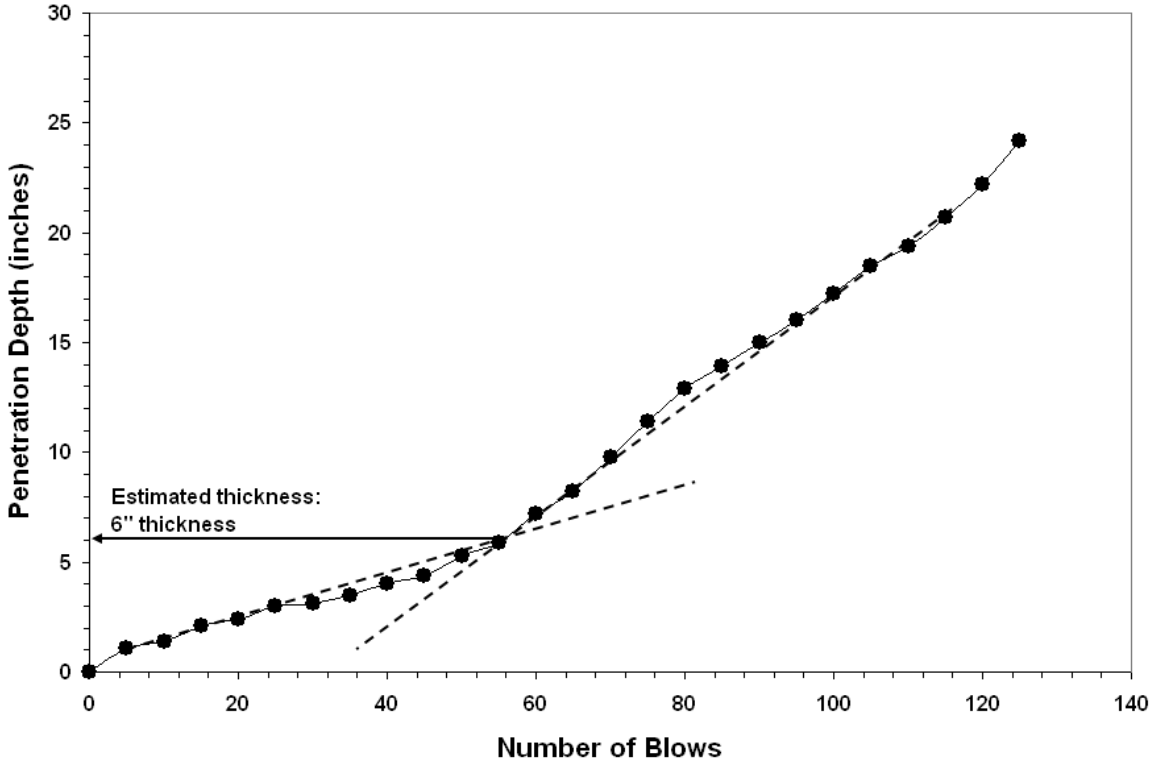

Figure C7. Estimating Base Thickness from DCP Data on Section G2S_6.

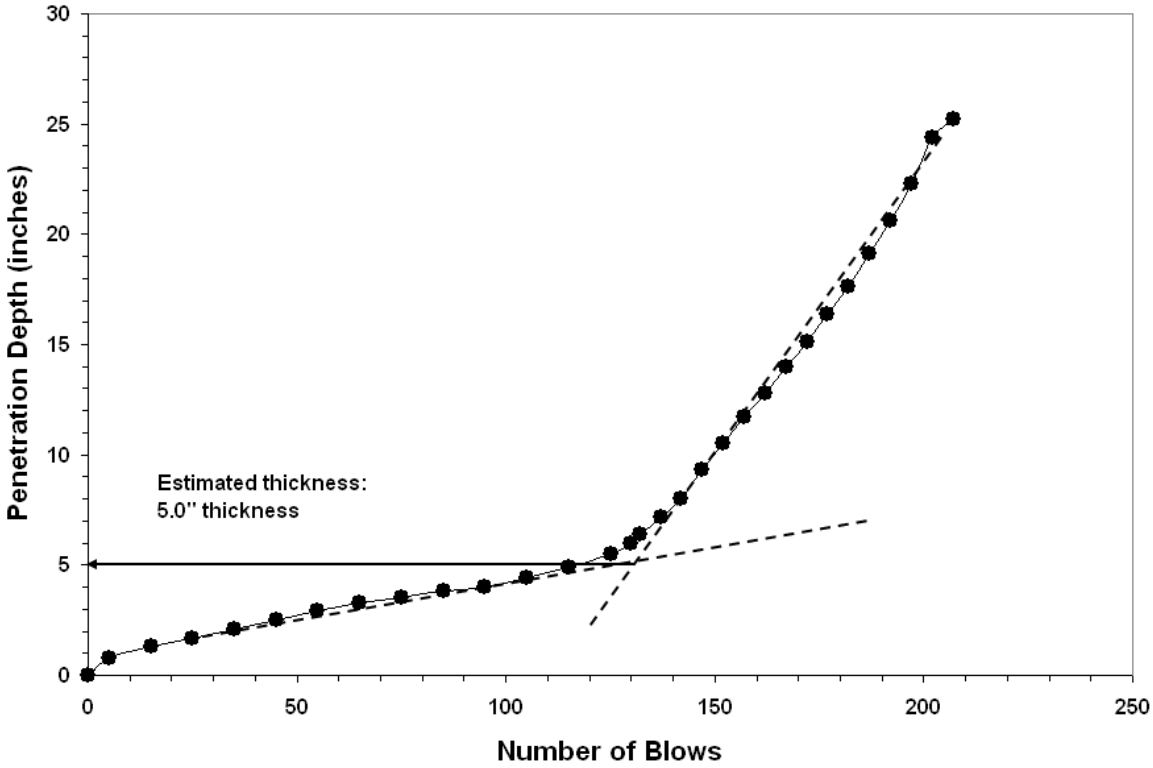

Figure C8. Estimating Base Thickness from DCP Data on Section CAS_6.

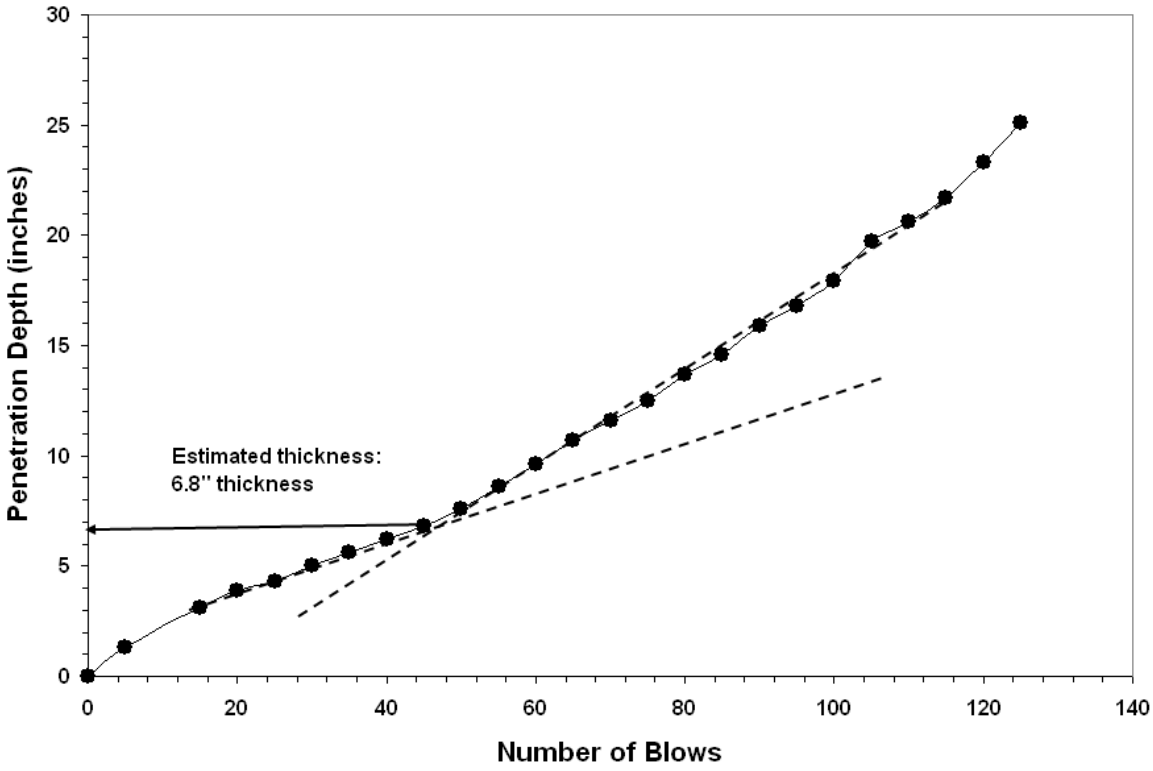

Figure C9. Estimating Base Thickness from DCP Data on Section UGS_6.

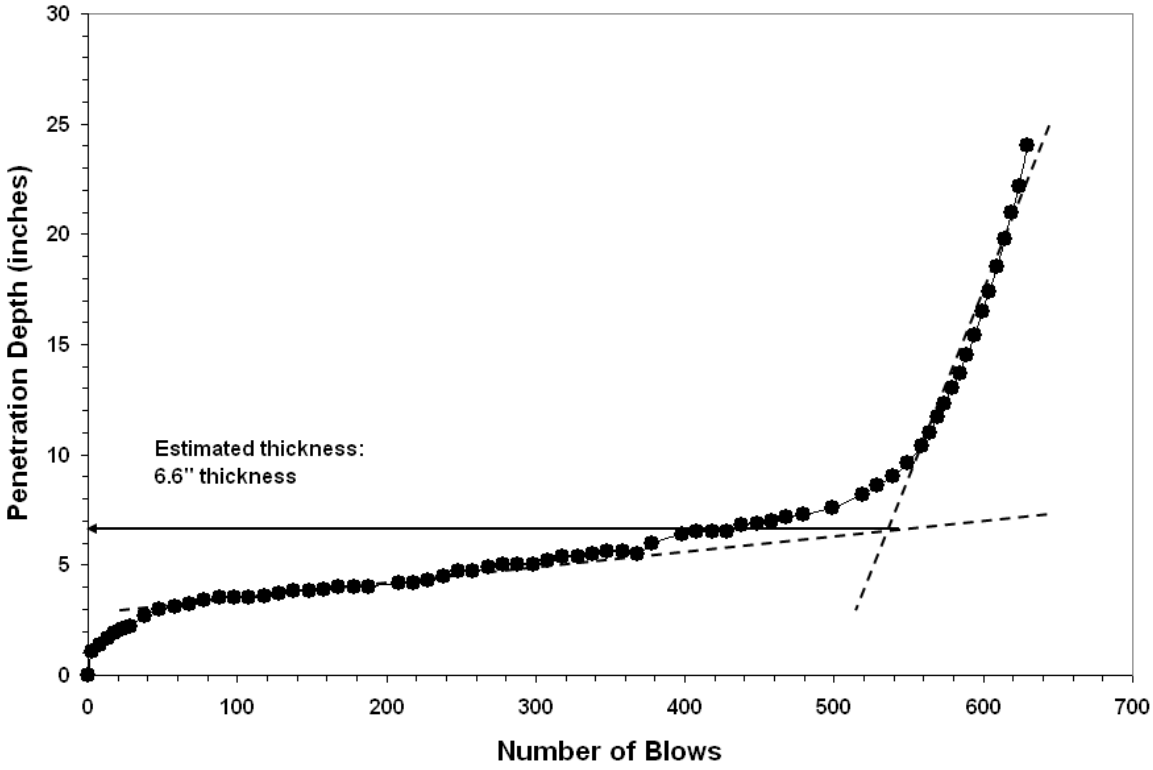

Figure C10. Estimating Base Thickness from DCP Data on Section SSS_6.

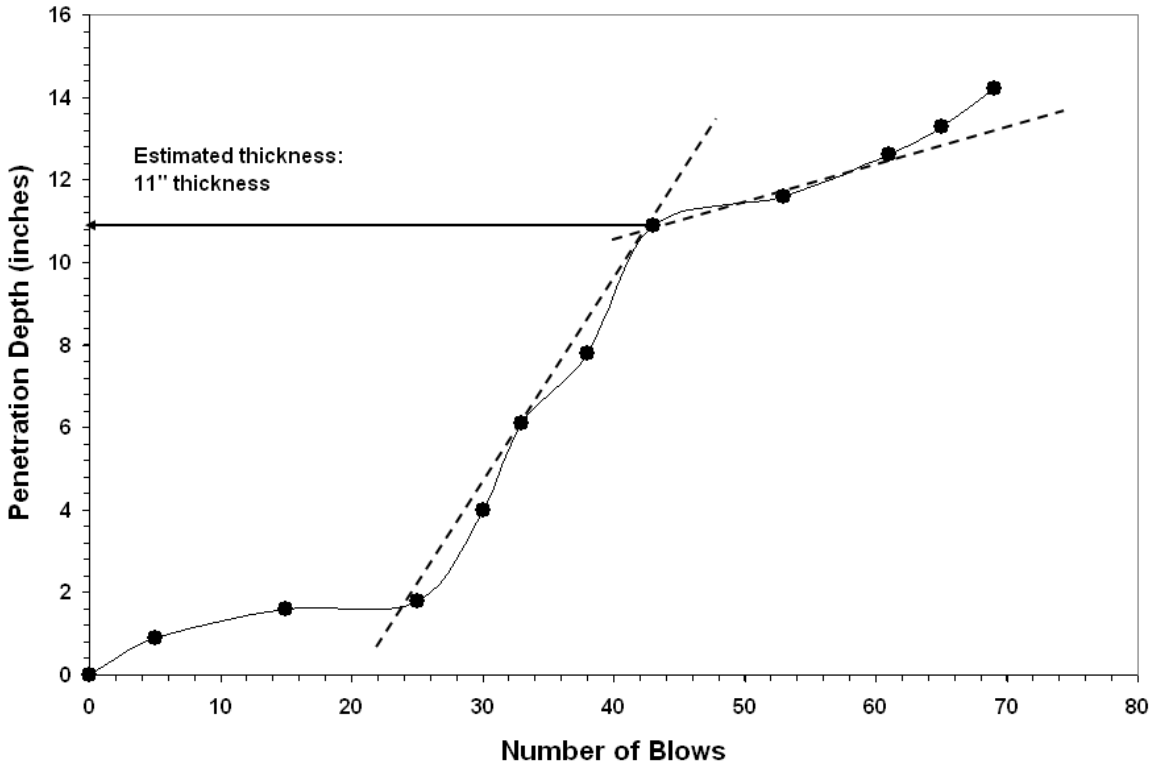

Figure C11. Estimating Base Thickness from DCP Data on Section G1S_12.

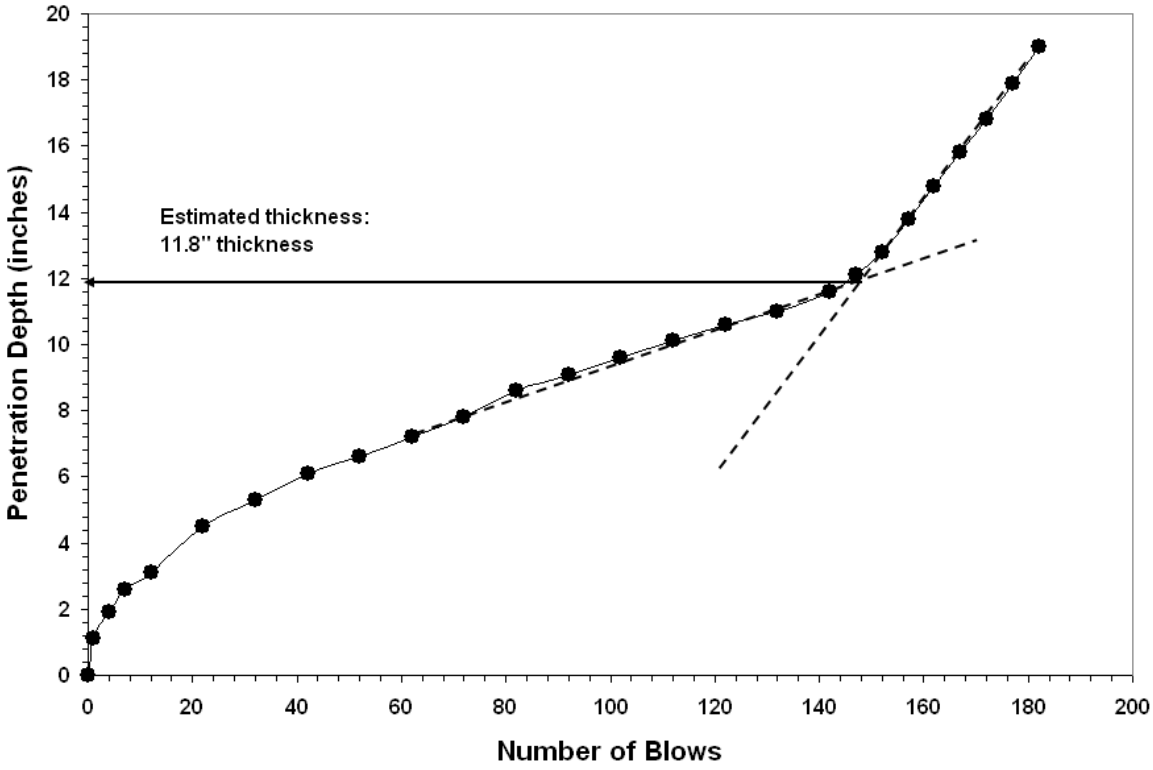

Figure C12. Estimating Base Thickness from DCP Data on Section G2S_12.

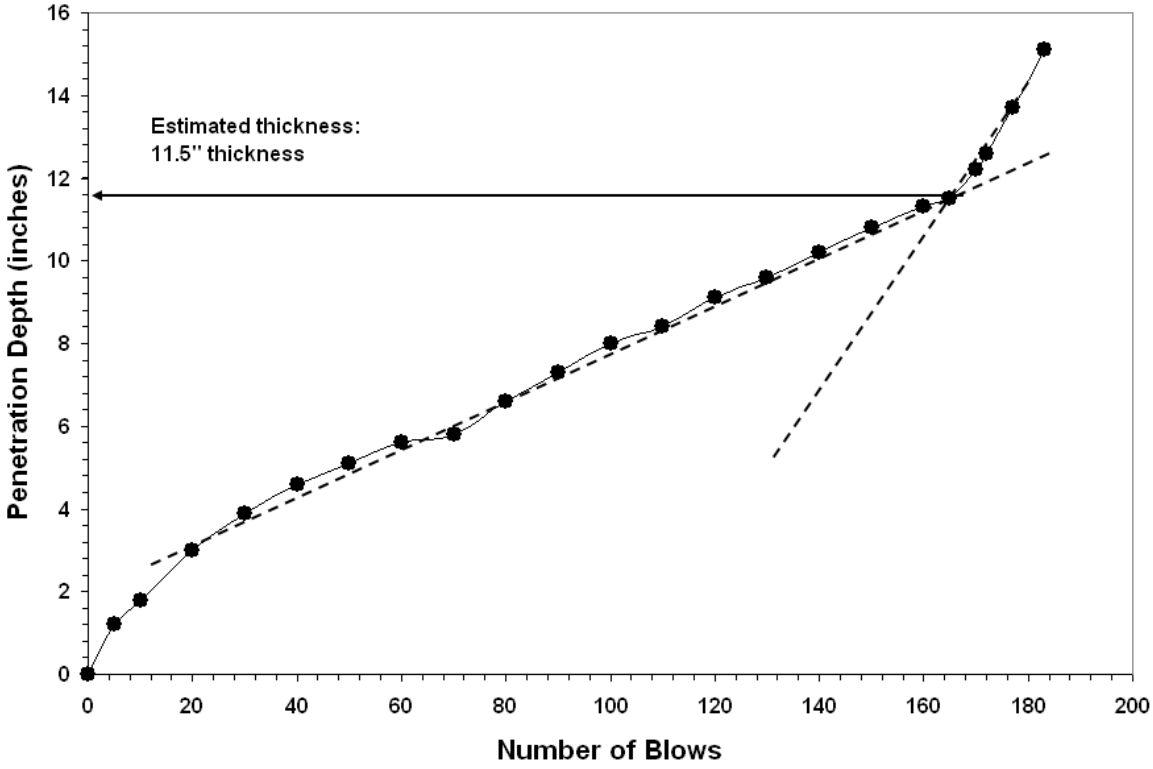

Figure C13. Estimating Base Thickness from DCP Data on Section CAS_12.

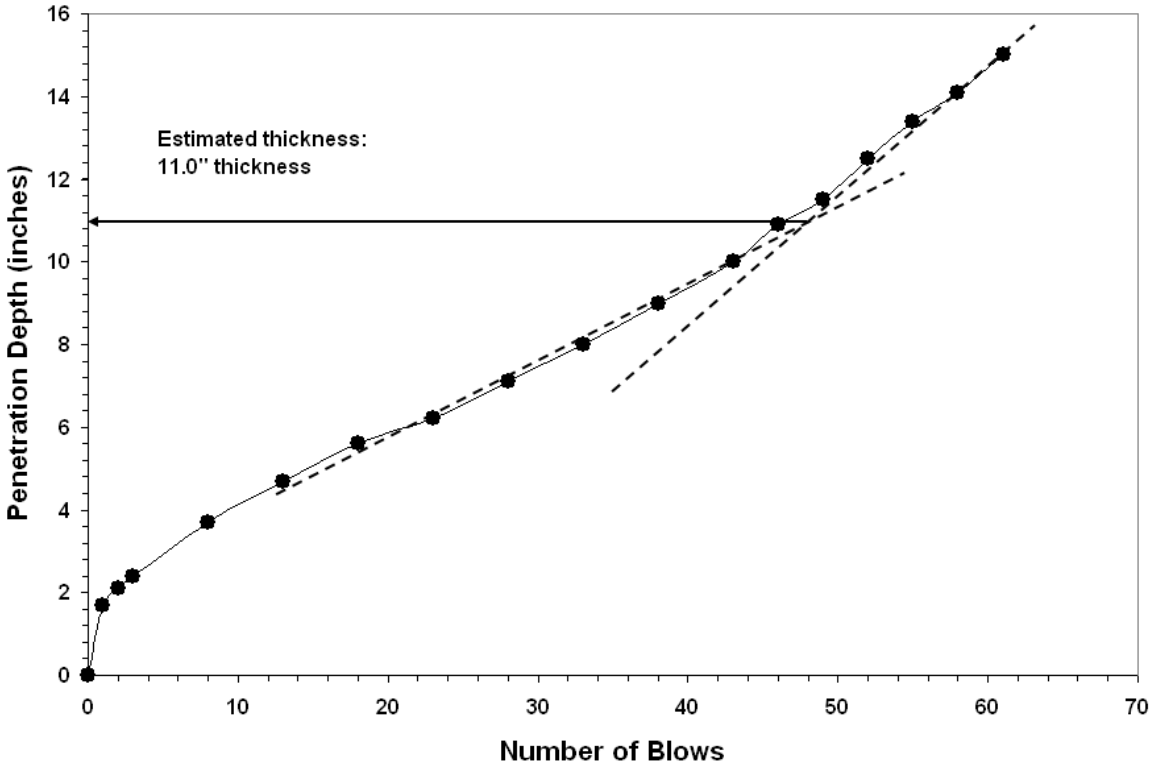

Figure C14. Estimating Base Thickness from DCP Data on Section UGS_12.

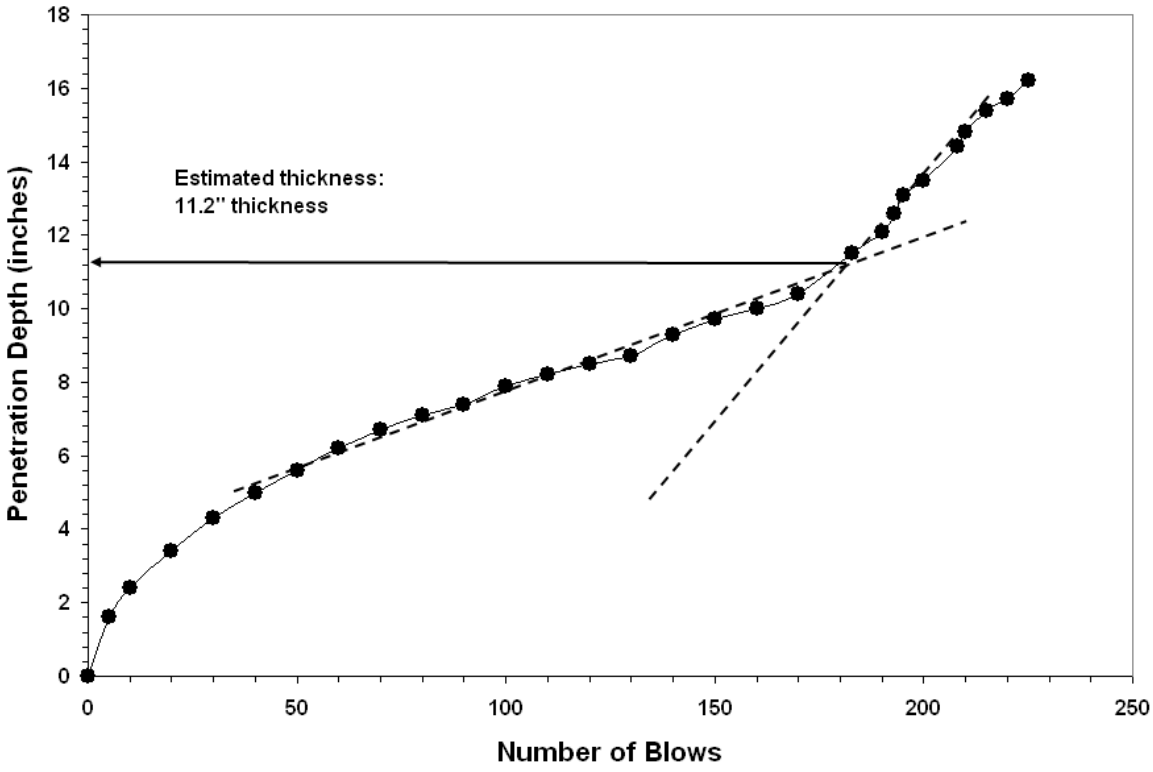

Figure C15. Estimating Base Thickness from DCP Data on Section SSS_12.

Table C15. Data from FWD Testing on Flexible Base Sections (Clay Subgrade).

Section	Station	Deflection (mils)		SCI (mils)	Backcalculated Modulus (ksi)	
		Sensor 1	Sensor 7		Base	Subgrade
SSC_12	1	63.3	3.2	35.9	16.4	7.4
	2	65.5	3.4	35.4	18.3	6.8
	3	58.2	3.0	29.3	16.7	7.9
	4	55.6	3.2	29.6	19.3	7.8
UGC_12	1	34.2	2.3	17.4	41.7	10.8
	2	37.0	2.3	19.4	38.0	10.6
	3	36.0	2.3	17.0	39.2	10.0
	4	33.1	2.2	17.5	41.6	10.4
CAC_12	1	55.7	2.7	27.6	18.6	8.6
	2	53.4	2.5	27.1	19.5	9.4
	3	59.2	2.8	30.6	16.5	7.7
	4	60.0	3.0	31.6	16.1	8.5
G2C_12	1	55.8	2.7	30.9	20.0	7.8
	2	57.9	2.6	32.4	19.5	8.2
	3	53.2	2.7	30.3	22.3	8.4
	4	50.5	2.6	30.6	24.2	8.6
G1C_12	1	50.9	2.6	29.4	20.4	9.9
	2	49.6	2.3	28.5	22.1	9.6
	3	53.8	2.5	31.0	18.5	9.5
	4	52.3	2.6	30.4	19.6	9.7
SSC_6	1	57.7	2.9	34.6	19.3	9.3
	2	56.0	2.5	31.9	21.0	8.8
	3	51.6	2.4	29.2	23.7	9.4
	4	54.2	2.5	31.1	25.1	8.6
UGC_6	1	49.7	2.3	28.4	30.4	9.0
	2	52.4	2.2	30.0	27.7	9.1
	3	52.1	2.2	31.3	27.3	9.5
	4	50.6	2.3	28.8	29.2	9.1
CAC_6	1	55.0	2.3	33.2	23.5	10.2
	2	56.6	2.3	35.7	20.5	10.2
	3	51.9	2.2	32.7	25.6	10.5
	4	55.6	2.5	36.2	21.5	10.5
G2C_6	1	39.4	2.1	23.4	40.6	11.3
	2	39.9	2.0	22.3	42.4	10.9
	3	38.3	2.0	24.0	39.2	11.8
	4	37.4	2.0	23.8	41.5	11.4
G1C_6	1	42.3	2.0	26.4	32.9	11.7
	2	42.4	2.3	24.3	34.1	11.5
	3	43.3	2.1	21.1	31.9	13.0
	4	43.4	2.2	24.7	29.9	12.6

Table C16. Data from FWD Testing on Flexible Base Sections (Sandy Subgrade).

Section	Station	Deflection (mils)		SCI (mils)	Backcalculated Modulus (ksi)	
		Sensor 1	Sensor 7		Base	Subgrade
G1S_6	1	36.8	2.6	18.2	61.4	11.4
	2	42.4	2.4	21.3	44.9	11.1
	3	32.2	2.5	13.3	84.3	11.3
	4	28.8	2.6	9.5	115.7	10.9
G2S_6	1	40.5	2.4	24.4	37.5	13.5
	2	38.0	2.5	18.5	49.4	12.3
	3	37.7	2.3	19.1	45.9	12.5
	4	35.0	2.4	19.4	53.2	13.7
CAS_6	1	36.4	2.7	15.1	61.3	10.9
	2	48.7	2.5	27.0	29.6	10.8
	3	40.2	2.5	20.9	49.0	11.3
	4	30.3	2.8	11.5	77.0	11.5
UGS_6	1	33.8	2.6	16.8	73.7	12.5
	2	38.7	2.3	20.9	51.8	12.2
	3	31.2	2.3	12.9	78.0	11.8
	4	29.3	2.4	13.1	84.0	13.1
SSS_6	1	24.9	2.6	9.2	150.0	13.0
	2	35.5	2.3	17.4	122.1	12.9
	3	46.7	2.2	25.0	80.8	12.0
	4	25.8	2.4	10.1	150.0	12.7
G1S_12	1	12.4	2.1	3.3	186.0	16.5
	2	13.5	1.9	4.1	146.4	16.9
	3	21.8	2.0	9.6	63.1	15.4
	4	14.1	2.0	4.6	120.0	16.8
G2S_12	1	43.3	2.0	28.2	23.5	16.0
	2	32.1	2.0	18.4	33.6	15.2
	3	44.1	2.0	23.4	22.4	15.8
	4	42.4	2.0	25.4	24.5	16.3
CAS_12	1	22.4	2.1	10.4	77.3	16.1
	2	24.7	2.0	10.2	70.8	14.8
	3	24.7	2.2	11.0	70.4	14.8
	4	17.7	2.1	5.8	114.7	15.3
UGS_12	1	52.9	2.2	30.4	20.8	12.8
	2	63.4	2.0	41.7	16.8	13.1
	3	35.0	1.9	17.6	31.1	13.5
	4	67.8	2.1	48.1	15.4	12.9
SSS_12	1	25.5	2.1	12.2	55.1	14.8
	2	28.4	2.0	14.9	47.4	15.3
	3	29.4	2.1	15.4	45.9	14.7
	4	25.1	2.1	12.0	53.8	14.8

Table C17. Data from FWD Testing on Stabilized Sections.

Section	Station	Deflection (mils)		SCI (mils)	Backcalculated Modulus (ksi)		
		Sensor 1	Sensor 7		Stabilized Material	Base[1]	Subgrade
Grade 2 with 4.5% cement on clay	1	13.4	2.3	1.6	1040.0		13.8
	2	25.4	2.1	6.8	580.0		14.5
	3	9.8	2.1	0.5	1040.0		18.6
	4	10.1	2.2	0.5	1040.0		17.4
Grade 2 with 3.0% cement on clay	1	21.9	2.4	6.7	260.7		12.9
	2	19.9	2.1	4.9	325.6		14.6
	3	20.1	2.2	7.8	223.7		12.1
	4	20.4	2.1	5.5	280.3		13.1
Uncrushed Gravel with 2% lime on clay	1	56.4	2.2	31.8	23.7		8.4
	2	49.8	2.2	30.4	27.1		9.3
	3	47.4	2.3	22.1	29.2		8.7
	4	44.6	2.3	22.2	34.3		9.2
Thin Type D HMAC on clay	1	35.8	2.2	12.6	144.8	25.0	8.1
	2	34.5	2.2	14.0	125.8	25.0	9.2
	3	33.6	2.2	13.0	139.3	25.0	9.6
	4	39.0	2.3	14.7	100.0	25.0	7.7
Thick Type D HMAC on clay	1	29.6	2.0	10.8	100.0	25.0	9.8
	2	27.4	2.2	11.0	107.0	27.2	10.7
	3	33.5	2.2	12.9	100.0	25.0	9.8
	4	40.1	2.3	15.1	100.0	25.0	8.0
Thick Type D HMAC on sand	1	23.7	2.1	11.8	200.0	36.3	13.0
	2	23.5	2.0	11.4	200.0	35.4	13.1
	3	22.5	2.0	10.3	200.0	40.4	12.3
	4	22.3	2.0	10.4	200.0	41.0	12.6
Thin Type D HMAC on sand	1	23.2	2.1	11.7	167.2	66.3	11.5
	2	22.7	2.0	11.0	161.8	67.6	11.4
	3	27.5	2.2	14.8	190.8	67.7	10.9
	4	22.9	2.1	10.9	155.4	54.5	10.5
Uncrushed Gravel with 2% lime on sand	1	28.1	2.3	14.2	83.9		12.3
	2	25.2	2.3	11.3	114.8		11.9
	3	36.5	2.3	20.3	33.9		11.1
	4	29.4	2.3	14.6	67.9		11.9
Grade 2 with 3.0% cement on sand	1	19.3	2.2	5.9	299.5		12.5
	2	36.0	2.1	18.8	49.7		11.7
	3	20.8	2.0	7.3	222.4		12.1
	4	17.3	2.1	4.5	419.3		12.4
Grade 2 with 4.5% cement on sand	1	11.9	2.0	1.6	540.0		13.5
	2	12.6	2.1	2.4	540.0		13.1
	3	16.2	2.1	3.2	540.0		10.4
	4	14.1	2.2	3.2	540.0		11.9

[1]Shaded cells indicate sections where the stabilized material is the base layer.

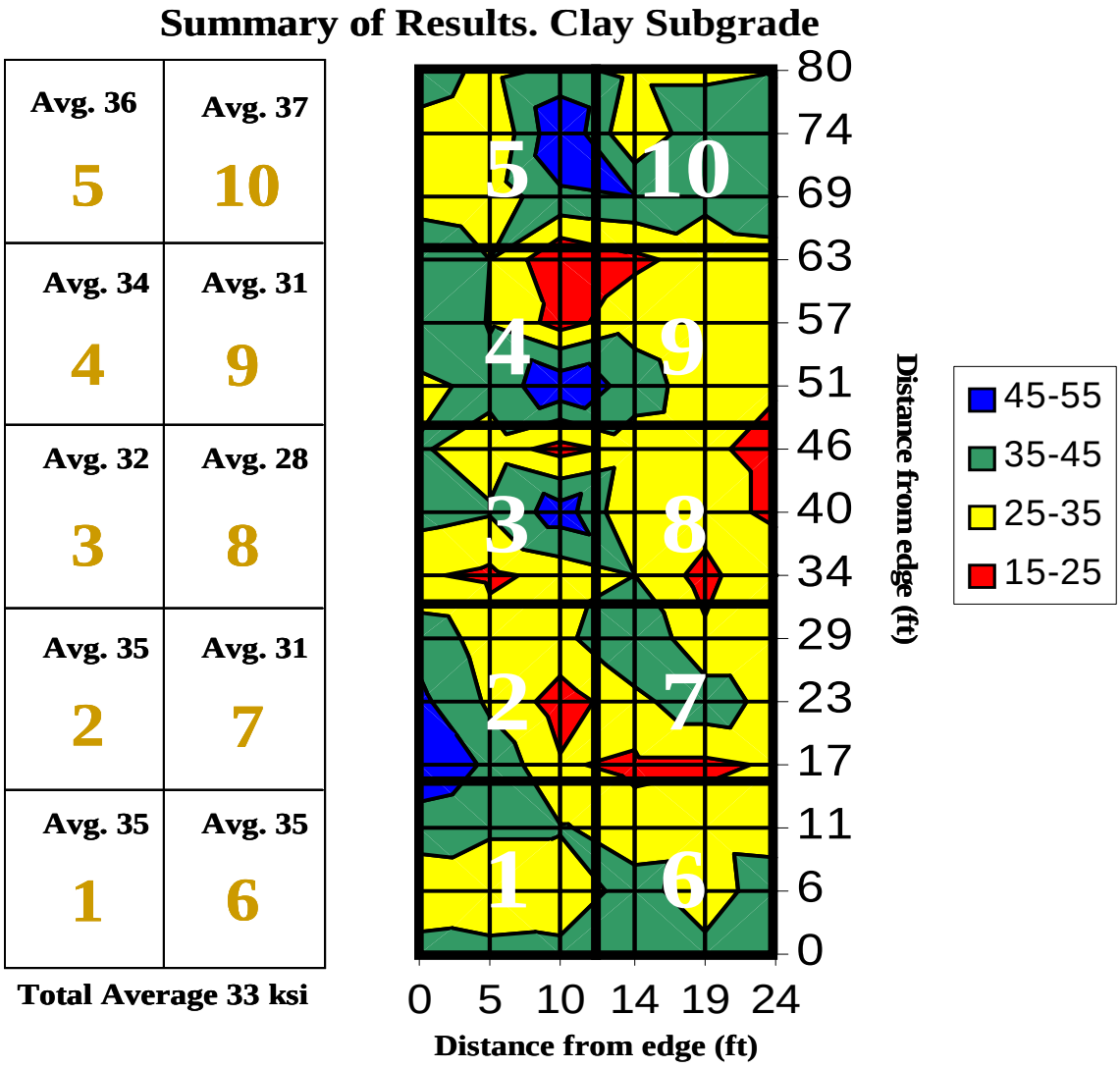

Figure C16. Summary of DSPA Test Results on Clay Subgrade Showing Average of DSPA Readings on Flexible Base Section Grid.

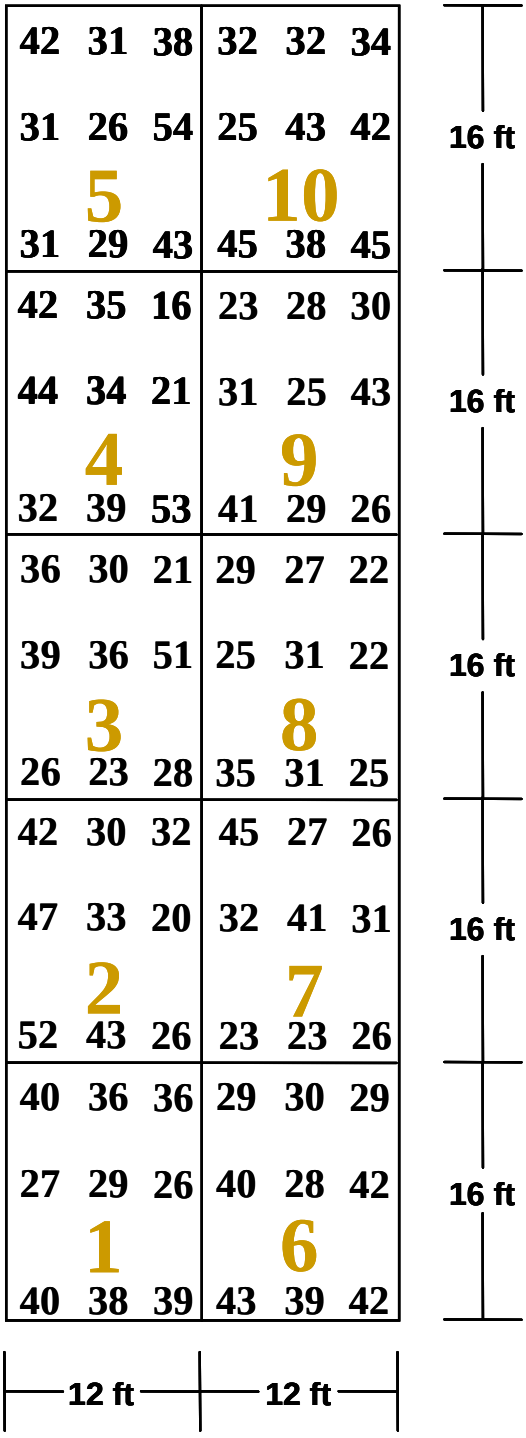

Figure C17. DSPA Test Results on Clay Subgrade Showing Individual DSPA Readings on Flexible Base Section Grid.

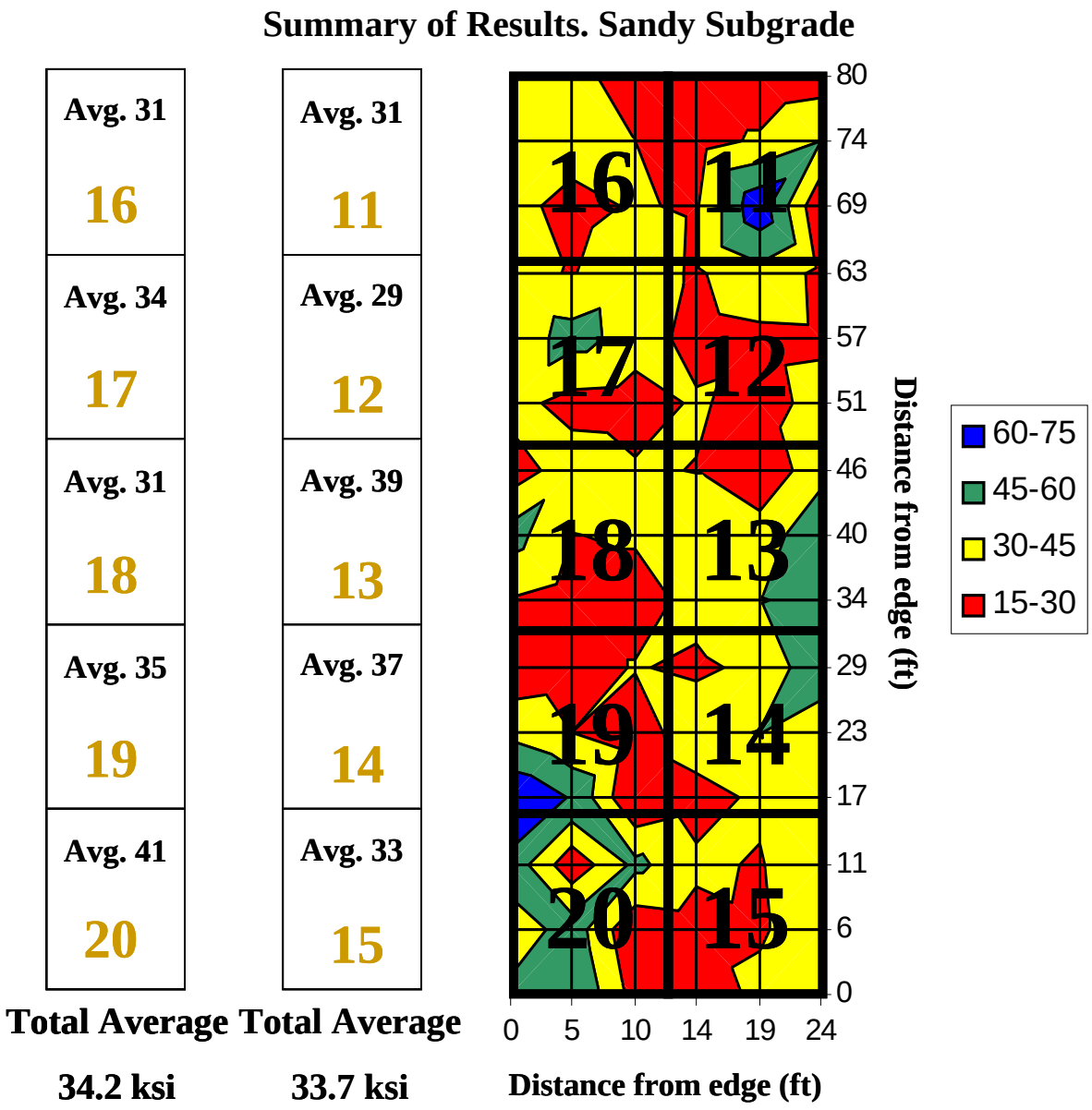

Figure C18. Summary of DSPA Test Results on Sandy Subgrade Showing Average of DSPA Readings on Flexible Base Section Grid.

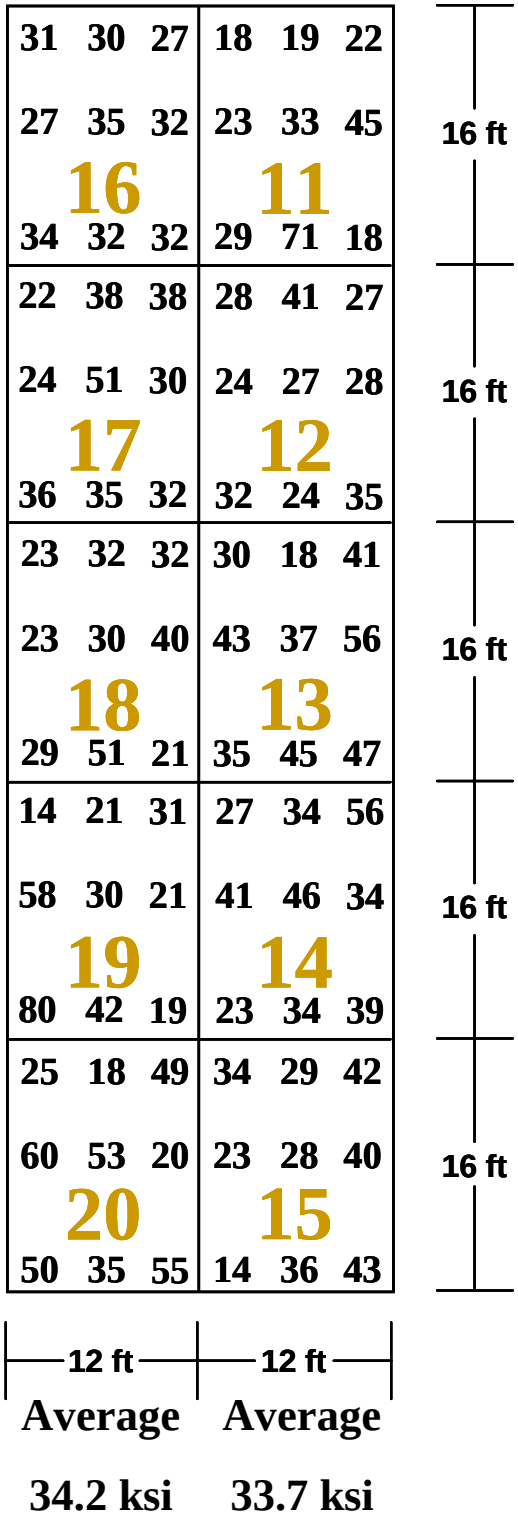

Figure C19. DSPA Test Results on Sandy Subgrade Showing Individual DSPA Readings on Flexible Base Section Grid.

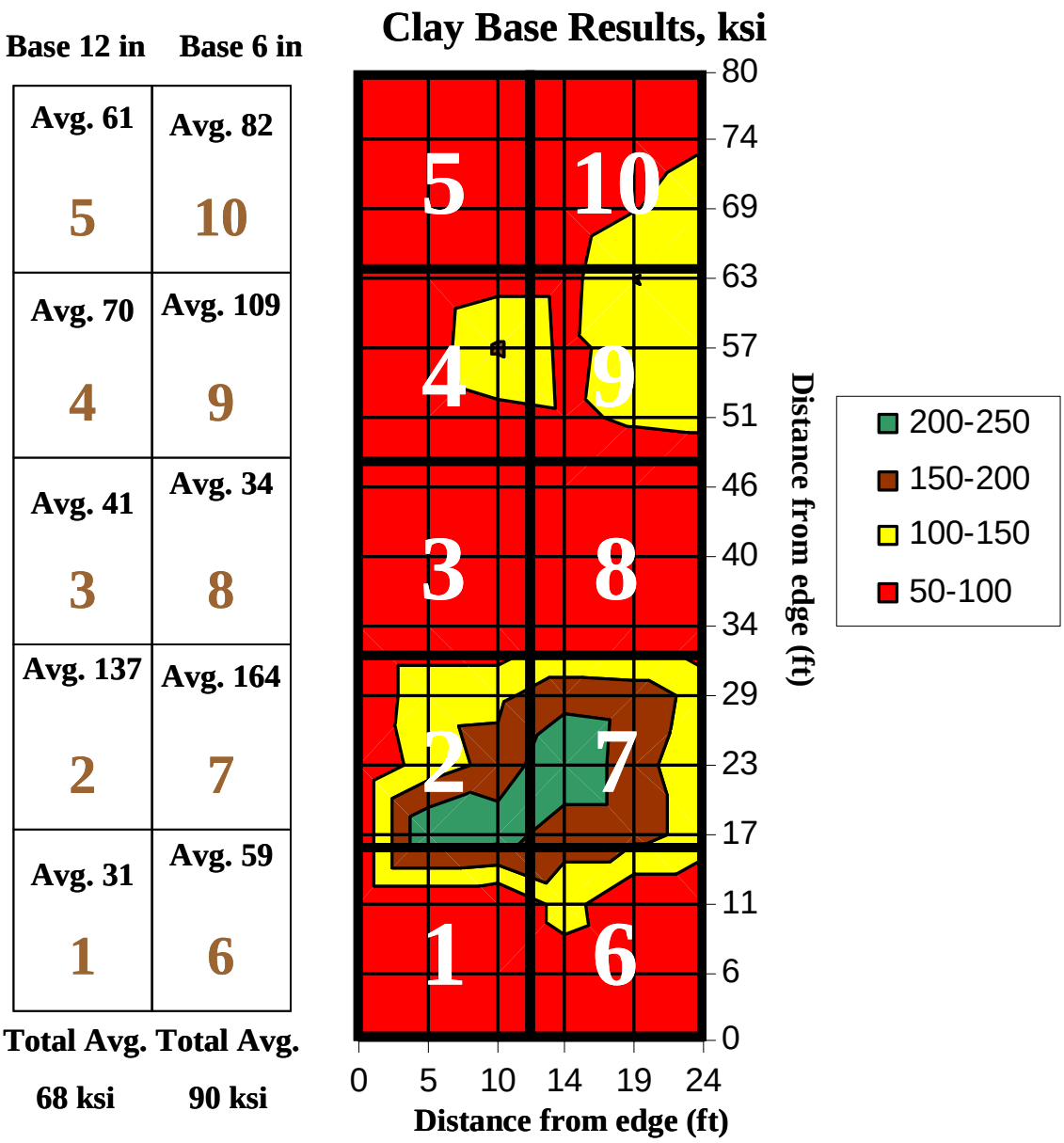

Figure C20. Summary of DSPA Test Results on Finished Flexible Base Sections on Clay Subgrade Showing Average of DSPA Readings.

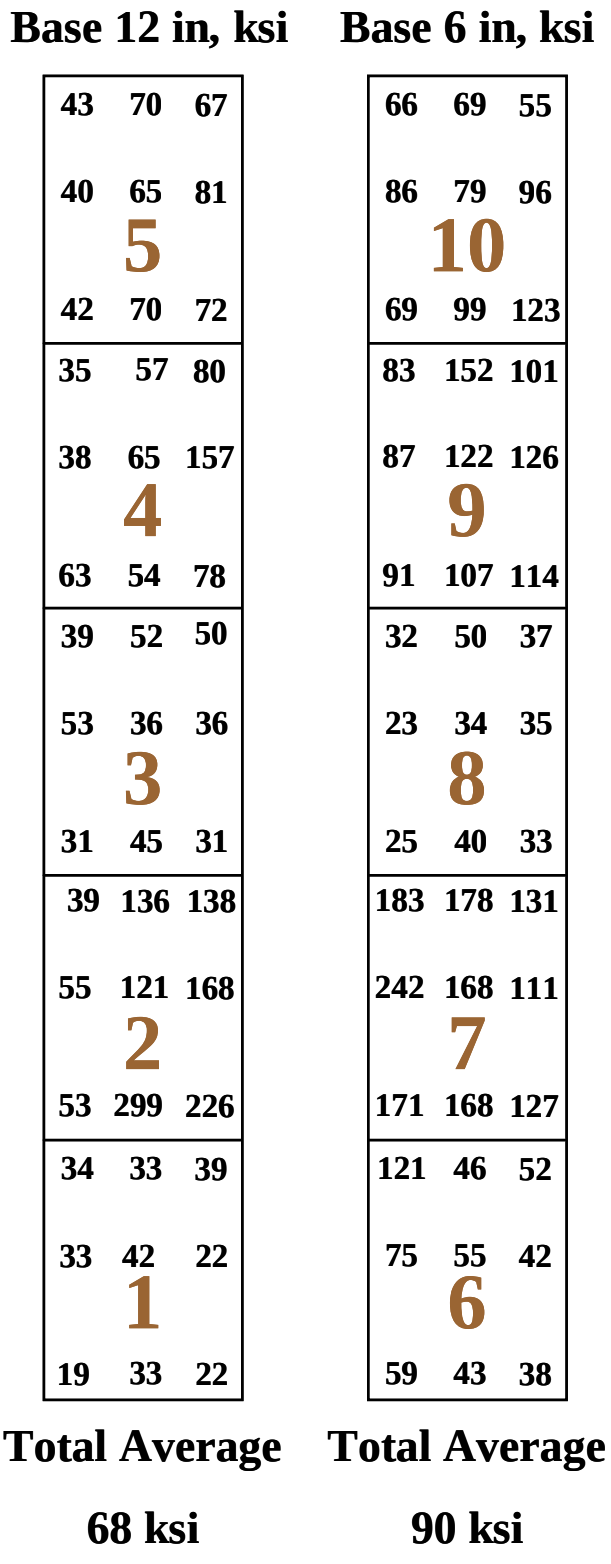

Figure C21. DSPA Test Results on Finished Flexible Base Sections on Clay Subgrade Showing Individual DSPA Readings.

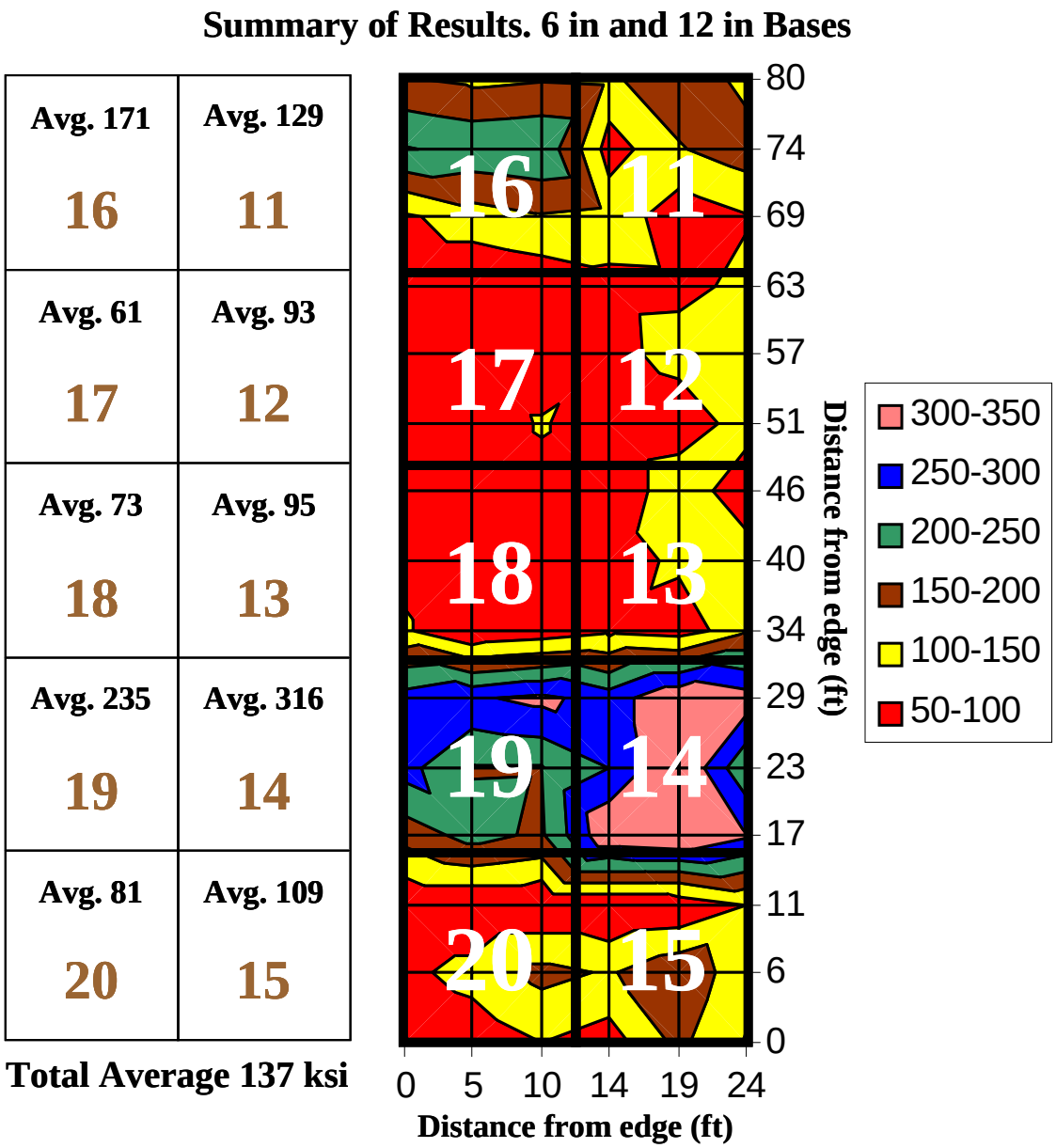

Figure C22. Summary of DSPA Test Results on Finished Flexible Base Sections on Sandy Subgrade Showing Average of DSPA Readings.

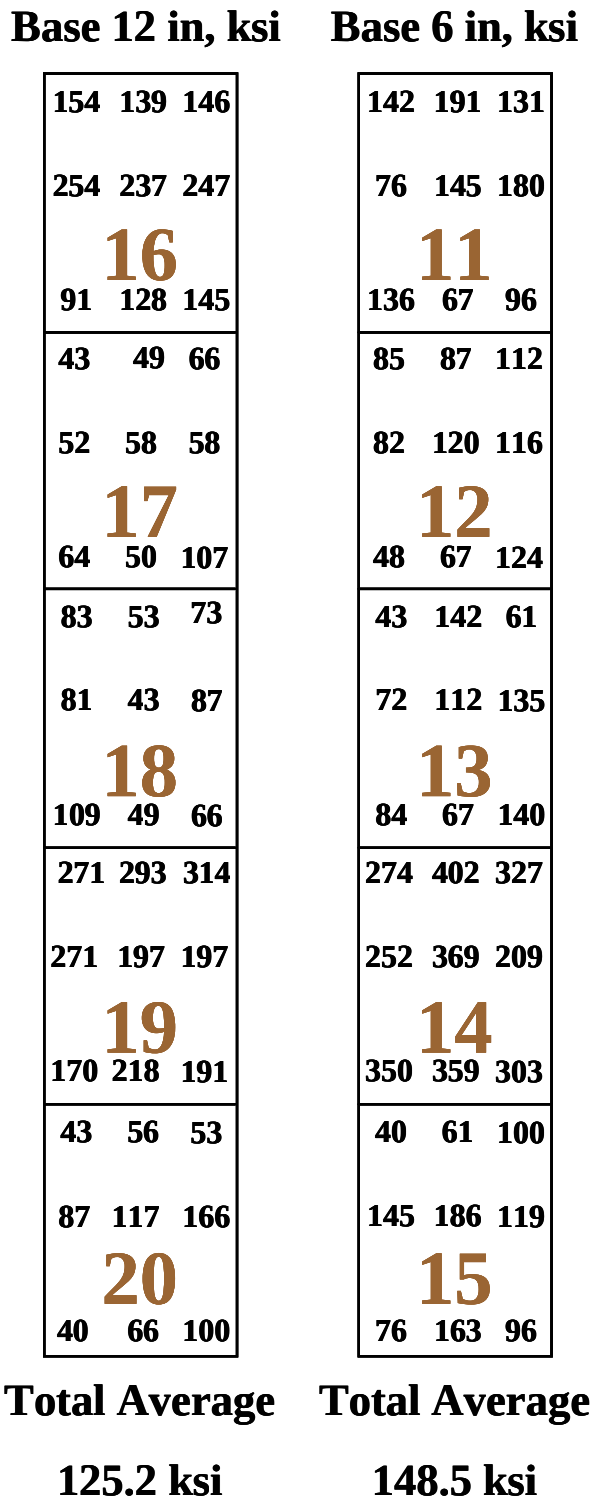

Figure C23. DSPA Test Results on Finished Flexible Base Sections on Sandy Subgrade Showing Individual DSPA Readings.

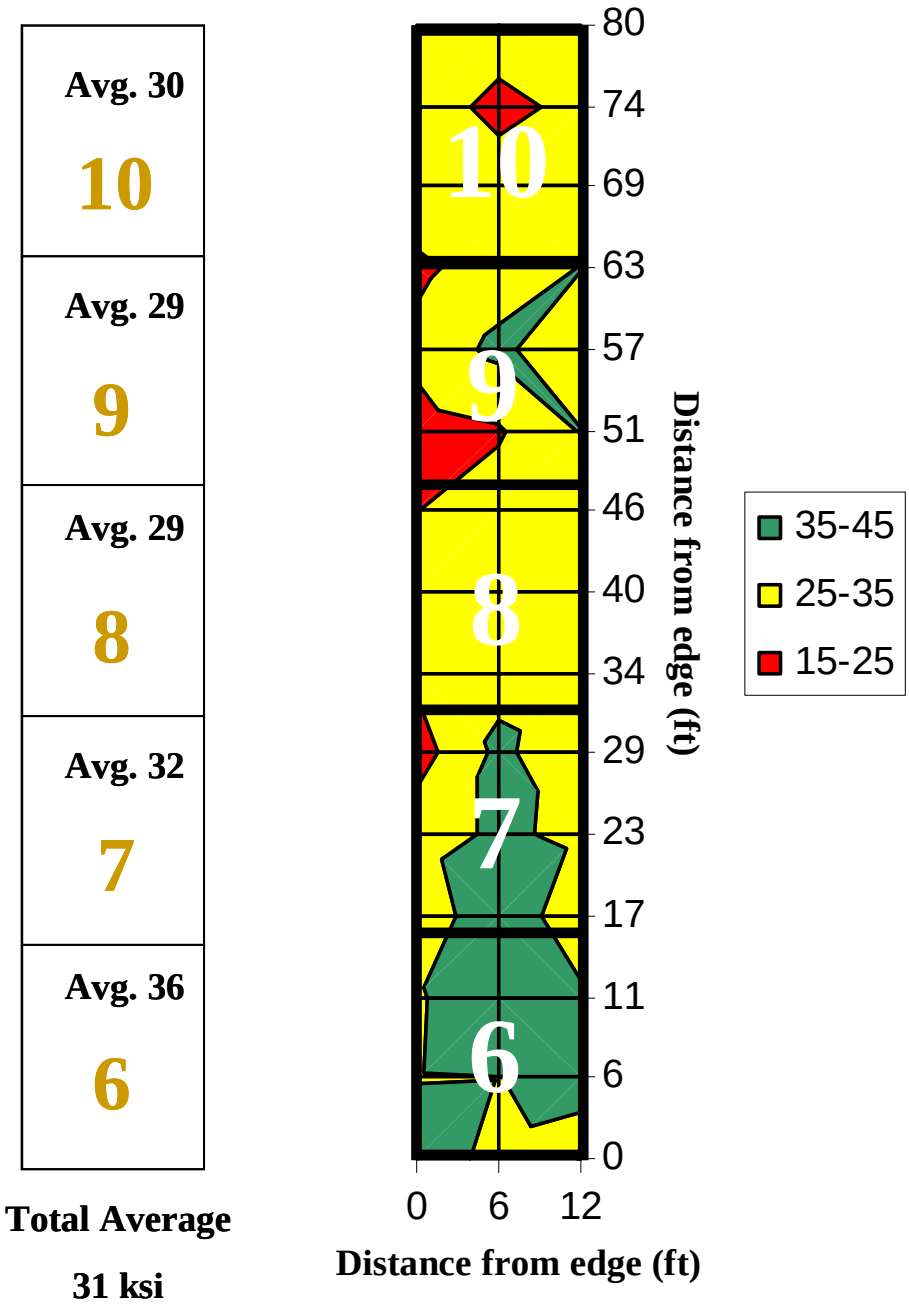

Figure C24. Summary of DSPA Test Results on Clay Subgrade Showing Average of DSPA Readings on Stabilized Section Grid.

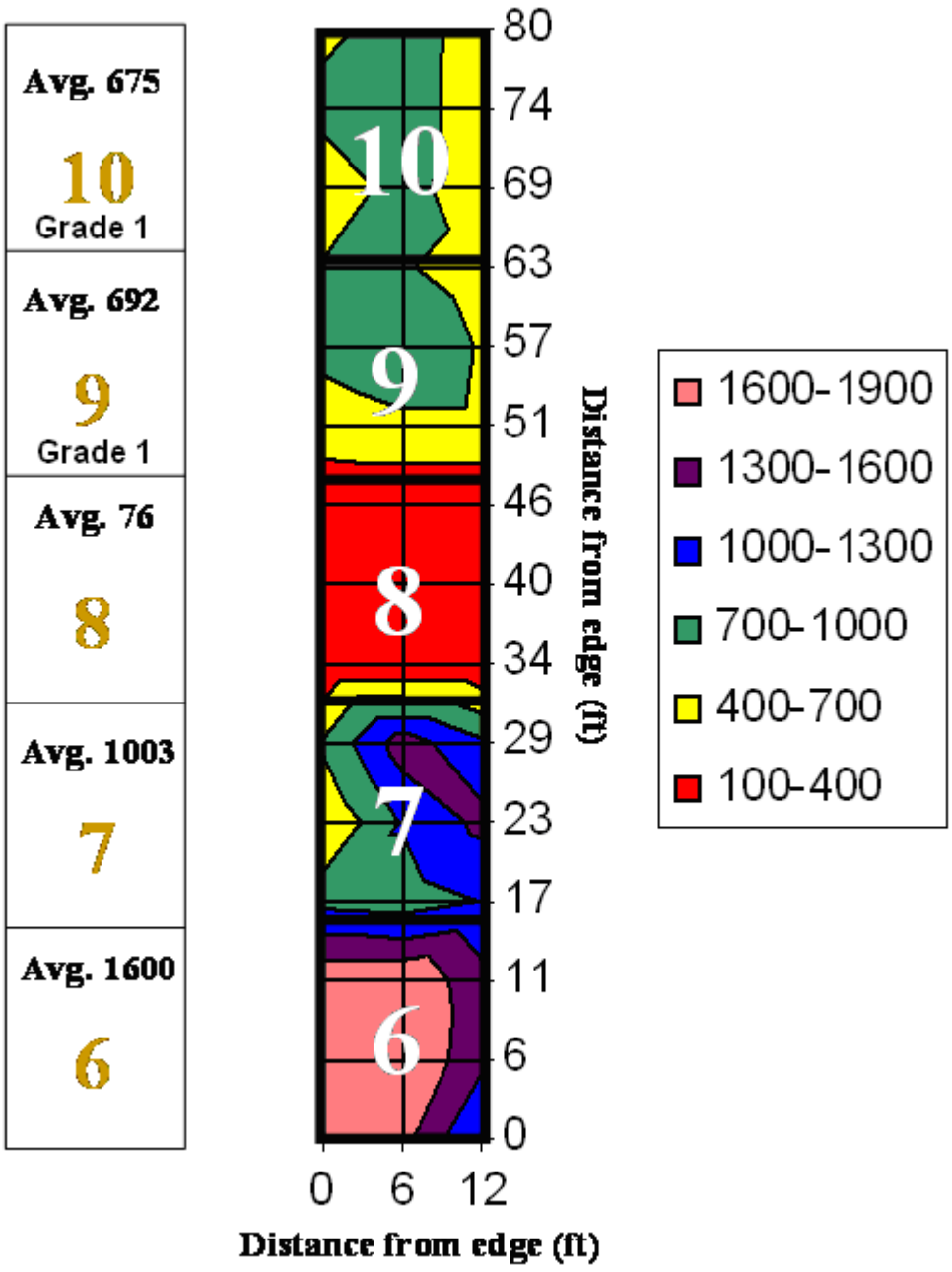

Figure C25. Summary of DSPA Test Results on Stabilized Base Layers Placed on Clay Subgrade Showing Average of DSPA Readings.

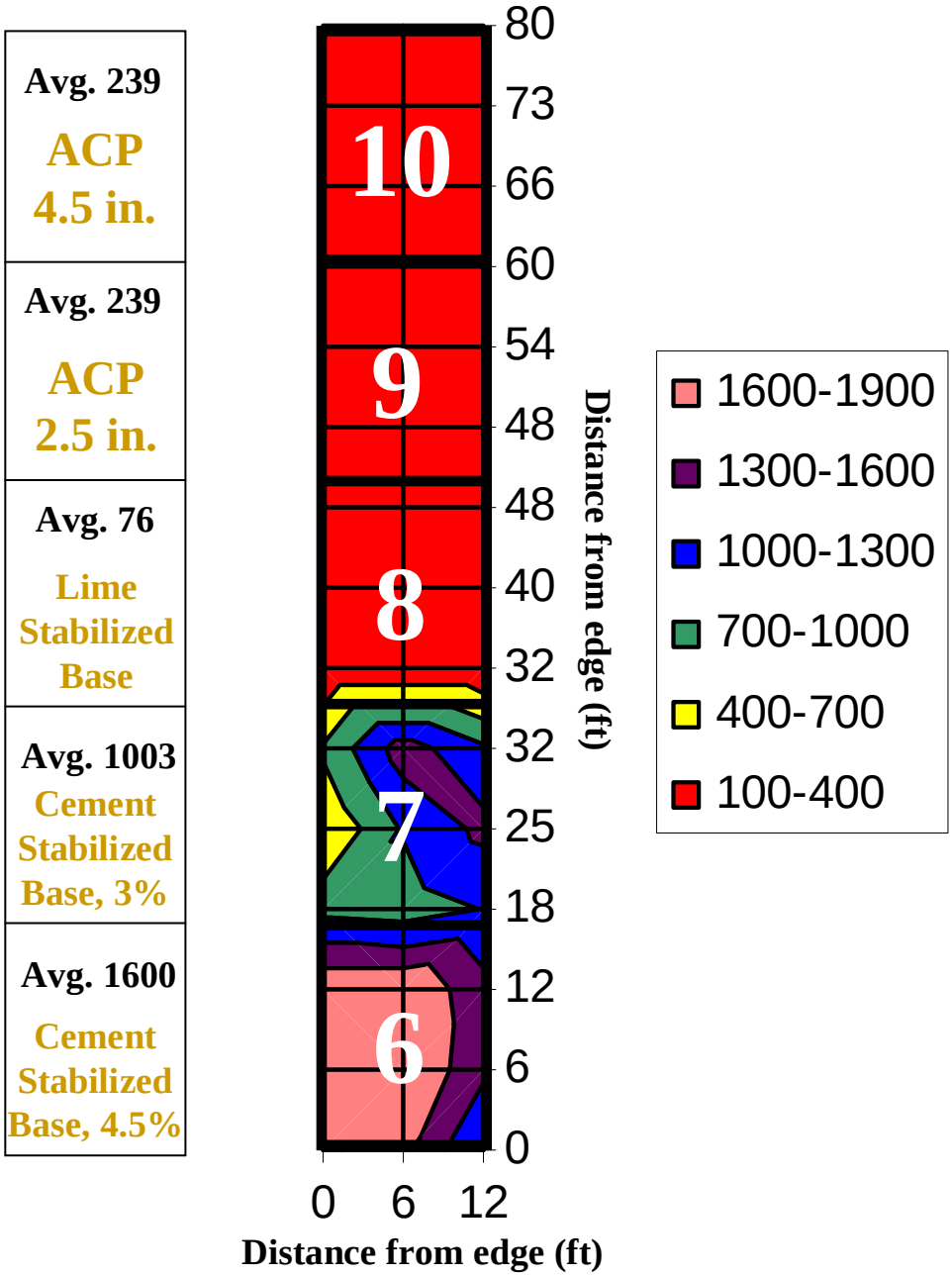

Figure C26. Summary of DSPA Test Results on Stabilized Sections Placed on Clay Subgrade Showing Average of DSPA Readings on Final Surface.

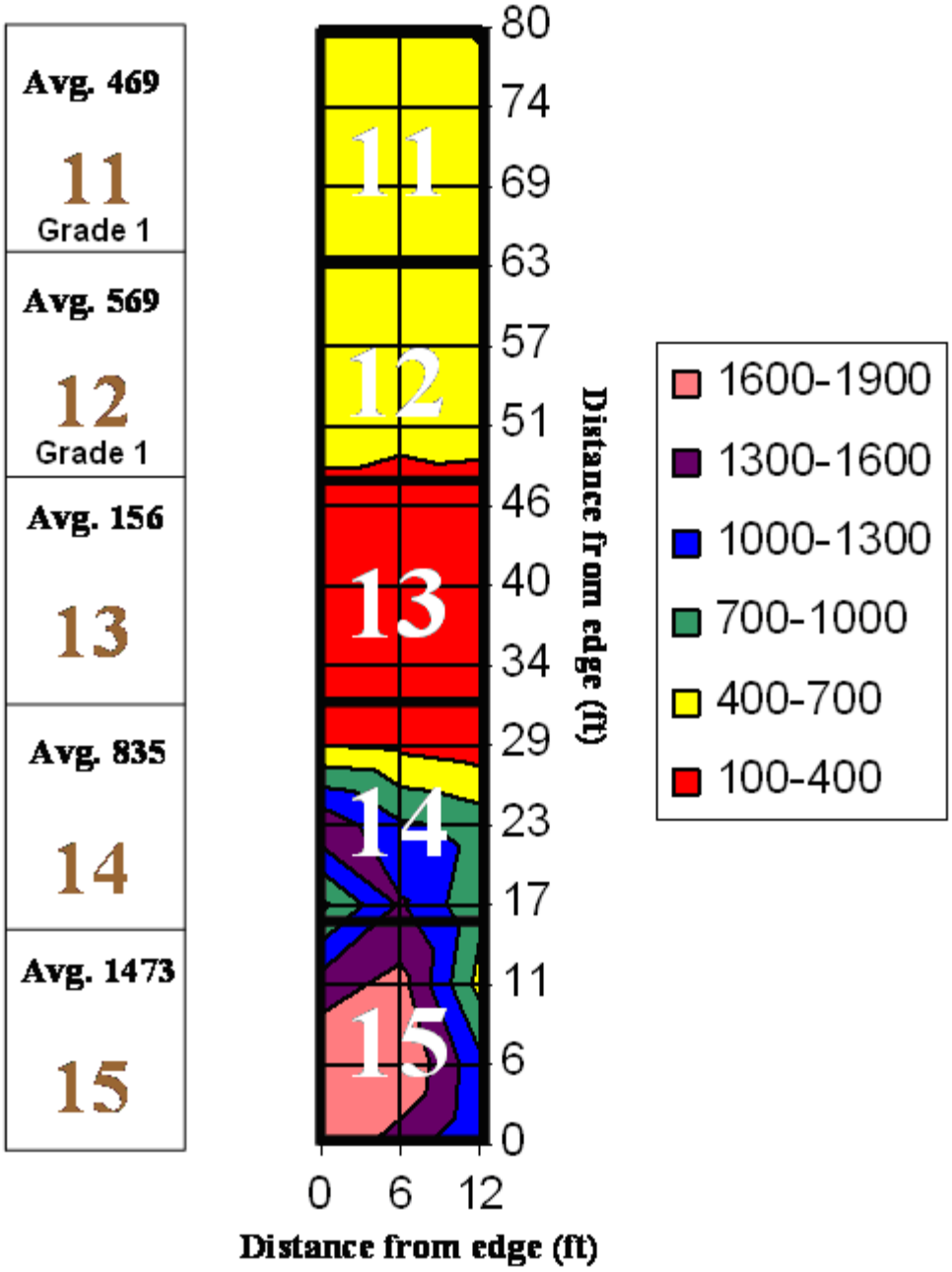

Figure C27. Summary of DSPA Test Results on Stabilized Base Layers Placed on Sandy Subgrade Showing Average of DSPA Readings.

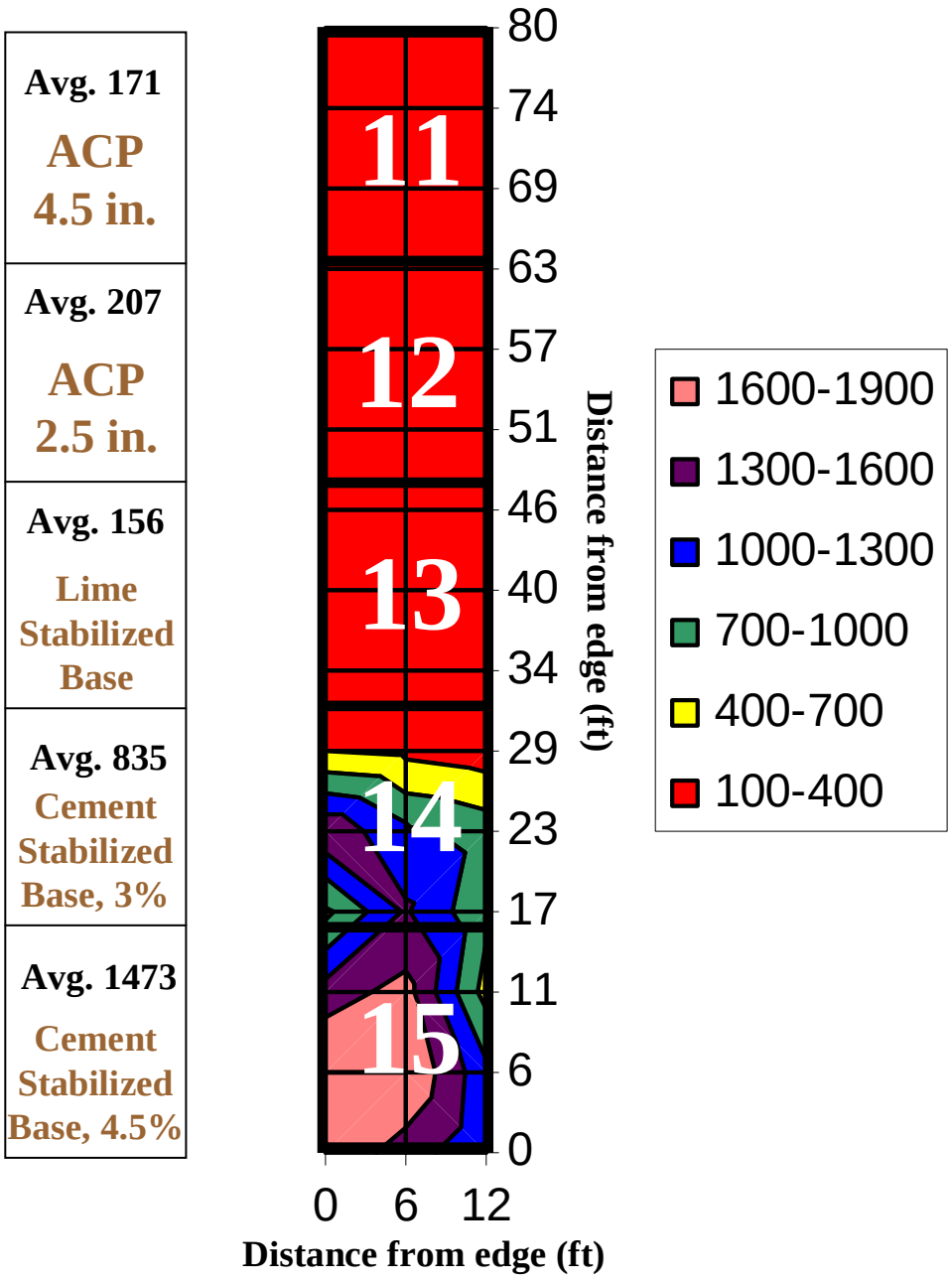

Figure C28. Summary of DSPA Test Results on Stabilized Sections Placed on Sandy Subgrade Showing Average of DSPA Readings on Final Surface.

Table C18. Phase I – Density Tests on Finished Sand Subgrade.

Test Section – Measurement Location	Density, %	Moisture, %
11-1	95.8	12.4
11-5	96.3	12.7
11-9	95.8	8.1
12-1	95.0	8.0
12-5	96.0	10.4
12-9	97.5	9.1
13-1	97.9	7.5
13-5	96.1	7.1
13-9	97.2	7.1
14-1	95.2	6.2
14-5	95.9	8.0
14-9	96.0	6.9
15-1	95.7	7.3
15-5	100.0	7.2
15-9	101.7	8.4
16-1	95.0	8.4
16-5	96.2	12.4
16-9	96.7	9.5
17-1	95.9	8.5
17-5	95.0	9.4
17-9	98.6	7.2
18-1	96.8	7.9
18-5	95.0	6.9
18-9	98.6	8.7
19-1	96.6	7.2
19-5	96.6	8.7
19-9	104.9	8.2
20-1	95.2	7.3
20-5	99.4	9.4
20-9	98.8	10.5

Table C19. Phase I – Density Tests on First 6-inch Lift of 12-inch Thick Sections at the Sand Site.

Test Section – Measurement Location	Density, %	Moisture, %	Base Material
16-1	100.0	7.9	Grade 1 Crushed Limestone
16-5	100.0	8.1	
16-9	100.3	7.4	
17-3	100.4	6.7	Grade 2 Crushed Limestone
17-5	101.5	7.2	
17-7	100.7	7.6	
18-3	101.4	17.4	Caliche
18-5	100.5	17.0	
18-7	100.8	18.2	
19-1	98.9	5.9	Uncrushed Gravel
19-5	98.8	6.5	
19-9	98.7	6.1	
20-1	100.1	6.5	Sandstone
20-3	99.7	5.8	
20-5	99.2	6.5	
20-7	101.0	5.7	
20-9	101.7	6.0	

Table C20. Phase I – Density Tests on Top 6-inch Lift of All Test Sections at the Sand Site.

Test Section – Measurement Location	Density, %	Moisture, %	Base Material
11-1	101.0	6.1	Grade 1 Crushed Limestone
11-5	100.3	5.4	
11-9	100.0	5.6	
12-1	99.3	6.0	Grade 2 Crushed Limestone
12-5	98.9	4.9	
12-9	99.0	5.8	
13-1	101.0	16.5	Caliche
13-5	101.5	16.3	
13-7	100.0	17.8	
14-3	99.1	5.2	Uncrushed Gravel
14-5	99.3	5.7	
14-7	99.8	5.2	
15-3	99.6	4.3	Sandstone
15-5	100.1	4.4	
15-7	100.4	4.2	
16-1	99.7	5.8	Grade 1 Crushed Limestone
16-5	100.0	6.3	
16-9	100.2	5.8	
17-1	99.2	6.2	Grade 2 Crushed Limestone
17-5	99.5	6.3	
17-9	99.3	7.2	
18-1	100.3	18.2	Caliche
18-5	100.5	17.7	
18-7	100.0	17.6	
19-1	99.0	6.1	Uncrushed Gravel
19-5	98.8	5.8	
19-9	99.3	6.1	
20-3	100.1	4.4	Sandstone
20-5	100.0	4.3	
20-7	99.6	4.3	

Table C21. Phase I – Density Tests on Subgrade at the Clay Site.

Test Section – Measurement Location	Density, %	Moisture, %
1-1	95.1	13.9
1-5	101.6	15.3
1-9	96.6	17.7
2-1	96.5	11.8
2-5	99.0	16.6
2-9	102.8	12.2
3-1	98.3	14.1
3-5	102.5	16.1
3-9	105.5	14.4
4-1	104.6	15.0
4-5	110.1	18.8
4-9	105.7	15.8
5-1	103.3	13.8
5-5	106.1	12.2
5-9	103.6	16.1
6-1	103.7	15.7
6-5	102.7	16.3
6-9	105.3	13.6
7-1	104.4	14.5
7-5	105.2	14.4
7-9	105.6	13.3
8-1	106.9	13.7
8-5	104.3	15.0
8-9	107.5	13.6
9-1	107.8	13.9
9-5	104.3	14.8
9-9	104.6	14.0
10-1	106.4	14.6
10-5	103.3	13.9
10-9	101.9	14.1

Table C22. Phase I – Density Tests on First 6-inch Lift of 12-inch Thick Sections at the Clay Site.

Test Section – Measurement Location	Density, %	Moisture, %	Base Material
1-3	99.6	4.2	Sandstone
1-5	101.0	5.4	
1-7	99.7	5.1	
2-3	98.8	4.7	Uncrushed Gravel
2-5	99.2	5.6	
2-7	99.4	5.9	
3-3	101.5	14.5	Caliche
3-5	99.9	16.6	
3-7	99.5	16.4	
4-3	101.0	4.9	Grade 2 Crushed Limestone
4-5	103.8	6.2	
4-7	101.9	5.3	
5-3	99.6	5.1	Grade 1 Crushed Limestone
5-5	100.9	5.1	
5-7	100.0	4.3	

Table C23. Phase I – Density Tests on Top 6-inch Lift of All Test Sections at the Clay Site.

Test Section – Measurement Location	Density, %	Moisture, %	Base Material
1-1	99.4	5.3	Sandstone
1-5	100.1	5.4	
1-9	98.3	5.3	
2-1	97.8	6.9	Uncrushed Gravel
2-5	101.3	6.4	
2-9	100.4	6.0	
3-1	97.7	19.6	Caliche
3-5	96.8	20.2	
3-9	97.6	20.8	
4-1	102.2	5.2	Grade 2 Crushed Limestone
4-5	101.9	5.6	
4-9	103.2	6.4	
5-1	99.9	5.1	Grade 1 Crushed Limestone
5-5	99.3	5.0	
5-9	99.7	5.5	
6-1	100.2	4.9	Sandstone
6-5	100.0	4.2	
6-9	100.5	4.6	
7-1	99.2	6.1	Uncrushed Gravel
7-5	100.1	6.2	
7-9	99.4	6.4	
8-1	100.7	16.3	Caliche
8-5	98.8	17.2	
8-9	101.8	16.2	
9-1	101.9	5.2	Grade 2 Crushed Limestone
9-5	99.8	6.2	
9-9	101.8	5.9	
10-1	99.3	3.4	Grade 1 Crushed Limestone
10-5	99.0	5.3	
10-9	100.4	4.6	

Table C24. Phase II – Density Tests on Finished Sand Subgrade.

Test Section – Measurement Location	Density, %	Moisture, %
11B-1	95.9	6.1
11B-5	96.3	5.1
11B-9	93.7	4.7
12B-1	98.3	6.2
12B-5	98.9	5.9
12B-9	95.8	6.7
13B-1	101.5	6.4
13B-5	97.4	9.7
13B-9	92.7	6.6
14B-1	97.4	6.9
14B-5	97.9	9.7
14B-9	98.8	8.1
15B-1	98.8	6.5
15B-5	97.9	7.4
15B-9	96.0	7.1

Table C25. Phase II – Density Tests on Finished Clay Subgrade.

Test Section – Measurement Location	Density, %	Moisture, %
6B-1	104.2	18.5
6B-5	106.6	13.5
6B-9	107.3	15.7
7B-1	103.1	18.5
7B-5	104.0	17.5
7B-9	103.9	18.4
8B-1	102.5	19.4
8B-5	100.6	19.5
8B-9	105.5	17.5
9B-1	101.3	17.7
9B-5	105.2	16.2
9B-9	107.7	16.5
10B-1	104.3	16.7
10B-5	104.2	16.2
10B-9	105.0	18.5

Table C26. Phase II – Density Tests on Finished Base Test Sections at the Sand Site.

Test Section – Measurement Location	Density, %	Moisture, %	Base Material
11B-2 11B-5 11B-8	100.7 100.0 102.1	7.3 7.8 7.6	Grade 1 Crushed Limestone
12B-2 12B-5 12B-8	98.2 100.6 101.4	8.7 7.6 7.3	Grade 1 Crushed Limestone
13B-2 13B-5 13B-8	97.7 99.2 97.5	7.0 6.2 7.1	Uncrushed Gravel with 2% lime
14B-2 14B-5 14B-8	98.3 97.5 97.1	7.3 7.2 7.7	Grade 2 with 3.0% Cement
15B-2 15B-5 15B-8	99.1 98.5 98.1	8.3 8.3 7.6	Grade 2 with 4.5% Cement

Table C27. Phase II – Density Tests on Finished Base Test Sections at the Clay Site.

Test Section – Measurement Location	Density, %	Moisture, %	Base Material
6B-2 6B-5 6B-8	99.0 98.4 97.8	9.0 8.4 9.1	Grade 2 with 4.5% Cement
7B-2 7B-5 7B-8	95.4 96.2 96.6	6.9 6.8 7.3	Grade 2 with 3.0% Cement
8B-2 8B-5 8B-8	98.3 97.4 98.0	6.5 6.0 6.2	Uncrushed Gravel with 2% lime
9B-1 9B-5 9B-8	100.1 99.6 100.4	7.4 6.2 5.5	Grade 1 Crushed Limestone
10B-1 10B-5 10B-8	99.5 99.8 99.9	8.0 7.4 7.5	Grade 1 Crushed Limestone

Table C28. Subgrade Moisture Contents Corresponding to Plate Bearing Tests.

Section	Base Material	Moisture Content, %	
		Clay	Sandy Soil
Flexible Base	Sandstone	22.6	6.2
	Uncrushed gravel	21.9	7.1
	Caliche with 2% lime	23.3	7.7
	Grade 2 crushed limestone	19.0	7.2
	Grade 1 crushed limestone	23.3	7.1
Stabilized Base	Grade 2 at 4.5% cement	16.0	7.0
	Grade 2 at 3.0% cement	18.1	7.9
	Uncrushed gravel with 2% lime	18.8	7.6
	Thin Type D HMAC over Grade 1	16.8	6.3
	Thick Type D HMAC over Grade 1	17.1	6.4

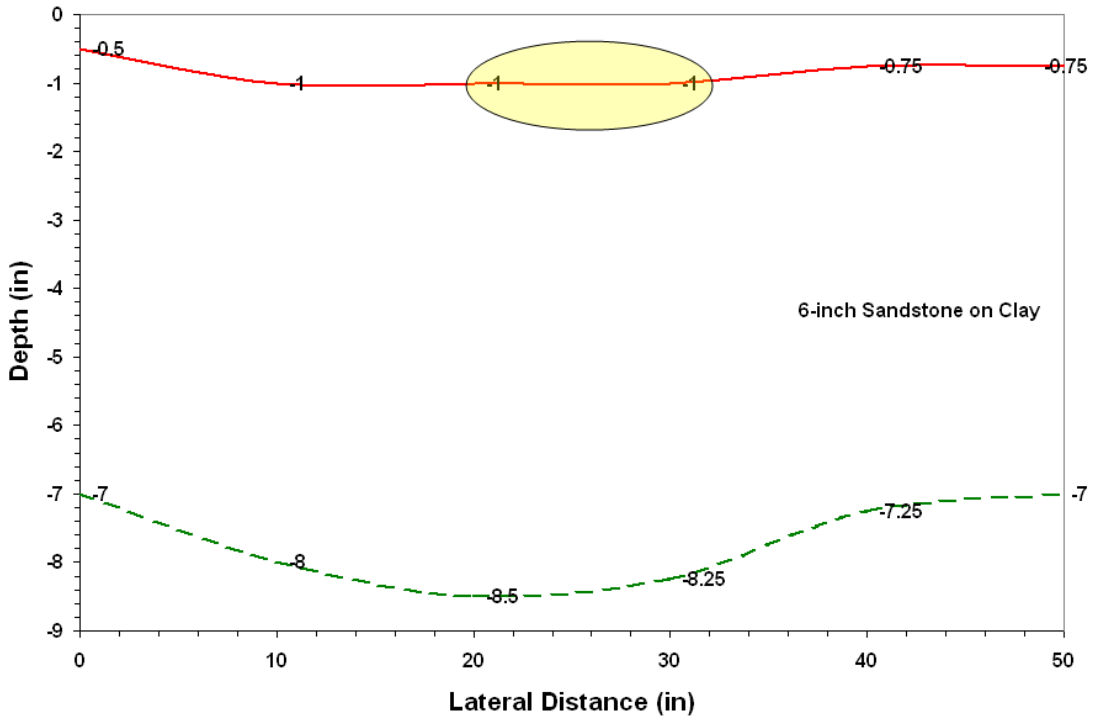

Figure C29. Cross-Sectional Profile from Trench Measurements (6-inch Sandstone Base on Clay).

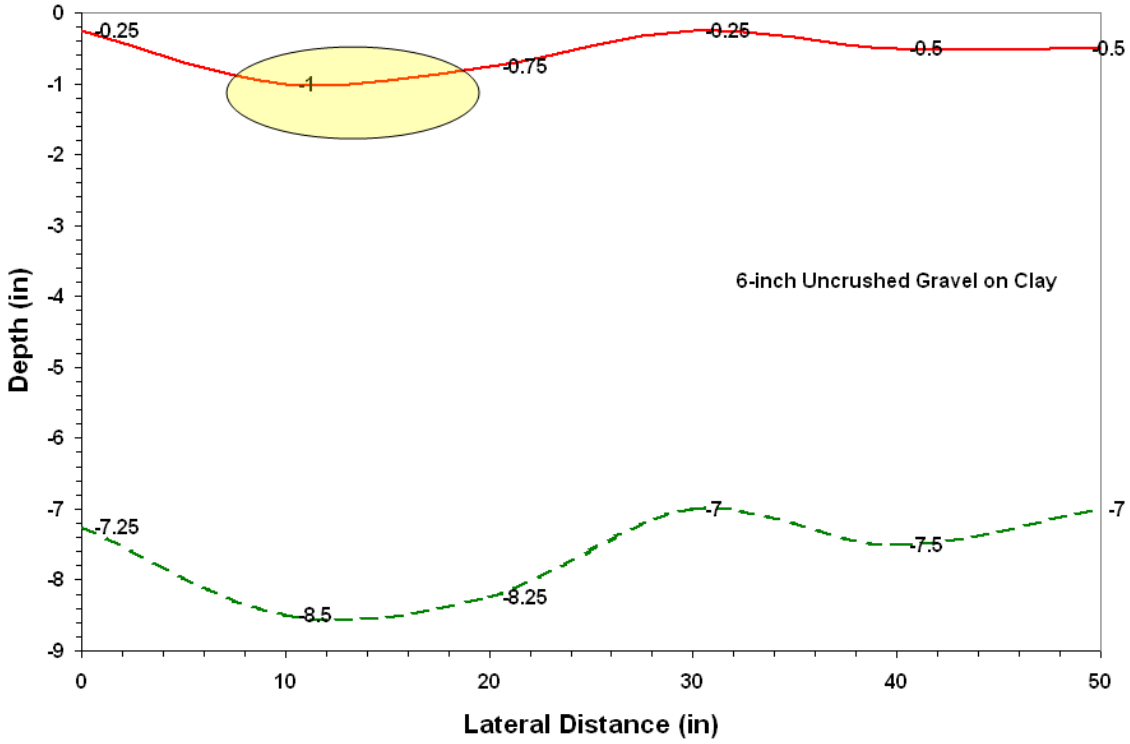

Figure C30. Cross-Sectional Profile from Trench Measurements (6-inch Uncrushed Gravel Base on Clay).

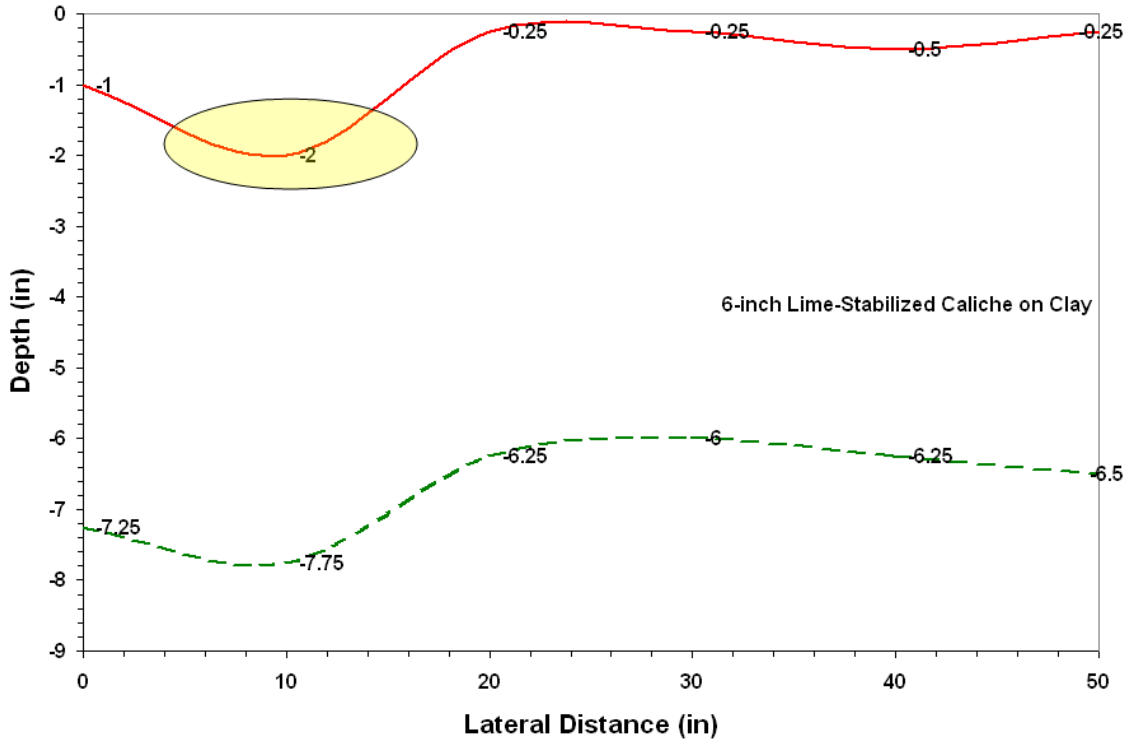

Figure C31. Cross-Sectional Profile from Trench Measurements (6-inch Lime-Stabilized Caliche on Clay).

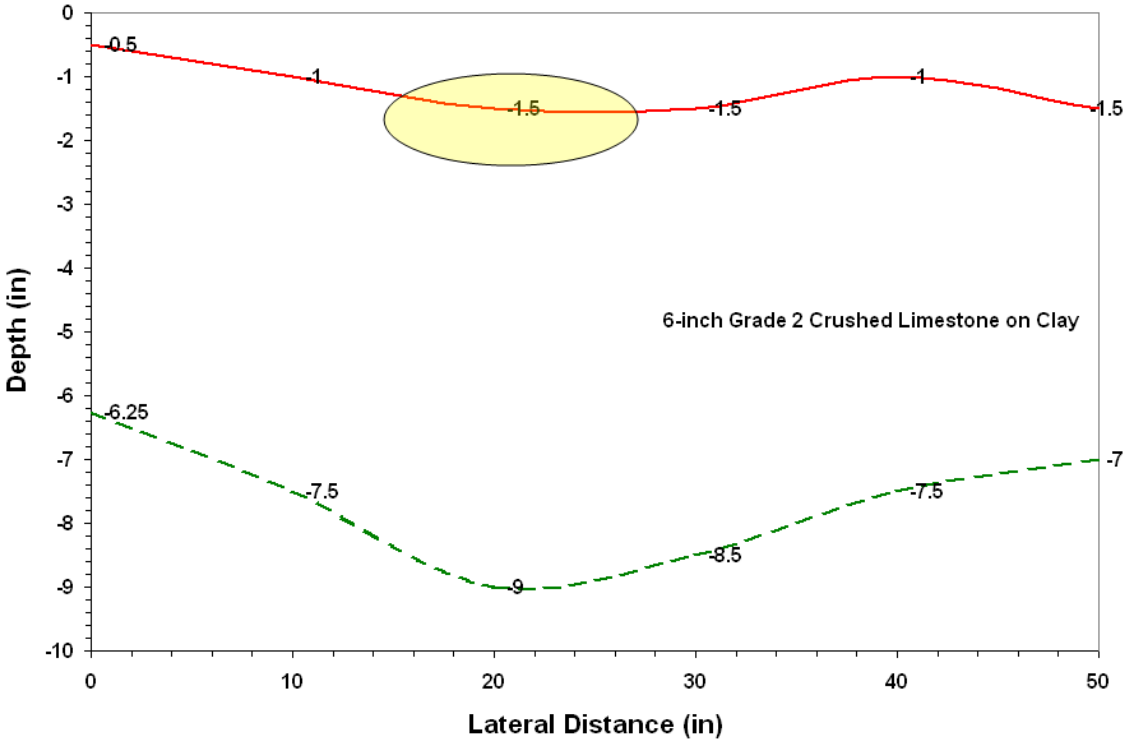

Figure C32. Cross-Sectional Profile from Trench Measurements (6-inch Grade 2 Crushed Limestone Base on Clay).

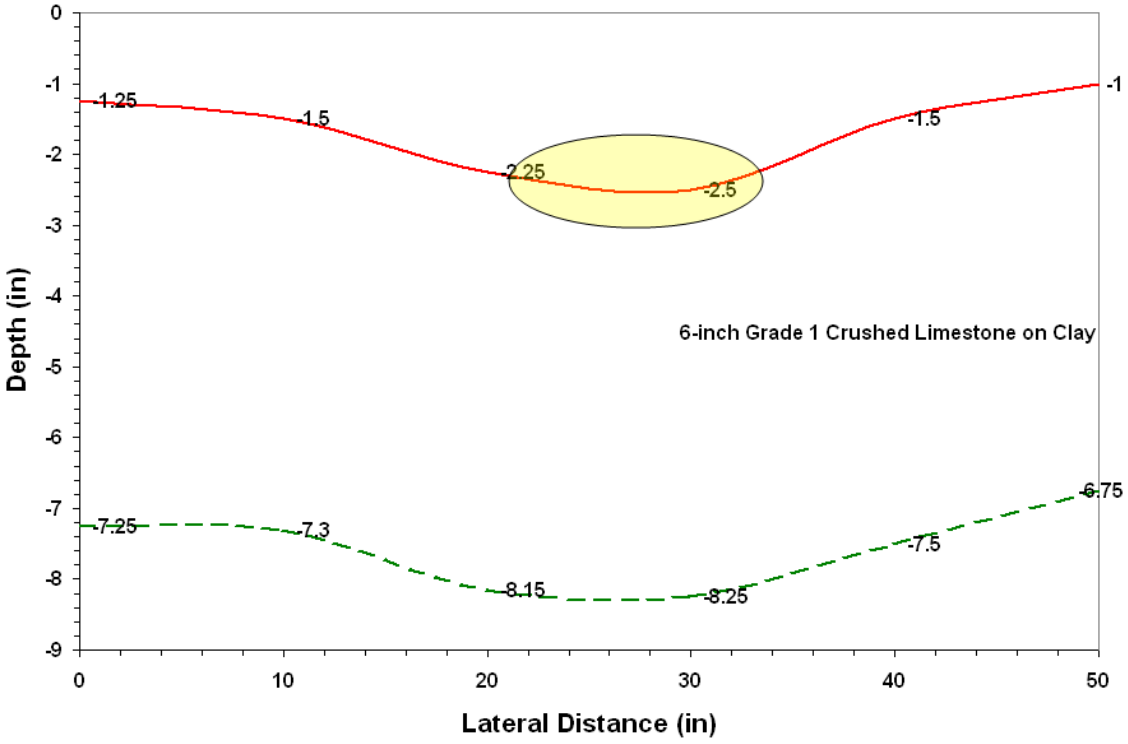

Figure C33. Cross-Sectional Profile from Trench Measurements (6-inch Grade 1 Crushed Limestone Base on Clay).

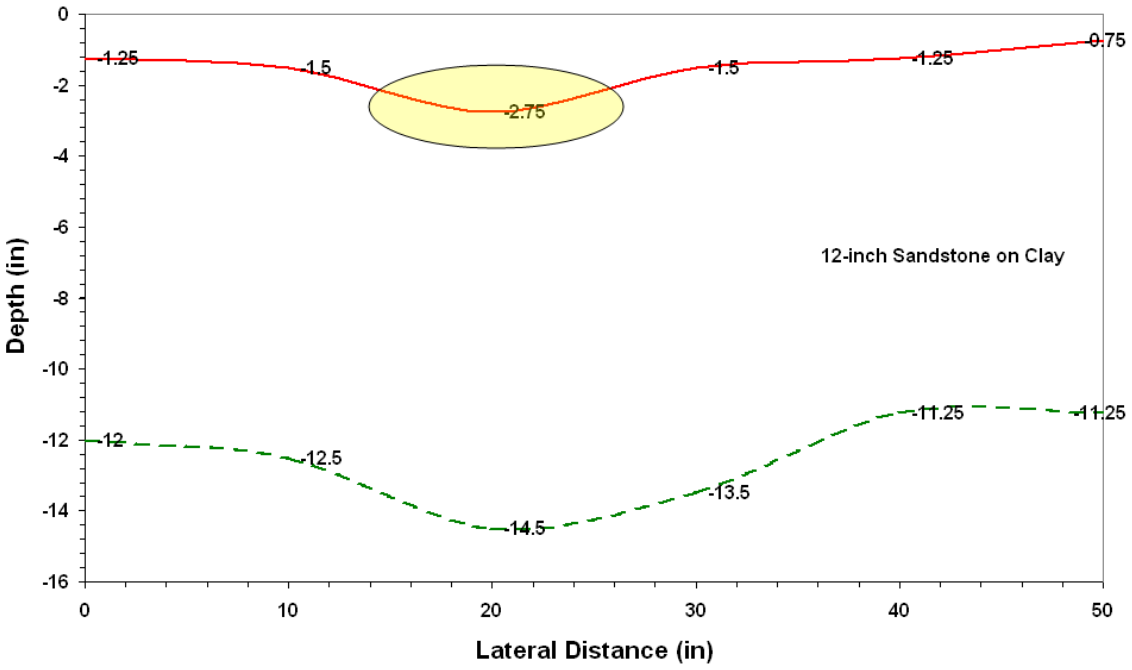

Figure C34. Cross-Sectional Profile from Trench Measurements (12-inch Sandstone Base on Clay).

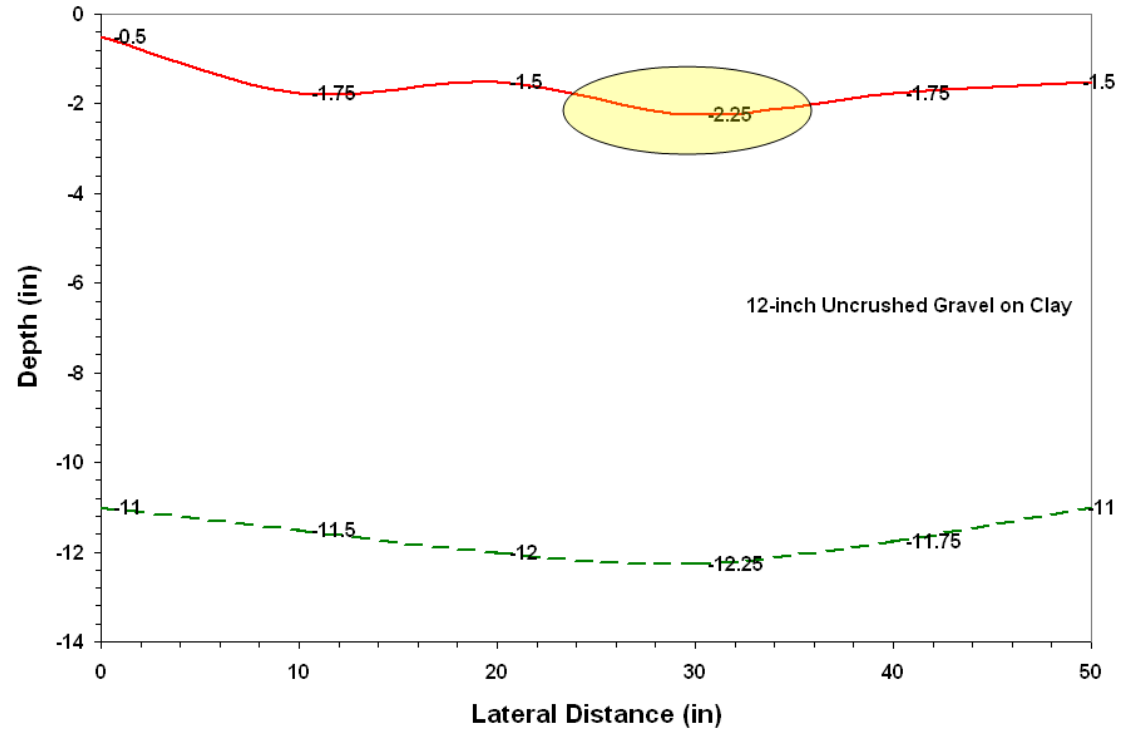

Figure C35. Cross-Sectional Profile from Trench Measurements (12-inch Uncrushed Gravel Base on Clay).

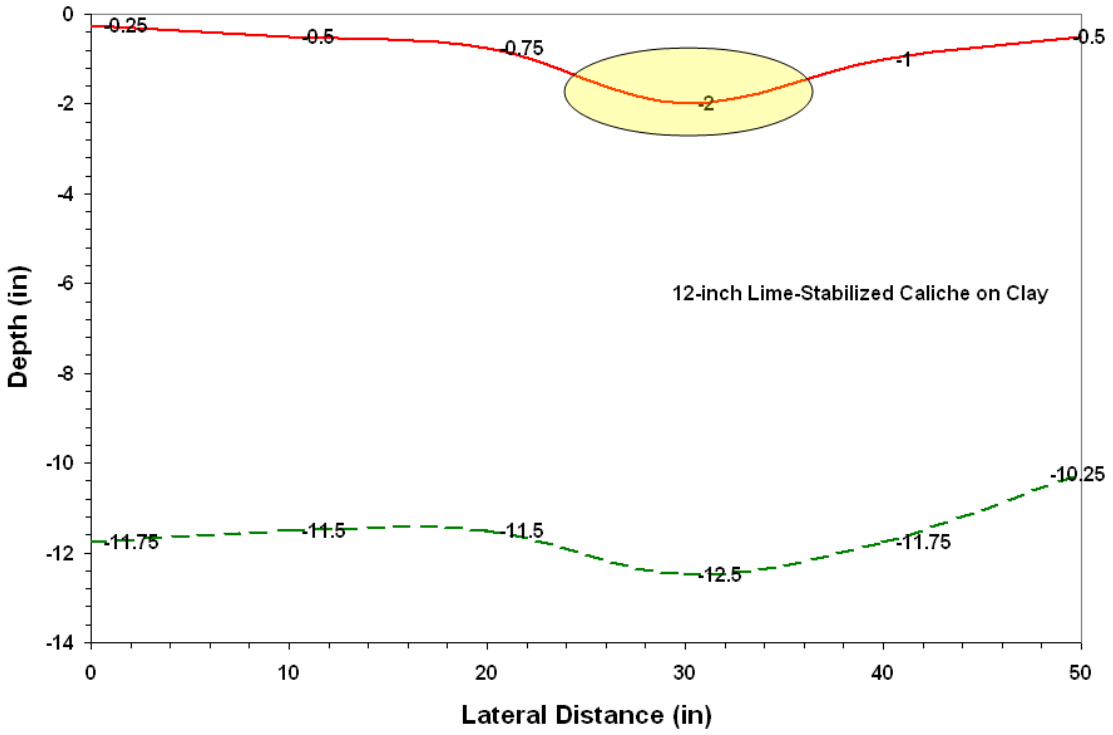

Figure C36. Cross-Sectional Profile from Trench Measurements (12-inch Lime-Stabilized Caliche on Clay).

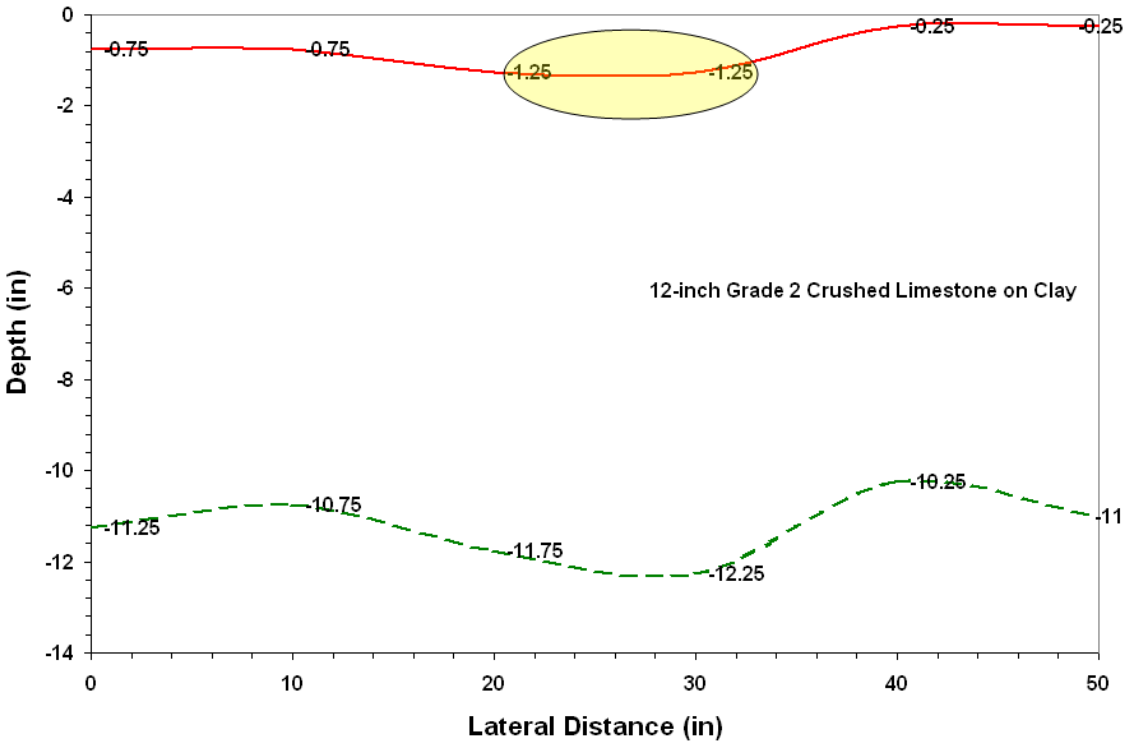

Figure C37. Cross-Sectional Profile from Trench Measurements (12-inch Grade 2 Crushed Limestone Base on Clay).

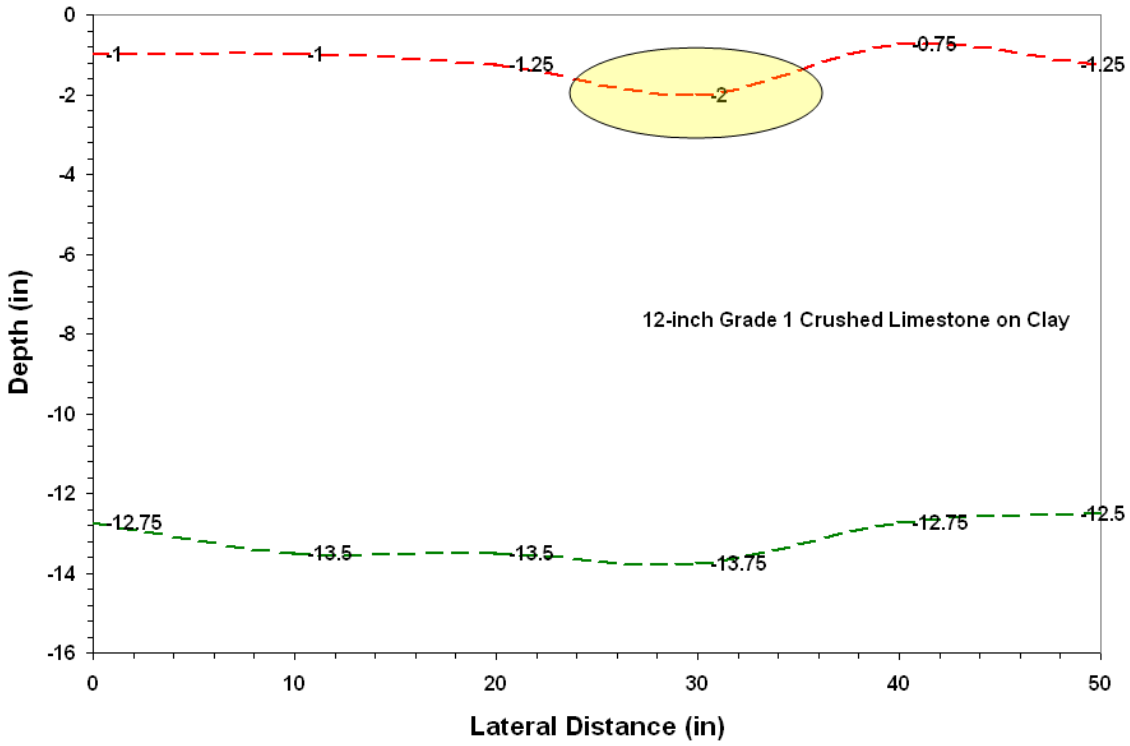

Figure C38. Cross-Sectional Profile from Trench Measurements (12-inch Grade 1 Crushed Limestone Base on Clay).

APPENDIX D. LOAD-DISPLACEMENT CURVES FROM PLATE BEARING TESTS ON FULL-SCALE PAVEMENT SECTIONS

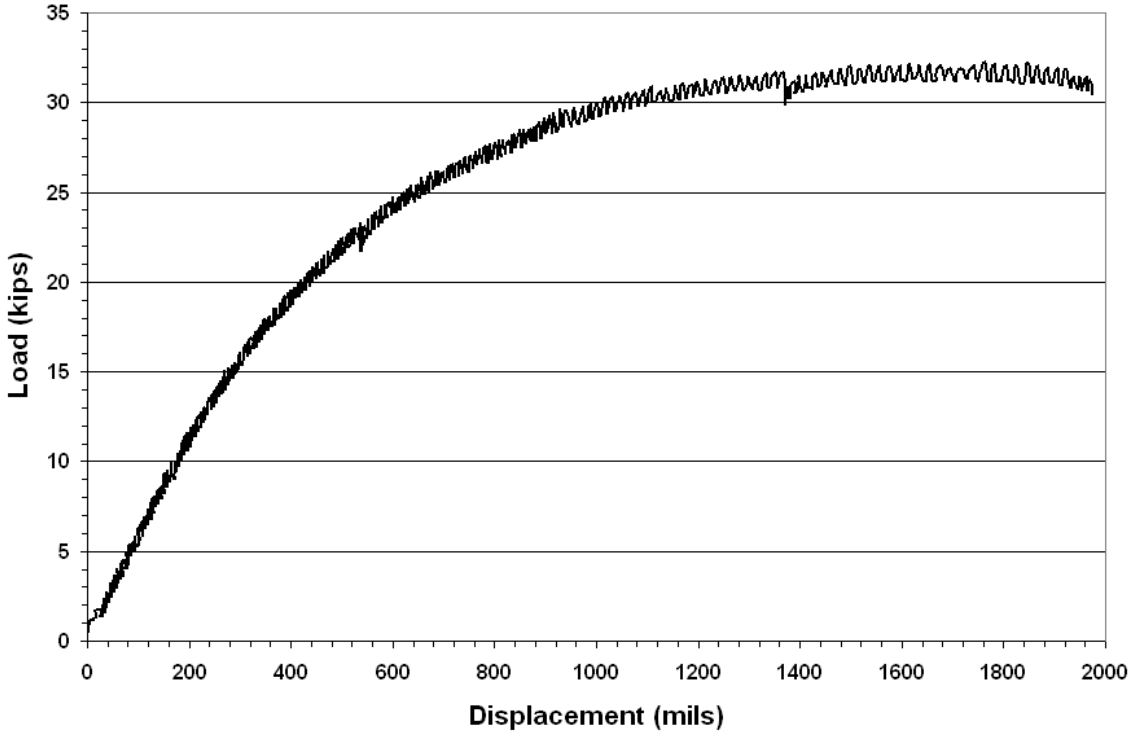

Figure D1. Load-Displacement Curve from Test on 12-inch Sandstone Base on Clay.

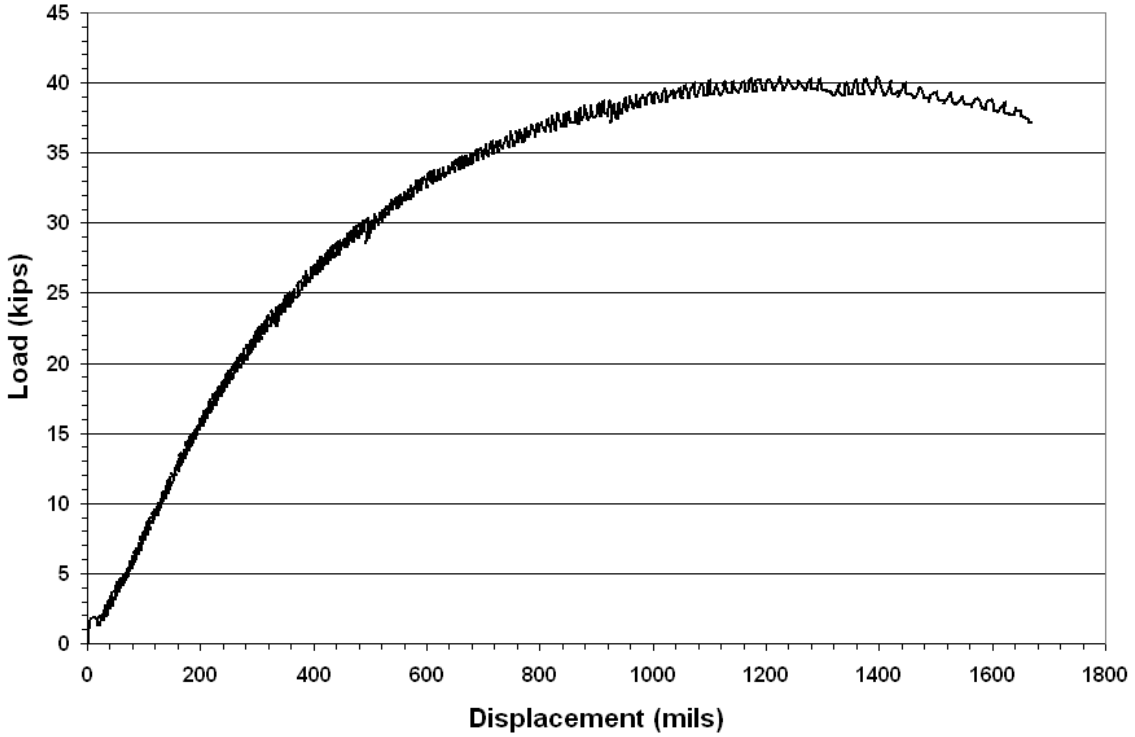

Figure D2. Load-Displacement Curve from Test on 12-inch Uncrushed Gravel Base on Clay.

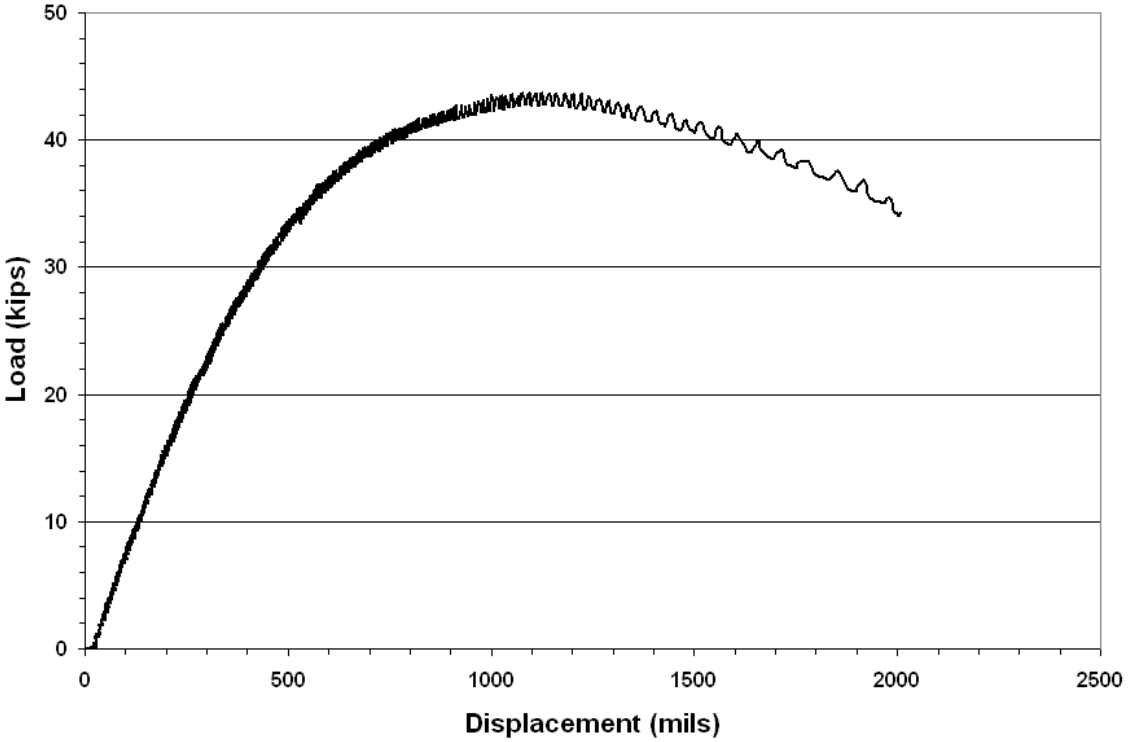

Figure D3. Load-Displacement Curve from Test on 12-inch Caliche Base on Clay.

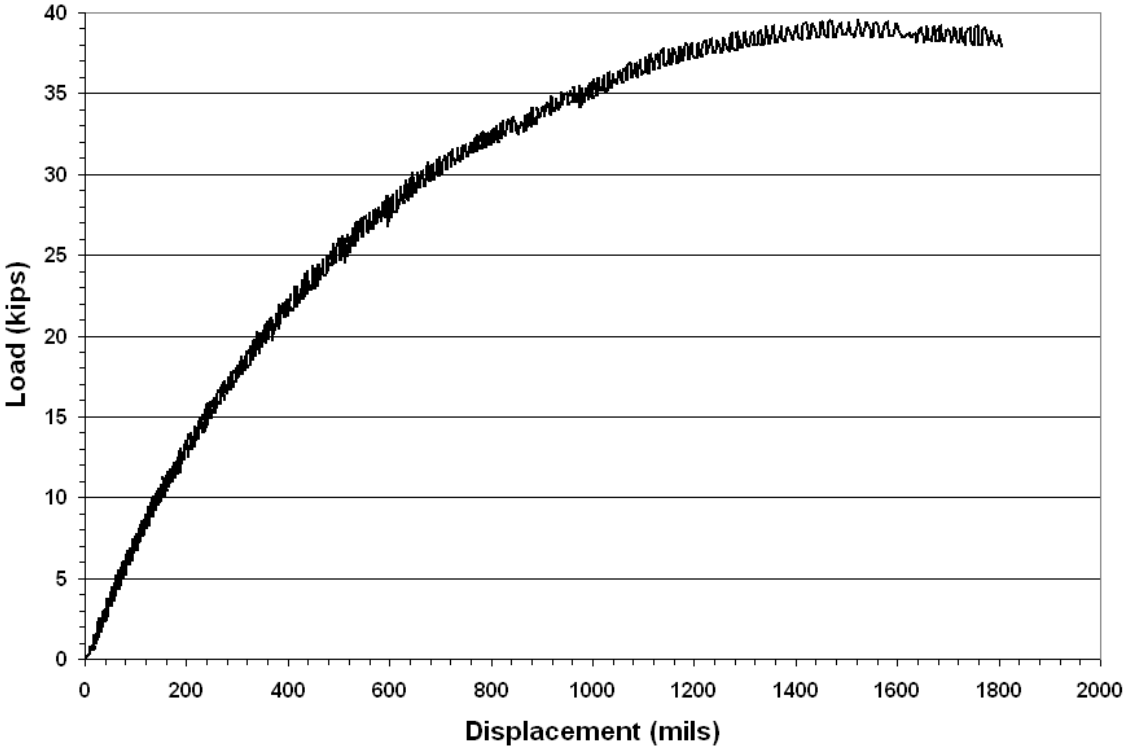

Figure D4. Load-Displacement Curve from Test on 12-inch Grade 2 Crushed Limestone Base on Clay.

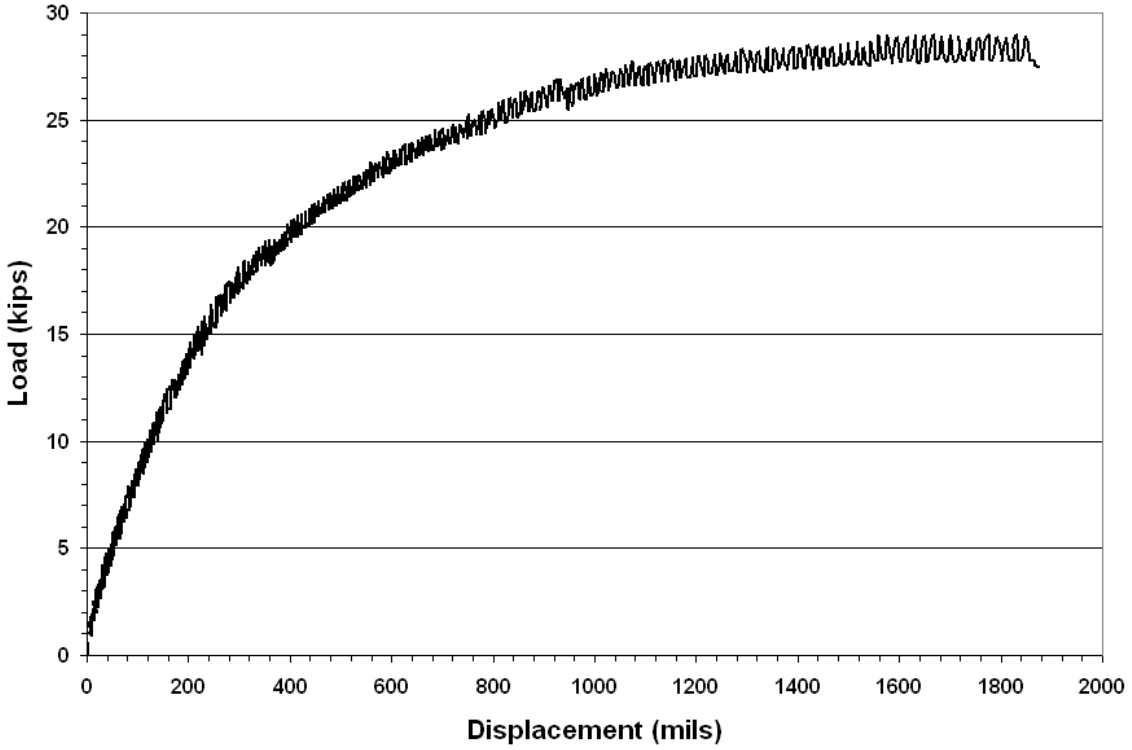

Figure D5. Load-Displacement Curve from Test on 12-inch Grade 1 Crushed Limestone Base on Clay.

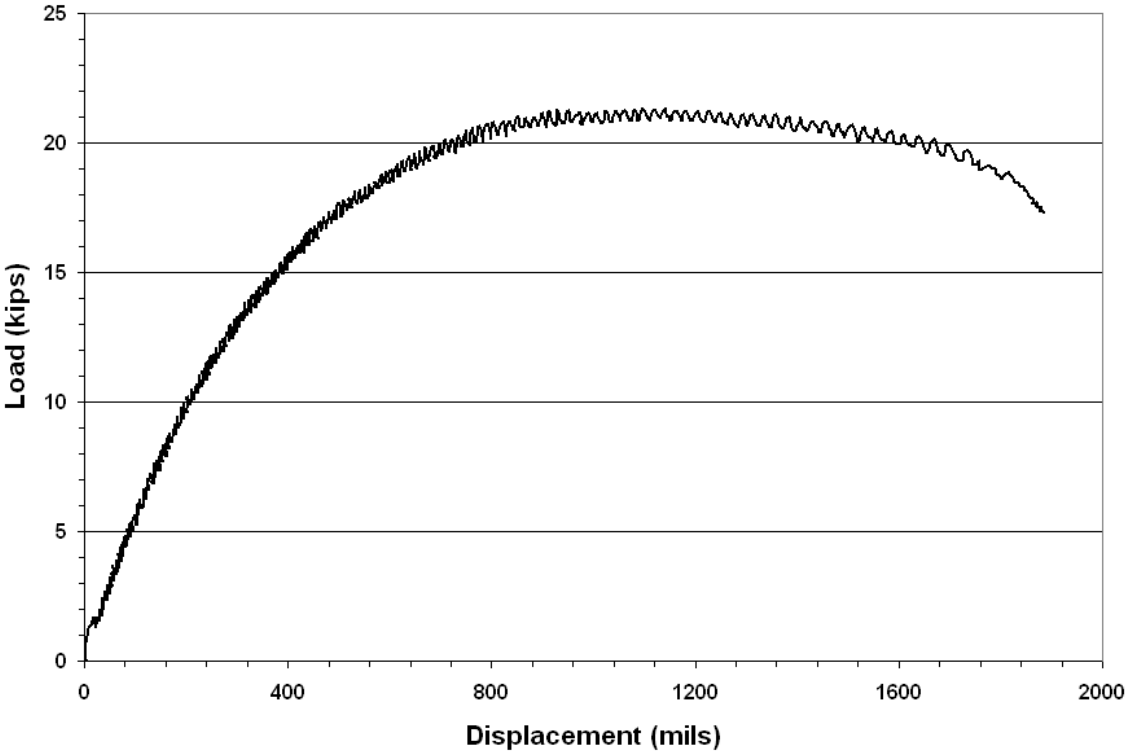

Figure D6. Load-Displacement Curve from Test on 6-inch Sandstone Base on Clay.

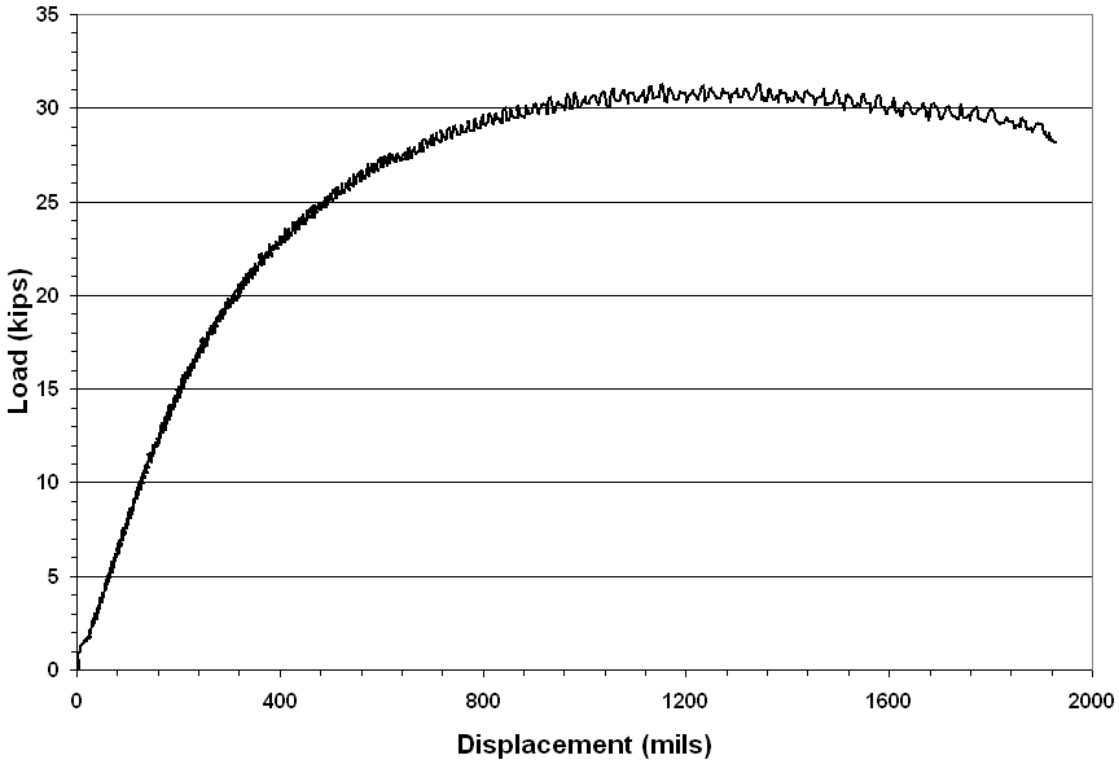

Figure D7. Load-Displacement Curve from Test on 6-inch Uncrushed Gravel Base on Clay.

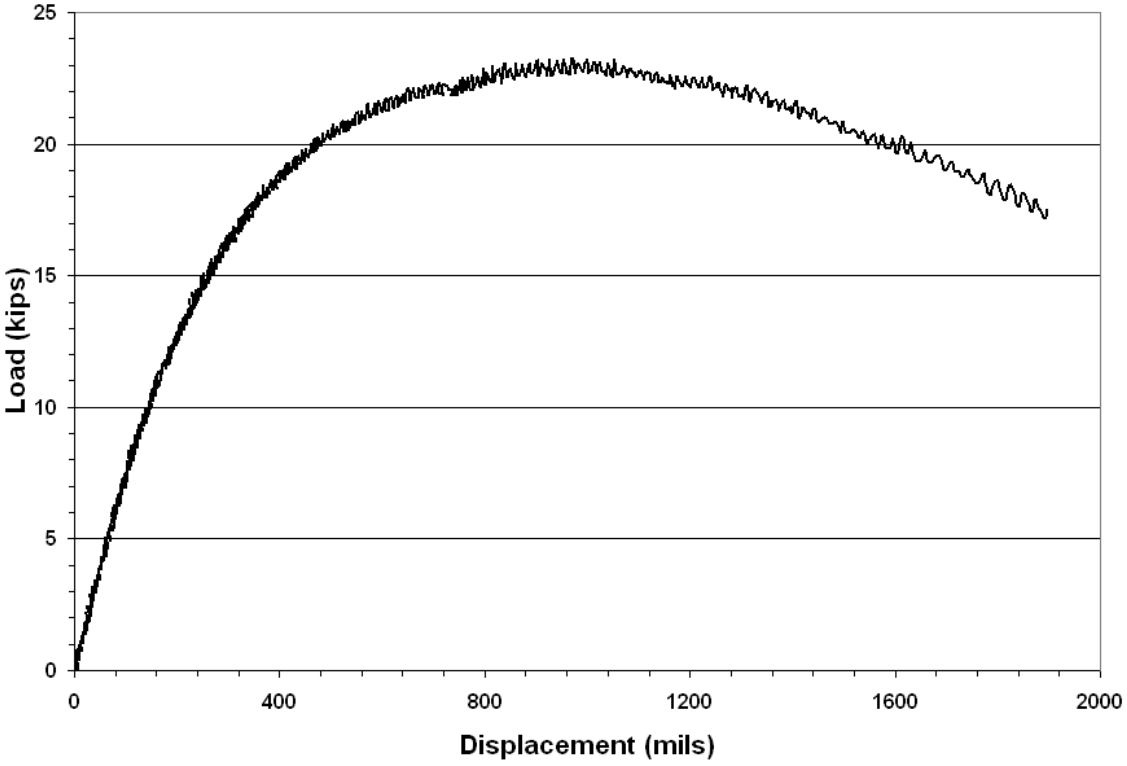

Figure D8. Load-Displacement Curve from Test on 6-inch Caliche Base on Clay.

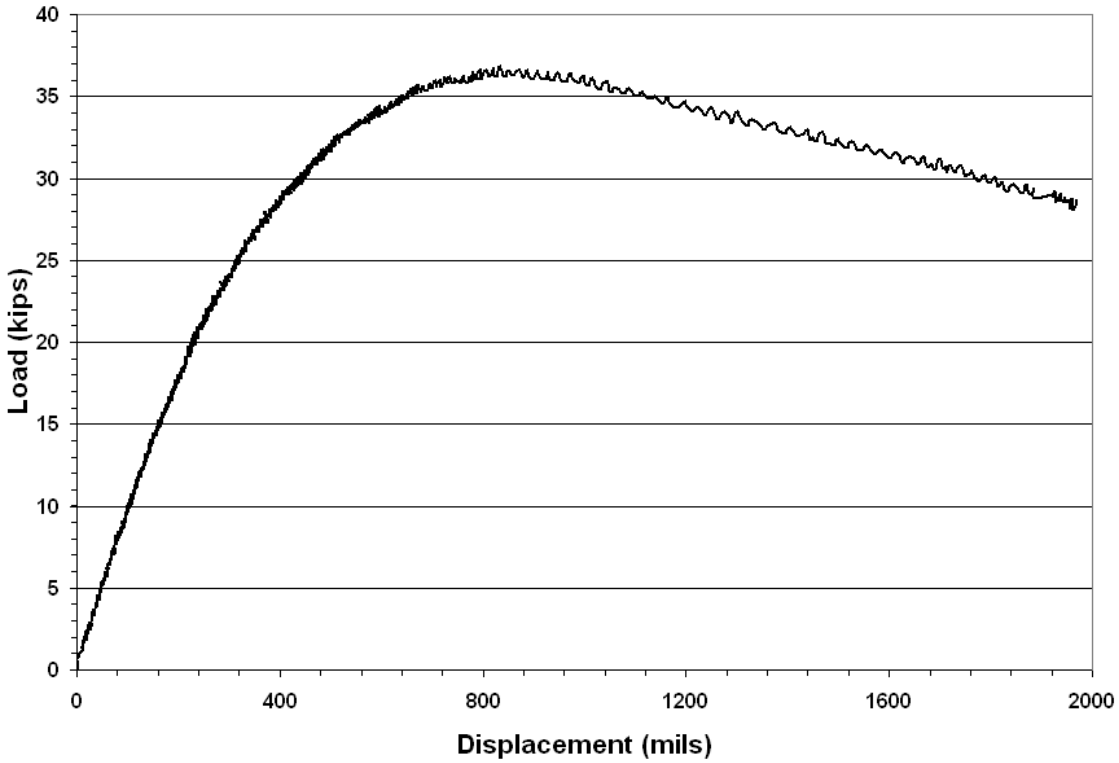

Figure D9. Load-Displacement Curve from Test on 6-inch Grade 2 Crushed Limestone Base on Clay.

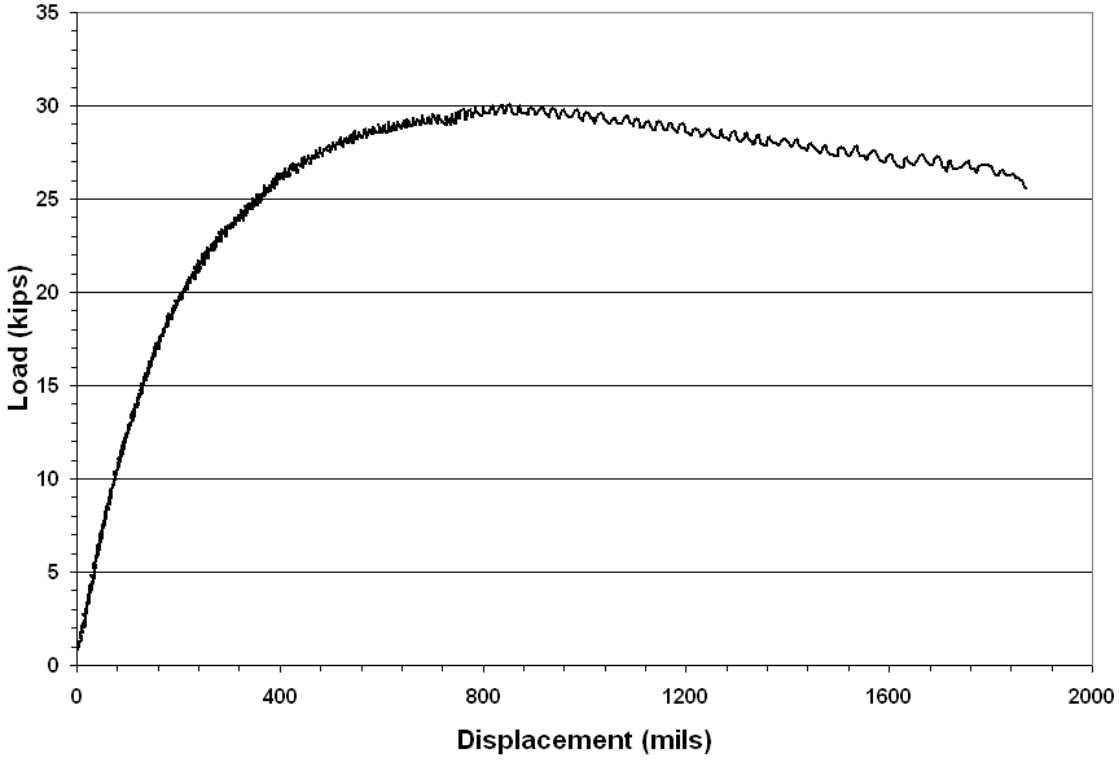

Figure D10. Load-Displacement Curve from Test on 6-inch Grade 1 Crushed Limestone Base on Clay.

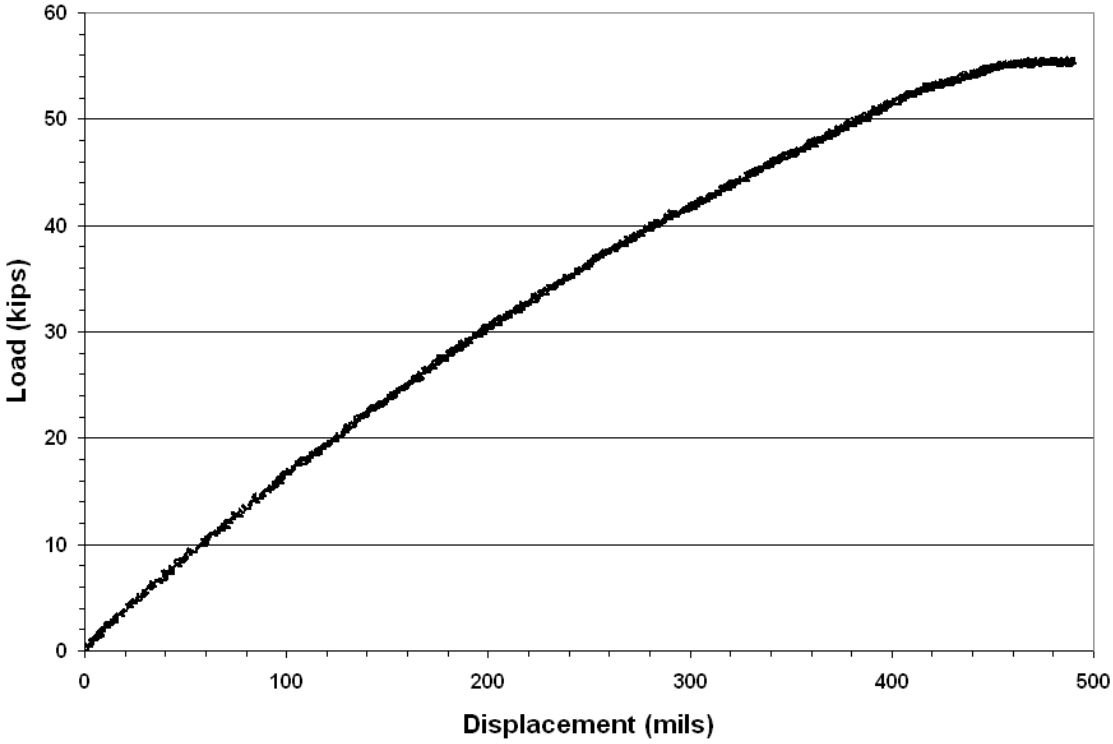

Figure D11. Load-Displacement Curve from Test on 6-inch Grade 1 Crushed Limestone Base on Sand.

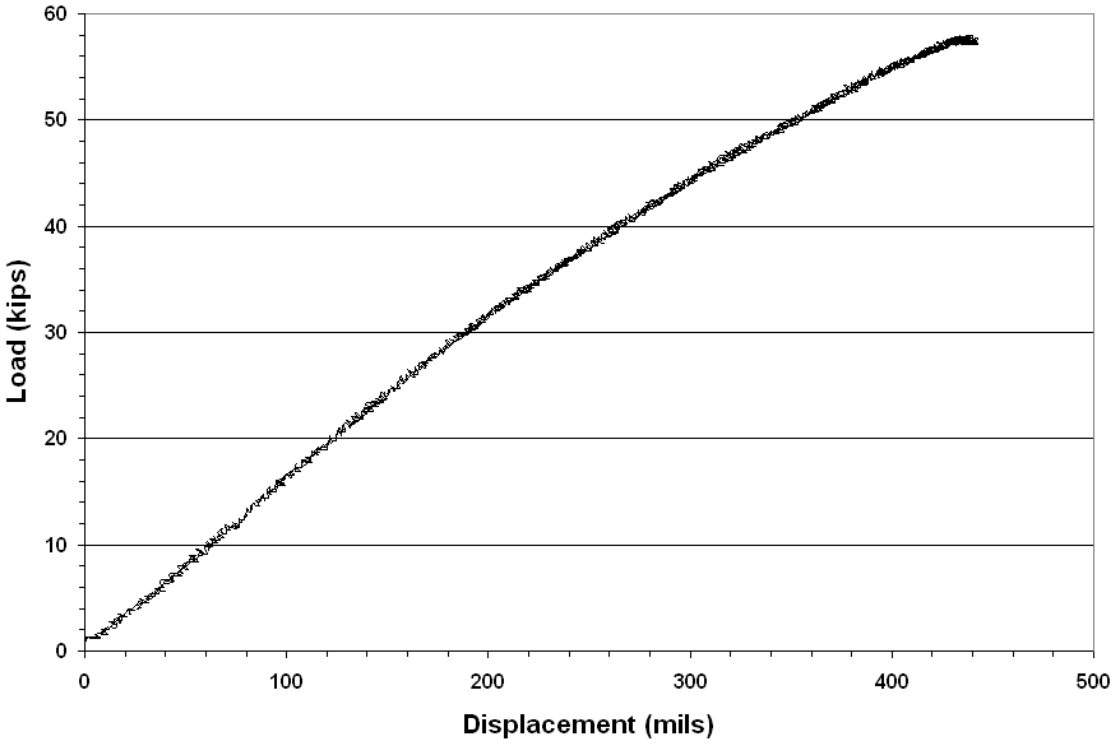

Figure D12. Load-Displacement Curve from Test on 6-inch Grade 2 Crushed Limestone Base on Sand.

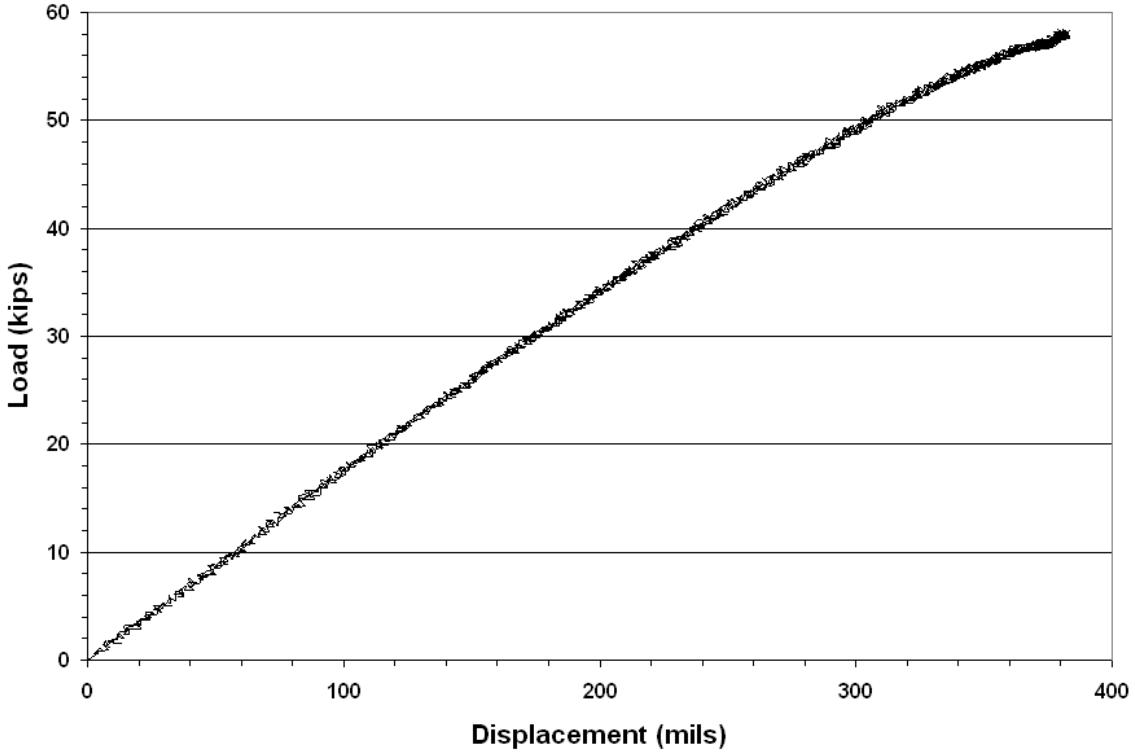

Figure D13. Load-Displacement Curve from Test on 6-inch Caliche Base on Sand.

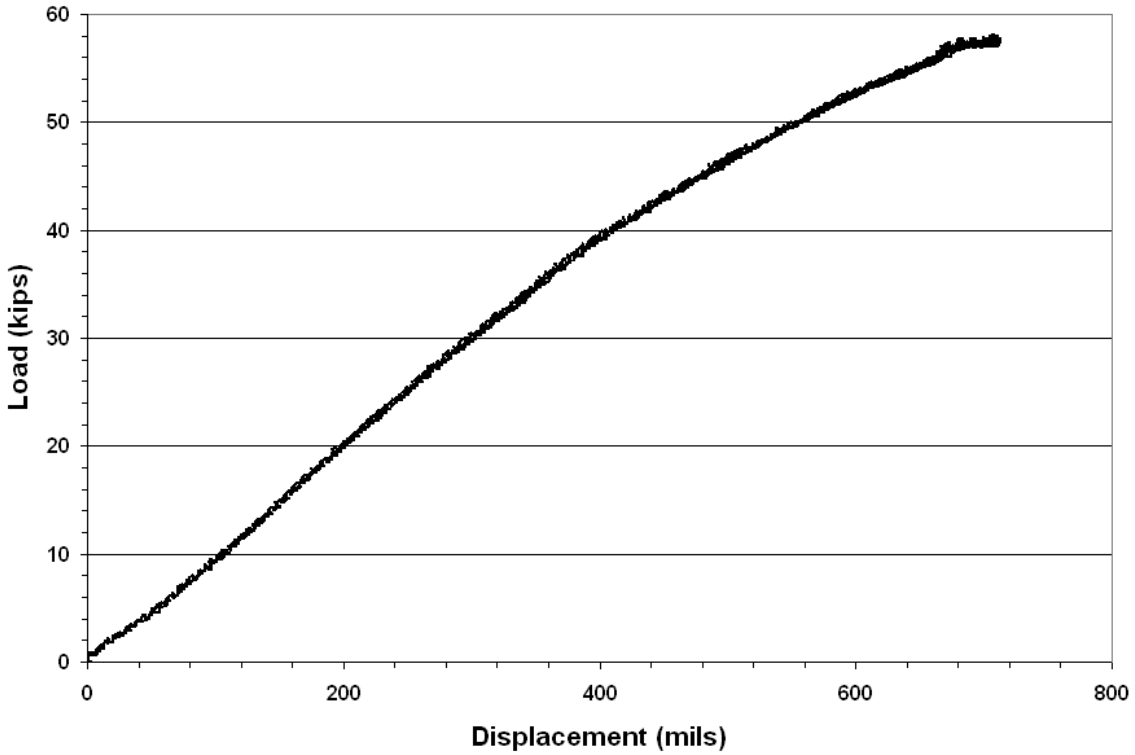

Figure D14. Load-Displacement Curve from Test on 6-inch Uncrushed Gravel Base on Sand.

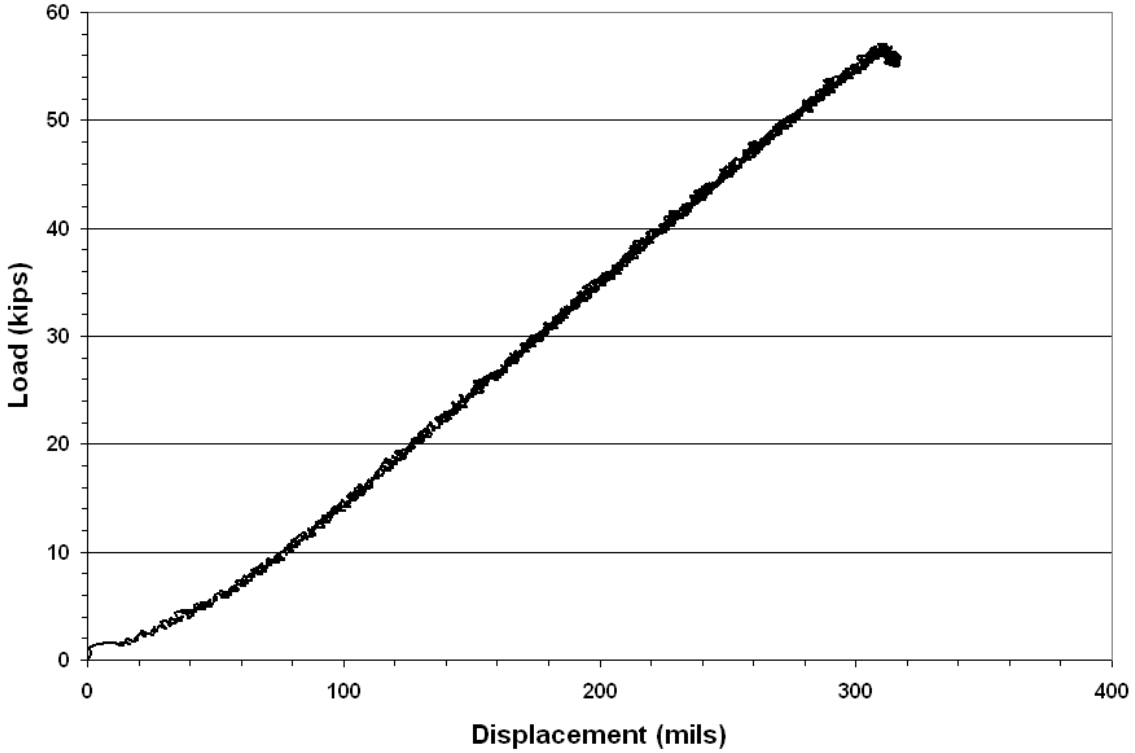

Figure D15. Load-Displacement Curve from Test on 6-inch Sandstone Base on Sand.

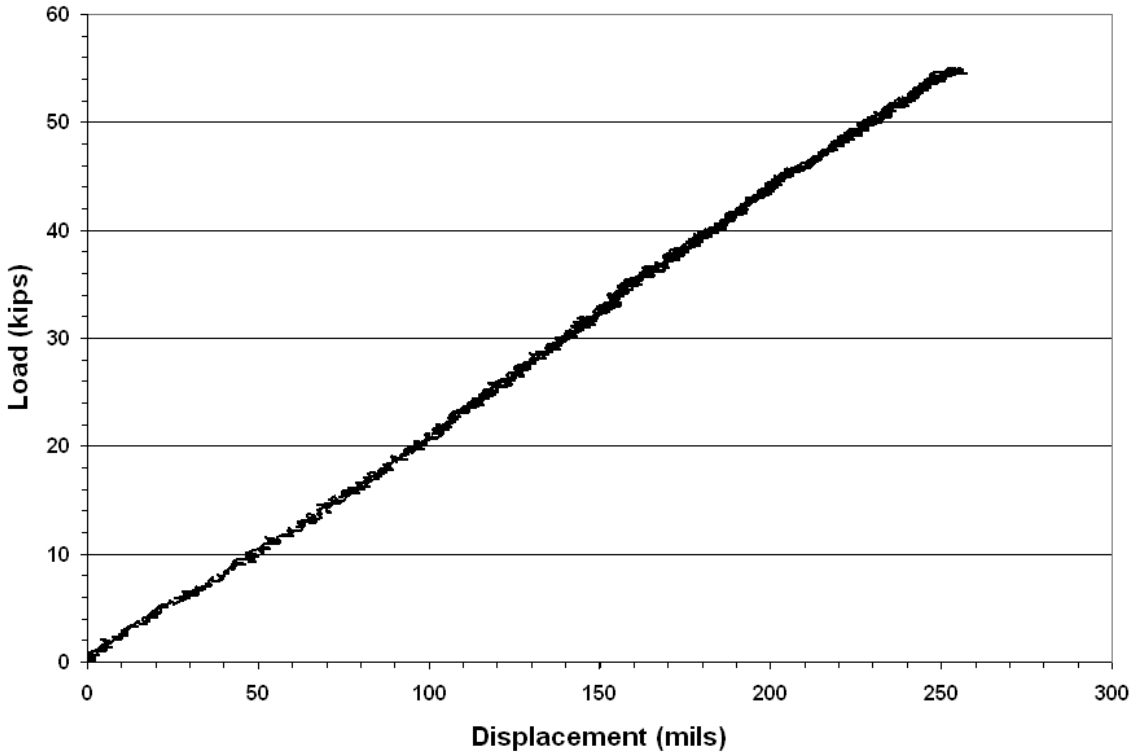

Figure D16. Load-Displacement Curve from Test on 12-inch Grade 1 Crushed Limestone Base on Sand.

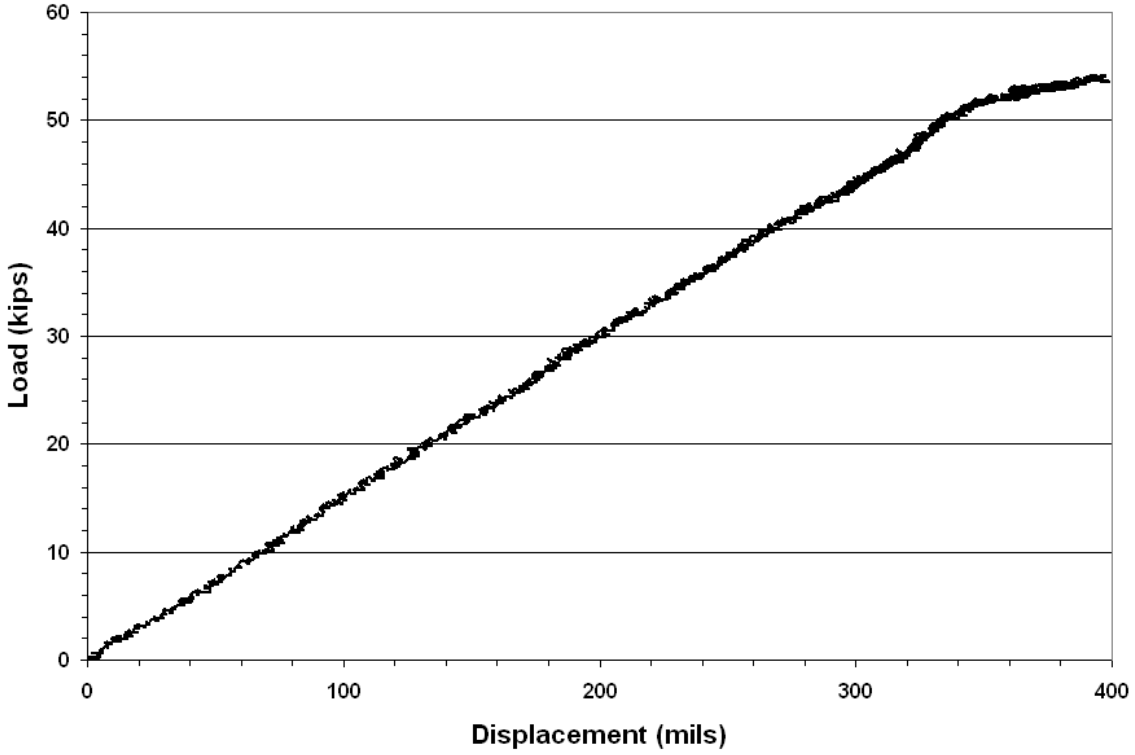

Figure D17. Load-Displacement Curve from Test on 12-inch Grade 2 Crushed Limestone Base on Sand.

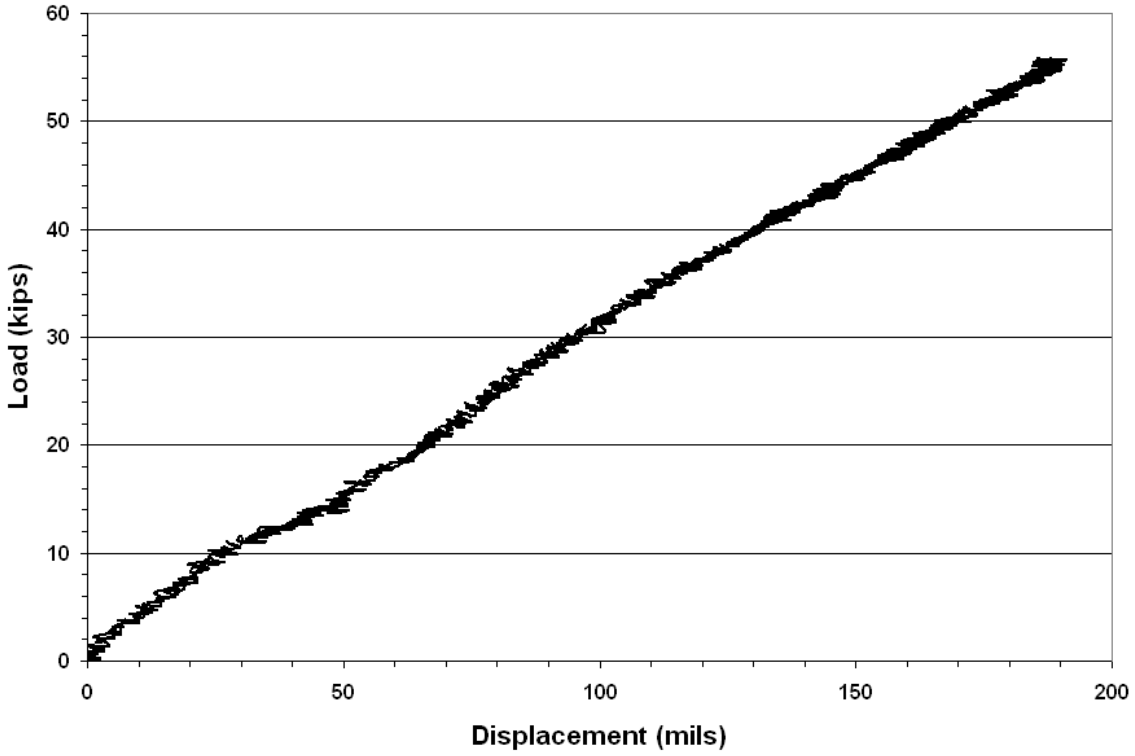

Figure D18. Load-Displacement Curve from Test on 12-inch Caliche Base on Sand.

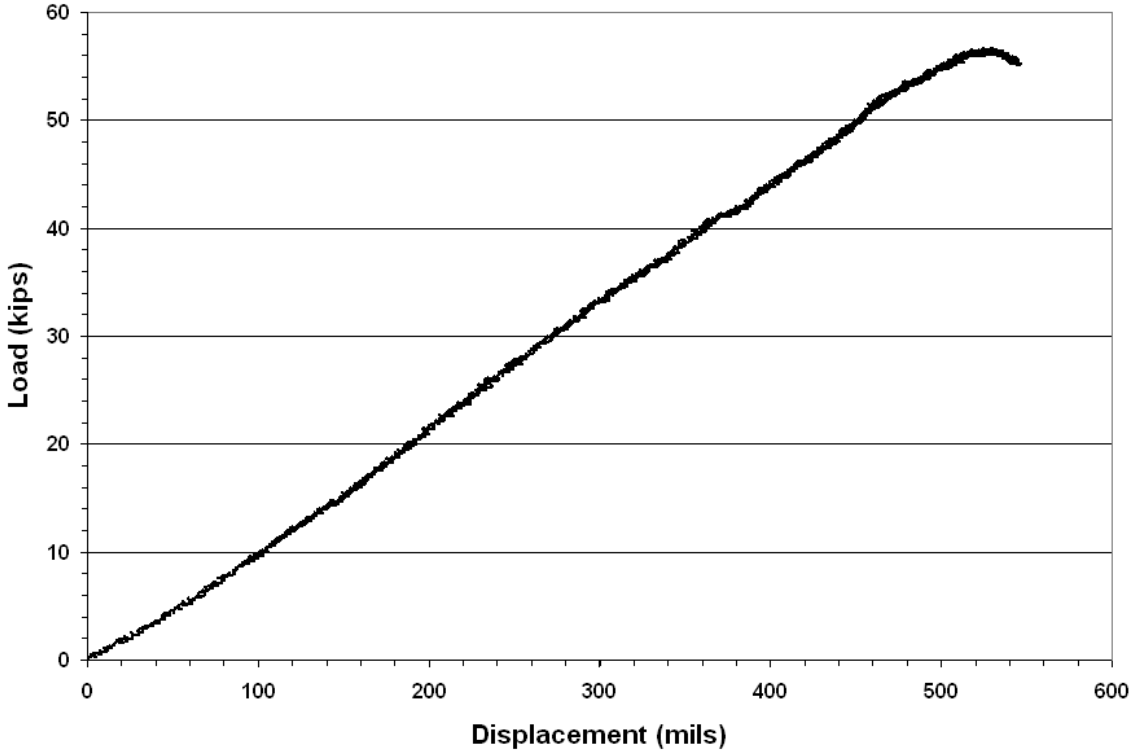

Figure D19. Load-Displacement Curve from Test on 12-inch Uncrushed Gravel Base on Sand.

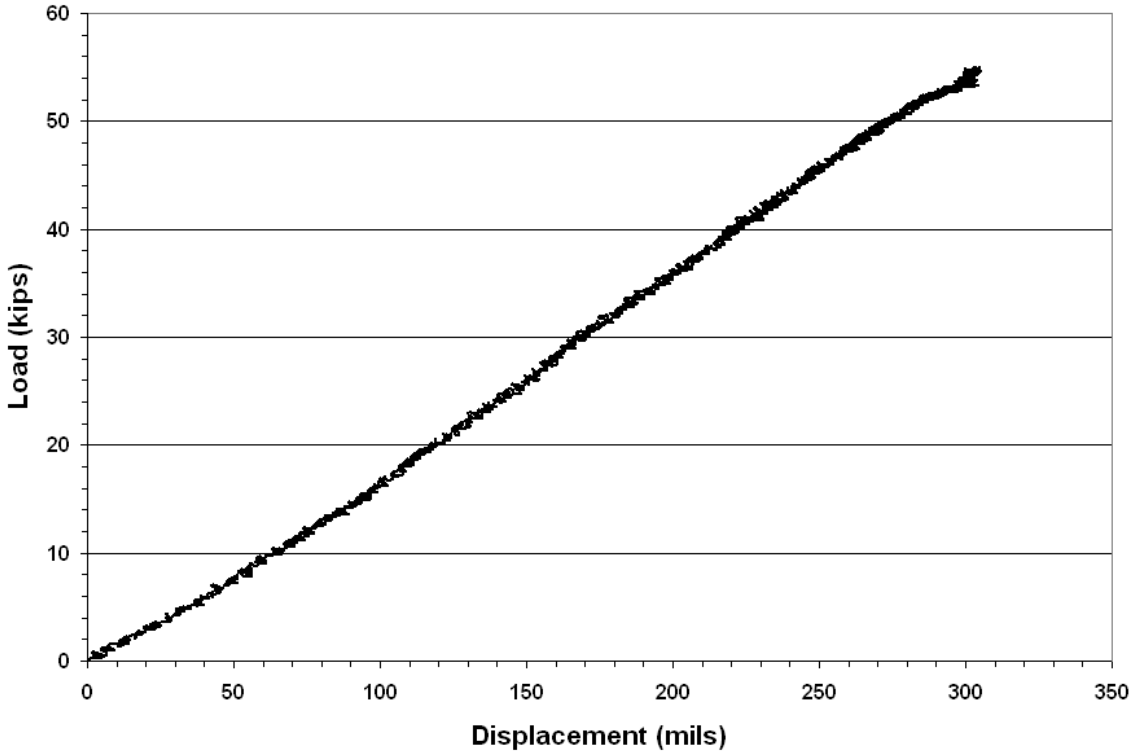

Figure D20. Load-Displacement Curve from Test on 12-inch Sandstone Base on Sand.

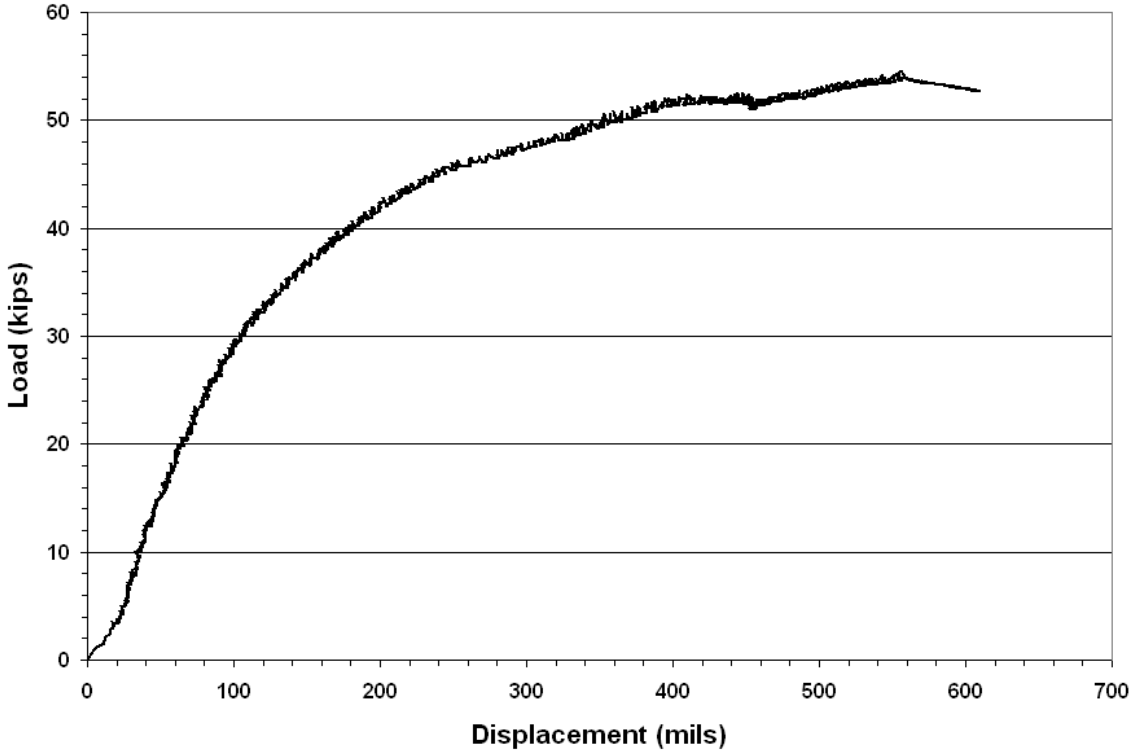

Figure D21. Load-Displacement Curve from Test on 4.5 Percent Cement-Treated Grade 2 Crushed Limestone Base on Clay.

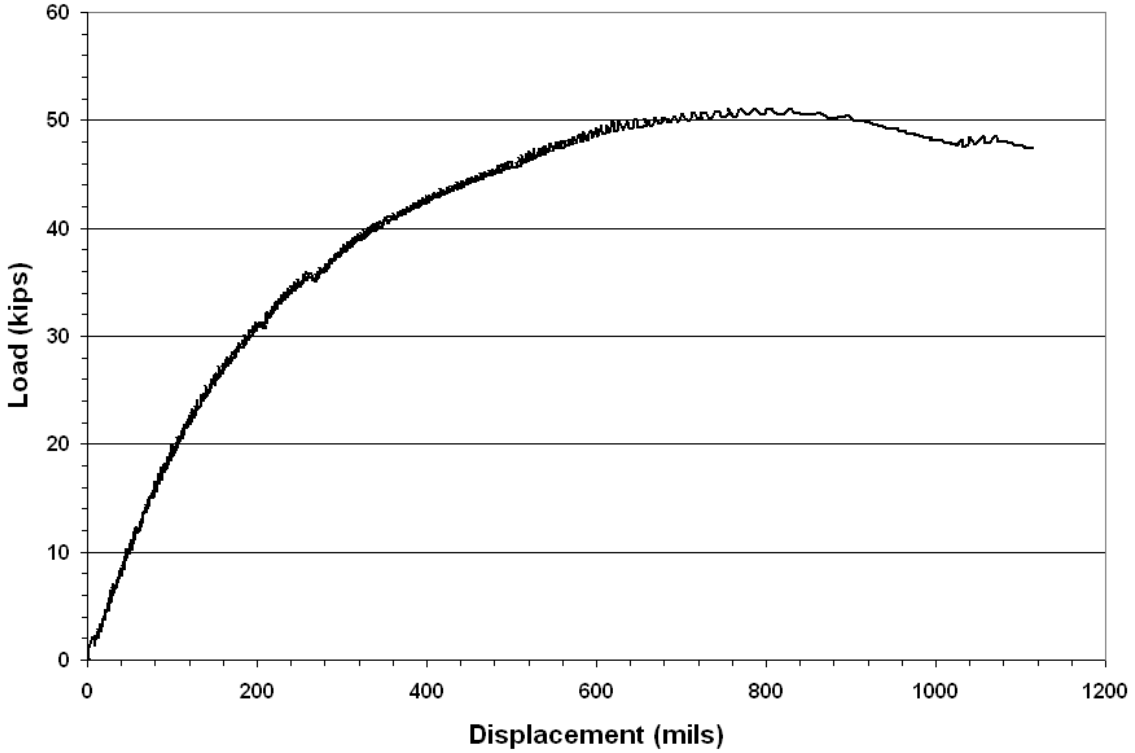

Figure D22. Load-Displacement Curve from Test on 3.0 Percent Cement-Treated Grade 2 Crushed Limestone Base on Clay.

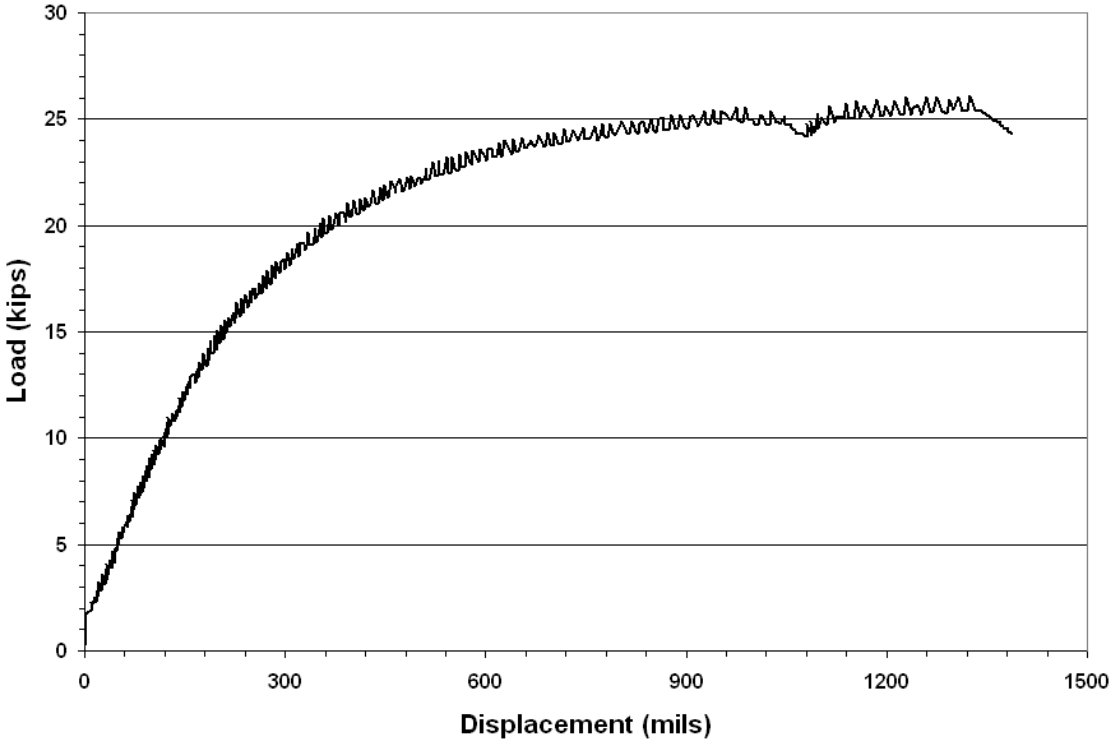

Figure D23. Load-Displacement Curve from Test on 2 Percent Lime-Stabilized Uncrushed Gravel on Clay.

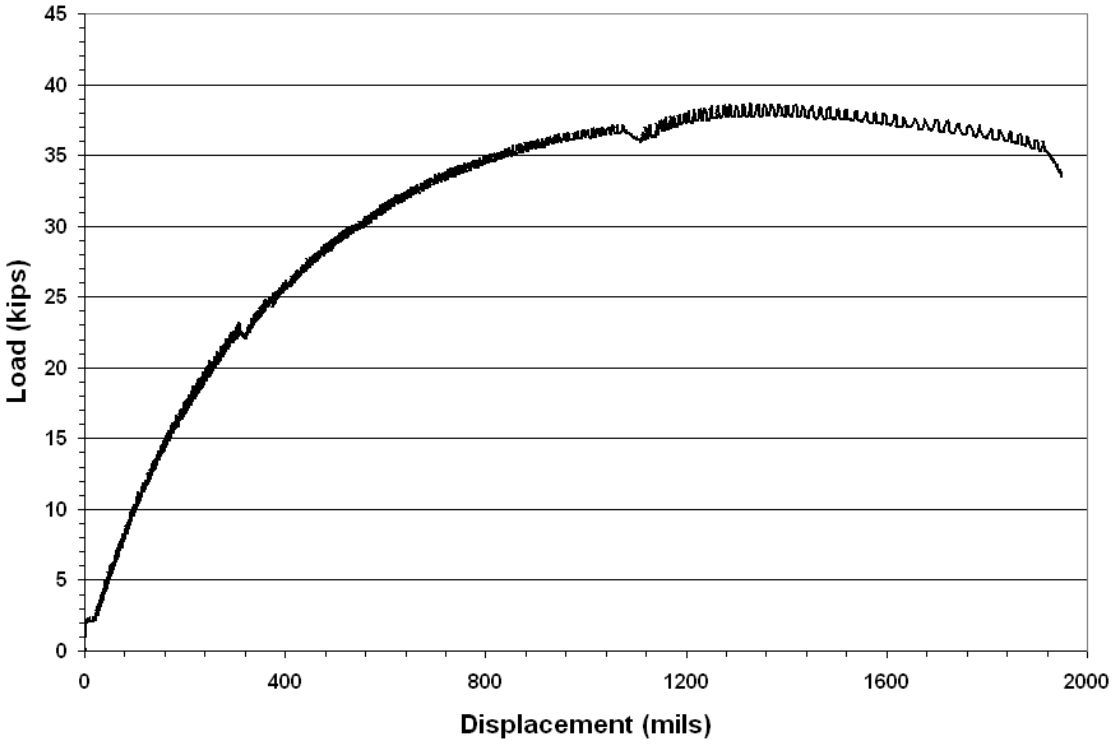

Figure D24. Load-Displacement Curve from Test on 2.5-inch Type D HMAC over Grade 1 Crushed Limestone on Clay.

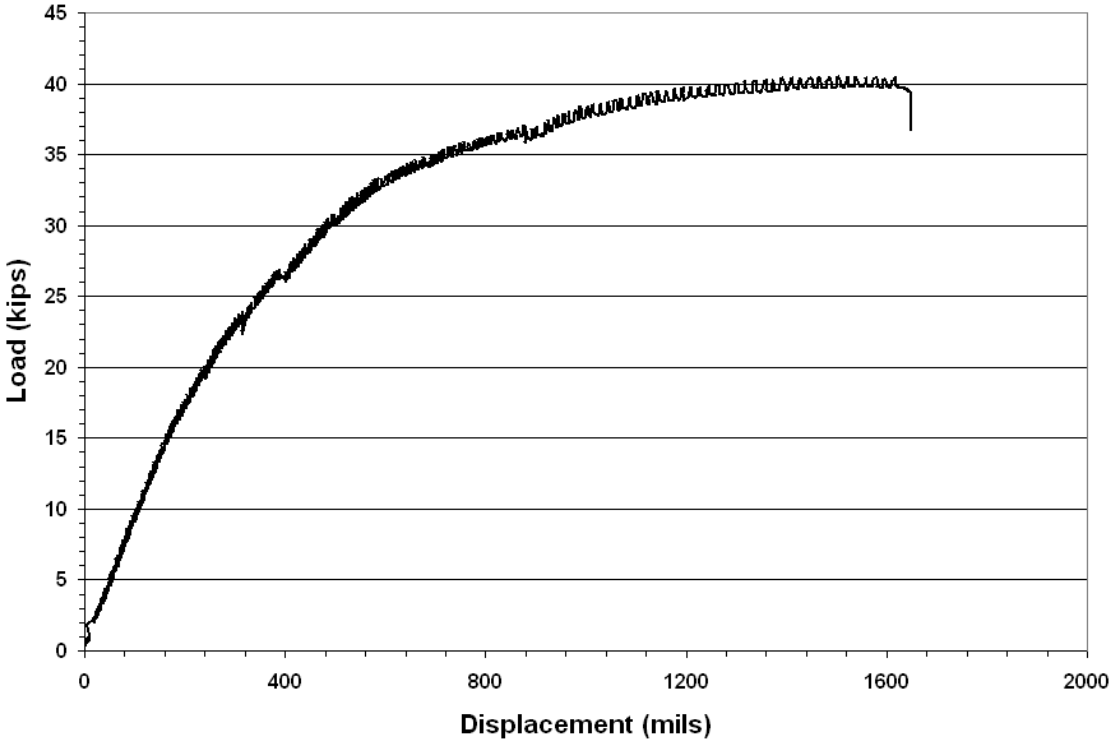

Figure D25. Load-Displacement Curve from Test on 4.5-inch Type D HMAC over Grade 1 Crushed Limestone on Clay.

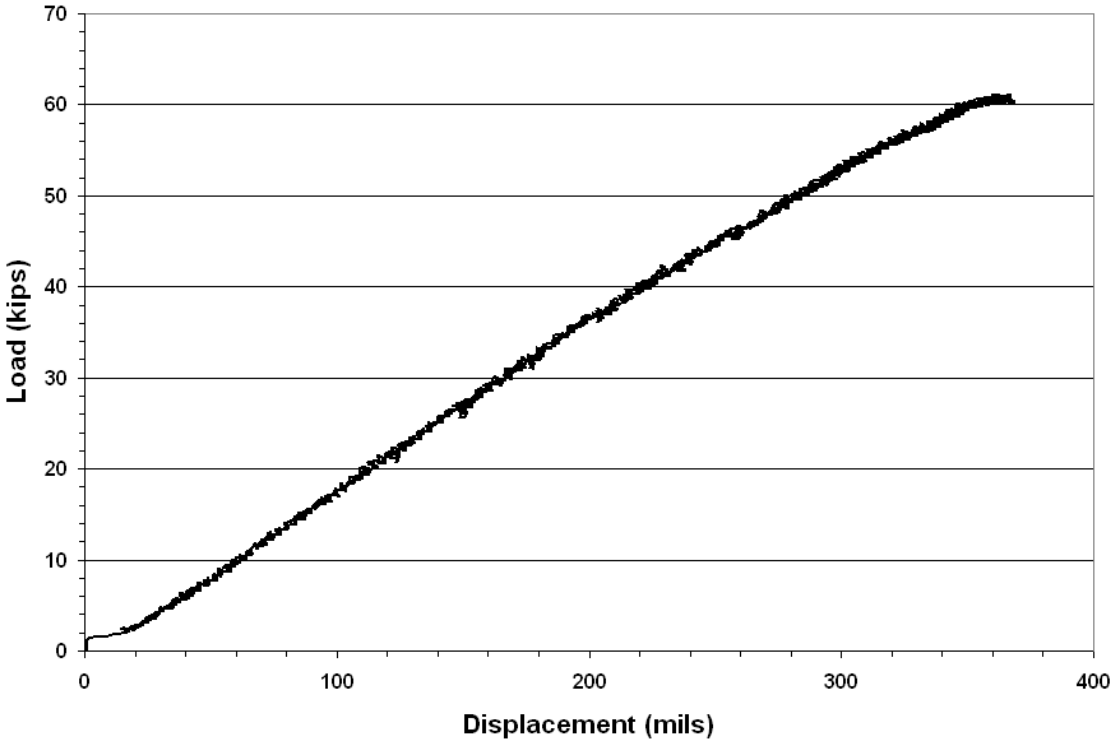

Figure D26. Load-Displacement Curve from Test on 4.5-inch Type D HMAC over Grade 1 Crushed Limestone on Sand.

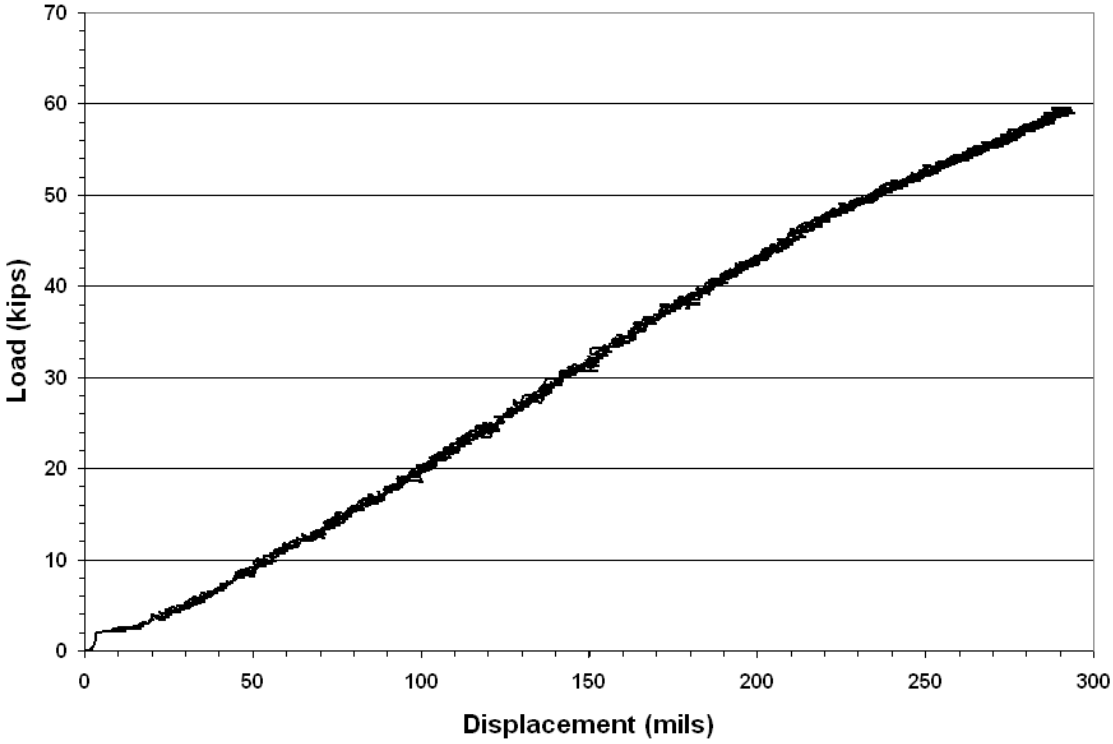

Figure D27. Load-Displacement Curve from Test on 2.5-inch Type D HMAC over Grade 1 Crushed Limestone on Sand.

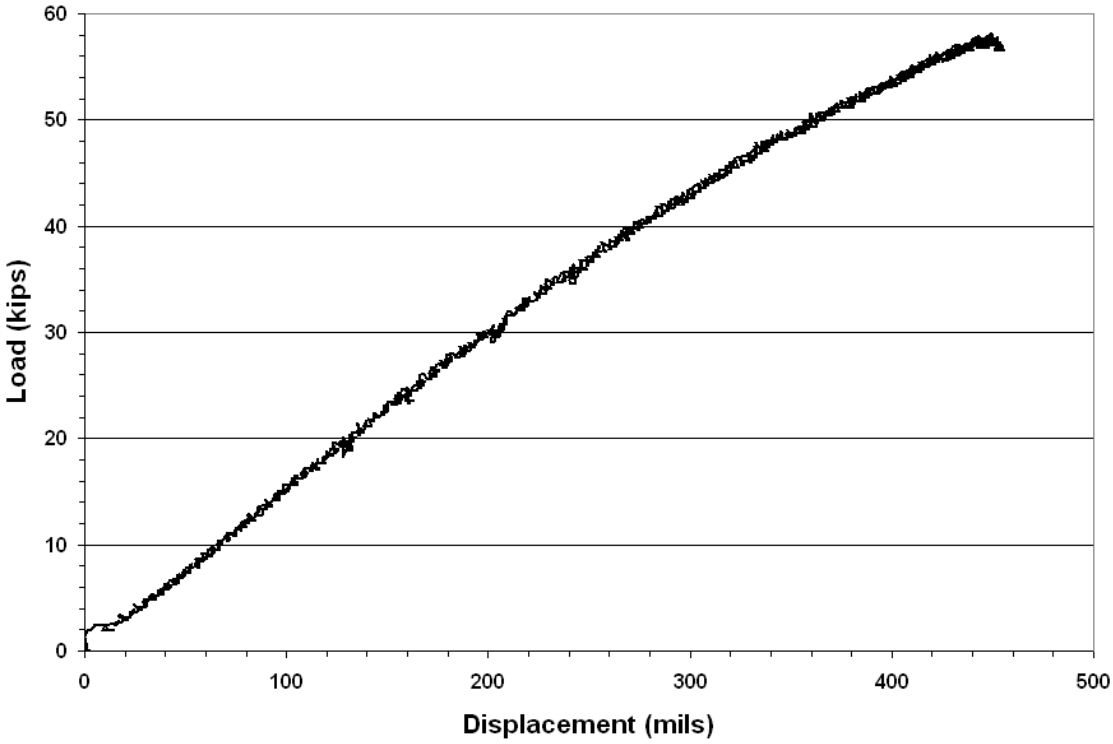

Figure D28. Load-Displacement Curve from Test on 2 Percent Lime-Stabilized Uncrushed Gravel on Sand.

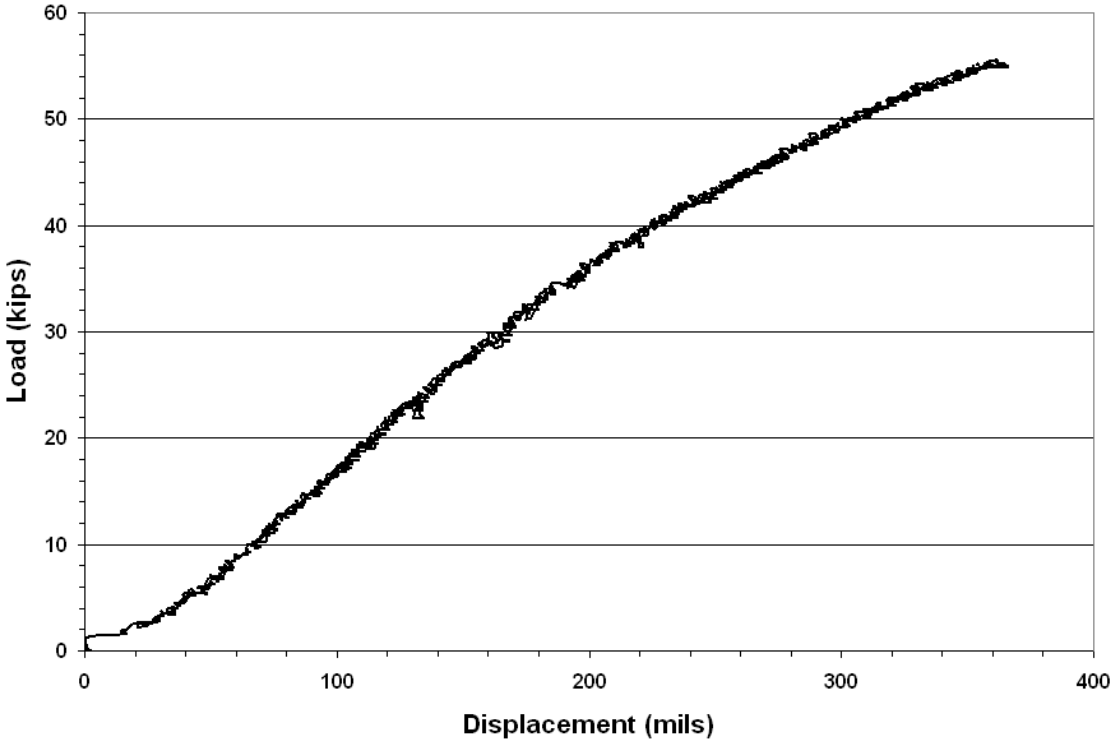

Figure D29. Load-Displacement Curve from Test on 3.0 Percent Cement-Treated Grade 2 Crushed Limestone Base on Sand.

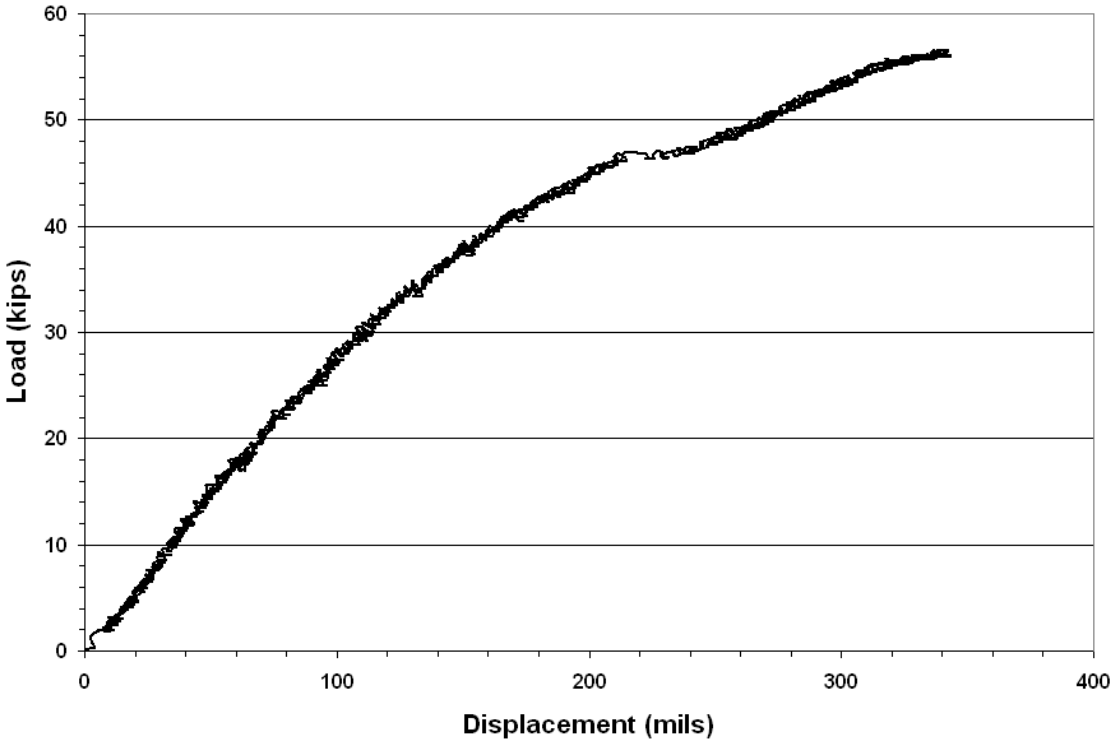

Figure D30. Load-Displacement Curve from Test on 4.5 Percent Cement-Treated Grade 2 Crushed Limestone Base on Sand.